


Spring 5-6-2017

The Rise and Fall of the Bovine Corpus Luteum

Heather Talbott

University of Nebraska Medical Center

Follow this and additional works at: <https://digitalcommons.unmc.edu/etd>

 Part of the [Biochemistry Commons](#), [Molecular Biology Commons](#), and the [Obstetrics and Gynecology Commons](#)

Recommended Citation

Talbott, Heather, "The Rise and Fall of the Bovine Corpus Luteum" (2017). *Theses & Dissertations*. 207.
<https://digitalcommons.unmc.edu/etd/207>

This Dissertation is brought to you for free and open access by the Graduate Studies at DigitalCommons@UNMC. It has been accepted for inclusion in Theses & Dissertations by an authorized administrator of DigitalCommons@UNMC. For more information, please contact digitalcommons@unmc.edu.

THE RISE AND FALL OF THE BOVINE CORPUS LUTEUM

by

Heather Talbott

A DISSERTATION

Presented to the Faculty of
the University of Nebraska Graduate College
in Partial Fulfillment of the Requirements
for the Degree of Doctor of Philosophy

Biochemistry and Molecular Biology
Graduate Program

Under the Supervision of Professor John S. Davis

University of Nebraska Medical Center
Omaha, Nebraska

May, 2017

Supervisory Committee:

Carol A. Casey, Ph.D.

Andrea S. Cupp, Ph.D.

Parmender P. Mehta, Ph.D.

Justin L. Mott, Ph.D.

ACKNOWLEDGEMENTS

This dissertation was supported by the Agriculture and Food Research Initiative from the USDA National Institute of Food and Agriculture (NIFA) Pre-doctoral award; University of Nebraska Medical Center Graduate Student Assistantship; University of Nebraska Medical Center Exceptional Incoming Graduate Student Award; the VA Nebraska-Western Iowa Health Care System Department of Veterans Affairs; and The Olson Center for Women's Health, Department of Obstetrics and Gynecology, Nebraska Medical Center.

Chapter 1: John S. Davis

Chapter 2: Crystal Krause, Xiaoying Hou, Pan Zhang, Sheikh M. K. Alam William B. Rizzo, Jennifer R. Wood, Robert A. Cushman, Andrea S. Cupp, and John S. Davis

Chapter 3: Crystal Krause, Xiaoying Hou, Pan Zhang, William B. Rizzo, Dragana Lagundzin, Nicholas T. Woods, Jennifer R. Wood, Robert A. Cushman, Andrea S. Cupp, and John S. Davis

Chapter 4: Xiaoying Hou, Fang Qiu, Pan Zhang, Chittibabu Guda, Fang Yu, Robert A. Cushman, Jennifer R. Wood, Cheng Wang, Andrea S. Cupp, and John S. Davis

Chapter 5: Abigail Delaney, Pan Zhang, Yangsheng Yu, Robert A. Cushman, Andrea S. Cupp, Xiaoying Hou, John S. Davis

The completion of this dissertation would have been impossible without the invaluable contributions of so many people, scientifically, educationally, professionally and personally.

First and foremost, I owe my enduring gratitude to my advisor Dr. John S. Davis who challenges me every day to strive to be the best citizen and scientist I can be.

My committee members, Dr. Carol Casey, Dr. Andrea Cupp, Dr. John Davis, Dr. Parmender Mehta, and Dr. Justin Mott. Thank you for your guidance, conversations, support, and understanding throughout the entirety of my graduate journey. You continue to remind me that success comes with persistent curiosity, thoughtful enquiry, and critical evaluation.

My husband and partner, Joseph Reed, who provided me with the love, editing, encouragement, thought-provoking conversations, and the final motivation that inspired me to complete my dissertation.

Holly Talbott, for her enduring motherly support, commas, and unwavering belief that I can do anything I put my mind to.

Christy Smith and Karen Hankins, for their friendship and assistance with grants, travel, and other administrative tasks which allowed me to focus on my work and succeed throughout my graduate education.

Annie Kosmacek, for her no-nonsense advice and friendship throughout which has kept me sane, motivated, and excited for life.

My grandparents, whose love and support will endure:

Helen Irene Day, 1927-2010; R. Trenton Day, 1926-2004; Donna Johansen, 1936-2017; R. Terry Johansen, 1935-2016; Dean Talbott, 1941-2011; Kyong Talbott, John Reed, 1937-2015; Marie Reed, 1937-2016; and Sherry Walsh.

My family who have supported me whole-heartedly throughout this entire adventure.

My lab mates both past and present for their assistance, support and friendship along the way.

In particular, Crystal Cordes, Chunbo He, Sharon Hou, Xiangmin Lv, Dulce Maroni, and Pan Zhang.

Collaborators for works both presented and not. Cheng Wang and lab, Andrea Cupp and lab, Jen Woods and lab, Bob Cushman and lab, Shyamal Roy and lab, Dr. Geoffrey Thiele and lab, Dr. William Rizzo and lab.

My classmates, for study sessions, humor, practice presentations and advice.

In particular, Ekta Agarwal, Mona Al-mugatoir, Shalis Ammons, Nick Griffin, Colleen Lambo, Raheleh Miralami, Tyler Scherr, Lucas Struble, and Kristin Wipfler.

McGoogan library staff, EHS staff, and UNMC Security

ABSTRACT: THE RISE AND FALL OF THE BOVINE CORPUS LUTEUM

Heather A. Talbott, Ph.D.

University of Nebraska, 2017

Supervisor: John S. Davis, Ph.D.

This dissertation describes a study of the mechanisms regulating the genesis and subsequent involution of the temporary endocrine structure, the corpus luteum (CL), through the use of a bovine model. The CL is essential for maintaining a suitable uterine environment for embryo implantation and early development through secretion of the steroid hormone progesterone. The “Rise and Fall” of the CL occurs within each estrous cycle whereby the CL must form from the ruptured follicle, secrete sufficient progesterone for uterine maturation, and at the end of the cycle (or pregnancy) regress to allow new follicular development. During the rise of the CL, the composition and regulation of lipid droplets (LDs) were studied and it was determined that LDs are a common luteal cell structure formed by day 3 post-ovulation, and store both cholesteryl esters and triglycerides. Additionally, the LD-associated proteome was examined and established that steroidogenic enzymes are enriched in purified LD fractions. Demonstrating that luteal LDs may serve as critical mediators of steroidogenesis by storing steroid precursors in close association with steroidogenic enzymes. At the fall of the CL, alterations in the luteal transcriptome revealed changes consistent with early activation of cytokine signaling. One such cytokine, C-X-C motif chemokine ligand 8 (previously IL-8), was assessed for its ability to regulate luteal cell function. CXCL8 expression was determined to be induced in bovine luteal cells via p38 and JNK signaling and could induce bovine neutrophil migration. However, neutrophils had no effect on progesterone secretion unlike activated peripheral blood mononuclear cells which could inhibit luteal cell progesterone secretion. In total, the studies described herein indicate that both LDs and cytokines play important roles in CL development, function, and regression.

GRAPHICAL ABSTRACT

The Rise and Fall of the Bovine Corpus Luteum

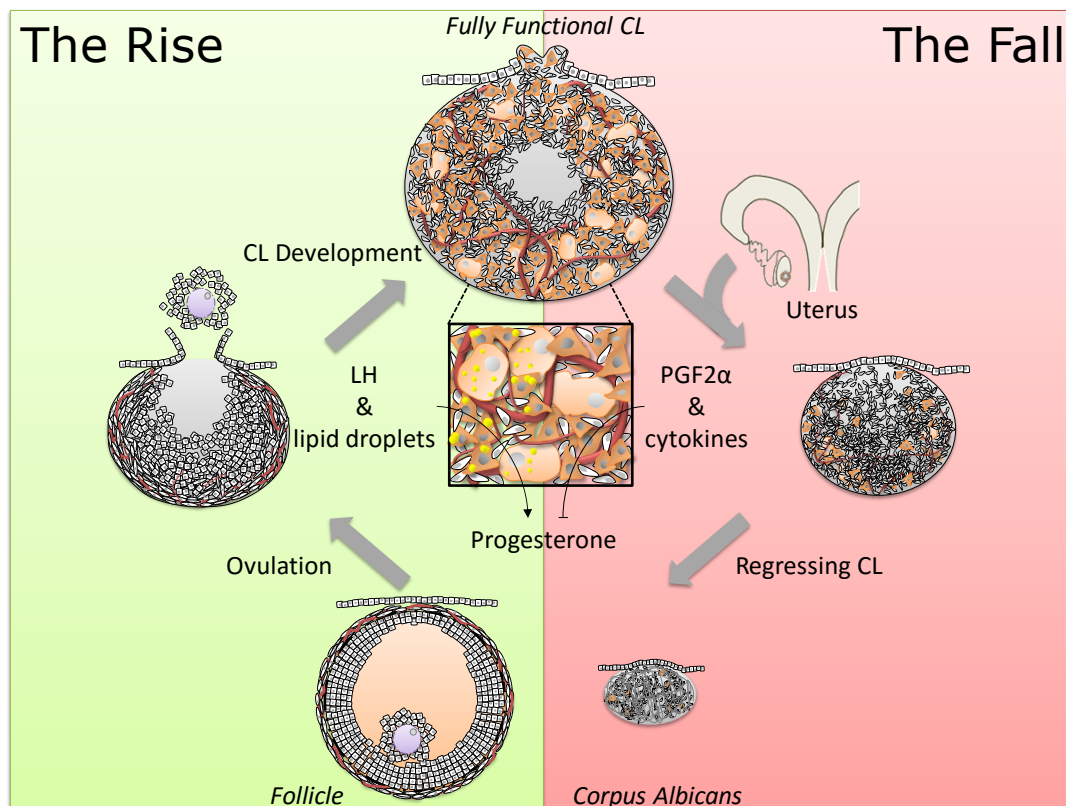


Diagram depicting the rise (left) and fall (right) of the bovine corpus luteum (CL). Development of the CL begins from a mature follicle (bottom left) with a well vascularized theca layer and multi-layered mural granulosa cells. Ovulation of the follicle begins the transformation into a functional CL (top) through angiogenic growth into the granulosa layer and differentiation of granulosa and theca cells into large and small luteal cells. During CL development, lipid droplets (LDs) form and store cholesteryl esters. These LDs may be an important source of luteinizing hormone (LH)-stimulated progesterone synthesis. At the end of the estrous cycle, prostaglandin F₂α (PGF₂α) released from the bovine uterus will trigger luteal regression, in part through stimulation of cytokine and cytokine signaling events. These processes result in decreased progesterone production and involution of the CL.

TABLE OF CONTENTS

ACKNOWLEDGEMENTS	i
ABSTRACT: THE RISE AND FALL OF THE BOVINE CORPUS LUTEUM	iii
GRAPHICAL ABSTRACT	iv
TABLE OF CONTENTS	v
LIST OF FIGURES	xi
LIST OF TABLES	xiii
LIST OF APPENDICES	xiv
LIST OF ABBREVIATIONS	xv
CHAPTER 1: INTRODUCTION	1
ABSTRACT	1
1.1. LIPID DROPLETS	2
1.2. AMP-ACTIVATED PROTEIN KINASE	8
1.3. LH INHIBITS AMPK	11
1.4. PGF _{2α} ACTIVATES AMPK	12
1.5. AUTOPHAGY	14
1.6. SUMMARY	17
CHAPTER 2: COMPOSITION OF THE LIPID DROPLETS OF THE BOVINE CORPUS LUTEUM	23
ABSTRACT	23
2.1. INTRODUCTION	24
2.1.1. <i>Formation and function of the CL</i>	24
2.1.2. <i>Luteal LDs</i>	24
2.1.3. <i>Functional role of LDs</i>	25
2.2. MATERIALS AND METHODS	25

2.2.1.	<i>Animals</i>	25
2.2.2.	<i>Lipid droplet staining in luteal tissue</i>	26
2.2.3.	<i>Transmission electron microscopy</i>	26
2.2.4.	<i>Isolation of large and small luteal cells</i>	26
2.2.5.	<i>Isolation of granulosa and theca cells</i>	27
2.2.6.	<i>Lipid droplet staining in freshly isolated cells.</i>	28
2.2.7.	<i>Progesterone assay</i>	28
2.2.8.	<i>Lipid droplet isolation from tissue</i>	28
2.2.9.	<i>Western blots</i>	29
2.2.10.	<i>Lipidomics</i>	29
2.2.11.	<i>High-performance thin layer chromatography (HPTLC)</i>	30
2.2.12.	<i>Reverse transcriptase-polymerase chain reaction (RT-PCR)</i>	31
2.3.	RESULTS	31
2.3.1.	<i>Animals</i>	31
2.3.2.	<i>Luteal LDs</i>	31
2.3.3.	<i>Lipid droplets in ovarian cells</i>	32
2.3.4.	<i>Expression of LD-associated proteins in the CL</i>	32
2.3.5.	<i>Lipid composition of LDs</i>	32
2.4.	DISCUSSION	33
2.4.1.	<i>Overview of study</i>	33
2.4.2.	<i>Lipid droplets in luteal tissue</i>	34
2.4.3.	<i>Lipid composition of LDs</i>	34
CHAPTER 3: LIPID DROPLETS ARE DYNAMICALLY REGULATED BY LUTEINIZING HORMONE SIGNALING IN THE BOVINE CORPUS LUTEUM		43
ABSTRACT		43
3.1.	INTRODUCTION	44
3.1.1.	<i>Regulation of CL formation</i>	44
3.1.2.	<i>Lipid droplets in the CL</i>	45

3.1.3.	<i>Regulation of LDs</i>	46
3.1.4.	<i>Hormone-sensitive lipase</i>	46
3.2.	MATERIALS AND METHODS	47
3.2.1.	<i>Isolation and culture of human granulosa cells</i>	47
3.2.2.	<i>Isolation of large and small luteal cells</i>	48
3.2.3.	<i>Isolation of granulosa and theca cells</i>	48
3.2.4.	<i>Luteal cell culture</i>	49
3.2.5.	<i>Differentiation of granulosa and theca cells to luteal cell types</i>	49
3.2.6.	<i>Western blots</i>	50
3.2.7.	<i>Progesterone assay</i>	50
3.2.8.	<i>Lipid droplet isolation from cells</i>	50
3.2.9.	<i>Proteomics</i>	51
3.2.10.	<i>Animals</i>	53
3.2.11.	<i>Lipid droplet isolation from tissue</i>	53
3.2.12.	<i>Western blots of LDs</i>	54
3.3.	RESULTS	54
3.3.1.	<i>Formation of LDs during differentiation</i>	54
3.3.2.	<i>Phosphorylation of HSL at Ser563 by LH and LH signaling intermediates</i>	55
3.3.3.	<i>Regulation of LDs</i>	55
3.3.4.	<i>PKA stimulation promotes alterations in the luteal LD proteome</i>	55
3.3.5.	<i>Luteal LDs are associated with steroidogenic enzymes</i>	56
3.4.	DISCUSSION	56
 CHAPTER 4: EARLY TRANSCRIPTOME RESPONSES OF THE BOVINE MID-CYCLE CORPUS LUTEUM TO PROSTAGLANDIN F2 ALPHA INCLUDES CYTOKINE SIGNALING		68
ABSTRACT		68
4.1.	INTRODUCTION	69
4.2.	MATERIALS AND METHODS	71

4.2.1.	<i>Animals</i>	71
4.2.2.	<i>Steroidogenic luteal cell culture</i>	72
4.2.3.	<i>Affymetrix bovine gene chip microarray</i>	74
4.2.4.	<i>Microarray statistics</i>	74
4.2.5.	<i>Self-organizing maps and statistics</i>	75
4.2.6.	<i>Dataset comparisons</i>	75
4.2.7.	<i>Pathway analysis</i>	75
4.3.	RESULTS	76
4.3.1.	<i>Bovine microarray</i>	76
4.3.2.	<i>Functional luteolysis</i>	78
4.3.3.	<i>Pathway analysis of short time-course</i>	79
4.3.4.	<i>PGF2α activates well-organized transcriptional cascades</i>	80
4.3.5.	<i>Dataset comparisons</i>	82
4.4.	DISCUSSION	83
4.4.1.	<i>Overview of study</i>	83
4.4.2.	<i>Induction of functional luteolysis</i>	84
4.4.3.	<i>Cytokine signaling</i>	85
4.4.4.	<i>PGF2α activates well-organized signaling cascades</i>	87
4.4.5.	<i>Dataset comparison and relationship to previous studies</i>	88
4.4.6.	<i>Conclusions from the study</i>	89
CHAPTER 5: EFFECTS OF CXCL8 AND IMMUNE CELLS ON THE REGULATION OF LUTEAL PROGESTERONE SECRETION		105
ABSTRACT		105
5.1.	INTRODUCTION	106
5.2.	MATERIALS AND METHODS	107
5.2.1.	<i>In vivo studies</i>	107
5.2.2.	<i>In vitro studies</i>	108
5.2.3.	<i>Isolation of bovine luteal cells</i>	108

5.2.4.	<i>Isolation of bovine endothelial and fibroblast cells</i>	108
5.2.5.	<i>Isolation of bovine neutrophils and migration assays</i>	109
5.2.6.	<i>Isolation of human neutrophils and degranulation assays</i>	110
5.2.7.	<i>Isolation of bovine peripheral blood mononuclear cells (PBMC)</i>	110
5.2.8.	<i>Co-culture experiments</i>	111
5.2.9.	<i>Neutrophil-luteal cell co-culture:</i>	111
5.2.10.	<i>PBMC-luteal cell co-culture:</i>	111
5.2.11.	<i>Western blot analysis</i>	112
5.2.12.	<i>Progesterone analysis</i>	112
5.2.13.	<i>Statistical analysis</i>	112
5.3.	RESULTS	112
5.3.1.	<i>PGF2α stimulates chemokine gene expression in vivo</i>	112
5.3.2.	<i>PGF2α stimulates CXCL8 expression in vitro</i>	113
5.3.3.	<i>CXCL8 induces migration of bovine neutrophils</i>	113
5.3.4.	<i>CXCL8 selectively stimulates signaling in bovine neutrophils</i>	114
5.3.5.	<i>Effect of CXCL8 and immune cells on progesterone secretion</i>	115
5.4.	DISCUSSION	115
CHAPTER 6: DISCUSSION		128
6.1.	OVERVIEW	128
6.2.	COMPOSITION OF THE LIPID DROPLETS OF THE BOVINE CORPUS LUTEUM	128
6.3.	LIPID DROPLETS ARE DYNAMICALLY REGULATED BY LUTEINIZING HORMONE SIGNALING IN THE BOVINE CORPUS LUTEUM	129
6.4.	EARLY TRANSCRIPTOME RESPONSES OF THE BOVINE MID-CYCLE CORPUS LUTEUM TO PROSTAGLANDIN F2 ALPHA INCLUDES CYTOKINE SIGNALING	130
6.5.	EFFECTS OF CXCL8 AND IMMUNE CELLS ON THE REGULATION OF LUTEAL PROGESTERONE SECRETION	131
6.6.	CONCLUSIONS	132

BIBLIOGRAPHY	134
---------------------	------------

APPENDIX A: SUPPLEMENTAL DATA FOR CHAPTER 3	176
--	------------

APPENDIX B: SUPPLEMENTAL DATA FOR CHAPTER 4	187
--	------------

LIST OF FIGURES

FIGURE 1-1 – LIPID DROPLETS IN BOVINE LARGE AND SMALL LUTEAL CELLS _____	18
FIGURE 1-2 – POTENTIAL ROLE OF HORMONE-SENSITIVE LIPASE IN LUTEAL CELLS _____	19
FIGURE 1-3 – ROLES OF LUTEINIZING HORMONE AND AMP-ACTIVATED KINASE IN PROGESTERONE SECRETION _____	20
FIGURE 1-4 – POTENTIAL MECHANISMS OF ACTIVATION AND INHIBITION OF HORMONE SENSITIVE LIPASE IN LUTEAL CELLS _____	21
FIGURE 1-5 – COUNTERACTING MECHANISMS OF LUTEINIZING HORMONE AND PROSTAGLANDIN F2A IN LUTEAL CELL STEROIDOGENESIS _____	22
FIGURE 2-1 – LUTEAL PERFORMANCE MEASURES OF DAY 3 AND DAY 10 BOVINE CORPUS LUTEA _____	36
FIGURE 2-2 – LIPID DROPLETS ANALYSIS OF IN VIVO TISSUE _____	37
FIGURE 2-3 – LIPID DROPLETS OF ISOLATED CELLS _____	39
FIGURE 2-4 – LIPID DROPLET-ASSOCIATED PROTEINS IN BOVINE TISSUE INCLUDING THE CL _____	40
FIGURE 2-5 – LIPID COMPOSITION OF LUTEAL LDS _____	41
FIGURE 2-6 – LIPID COMPOSITION OF SUBCELLULAR COMPARTMENTS OF LUTEAL TISSUE _____	42
FIGURE 3-1 – LIPID DROPLET-ASSOCIATED PROTEINS WERE EXPRESSED AT GREATER AMOUNTS IN LUTEAL CELLS AT BOTH TRANSCRIPTIONAL AND PROTEIN LEVELS _____	61
FIGURE 3-2 – LIPID DROPLETS AND LD-ASSOCIATED PROTEINS HSL AND PLIN2 INCREASE DURING DIFFERENTIATION OF GRANULOSA CELLS TO LUTEAL CELLS _____	62
FIGURE 3-3 – PHOSPHORYLATION OF HSL AT SER-563 IS INCREASED BY LH AND PROTEIN KINASE A ACTIVATING COMPOUNDS _____	63
FIGURE 3-4 – HORMONE-STIMULATED PROGESTERONE PRODUCTION CAN BE INHIBITED WHEN HSL ACTIVITY IS BLOCKED _____	64
FIGURE 3-5 – PHOSPHORYLATION OF HSL RESULTS IN ITS TRANSLOCATION TO LDS IN BOVINE LUTEAL TISSUE _____	65
FIGURE 3-6 – WESTERN BLOT ANALYSIS OF LD ASSOCIATED PROTEINS FROM FUNCTIONAL BOVINE CL CONFIRMS PROTEOMIC IDENTIFICATION OF LD-ASSOCIATED STEROIDOGENIC ENZYMES _____	66

FIGURE 3-7 – PROPOSED ORGANIZATION OF LUTEAL LDS, MITOCHONDRIA, AND ENDOPLASMIC RETICULUM TO FACILITATE STEROIDOGENESIS _____	67
FIGURE 4-1 - TIME-COURSE OF THE TRANSCRIPTOMIC RESPONSE TO PGF2A _____	91
FIGURE 4-2 – PGF2A INDUCED REDUCTIONS IN PROGESTERONE ARE CORRELATED WITH REDUCTIONS IN THE EXPRESSION OF GENES CONTROLLING INTRACELLULAR CHOLESTEROL AVAILABILITY _____	93
FIGURE 4-3 – IN VIVO TREATMENT WITH PGF2A PREDICTS CLASSICAL PGF2A AND CYTOKINE SIGNALING _____	94
FIGURE 4-4 – TEMPORAL RESPONSE WAVES TO PGF2A _____	96
FIGURE 4-5 – COMMON GENE ALTERATIONS IN RESPONSE TO PGF2A _____	98
FIGURE 5-1 – INDUCTION OF CHEMOKINES FOLLOWING TREATMENT WITH PGF IN VIVO AND IN VITRO _____	120
FIGURE 5-2 – STIMULATORY EFFECTS OF CXCL8 ON NEUTROPHILS. _____	121
FIGURE 5-3 – IL8 STIMULATES EARLY SIGNALING RESPONSES IN BOVINE NEUTROPHILS. _____	122
FIGURE 5-4 – CXCL8 STIMULATED NEUTROPHIL MIGRATION IS INDEPENDENT OF ERK SIGNALING. _____	123
FIGURE 5-5 – CXCL8 AND NEUTROPHILS DO NOT INHIBIT LUTEAL PROGESTERONE PRODUCTION. _____	124
FIGURE 5-6 – COCULTURES OF LUTEAL CELLS WITH ACTIVATED PERIPHERAL BLOOD MONONUCLEAR CELLS (PBMCS) INHIBIT LUTEAL PROGESTERONE PRODUCTION. _____	125

LIST OF TABLES

TABLE 4-1 – TOP TEN UP-REGULATED GENES AT EACH TIME-POINT _____	99
TABLE 4-2 – TOP TEN DOWN-REGULATED GENES AT EACH TIME-POINT _____	100
TABLE 4-3 – TOP FIVE CANONICAL PATHWAYS PREDICTIONS DURING EACH TIMEPOINT DURING THE EARLY RESPONSE TO PGF2A TREATMENT _____	101
TABLE 4-4 – COMMON TRANSCRIPTS DIFFERENTIALLY EXPRESSED IN RESPONSE TO PGF2A TREATMENT _	102
TABLE 5-1 – BOVINE PRIMERS FOR QPCR _____	126
TABLE 5-2 – ANTIBODIES USED FOR CELL SIGNALING, WESTERN BLOTS, AND FLOW ANALYSIS _____	127

LIST OF APPENDICES

APPENDIX A-1 – VERIFICATION OF CAY10499 ON-TARGET EFFECTS _____	176
APPENDIX A-2 – LUTEAL LIPID DROPLET-ASSOCIATED PROTEINS DETERMINED BY PROTEOMICS _____	177
APPENDIX A-3 – QUANTIFICATION OF LD-ASSOCIATED PROTEIN BY WESTERN BLOT _____	186
APPENDIX B-1 – PRIMERS USED FOR QPCR _____	187
APPENDIX B-2 – DIFFERENTIALLY EXPRESSED TRANSCRIPTS FROM A SHORT PGF2A TIME-COURSE _____	188
APPENDIX B-3 – BIOLOGICAL PROCESS ANNOTATION OF DIFFERENTIALLY EXPRESSED GENES FROM EACH TIME POINT _____	192
APPENDIX B-4 – PHYSIOLOGICAL CHARACTERISTICS OF THE STUDY ANIMALS _____	193
APPENDIX B-5 – DIFFERENTIALLY EXPRESSED TRANSCRIPTS INCLUDED WITHIN EACH SOM _____	195

LIST OF ABBREVIATIONS

Protein/*Gene* Name

3 β HSD/ <i>HSD3B1</i>	hydroxyl-delta-5-steroid dehydrogenase, 3 beta and steroid delta-isomerase 1
ABCA1/ <i>ABCA1</i>	ATP binding cassette subfamily A member 1
ABCG1/ <i>ABCG1</i>	ATP binding cassette subfamily G member 1
ACC	Acetyl-CoA carboxylase
<i>ACTB</i>	Beta-actin
AICAR	5-amino-imidazole-4-carboxamide riboside
AKR1C2	Aldo-keto reductase family 1 member C2
AMP	Adenosine monophosphate
AMPK	Adenosine monophosphate-activated protein kinase
ANOVA	Analysis of variance
APC	Allophycocyanin
APOA1/ <i>APOA1</i>	Apolipoprotein A1
APOE/ <i>APOE</i>	Apolipoprotein E
ATF3/ <i>ATF3</i>	Activating transcription factor 3
ATG	Autophagy-related
ATGL	Adipose triglyceride lipase
ATP	Adenosine triphosphate
Bak1	Bcl2-antagonist/killer 1
Bcl2	B-cell lymphoma 2
Becn1	Beclin 1
BMB-15/ <i>BMP15</i>	Bone morphogenetic protein 15
BSA	Bovine serum albumin
CAMKK2	Calcium/calmodulin-dependent protein kinase kinase 2
cAMP	Cyclic adenosine monophosphate
CCL/ <i>CCL</i>	C-C motif chemokine
ITGAM	Integrin subunit alpha M (also: CD11b)
CD66b	Carcinoembryonic antigen-related cell adhesion molecule 8 (also: CEACAM8)
CE	Cholesteryl esters
CEBPD	CCAAT/enhancer binding protein delta
CG	Chorionic gonadotropin
cGMP	Cyclic guanine monophosphate
CL	Corpus luteum
COC	Cumulus-oocyte complex
cPLA2/ <i>PLA2G4A</i>	Cytosolic phospholipase A2
CPT1A	Carnitine palmitoyltransferase 1A
CXCL/ <i>CXCL</i>	C-X-C motif chemokine
CYP17/ <i>CYP17A1</i>	Steroid 17-alpha-hydroxylase/17,20 lyase cytochrome P450 family 17 subfamily A member 1
DAG	Diglyceride/diacylglycerol
Dapk	Death-associated protein kinase 1
DMEM	Dulbecco's modified eagle medium
DMSO	Dimethylsulfoxide

DNA	Deoxyribonucleic acid
ECGS	Endothelial cell growth supplement
EGR/ <i>EGR</i>	Early growth response protein
ERF/ <i>ERF</i>	ETS2 repressor factor
ERK	Extracellular signal-regulated kinase
FA	Fatty acids
FADH ₂	flavin adenine dinucleotide
FBS	Fetal bovine serum
FITC	Fluorescein isothiocyanate
FOS/ <i>FOS</i>	Finkel-Biskis-Jinkins murine osteosarcoma viral oncogene homolog
FSH	Follicle stimulating hormone
GADPH	Glyceraldehyde-3-phosphate dehydrogenase
GC	Granulosa cells
GDF-9	Growth/differentiation factor 9
GEO	Gene expression omnibus
GnRH	Gonadotropin-releasing hormone
H&E	Hematoxylin and eosin
HBSS	Hank's balance salt solution
hCG	Human chorionic gonadotropin
HDL	High-density lipoprotein
HIF-1 α / <i>HIF1A</i>	Hypoxia inducible factor 1 alpha subunit
HLM	Hypotonic lysis medium
HMG-CoA reductase/ <i>HMGCR</i>	3-hydroxy-3-methylglutaryl-CoA reductase
HPLC	High-performance liquid chromatography
HPTLC	High-performance thin layer chromatography
HRP	Horse radish peroxidase
HSL/ <i>LIPE</i>	Hormone-sensitive lipase
IFN γ / <i>IFNG</i>	Interferon gamma
IFN τ / <i>IFNT</i>	Interferon tau
IL-/ <i>IL</i>	Interleukin
IPA	Ingenuity Pathway Analysis
ITS	Insulin-transferrin-selenium
I κ B α / <i>NFKB1A</i>	Inhibitor of kappa B alpha
I κ B ζ / <i>NFKBIZ</i>	NF- κ B inhibitor zeta
JNK	JUN N-terminal kinase
JUN/ <i>JUN</i>	Jun proto-oncogene
LC3	Microtubule-associated protein light chain 3
LD	Lipid droplet
LDL	Low density lipoprotein
LDLR/ <i>LDLR</i>	Low density lipoprotein receptor
LH	Luteinizing hormone
LHCGR	Luteinizing hormone/chorionic gonadotropin receptor
LIF	Leukemia inhibitory factor
LKB1	Tumor suppressor liver kinase B1 (also: serine and threonine kinase 11, STK11)

LLC	Large luteal cells
M199	Medium 199
MAM	Mitochondria-associated endoplasmic reticulum membrane
MAPK	Mitogen-activated protein kinase
MAPK1	Mitogen-activated protein kinase 14 (also: ERK2)
MAPK14	Mitogen-activated protein kinase 14 (also: p38)
MAPK3	Mitogen-activated protein kinase 3(also: ERK1)
MAPK8	Mitogen-activated protein kinase 8 (also: JNK)
MMP	Matrix metalloproteinase
MRM	Multiple reaction monitoring
mRNA	Messenger ribonucleic acid
MS/MS	Tandem mass spectrometry
Mt	Mitochondria
MTOR	Mechanistic target of rapamycin
MYC/ <i>MYC</i>	V-Myc avian myelocytomatosis viral oncogene homolog
NADH	Nicotinamide adenine dinucleotide
NFIB/ <i>NFIB</i>	Nuclear factor I B
NFIL3/ <i>NFIL3</i>	Nuclear factor interleukin 3 regulated
NF- κ B/ <i>NFKB1</i>	Nuclear factor kappa B
NR1D1/ <i>NR1D1</i>	Nuclear receptor subfamily 1 group D member 1
NR1H/ <i>NR1H</i>	Nuclear receptor family 1 subfamily H members
NR2C2/ <i>NR2C2</i>	Nuclear receptor subfamily 2 group C member 2
NR2F1/ <i>NR2F1</i>	Nuclear receptor subfamily 2 group F member 1
NR4A/ <i>NR4A</i>	Nuclear receptor subfamily 4 group A members
NS	Not significant
O.C.T.	Optimal cutting temperature compound
ORO	Oil red O
P450 _{scc} / <i>CYP11A11</i>	Cytochrome P450 family 11 subfamily A member 1
PBMC	Peripheral blood mononuclear cells
PBS	Phosphate-buffered saline
PC	Phosphatidylcholine
PCR	Polymerase chain reaction
PE	Phosphatidylethanolamine
PGE2	Prostaglandin E 2
PGES2/ <i>PTGES</i>	Prostaglandin E synthase 2
PGF2 α	Prostaglandin F 2 alpha
PGHS-2	Prostaglandin G/H synthase 2 (also: COX2)
PGI2	Prostaglandin I 2
PI	Phosphoinositol
PKA	Protein kinase A
PKC/ <i>PKCD</i>	Protein kinase C
PKC β II	Protein kinase C beta two
PKC ϵ	Protein kinase C epsilon
PLIN	Perilipin
PMA	Phorbol myristate acetate

PNS	Post-nuclear supernatant
PTGFR/ <i>PTGFR</i>	Prostaglandin F receptor
PVDF	Polyvinylidene difluoride
qPCR	Quantitative real-time polymerase chain reaction
RMA	Robust multi-array average
Rock1	Rho-associated coiled-coil containing protein kinase 1
RPMI	Roswell Park Memorial Institute 1640 medium
RT-PCR	Reverse transcriptase polymerase chain reaction
SCRB1/ <i>SCARB1</i>	Scavenger receptor class B member 1
SDS	Sodium dodecyl sulfate
SEM	Standard error of the mean
SLC	Small luteal cells
SLCO2A1	Solute carrier organic anion transporter family member
SM	Sphingomyelin
SOCs/ <i>SOCs</i>	Suppressor of cytokine signaling
SOM	Self-organizing map
SOX4/ <i>SOX4</i>	Sex determining region Y-box 4
SREBF/ <i>SREBF</i>	Sterol regulatory element binding transcription factor 1/2
sMRM	Scheduled multiple reaction monitoring
ST	Sterols
ST loop	Serine/threonine rich loop
StAR/ <i>StAR</i>	Steroidogenic acute regulatory protein
STAT	Signal transducer and activator of transcription
STK4/ <i>STK4</i>	Serine/threonine-protein kinase 4 (also: MST1)
TAG	Triglyceride/triacylglyceride
TC	Theca cells
TEM	Transmission electron microscopy
TGF β / <i>TGFB</i>	Transforming growth factor beta 1/2
TNF α / <i>TNF</i>	Tumor necrosis factor alpha
VDAC	Voltage-dependent anion channel
VE-cadherin	Vascular endothelial cell cadherin
VEGF	Vascular endothelial growth factor
FFA	Free fatty acids

CHAPTER 1: INTRODUCTION

*Luteal Lipid Droplets and Metabolic Pathways Regulate Steroidogenesis in the Corpus Luteum **

Abstract

This review focuses on recent advances in the understanding of metabolic processes used by the corpus luteum to control steroidogenesis and other cellular functions. The corpus luteum (CL) has abundant lipid droplets that are believed to store cholesteryl esters and triglycerides. Recent studies in other tissues indicate that cytoplasmic lipid droplets serve as platforms for cell signaling and interactions with other organelles. Lipid droplets are also critical organelles for controlling cellular metabolism. Emerging evidence demonstrates that luteinizing hormone (LH) via activation of the cAMP and the protein kinase A (PKA) signaling pathway stimulates the phosphorylation and activation of hormone-sensitive lipase (HSL) an enzyme that hydrolyzes cholesteryl esters stored in lipid droplets to provide cholesterol for steroidogenesis and fatty acids for utilization by mitochondria for energy production. The energy sensor adenosine monophosphate (AMP)-activated protein kinase (AMPK) can inhibit steroidogenesis by interrupting metabolic pathways that provide cholesterol to the mitochondria or the expression of genes required for steroidogenesis. In addition to lipid droplets, autophagy also contributes to the regulation of the metabolic balance of the cell by eliminating damaged organelles and providing cells with essential nutrients during starvation. Autophagy in luteal cells is regulated by signaling pathways that impact AMPK activity and lipid droplet homeostasis. In summary, a number of signaling pathways converge on luteal lipid droplets to regulate steroidogenesis and metabolism. Knowledge of metabolic pathways in luteal cells is fundamental to understanding events that control the function and life span the corpus luteum.

* The material presented in this chapter was previously published: Talbott and Davis. Lipid Droplets and Metabolic Pathways Regulate Steroidogenesis in the Corpus Luteum. *The Life Cycle of the Corpus Luteum* 2017 ¹⁶¹

Recent research has provided great insight into mechanisms contributing to corpus luteum formation, function, and regression. Many of these studies have focused on changes in gene and protein expression and activity. The availability of new techniques for metabolomics, lipidomics, and proteomics has renewed interest in determining how cellular metabolic events control steroidogenesis. Specifically, there is an interest in understanding how lipids are stored and utilized during the lifespan of the corpus luteum. One of the notable features observed during luteal development is the acquisition of cytoplasmic lipid droplets (LDs). These unique organelles are surrounded by a phospholipid monolayer which coats a core of neutral lipids including cholesteryl esters and triglycerides. Lipid droplets have been most extensively studied in adipocytes and preadipocytes, for their pivotal role in energy conservation and homeostasis ^{1,2}, however, LDs have been observed in nearly all cell types, from prokaryotes ³ to hepatocytes ⁴, cardiac myocytes ⁵, macrophages ⁶, and steroid-secreting cells ^{7,8}. In many of these cells, LDs are a sign of pathological stress because of an overabundance of environmental lipids (e.g., the foamy macrophage seen in atherosclerotic lesions ⁶). However, LD formation and presence in steroidogenic tissues such as the ovarian follicle and corpus luteum appears to be non-pathological and required for healthy, fully-functional steroidogenic ovarian cells.

1.1. Lipid droplets

Recent reviews point to cytoplasmic LDs as critical mediators of metabolic health and disease ^{1,9,10}. Intracellular LDs store triglycerides and cholesteryl esters as reservoirs for energetic substrates (fatty acids) or cholesterol for membrane biosynthesis or sterol production ^{11,12}. They also serve to protect cells from lipotoxicity ¹³. The key to understanding LD size and activity is the presence or absence of specific LD coat proteins ¹⁴. The family of perilipin (PLIN) proteins (PLIN1-5) serves as LD coat proteins and organizing centers for enzymes and transporters in lipid metabolism ¹⁵⁻¹⁷. The PLIN family of proteins is composed of PLIN1 (also called perilipin), PLIN2 (adipophilin or ADRP), PLIN3 (previously Tip47), PLIN4 (previously S3-12) and PLIN5

(previously OXPAT). PLIN1 and PLIN4 are highly expressed in white adipose ¹⁶; whereas PLIN2, PLIN3 and PLIN4 are widely expressed; PLIN2 is abundant in liver and PLIN5 is found in oxidative tissues like heart and brown adipose ¹⁸. *Plin1* null mice have a distinct phenotype of reduced fat mass, increased lipolysis and increased β -oxidation ¹⁹. *Plin2* null mice are resistant to high fat diet-induced obesity ²⁰, and *Plin3* compensates for the loss of *Plin2* in these mice ²¹. Inactivation of *Plin4* down-regulates *Plin5* and reduces cardiac lipid accumulation in mice ²². It seems, therefore, that the level of PLIN proteins in specific cell types regulates lipolysis in target tissues. Reports in the monkey ²³ and mouse ²⁴ indicate that the ovary expresses PLIN2, an LD coat protein associated with cholesteryl ester storage ²⁵. We have found that the bovine corpus luteum predominantly expresses mRNA for *PLIN2* and *PLIN3* with low levels of *PLIN1*, a different pattern of *PLIN* transcript expression when compared to adipose tissue (Figure 1-1 A). Bovine large and small luteal cells express comparable levels of *PLIN2* and *PLIN3* mRNA but different levels of *PLIN1* and *PLIN4* mRNA (Talbot, Krauss, and Davis, unpublished). Exactly how the LD-associated PLINs impact luteal LDs and steroidogenesis are subjects of current investigation.

Hormone-sensitive lipase (HSL) is a key cytosolic enzyme in the regulation of lipid stores in adipocytes that translocates to the LD in response to catecholamine stimulation ²⁶⁻²⁸. A current view of the mechanisms regulating lipolysis in adipose tissue suggests that the LD-associated PLIN1 coats the LD and functions as a scaffold in the regulation of lipolysis ^{16,29,30}. Under basal conditions, PLIN1 acts as a barrier to the hydrolysis of lipids within the LD by preventing access of adipose triglyceride lipase (ATGL) and HSL, the major lipases in adipose cells. Following β -adrenergic stimulation of cAMP and protein kinase A (PKA) signaling, PLIN1 and HSL are phosphorylated, which leads to the movement of HSL from the cytosol to the LD ³¹. The phosphorylation of HSL facilitates its association with the LD and with lipid substrates once associated with the LD ³² permitting lipid hydrolysis to proceed. Phosphorylation of HSL by PKA

occurs on multiple sites, including Ser-563 and Ser-660, which stimulate catalytic activity and translocation of HSL to LDs^{33–36}. Phosphorylation of HSL also occurs at Ser-565, a non-PKA site, which is a negative regulator of HSL activity and is believed to be mutually exclusive with phosphorylation on the Ser-563 site³⁷. Thus, hormonal cues that signal for elevations in systemic energy stimulate PKA to phosphorylate HSL which contributes to lipolysis to maintain energy homeostasis.

The presence of both PLIN coat proteins³⁸ and HSL³⁹ in the ovary suggests that LH via a cAMP/PKA signaling pathway may regulate the phosphorylation of PLINs and HSL to hydrolyze cholesteryl esters stored in luteal LDs to produce substrate for synthesis of steroids such as progesterone, which is an obligate precursor of all biologically active steroids. Studies with HSL-null mice revealed that knockout of HSL resulted in decreased steroidogenesis in the adrenals and inhibited sperm production in the testis^{40,41}. These findings suggest that HSL is involved in the intracellular processing and availability of cholesterol for adrenal and gonadal steroidogenesis. Manna *et al.* recently reported that activation of the PKA pathway in MA-10 mouse Leydig cells, the testosterone-producing cells of testes, enhanced expression of HSL and its phosphorylation at Ser-563 and Ser-660⁴². Inhibition of HSL activity suppressed cAMP-induced progesterone synthesis and resulted in increased cholesteryl ester levels in MA-10 cells. Also of interest is a report⁴³ demonstrating an interaction between StAR (steroidogenic acute regulatory protein) and HSL in the rat adrenal following treatment with adrenocorticotrophic hormone. Co-expression of StAR and HSL resulted in elevated HSL activity and mitochondrial cholesterol content. These observations suggest that the proteins that produce and transport cholesterol may co-localize in LDs and mitochondria. Furthermore, we have observed that mitochondria are closely associated with cytoplasmic LDs in bovine luteal cells (Figure 1-1 B) indicating that luteal LDs and mitochondria may interact to facilitate steroidogenesis. While the evidence points to an important

role for HSL in steroidogenesis, there is little information concerning the LD and the events that control these early steps in ovarian steroidogenesis ⁴⁴.

Despite the renewed interest in cytoplasmic LD as platforms for cell signaling, interactions with other organelles, and metabolic control ^{45,46}, few studies have characterized the protein and lipid composition of the LD. The LD proteome has been characterized to varying degrees in a few mammalian tissues or cell lines [mouse mammary epithelial cells ⁴⁷ and 3T3-L1 adipocytes ^{48,49}, rat liver and mouse muscle tissue ^{50,51}, and human cell lines ⁵²⁻⁵⁴]. Khor *et al.* compared the proteome of LDs from rat granulosa cells treated *in vitro* with either high-density lipoproteins or fatty acids to enrich cytoplasmic LDs with cholesteryl esters or triacylglycerides, respectively ⁵⁵. When comparing the LD proteomes a large number of proteins (278) were common to the LDs prepared from either treatment. These proteins included PLIN2 and were similar to other studies on LD proteomes. They also identified 61 proteins unique to the cholesteryl ester-rich LDs and 40 unique proteins unique to triacylglycerol-rich LDs. Notably, they identified steroidogenesis associated proteins, Hsd3b1, vimentin, and voltage-dependent anion channel (Vdac1) proteins enriched in the cholesteryl ester-rich LDs. Recent reports on the proteomic analysis of LD isolated from the mouse Leydig tumor cell line MLTC-1 ⁵⁶, and mouse testes ⁵⁷ also revealed the presence of PLIN family proteins and enzymes involved in the synthesis of steroid hormones. Despite the recent work on characterization of the LD proteome in various tissues, there is still a lack of information about the protein composition of luteal LDs and the effects of hormones or metabolic alterations on luteal LD properties. In our studies (Talbot, Krauss, and Davis, unpublished) the LDs isolated from bovine luteal tissue predominantly contain PLIN2 and PLIN3 coat proteins, as well as HSL, HSD3B1, CYP11A1, and StAR. Collectively, these studies indicate that the LD may serve as a novel hormonally-responsive platform that is essential for steroidogenesis.

Comprehensive analysis of the lipid composition of LDs in other tissues is just beginning to be evaluated ⁵⁸. The protein composition of LDs, particularly the PLIN family of LD coat proteins is believed to influence the type of lipids stored in LDs and metabolic activity of tissues ^{1,59}. The lipid composition of ovarian LDs and the effects of hormones on the lipids contained therein are currently unknown. Our preliminary studies indicate that compared to granulosa and theca cells, the total lipid content of luteal cells is increased. Several studies reported the types and changes of lipids in the intact corpus luteum of rats ⁶⁰, pigs ^{61,62}, sheep ⁶³ and humans ⁶⁴. These studies reported that cholesteryl esters and free fatty acids remain relatively constant during the functional phases of the luteal lifespan while triglycerides accumulated in the regressing corpus luteum. The increased lipid content of luteal cells is likely to be stored exclusively within the LDs; however, this remains to be shown experimentally. Additional studies are needed to determine the role and fate of lipids in LDs during both function and regression of the corpus luteum.

Bovine and ovine corpora lutea have two distinct steroidogenic cells, large and small luteal cells, with different abilities to produce progesterone ⁶⁵⁻⁶⁷. The small luteal cells respond to LH with large increases in progesterone secretion while the large luteal cells have a high basal rate of progesterone secretion and respond to LH with a comparatively modest fold increase in progesterone secretion. The luteal tissue of women, monkeys, pigs, and rodents also possess large and small luteal cells, although the basal and LH-stimulated progesterone secretion differ from the bovine corpus luteum ⁶⁸. Our preliminary data indicate that bovine large and small luteal cells have LDs with distinctive morphology. As indicated by BODIPY 493/503 staining of neutral lipids (green) and the LD protein ATGL small luteal cells have large LDs, whereas large cells have abundant dispersed small LDs (Figure 1-1 C & D). Whether and how the LDs in either cell type contribute to the ability to respond to LH or to the basal rate of progesterone secretion is currently unknown. Studies in other tissues indicate that PKA-dependent phosphorylation of

PLIN1 induces dispersion of clustered LDs in HEK293 cells, fibroblasts, and 3T3L1 adipocytes^{69,70}. Based on these findings it seems possible that the dispersed LDs observed in bovine large luteal cells may be the result of constitutive PKA activity reported to be present in large luteal cells⁷¹.

Fatty acids (either synthesized *de novo* or provided by the hydrolysis of stored cholesteryl esters, triglycerides or phospholipids) are essential for energy production and the synthesis of most lipids, including those found in membranes and lipids involved in cellular signaling. Despite their fundamental physiological importance, an oversupply of non-esterified fatty acids can be detrimental to the cellular function¹⁰. Fatty acids are transported across the outer mitochondrial membrane by carnitine palmitoyltransferase I (CPT1A), the rate-limiting step in fatty acid oxidation. Fatty acids are consumed by mitochondria through β -oxidation to produce acetyl-CoA and nicotinamide adenine dinucleotide (NADH) and flavin adenine dinucleotide (FADH₂) for use in the electron transport chain to produce adenosine triphosphate (ATP)⁷². The hydrolysis of cholesteryl esters by HSL liberates cholesterol and fatty acids (Figure 1-2). The fatty acids are either re-esterified and stored in LDs or membranes or used for β -oxidation producing reducing equivalents and acetyl-CoA for the citric acid cycle⁷². Although little is known about the role of fatty acid β -oxidation in luteal cells, recent studies indicate that fatty acid β -oxidation plays a key role in cumulus-oocyte complex metabolism and oocyte maturation^{73,74}. These studies found that promoting β -oxidation with *L*-carnitine improved embryo development and pharmacologic inhibition of fatty acid β -oxidation with etomoxir, a CPT1A inhibitor, impaired oocyte maturation and embryo development. Steroidogenic tissues use glycolysis to support steroidogenesis⁷⁵, however, it seems likely that the production of large quantities of progesterone by luteal cells would also require β -oxidation of fatty acids to provide the energy needed for optimal steroidogenesis under basal conditions, but this remains to be critically evaluated. It seems likely that large and small luteal cells may have different energy processing requirements, based on the

pronounced differences in the ability of large and small luteal cells to produce progesterone under basal and stimulated steroidogenesis. Our preliminary studies indicate that *CPT1A* mRNA expression in large luteal cells is 5.6 fold greater than in granulosa cells, whereas no difference in *CPT1A* mRNA expression was observed between theca and small luteal cells. This data supports our idea that β -oxidation may play an important role in the metabolic regulation of large luteal cells. Given the intense interest in pathologies that result in lipid accumulation and conditions (i.e. obesity, diabetes, metabolic syndrome) that elevate free fatty acids and alter metabolism, understanding how LDs, glycolysis, and β -oxidation are regulated in the corpus luteum may provide clues for improving ovarian function, treating ovarian disorders, and enhancing fertility.

1.2. AMP-activated protein kinase

AMP-activated protein kinase (AMPK) is a master regulator of cellular metabolism^{72,76}. The AMPK complex is a heterotrimer consisting of an α catalytic subunit, and non-catalytic β and γ regulatory subunits⁷⁷. Studies from a number of investigators demonstrated that AMPK is present in the oocyte, granulosa and theca cells as well as luteal cells [reviewed in Bertoldo *et al.*⁷⁸]. As its name suggests, AMPK is allosterically activated by adenosine monophosphate, AMP. The enzyme is activated by increases in AMP : ATP or ADP : ATP ratios, which occur when cellular energy status has been compromised by metabolic stresses that either interfere with ATP production or that accelerate ATP consumption⁷⁹. AMPK acts to restore energy homeostasis by activating alternate catabolic processes generating ATP while inhibiting energy-consuming processes, e.g., protein, carbohydrate, and lipid biosynthesis, as well as cell growth and proliferation (Figure 1-3). AMPK acts via direct phosphorylation of metabolic enzymes, and by longer-term effects via phosphorylation of transcription regulators^{80,81}.

AMPK can be activated by a number of synthetic allosteric effectors (A-769662, 991, MT 63-78) identified by Abbott laboratories using high throughput screens for AMPK. Other allosteric effectors are salicylate, the major breakdown product of aspirin, and pro-drugs: 5-

amino-imidazole-4-carboxamide riboside (AICAR) and C13, which are converted into AMP analogs following cellular uptake. For example, AICAR, a widely used AMPK activator, is taken into cells and then converted to the monophosphorylated derivative ZMP, which mimics the effect of AMP both on the allosteric activation of the kinase and inhibition of the dephosphorylation of Thr-172 on AMPK. Pharmacological AMPK activators (e.g., metformin, berberine, resveratrol, and hydrogen peroxide) are typically viewed as metabolic poisons that inhibit ATP synthesis and stimulate AMPK indirectly by increasing cellular AMP levels ⁷⁹. Activation of AMPK by upstream kinases occurs by phosphorylation of a conserved threonine within the 'activation loop' of the kinase domain (Thr-172). The primary upstream kinases that phosphorylate Thr-172 are the tumor suppressor liver kinase B1 (LKB1) (also known as serine and threonine kinase 11 or STK11), and the calcium/calmodulin-dependent protein kinase kinase 2, CAMKK2. The latter is activated when intracellular Ca^{2+} is increased by the action of hormones.

The AMPK likely controls multiple aspects of metabolism in ovarian cells. AMPK phosphorylates and inactivates acetyl-CoA carboxylase (ACC) and 3-hydroxy-3-methylglutaryl-CoA reductase (HMGCR), key enzymes involved in regulating de novo biosynthesis of fatty acids and cholesterol (Figure 1-3). Activation of AMPK also blocks the activation of the mechanistic target of rapamycin (MTOR) and protein synthesis by phosphorylating the key regulatory proteins, raptor and tuberous sclerosis proteins ⁸¹. Another immediate consequence of enhanced AMPK activity is the phosphorylation of HSL at Ser-565, which precludes activation of HSL by PKA ⁸². Conversely, conditions that stimulate PKA-induced phosphorylation of HSL at Ser-660 and Ser-563 suppress the phosphorylation of HSL at the AMPK site Ser-565. *In vitro* kinase assays using purified PKA and AMPK support the notion that phosphorylation of HSL at Ser-563 and Ser-565 is mutually exclusive. Thus, in steroidogenic tissues, activation of AMPK can inhibit HSL-mediated hydrolysis of cholesteryl esters and prevent the release of free

cholesterol for steroidogenesis⁸³. The observation that HSL is a key enzyme in adipocytes and steroidogenic cells strategically positions AMPK to control the expression of genes required for steroidogenesis and the availability of cholesterol for ovarian progesterone synthesis (Figure 1-4).

Reports from the DuPont laboratory^{84,85} demonstrate that AMPK activators metformin and AICAR inhibit the secretion of progesterone and/or estradiol by granulosa cells in a manner dependent on the state of cellular differentiation and the species investigated^{78,84,86}. In rat and bovine granulosa cells, AMPK activation induced by metformin reduced the expression of mRNA for key enzymes required for progesterone synthesis, *HSD3B1*, *CYP11A1* and *StAR*^{85,87}. In the human KGN granulosa cell line (Huang, Hou and Davis, unpublished) treatment with the AMPK activator metformin inhibited *StAR* mRNA expression and progesterone synthesis. In general, the studies in granulosa cells suggest that the reduction in steroidogenesis was a result of a reduction in the transcription of genes in the steroidogenic pathway. Other studies showed that metformin impairs proliferation of bovine granulosa cells and rat theca cells via mechanisms involving AMPK-mediated inhibition of MTOR signaling and protein synthesis⁸⁸⁻⁹⁰.

Bowdridge *et al.* recently reported increases in the expression of AMPK α , β , and γ subunits during the maturation of the bovine corpus luteum, with the exception of AMPK $\gamma 1$ and $\gamma 2$ subunits⁹¹. Other studies from the Flores laboratory provide evidence for increased expression of genes encoding distinct protein kinase C isoforms and genes participating in Ca^{2+} homeostasis during luteal maturation⁹². Goravanahally *et al.*⁹³ reported that CAMKK2, a downstream target of Ca^{2+} and upstream regulator of AMPK is also more highly expressed in mature bovine corpus luteum than in newly formed luteal tissue. It should be noted that two important physiologic processes occur during this developmental period; 1) the corpus luteum develops its maximal capacity for progesterone secretion and 2) the corpus luteum develops the capacity to undergo luteolysis in response to $\text{PGF}_{2\alpha}$. Based on the high rate of progesterone production during the mid-luteal phase and pregnancy, it seems likely that any factors that influence metabolic activity

in steroidogenic cells would increase or decrease AMPK activity and impact steroid secretion. Hou *et al.*⁹⁴ reported that treatment of primary cultures of bovine luteal cells with AICAR rapidly increased AMPK activity and significantly reduced LH-stimulated MTOR activity and progesterone secretion. Additional findings in this report indicated that the inhibition of MTOR with rapamycin did not contribute to the reduction in LH-stimulated progesterone secretion. More recently, Bowdridge *et al.* observed that treatment of bovine luteal tissue slices with either metformin or AICAR acutely reduced basal progesterone secretion⁹¹. These results indicate that AMPK activators acutely inhibit luteal progesterone synthesis indicating that the energy status of luteal cells is an important regulator of steroidogenesis.

1.3. LH inhibits AMPK

The C-terminal domains of AMPK α subunit isoforms in vertebrates contain a serine/threonine (ST)-rich insert of 50–60 amino acids, the so-called ‘ST loop’⁹⁵. Phosphorylation of the ST loop serves as a means for negative regulation of AMPK. The amino acid residues defining the ends of this loop are close to the Thr-172 residue and contain a number of regulatory phosphorylation sites. The best characterized of these sites is Ser-485 on the AMPK $\alpha 1$ subunit. The Ser-485 site is phosphorylated by the cyclic AMP-dependent protein kinase, PKA⁹⁶ or AKT⁹⁷, which subsequently inhibits the phosphorylation of the AMPK α subunit Thr-172 residue by upstream kinases, LKB1 or CaMKK2⁹⁵. The AMPK- $\alpha 2$ subunit contains a similar conserved ST loop and phosphorylation of Ser-491 is likely to exert the same inhibitory effect, although Ser-491 is a poor substrate for AKT and appears to be also modified by autophosphorylation⁹⁵. Additionally, PKA can phosphorylate the Ser-173 residue (adjacent to Thr-172 within the activation loop), which can inhibit Thr-172 phosphorylation⁹⁸. In a study using primary cultures of bovine luteal cells, Hou *et al.* reported that treatment with LH rapidly inhibited AMPK activity as evidenced by reduced AMPK Thr-172 phosphorylation and reduced

phosphorylation of the AMPK substrate ACC⁹⁴. Treatment with LH also increased phosphorylation of AMPK on Ser-485, which is associated with inhibition of AMPK activity⁹⁴.

In contrast to granulosa cells, bovine luteal cells contain the required steroidogenic machinery including HSL, which enables luteal cells to respond to LH or cAMP with rapid increases in progesterone synthesis. The increases in progesterone occur within 10-30 min⁹⁹⁻¹⁰¹ and precede the LH-induced increase in StAR expression, which is typically observed 2-4 hours after treatment¹⁰². These changes are associated with reduced phosphorylation of HSL at the inhibitory AMPK phosphorylation site Ser-565 and increased phosphorylation of HSL at Ser-563 and 660, residues that are required for HSL activity (Krause, Talbott, Hou and Davis, unpublished). Thus, the ability of LH to reduce AMPK activity may allow optimal LH- and PKA-dependent activation of HSL and provide cholesterol for the already existing steroidogenic machinery. An experimental model of the proposed interaction among PKA and AMPK regulation of HSL is shown in Figure 1-4. Physiologic conditions that increase the activity of AMPK require phosphorylation of the AMPK α subunit on Thr-172 residues¹⁰³. This leads to the phosphorylation of the AMPK substrates: ACC (Ser-79) and HSL (Ser-565), which could reduce the ability of luteal cells to provide cholesterol substrate in response to a pulse of LH. LH or PKA activators attenuate AMPK activity through modulation of at least two AMPK α -subunit phosphorylation sites, Thr-172 (reduced) and Ser-485 (increased). Reduced HSL phosphorylation by AMPK allows PKA to phosphorylate HSL on Ser-563 and Ser-660 resulting in increased HSL activity which presumptively provides cholesterol for progesterone synthesis.

1.4. PGF_{2 α} activates AMPK

Early studies established that PGF_{2 α} binds to and activates its cognate G_q protein-coupled receptor, the prostaglandin F receptor, PTGFR. This initial event provokes the rapid activation of phospholipase C, which leads to increases in both cytoplasmic Ca²⁺ and activation of protein kinase C. These early events contribute to the activation of additional protein kinase cascades like

the mitogen-activated protein kinases (ERK1/2, p38, and Jun N-terminal kinase (JNK))¹⁰⁴ that contribute to the induction of early responses genes like Finkel-Biskis-Jenkins murine osteosarcoma viral oncogene homolog (FOS), Jun proto-oncogene (JUN), early growth response protein 1 (EGR1), and activating transcription factor 3 (ATF3)^{105–108}. While these early response genes have been implicated in the luteolytic response to PGF_{2α}, it is not clear how or whether they impact metabolic events in luteal cells. The developmental-specific expression of protein kinase C and CAMKK2 isoforms, proteins involved in Ca²⁺ homeostasis, and AMPK have been implicated in the cellular mechanisms of acquisition of luteolytic capacity by bovine corpus luteum^{92,93,109}. Based on these observations it seems reasonable to predict that PGF_{2α} could activate Ca²⁺/CAMKK2 pathways leading to the activation and phosphorylation of AMPK on Thr-172.

Bowdridge *et al.* recently reported that PGF_{2α} rapidly (2 min) and transiently stimulated the phosphorylation of AMPK on the Ser-485 site in dispersed bovine luteal cells⁹¹. The response was prevented by treatment with STO-609, a CAMKK2 inhibitor. Treatment with STO-609 also prevented the modest inhibitory effect of PGF_{2α} on progesterone synthesis in overnight incubations of dispersed luteal cells⁹¹. In recent studies using bovine large luteal cells, we have observed that PGF_{2α} rapidly stimulates the phosphorylation of AMPK on the stimulatory Thr-172 residue as well as the inhibitory Ser-485 residue (Hou, Zhang, Talbott, and Davis, unpublished data). The phosphorylation of AMPK was coupled to the phosphorylation of the AMPK target ACC, indicating that AMPK was activated by PGF_{2α}. The observation that PGF_{2α} can target multiple sites on AMPK is consistent with findings that PGF_{2α} activates multiple protein kinase pathways in luteal cells; pathways linked to calcium signaling, protein kinase C, mitogen-activated protein kinases, and MTOR signaling¹¹⁰. While additional studies are needed to determine exactly how PGF_{2α} regulates AMPK in luteal cells, it seems clear that activation of AMPK with pharmacologic tools disrupts luteal progesterone synthesis (Figure 1-5). Studies are

also needed to determine whether AMPK is activated *in vivo* during natural and PGF_{2α}-induced luteolysis. It is conceivable that changes in luteal blood flow, hypoxia, and the presence of inflammatory mediators all contribute to altering the metabolic status of steroidogenic luteal cells, resulting in the activation of AMPK and disrupting progesterone synthesis.

1.5. Autophagy

Autophagy plays an important role in cellular and tissue physiology^{111–113}. The main function of autophagy is to protect cells against starvation by allowing cells to salvage nutrients by digesting organelles and macromolecules at times of nutrient scarcity as well as to ensure cell homeostasis by eliminating damaged organelles and misfolded proteins. Three different types of autophagy (macroautophagy, microautophagy, and chaperone-mediated autophagy) have been described, based largely on the processes by which cargo is delivered to lysosomes. In general, autophagy can be induced by limitations in amino acids, growth factors, energy, and oxygen. The formation of autophagosomes requires the activation of a number of protein complexes: the autophagy-related 1 (Atg1)–Unc-51-like kinase complex, which is a key signaling intermediate that is regulated by MTOR and AMPK; the autophagy-specific class III phosphatidylinositol 3-kinase Vps34 complex (consisting of Vps34, Beclin 1, Vsp15 and Atg14L), which produce a pool of phosphatidylinositol-3-phosphate that is necessary for autophagosome formation; and a complex of ubiquitin-like proteins: Atg12, Atg5, Atg16 and LC3-I (Atg8) and their conjugation machinery, which leads to the lipidation of microtubule-associated protein light chain 3 (LC3) with phosphatidylethanolamine, a process required for autophagosome formation and closure. The presence of LC3-II, an LC3 cleavage product, inside the mature autophagosome is generally used as a marker of autophagy.

Autophagy has been shown to occur in oocytes, granulosa cells, and luteal cells and is often associated with apoptosis. Genetic mouse models demonstrate that *Atg7* (-/-) ovaries¹¹⁴ or germ cell-specific deletion of *Atg7*¹¹⁵ compromised autophagy in the perinatal mouse ovary resulting

in the early loss of female germ cells. Loss of Beclin 1 (*Becn1*), which plays a central role in the regulation of autophagy through activation of the Vps34 complex, also resulted in a significant loss of germ cells at birth ¹¹⁴. These findings indicate that autophagy may promote survival of germ cells during ovarian development. Other studies provide evidence for the presence of autophagosomes in the granulosa cells of atretic follicles of several species ^{116,117}. Studies in the rat support the idea that activation of the AKT/MTOR signaling pathway suppresses autophagy as assessed by levels of LC3-II in granulosa cells ¹¹⁶.

The presence of lysosomes and autophagosomes in the corpus luteum was described over 45 years ago ^{118–121}. Recent studies have documented the presence of autophagy-related proteins: Beclin 1 and LC3 in the luteal tissue of rodents, cows, and humans ^{122–125}. However, in luteal cells, it remains unclear whether a certain level of autophagy promotes cell survival versus cell death. In the rat, LC3-II positive autophagosomes were identified during the late luteal phase and were correlated with luteal cell apoptosis ^{125,126}. Furthermore, treatment of rat luteal cells with PGF_{2α} under serum-free conditions increased autophagosomes, LC3-II protein, and luteal cell apoptosis, suggesting that autophagy may be involved in luteal cell death. Choi *et al.* observed that although PGF_{2α} increased both ERK1/2 and MTOR activity in rat luteal cells, autophagy could be prevented by inhibition of ERK1/2 signaling and appeared to be independent of phosphatidylinositol 3-kinase/AKT/MTOR activity ¹²⁶. It will be important to understand the sequence of events *in vivo* and to determine whether the stimulatory effects of PGF_{2α} on AMPK activation are linked in some way to autophagy in the corpus luteum.

Gawriluk *et al.* reported that *Becn1* deficiency in the mouse ovary resulted in a reduction of progesterone production and preterm labor ¹²². To avoid the loss of germ cells associated the *Becn1* knockout animal, this group targeted *Becn1* deletion to the granulosa cells and as a result, they were able to follow luteal function throughout pregnancy. Although ovulation, implantation, and progesterone levels during early pregnancy were not affected by *Becn1* ablation, they found

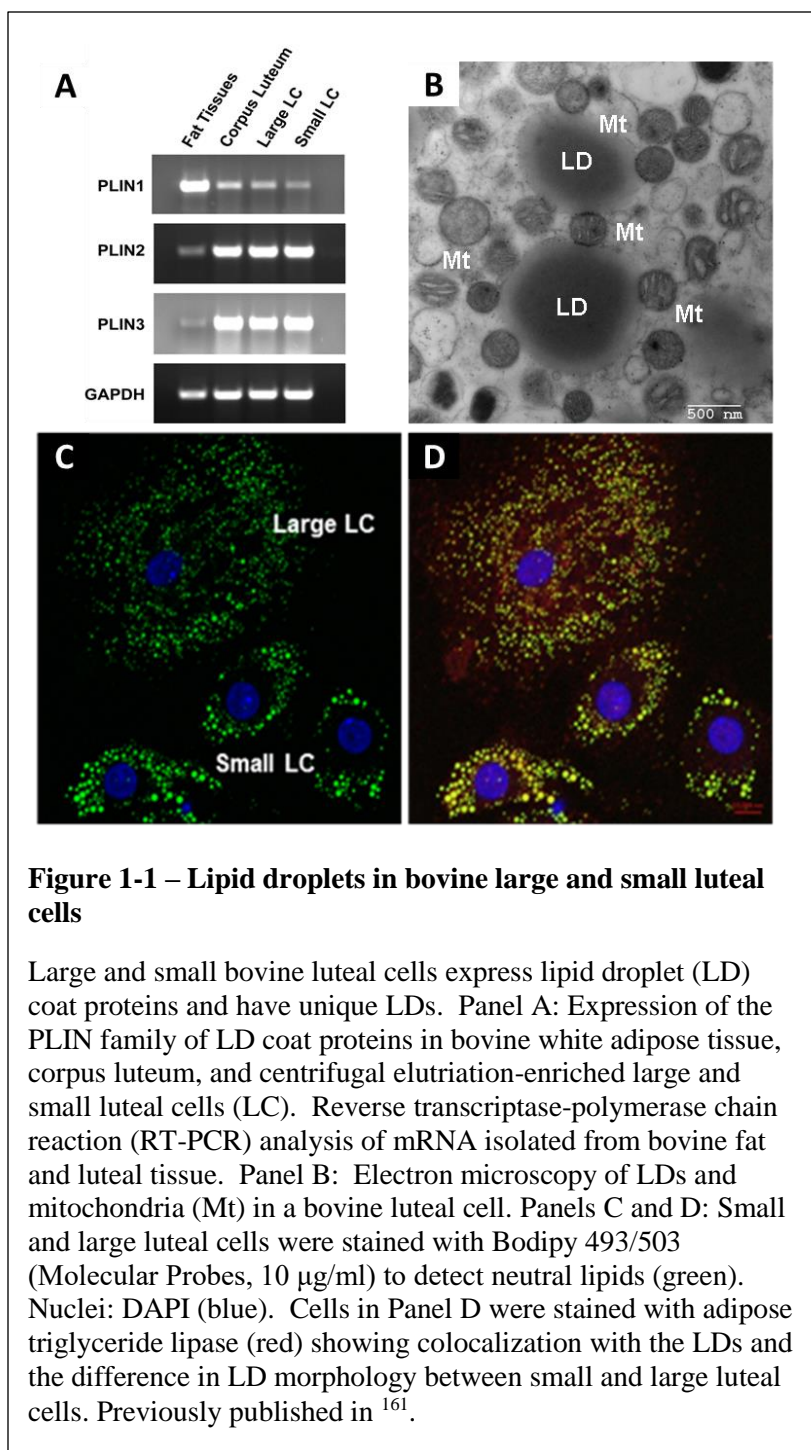
that *Becn1* abrogation resulted in a reduction of circulating progesterone in mid to late pregnancy. The reduction in progesterone resulted in early parturition, which was reversed by treatment with exogenous progesterone. Of relevance to luteal metabolism were the findings that the numbers of LDs were reduced and the mitochondria were smaller in the *Becn1* deficient ovaries compared to controls. These changes were not accompanied by changes in the expression of genes important for the synthesis of progesterone. Exactly how the reduction in LDs and reduced autophagy contributed to reduced progesterone synthesis remains to be firmly established, but could be a consequence of impaired lipid transport mechanisms and reduced expression of key receptors (hormone and cholesterol-uptake) on the luteal cells ¹²². Studies in other systems indicate that *Becn1* expression and activity is controlled via transcriptional regulation, miR-30a, and by post-translational modifications (reviewed in ¹²⁷). Recent studies in cardiac tissue showed that the transcription factor ATF3 binds to the ATF/cAMP response element of the *Becn1* promoter and that ATF3 is capable of reducing autophagy via suppression of the *Becn1*-dependent autophagy pathway ¹²⁸. Since PGF_{2α} rapidly increases activation of mitogen-activated protein kinases (ERK1/2, p38, and JNK) and ATF3 expression in bovine and rat luteal cells *in vivo* and *in vitro* ^{104,107}, it is important to determine whether PGF_{2α} inhibits autophagy through changes in *Becn1* expression or activity during luteal regression.

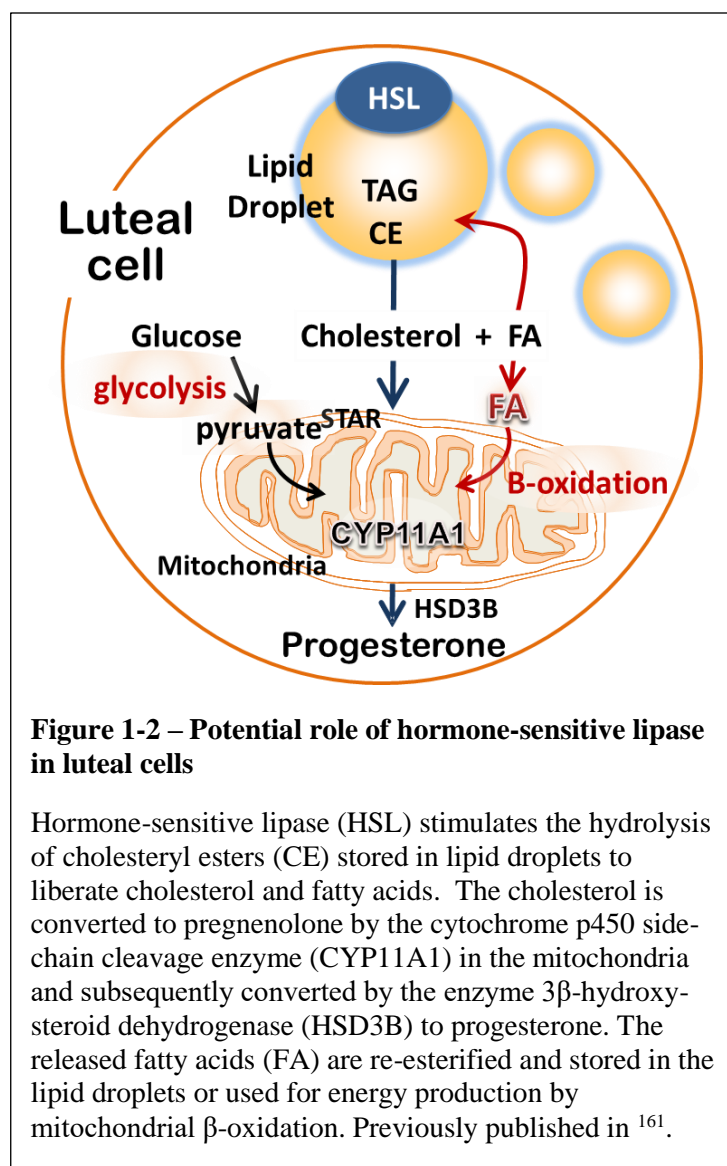
It should also be appreciated that *Becn1* directly interacts with B-cell lymphoma 2 (*Bcl2*) family proteins (*Bcl2* and *Bcl2/XL*) in a manner that negatively regulates autophagy. To complicate matters, a variety of ligands that regulate intracellular protein kinases, including Dapk, Rock1, Mst1, and Mapk8, (death-associated protein kinase 1, rho-associated coiled-coil containing protein kinase 1, macrophage stimulating 1, mitogen-activating protein kinase 8, respectively), can positively or negatively regulate *Becn1/Bcl2* effects on autophagy ¹²⁷. *Beclin 1* can also secondarily affect apoptosis through regulation of anti-apoptotic and pro-apoptotic BH3 domain-containing proteins. In addition to the *Bcl2* family, the VDAC (voltage-dependent anion

channel) family is also involved in ovarian apoptosis and autophagy regulation ¹²⁹. Vdac2 directly interacts with Bcl2-antagonist/killer 1 (Bak1) to inhibit its oligomerization, thus suppressing cell apoptosis. Yuan *et al.* recently reported that Vdac2 inhibits autophagy in the developing ovary by interacting with Becn1 and Bcl2L1 to stabilize the Becn1 and Bcl2L1 complex ¹²⁹. Recent work by several groups has found a close relationship between autophagy and LDs ^{130–132}. In particular, LC3 ¹³¹, ATG2 ¹³³, ATG7 ¹³⁰ and several VDAC ^{56,57} proteins are often associated with LDs and appear to play important roles in LD formation and function. This suggests that events associated with autophagy may also impact the formation and function of ovarian LDs. Further work is needed to understand how LDs and autophagosome components influence both autophagy and apoptosis and thereby affect luteal function and lifespan.

1.6. Summary

Metabolic processes in the corpus luteum are tightly controlled by luteotropic and luteolytic factors. Signaling cascades involving LD homeostasis, PKA, AMPK, and autophagy are clearly important in the control of steroidogenesis. It remains to be determined how these cellular events are integrated into a physiologic context over the lifespan of the corpus luteum. Understanding the complex interplay of metabolic and hormonal clues underpinning steroidogenesis is essential to understanding and developing new therapies for infertility, particularly in the setting of increasing prevalence of obesity and metabolic diseases such as diabetes and polycystic ovary syndrome.





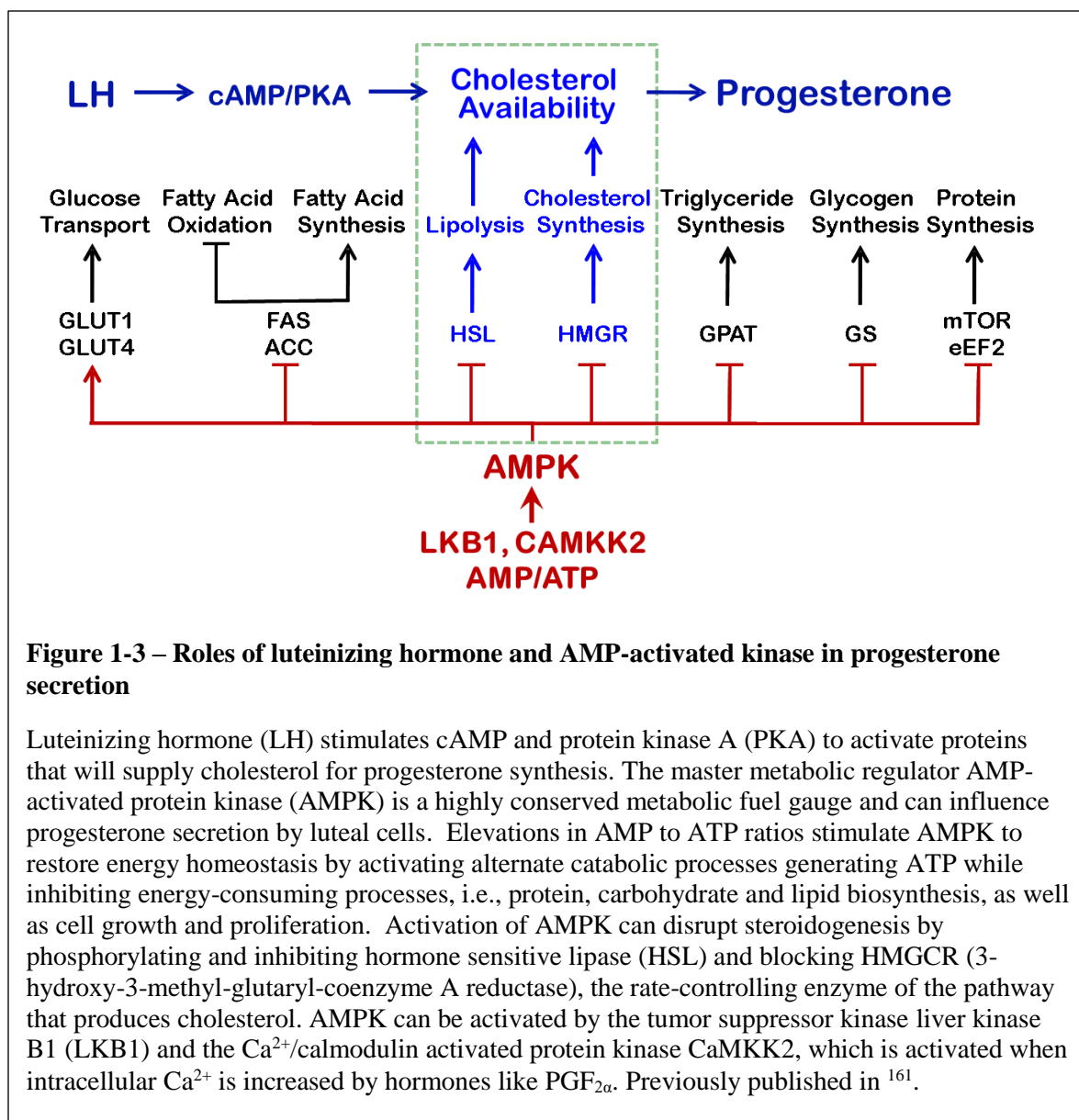


Figure 1-3 – Roles of luteinizing hormone and AMP-activated kinase in progesterone secretion

Luteinizing hormone (LH) stimulates cAMP and protein kinase A (PKA) to activate proteins that will supply cholesterol for progesterone synthesis. The master metabolic regulator AMP-activated protein kinase (AMPK) is a highly conserved metabolic fuel gauge and can influence progesterone secretion by luteal cells. Elevations in AMP to ATP ratios stimulate AMPK to restore energy homeostasis by activating alternate catabolic processes generating ATP while inhibiting energy-consuming processes, i.e., protein, carbohydrate and lipid biosynthesis, as well as cell growth and proliferation. Activation of AMPK can disrupt steroidogenesis by phosphorylating and inhibiting hormone sensitive lipase (HSL) and blocking HMGCR (3-hydroxy-3-methyl-glutaryl-coenzyme A reductase), the rate-controlling enzyme of the pathway that produces cholesterol. AMPK can be activated by the tumor suppressor kinase liver kinase B1 (LKB1) and the Ca^{2+} /calmodulin activated protein kinase CaMKK2, which is activated when intracellular Ca^{2+} is increased by hormones like $\text{PGF}_{2\alpha}$. Previously published in ¹⁶¹.

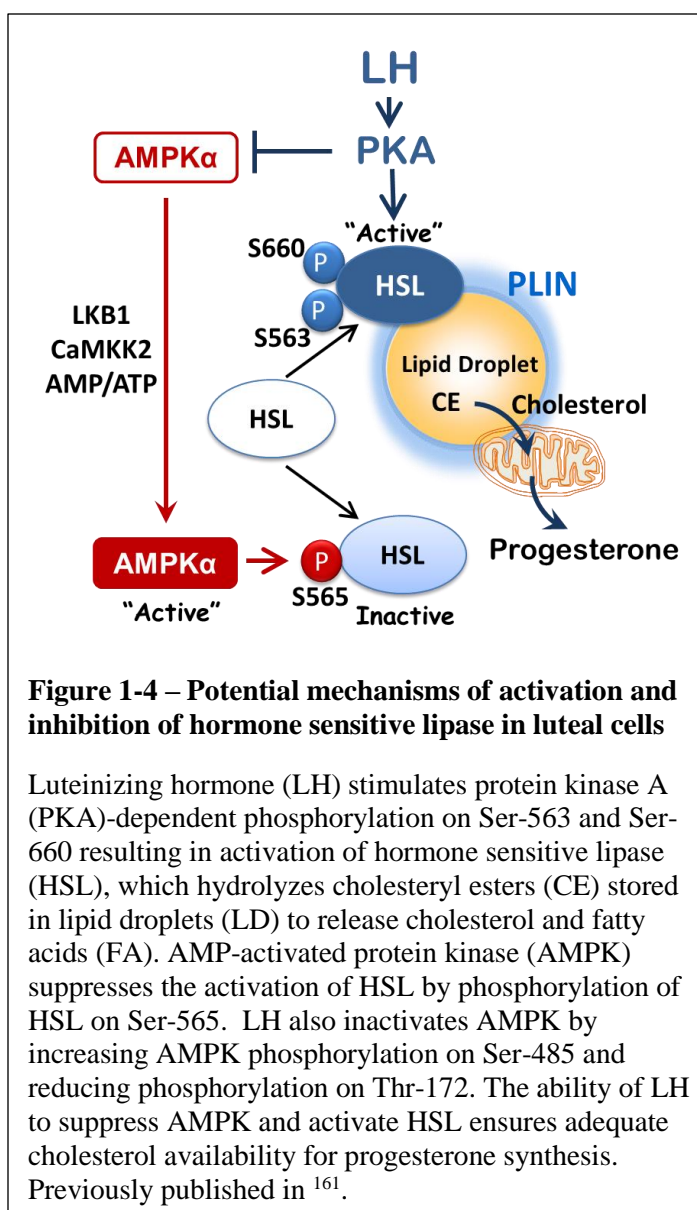


Figure 1-4 – Potential mechanisms of activation and inhibition of hormone sensitive lipase in luteal cells

Luteinizing hormone (LH) stimulates protein kinase A (PKA)-dependent phosphorylation on Ser-563 and Ser-660 resulting in activation of hormone sensitive lipase (HSL), which hydrolyzes cholesteryl esters (CE) stored in lipid droplets (LD) to release cholesterol and fatty acids (FA). AMP-activated protein kinase (AMPK) suppresses the activation of HSL by phosphorylation of HSL on Ser-565. LH also inactivates AMPK by increasing AMPK phosphorylation on Ser-485 and reducing phosphorylation on Thr-172. The ability of LH to suppress AMPK and activate HSL ensures adequate cholesterol availability for progesterone synthesis. Previously published in ¹⁶¹.

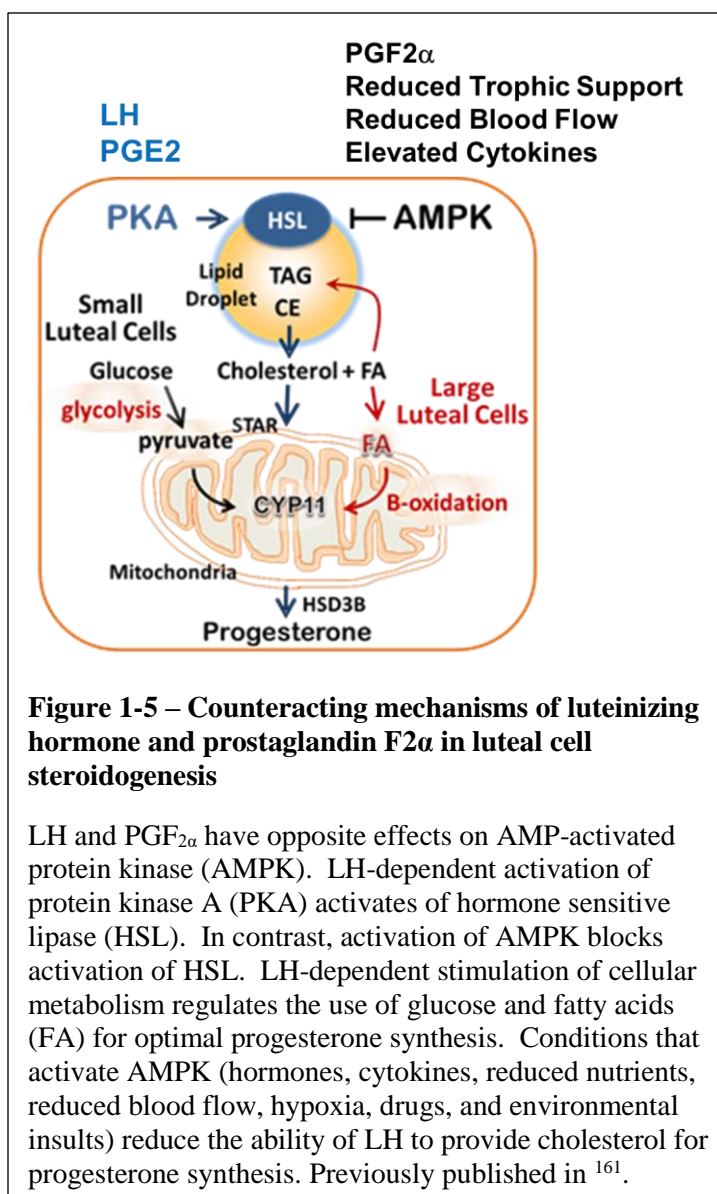


Figure 1-5 – Counteracting mechanisms of luteinizing hormone and prostaglandin F2 α in luteal cell steroidogenesis

LH and PGF_{2 α} have opposite effects on AMP-activated protein kinase (AMPK). LH-dependent activation of protein kinase A (PKA) activates of hormone sensitive lipase (HSL). In contrast, activation of AMPK blocks activation of HSL. LH-dependent stimulation of cellular metabolism regulates the use of glucose and fatty acids (FA) for optimal progesterone synthesis. Conditions that activate AMPK (hormones, cytokines, reduced nutrients, reduced blood flow, hypoxia, drugs, and environmental insults) reduce the ability of LH to provide cholesterol for progesterone synthesis. Previously published in ¹⁶¹.

CHAPTER 2: COMPOSITION OF THE LIPID DROPLETS OF THE BOVINE CORPUS LUTEUM[†]

Abstract

Establishment and maintenance of pregnancy are dependent on the ability of the ovarian corpus luteum (CL) to synthesize progesterone. The ovulatory surge of luteinizing hormone (LH) prompts development of the CL and differentiation of the follicular cells. During differentiation, there is an increase in expression of steroidogenic enzymes, proteins that transport cholesterol, and lipid droplet (LD)-associated proteins important for storing cholesteryl esters (CE). Our purpose was to identify the composition of LDs in ovarian steroidogenic cells. We hypothesized that LDs are a common feature of steroidogenic luteal cells and could store CE. Bovine ovaries with functional CLs at days 3 and 10 after ovulation were used for whole tissue analysis. Further analyses were performed on isolated granulosa, theca, small, and large luteal cells. LDs were isolated by a step-wise sucrose gradient for subsequent lipid and protein analyses. Luteal LD-associated proteins were determined by Western blot and included classic LD-associated proteins: PLIN2, PLIN3, PLIN5, vimentin, and adipose triglyceride lipase (ATGL). The neutral core of luteal LDs was composed primarily of triglyceride (TAG) (168 pmol/μg protein), diglyceride (5.62 pmol/μg protein) and CE (2.78 pmol/μg protein). Compared to adipocyte LDs, bovine luteal LDs were enriched in CE, and nearly all CE present in the CL tissue were present in the LD fraction. The results indicate that bovine luteal LDs are not similar to LDs isolated from adipose tissue and contain deposits of CE, although TAGs are still the predominant lipid species.

[†] The material presented in this chapter is in preparation to be as submitted as a manuscript: Talbott *et al.* Composition of the Lipid Droplets of the Bovine Corpus Luteum.

2.1. Introduction

2.1.1. Formation and function of the CL

Multiple fertile cycles in mammals depend on the formation of a transient endocrine structure in the ovary termed the corpus luteum (CL) ¹³⁴. The CL forms at the beginning of each estrus cycle and synthesizes progesterone, a hormone critical for early embryonic survival during pregnancy ^{135–137}. The CL has a tremendous ability to synthesize progesterone, 40 mg/day in humans ^{138,139}, and the bovine CL can produce ~10-fold more progesterone than in humans ¹⁴⁰. Steroids in the bovine CL are derived primarily through high-density lipoprotein (HDL)-derived cholesteryl esters ^{141–143}, with smaller amounts from low-density lipoproteins, and minor contributions from de novo cholesterol synthesis ¹⁴⁴. These cholesteryl esters can serve as precursors for steroid synthesis after removal of the fatty acid. The CL provides an ideal tissue for studying the mechanisms of steroidogenesis, due to its high steroidogenic output; therefore, changes in steroid synthesis are easier to detect than may be masked in other tissues. As well, progesterone is a necessary precursor of androgens, estrogens, glucocorticoids and mineralocorticoids.

2.1.2. Luteal LDs

For over 40 years, luteal cells have been noted as containing LDs ^{145,146}. One report determined that LDs made up 1.6–9.2% of identifiable subcellular components (mitochondria, granules, etc.) during the functional life span of the CL ¹⁴⁷. Armstrong *et al.* demonstrated that in rats and rabbits these LDs were primarily composed of cholesteryl esters and that treatment with LH reduced the total amount of cholesteryl esters present ¹⁴⁸. As well, several research groups showed cholesterol and cholesteryl ester storage using the cholesterol sensing Schultz reagent ^{149–154}. Reports by Armstrong, Claesson, Gurarya, and others indicated that luteal LDs in various species could be altered by treatment with LH and prostaglandin F₂ α , which is important in the involution of the CL ^{148,155–157}. Additionally, they determined that the small luteal cells contained ~400 LDs/cell and large luteal cells had upwards of 1250 LDs/cell indicating a likely role for this

common luteal cell structure¹⁵⁸. Luteal LDs are postulated to store cholesteryl esters that could be used for steroidogenesis¹⁵⁹.

2.1.3. *Functional role of LDs*

Lipid droplets are unique organelles that store neutral lipids within a phospholipid monolayer, as opposed to the bilayer surrounding most other organelles^{4,160–162}. LD-associated proteins coat the LD, often through unique domains that allow for interaction with a monolayer^{17,29,163,164}. These proteins can protect the LD-contained lipids from hydrolysis, as well as protect the cell from toxic lipid accumulations¹⁶. As well, the LD coat proteins can interact with proteins that insert new lipids into the LD core, export and/or modify the neutral lipids for use in the cell. Finally, the coat proteins allow the trafficking and association of LDs with other cellular structures^{165–168}. LDs have been most extensively studied in adipose cells, where they form large unilocular droplets^{31,169}, though, LDs have been observed in nearly every tissue, as well as organisms from all domains of life^{3–5}. However, in many of these conditions, other than adipose tissue, LD formation is related to pathological conditions, usually due to an oversupply of fats, including the foamy macrophage in atherosclerotic lesions, and fatty liver disease due to liver damage^{4,162,170,171}.

2.2. Materials and Methods

2.2.1. *Animals*

Post-pubertal multiparous female cattle (n = 15) of composite breeding (½ Red Angus, Pinzgauer, Red Poll, Hereford and ½ Red Angus and Gelbvieh) were synchronized using two intramuscular injections of PGF2α (25mg; Lutalyse®, Zoetis Inc., Kalamazoo Michigan, MI) 11 days apart. At day 3 or day 10 after ovulation, 3-5 cows were subjected to a bilateral ovariectomy through a right flank approach under local anesthesia^{277,278}. The CL was removed from the ovary, weighed and < 5 mm³ sections were snap-frozen in liquid N₂ for subsequent protein and RNA analysis. All animal procedures were completed under an IACUC-approved protocol and

performed at the University of Nebraska—Lincoln, Animal Sciences Department. Statistical differences in animal characteristics were determined using one-way analysis of variance in GraphPad Prism (La Jolla, CA).

2.2.2. *Lipid droplet staining in luteal tissue*

Tissue sections were frozen in optimal cutting temperature (O.C.T.) compound (Tissue-Tek) transported back to the lab on dry ice. Frozen samples were kept at -80 C until sectioning using a Leica CM3050S instrument and attached to silane-coated slides before fixation in 10% phosphate-buffered formalin for 1 h. Fixed slides were stained with oil red O and counterstained with Harris' hemotoxin using an automated slide staining setup at the University of Nebraska Medical Center Tissue Sciences Facility. Slides were scanned at 40x using Ventana's Coreo Au Slide Scanner. Images were analyzed by Definiens Tissue Studio (Munich, Germany) to count nuclei and area occupied by oil red O.

2.2.3. *Transmission electron microscopy*

Coronal sections (through the stomata) of luteal tissue were fixed in 3% (w/v) paraformaldehyde and 0.2% glutaraldehyde in phosphate-buffered saline (PBS), pH 7.4, post-fixed in 2 % OsO₄, resin-embedded, and ultra-thin sectioned for electron microscopy. Transmission electron microscopy (TEM) images were captured using a Hitachi H7500 at the University of Nebraska-Lincoln Center for Biotechnology. Three images (magnification: 8,000x) from each CL were used for quantification of LD number and area using ImageJ¹⁷².

2.2.4. *Isolation of large and small luteal cells*

For luteal cell preparations, bovine ovaries were collected during early pregnancy (fetal crown-rump length < 12 cm) from a local abattoir (JBS USA, Omaha, NE) and transported to the laboratory on a cold pack. The luteal tissue was dissociated with collagenase as described previously¹⁷³. The cell viability was determined by the trypan blue exclusion test, and luteal cell preparations with more than 90% viability were used. Small and large luteal cells (SLC, LLC

respectively) were isolated essentially as previously described¹⁰⁴. Briefly, the mixed luteal cells were resuspended in elutriation medium (calcium-free Dulbecco's modified eagle medium (DMEM) [US Biological D9800-10], supplemented with 25 mM HEPES, 3.89 g/L sodium bicarbonate, and 3 mg/mL glucose). Resuspended cells were subjected to centrifugal elutriation with continuous flow using a Beckman Coulter Avanti J-20 XP centrifuge equipped with a Beckman JE-5.0 elutriator rotor. The fractions containing SLC and LLC were pelleted and resuspended in basal M199 (0.1% BSA, 100 U/ml penicillin-G-sodium, 100 µg/ml streptomycin sulfate, and 10 µg/ml gentamicin sulfate). The average purity of SLC was 90% and LLC in were 75%.

2.2.5. *Isolation of granulosa and theca cells*

Follicular granulosa and theca cells were prepared from bovine ovaries collected from a local abattoir (JBS USA, Omaha, NE). Large follicles (> 0.8 cm) were punctured with a 20-gauge needle and follicular fluid was removed, the needle was reinserted and the granulosa cells were resuspended in an equal volume of elutriation medium containing 20 µg/mL DNase (Worthington). After the granulosa cells were removed, the follicle was opened and the theca was removed from the surrounding stroma and stored in elutriation medium. Small antral follicles (< 0.8 cm) were opened with a scalpel and the granulosa cells were gently scraped from the follicle wall using the blunt side of the scalpel and resuspended in elutriation medium. Theca were removed from surrounding stroma and placed in Elutriation Medium. Granulosa cells were washed by centrifugation three times at 150 rcf for 5-10 min and filtration through a 70 µm mesh. Theca cells were resuspended in 0.2 mg/mL Collagenase 2 (Atlanta Biologicals) in elutriation medium and dispersed using constant agitation at 37 °C for 1 h. Dispersed theca were removed from the undigested tissue by filtration through a 70 µm mesh then washed by centrifugation three times at 150 rcf for 5-10 min. Red blood cells were removed by resuspending theca cells in dH₂O and immediate addition of 2x PBS.

2.2.6. *Lipid droplet staining in freshly isolated cells.*

Cells in suspension were affixed to glass slides using Cytofuge (6.5 g, 5 min) and immediately fixed in 10% phosphate-buffered formalin. Slides were washed well with PBS, then stained with oil red O (ORO) in isopropanol for 15 min, rinsed with dH₂O and then the nuclei were briefly counterstained using filtered Harris' hematoxylin. Coverslips were affixed using fluromount G.

2.2.7. *Progesterone assay*

Jugular blood samples were collected into heparinized tubes and plasma samples were frozen at -80 °C until analysis could be performed. Progesterone concentration in plasma was determined using a commercial radioimmunoassay (Progesterone CT 07-270102, MP Biomedicals, LLC, Solon, OH). The intra-assay coefficient of variation of 9.13% and inter-assay coefficient of variation of 7.99%.

2.2.8. *Lipid droplet isolation from tissue*

Tissue (~2.5 g) was washed thoroughly in TE buffer (10 mM Tris, 1 mM EDTA, pH 7.4). Minced tissue was resuspended in 10 mL tissue homogenate buffer (60% sucrose w/v in TE buffer containing protease and phosphatase inhibitor cocktail) and homogenized with a Teflon Dounce homogenizer in a glass vessel. The post-nuclear supernatant (PNS) fraction was obtained after centrifugation at 2000 rcf for 10min. The supernatant was loaded into a 30 mL ultracentrifuge tube and overlaid sequentially with 40%, 25%, 10%, and 0% sucrose w/v in TE buffer containing protease and phosphatase inhibitor cocktails. Samples were centrifuged at 110,000 x g (r_{avg}) for 30 min at 4 °C with no brake in a Beckman Coulter Avanti J-20 XP ultracentrifuge using an SW 32 Ti rotor. The LDs concentrated in a yellow/white band at the top of the gradient were harvested and concentrated by centrifugation at 2000 rcf for 10 min at 4 °C protocol was modified from ^{174,175}.

2.2.9. *Western blots*

Tissue samples were weighed and homogenized (~100 mg/mL) in cell lysis buffer (20mM Tris [pH 7.4], 150 mM NaCl, 1 mM EDTA, 1 mM EGTA, 1% Triton x-100, protease and phosphatase inhibitor cocktails) using OMNI Tissue homogenizer then sonicated for 3 s. Lysates were centrifuged at 18,350 x g for 15 min at 4 C and the supernatant was collected for SDS-PAGE analysis. Protein concentration was determined by Bradford reaction (Bio-Rad 500-0006). Aliquots of samples (10-30 µg protein) were suspended in protein loading buffer (50 mM Tris pH 6.8, 300 mM glycerol, 25 mM SDS, 45 mM DTT, 260 mM 2-mercaptoethanol, bromophenol) separated on 10% SDS-PAGE gel and transferred to nitrocellulose membranes. Membranes were blocked in TBST (10 mM Tris-HCl, 150 mM NaCl, 0.1% Tween 20; pH 7.5) with 5% fat-free milk for 1 h at room temperature. Membranes were incubated either overnight at 4 C or for 2 h at room temperature with primary antibody diluted in TBST with 1% non-fat milk or 5% BSA. After washing, membranes were incubated for 1 h at room temperature with 1:20,000 anti-rabbit or anti-mouse HRP-conjugated IgG diluted in TBST with 1% non-fat milk. After washing, protein bands were detected with SuperSignal West Femto (Thermo).

2.2.10. *Lipidomics*

Lipids from CL tissue LDs were extracted using a standard Bligh and Dyer extraction protocol¹⁷⁶ and then dried and sent to Avanti Polar Lipids for lipidomics analysis. Extracts were received as dried residues in glass vials and were immediately stored at -80 °C until analysis. The samples were provided for lipidomic profiling of free sterols, cholesteryl esters, triacyl- and diacyl-glycerols, phospholipids, and sphingolipids. The molecular species within each class were identified, quantified and summed to report the average lipid profile of bovine luteal LDs. To provide resolution and quantitative ability beyond the mass resolution of the tandem quadrupole mass spectrometers employed, molecular species were resolved by reversed-phase liquid chromatography in the presence of class and sub-class specific internal standard compounds added to each sample. The compounds were detected by tandem mass spectrometry (MS/MS) for

mass specific fragment ions according to lipid class and molecular weight of the compound, known as multiple reaction monitoring (MRM). Selectivity was further enhanced by scheduling the detection of each compound according to its elution from the high-performance liquid chromatography (HPLC) column, known as scheduled MRM (sMRM). The semi-quantization was calculated using the integrated area of each analytes MRM peak, divided by the appropriate internal standard peak area, multiplied by its known concentration. Quantization of cholesterol and cholesteryl esters were directly calculated with standards and internal standards from calibration response curves. Lipid concentrations were normalized to the corresponding protein concentration of each sample.

2.2.11. *High-performance thin layer chromatography (HPTLC)*

For lipid analyses, 0.25 mL of cell homogenate was extracted overnight with 2.5 mL of chloroform-methanol (1:1). After removing insoluble material by centrifugation, lipid extracts were washed according to Folch, Lees, and Sloane Stanley¹⁷⁷ before analysis. The cholesteryl esters and triglycerides were separated by HPTLC on 10 cm plates using a single solvent system described by Mangold and Malins 1960¹⁷⁸. The plates were prewashed by development with chloroform-methanol-water (60:35:8) followed by chloroform-methanol-acetic acid-formic acid-water (35:15:6:2:1). Lipids were dissolved in chloroform-methanol (1:1), and 10 uL was spotted in a 0.6 cm line at the origin (1 cm above the bottom of the plate). The plate was developed using petroleum ether (b.p. 60-70 °C)-ethyl ether-acetic acid (45:5:0.5). The plate was sprayed with 10% CuSO₄ in phosphoric acid, and lipids were visualized by heating at 180 °C for 5 minutes. The plates were scanned (instrument) and the images were analyzed using UVP Vision Works LS software by calculating the area under the curve after lane specific straight line background correction. A mixture of the following standard lipids was co-chromatographed: phosphatidylcholine, cholesterol, triglyceride, cholesterol palmitate, oleic acid. Preliminary analyses were completed to establish the linearity of detection for each lipid class to ensure that

lipids did not exceed the linear range for quantitation. For every plate of cellular lipids, five lanes of varying amounts of lipid standards were simultaneously run to generate standard curves for quantitation. The amount of each cellular lipid was expressed as $\mu\text{g lipid/mg cell protein}$.

Adapted from ¹⁷⁹.

2.2.12. Reverse transcriptase-polymerase chain reaction (RT-PCR)

Target transcript expression was evaluated by isolating RNA from target tissue, reverse transcription of 1 μg RNA using SuperScript II Reverse Transcriptase (Invitrogen, Grand Island, NY) followed by RT-PCR using gene-specific primers.

2.3. Results

2.3.1. Animals

Synchronized multiparous cows were subjected to a bilateral ovariectomy at either day 3 or day 10 after ovulation. Day 10 CLs weighed significantly more than day 3 CLs (4.7 ± 0.46 , 2.8 ± 0.65 g, respectively). Serum progesterone concentrations were also elevated in day 10 (13.05 ± 4.14 ng/mL, $P = 0.2$) compared to day 3 (4.85 ± 1.47 ng/mL) (Figure 2-1).

2.3.2. Luteal LDs

Lipid droplets were a prominent feature in both day 3 and day 10 *in vivo* CLs, oil red O staining of frozen section of luteal tissue demonstrated that oil red O occupied an area of $26\text{-}36 \mu\text{m}^2$ per nucleus regardless of luteal age (Figure 2-2, A- C). Analysis of TEM images did not demonstrate a difference in the number of LDs in day 3 and day 10 CLs. As well, TEM images demonstrated that LDs are abundant within luteal tissue, but characterization of the size of individual LDs indicated no differences between in LD size between day 3 and day 10 CL (0.41 ± 0.04 , $0.41 \pm 0.03 \mu\text{m}^2/\text{LD}$, respectively) (Figure 2-2 D, E, & F). Finally, there are no clear differences in the luteal tissue architecture (Figure 2-2 G, & H) though the total size of the CL is increased and progesterone secretion is increased in day 10 compared to day 3 CLs (Figure 2-1).

Discontinuous sucrose gradients were used to separate LDs from whole tissue and created a distinct yellow band at the top of the sucrose gradient (Figure 2-2 I).

2.3.3. *Lipid droplets in ovarian cells*

Granulosa and theca cells are precursors to the steroidogenic cells of the CL. Lipid droplet content of these follicular precursors was compared to the steroidogenic SLC and LLC. Confocal images of isolated cell types demonstrated that granulosa and theca cells have fewer and smaller LDs than the luteal counterparts (Figure 2-3 A & B). As well, SLC appeared to have fewer, but larger LDs than LLC which contained many small LDs.

2.3.4. *Expression of LD-associated proteins in the CL*

Western blot and RT-PCR analysis of proteins known to associate with LDs from bovine fat, liver, heart and CL tissue demonstrated that the bovine PLIN1 expression is greatest in bovine adipose tissue. Whereas PLIN2 is greatest in the heart and CL. Both PLIN3 and PLIN5 were found in all the tissues examined. Adipose triglyceride lipase (ATGL) expression was greatest in adipose and heart tissue where as abhydrolase domain-containing protein 5 (ABHD5), a coactivator of ATGL was found in all tissues examined. The cholesteryl ester synthesizer, sterol O-acyltransferase1 (SOAT1) protein was highest in bovine liver. Finally, HSL, a cholesteryl esterase, was high in luteal tissue and extremely abundant in adipose tissue (Figure 2-4).

2.3.5. *Lipid composition of LDs*

Lipids from CL tissue LDs were extracted and assessed for their relative lipid content. Triacylglycerides were the predominant lipid species in luteal LDs ($168 \text{ pmol}/\mu\text{g protein} \pm 41.9$). Other neutral lipids included diacylglycerol ($5.62 \pm 2.1 \text{ pmol}/\mu\text{g protein}$) and cholesteryl esters ($2.78 \pm 0.70 \text{ pmol}/\mu\text{g protein}$). Sterols were undetectable in all but one LD sample. Polar lipids were primarily composed of phosphatidylcholine ($5.73 \pm 1.49 \text{ pmol}/\mu\text{g protein}$), sphingomyelin ($2.68 \pm 0.28 \text{ pmol}/\mu\text{g protein}$), phosphatidylinositol ($1.69 \pm 0.61 \text{ pmol}/\mu\text{g protein}$), and phosphatidylethanolamine ($1.39 \pm 0.38 \text{ pmol}/\mu\text{g protein}$) (Figure 2-5 A). The fatty acids of

cholesteryl esters were composed primarily of oleic acid (18:1, 15% of total), pentadecanoic acid (15:0, 13%), adrenic acid (22:4, 12%), and erucic acid (22:1, 10%) and smaller amount of other fatty acids (Figure 2-5 B).

Analysis of whole tissue lipid content was performed on both bovine CL and adipose tissues by HPTLC. Luteal tissue had 7.4-fold more cholesterol over adipose tissue and 8.2-fold more cholesteryl esters (Figure 2-5 C). The follicular granulosa and theca cells both had low levels of lipids and SLC and LLC had significantly more free fatty acids, cholesterol, cholesteryl esters and triacylglycerides than their follicular counterparts. However, there were no differences in major lipid classes between granulosa and theca cells or LLC and SLC (Figure 2-5 D).

Purified LDs were compared to the lipid content of whole tissue, post-nuclear supernatant, and post-nuclear supernatant after removal of LDs. Cholesteryl esters and triglycerides were found predominately within luteal LDs, and not in other tissue components. Whereas, cholesterol was not found in the LDs but elsewhere in the tissue, consistent with the lipidomics data. Free fatty acids were stored equally in LDs and other cellular components (Figure 2-6).

2.4. Discussion

2.4.1. Overview of study

Within the bovine CL, LDs are a prominent feature which are established by day 3 post-ovulation and maintained at mid-cycle (day 10). These LDs are enriched in several proteins including classic LD-associated proteins as well as steroidogenic enzymes. Although the major constituent of bovine LDs is triglyceride, cholesteryl esters constitute 2.78 ± 0.70 pmol/ μ g protein. Bovine luteal cells are enriched in cholesterol and cholesteryl esters compared to bovine visceral adipose tissue, likely for use in steroidogenesis. In contrast, the granulosa and theca cells of the follicle have few LDs and have reduced lipid content (of all major classes) compared to the steroidogenic luteal cells. Although, there does not appear to be a difference in lipid composition of granulosa and theca cells or of the luteal LLC and SLC.

2.4.2. *Lipid droplets in luteal tissue*

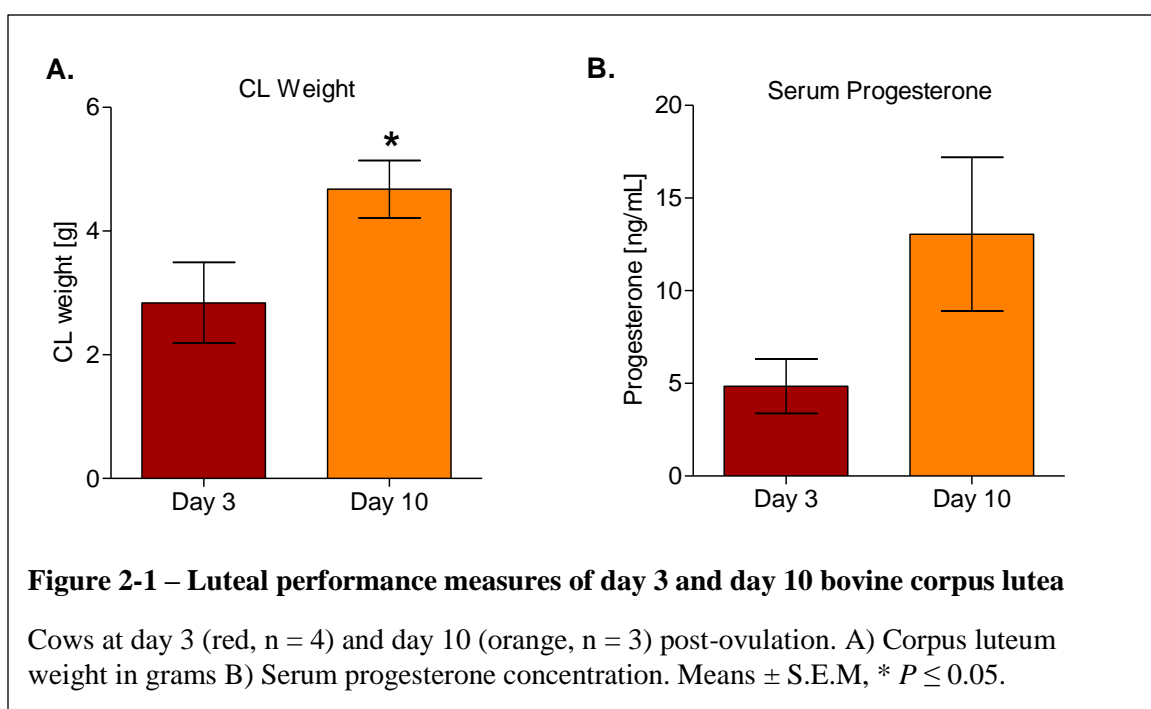
Lipid droplets are a large component of both early (day 3) and mid-cycle CL (day 10) comprising approximately 26 - 36 μm^2 /nuclei, which would be approximately 5-16% of luteal cell area based on other group's luteal cell area measurements (SLC: 201-216 μm^2 , LLC 566-581 μm^2) in agreement with other studies examining LD /luteal cell area or volume ^{156,158,180}. Lipid droplets occupied ~2% of the luteal cell volume in a recent study examining ovine luteal cell LDs ¹⁵⁸. Since LDs are rarely seen in luteal endothelial cells, the percentage of the luteal cells occupied by LDs could be even higher. Individual luteal LDs have a mean area of 0.41 μm^2 which does not differ between day 3 and day 10 CLs. Together this indicates that luteal LDs are an established feature of luteal tissue by day 3 and does not differ between day 3 and day 10 CLs. Thus, luteal LDs must form prior to day 3 post-ovulation. This is in keeping with studies by Guraya *et al.* who described that granulosa cells in humans developed fine "lipid granules" and "heterogeneous lipid bodies" within newly ruptured follicles, and that the theca interna cells of newly ruptured follicles are filled with sudanophilic lipids, including cholesterol and its esters ¹⁸¹. As well, LDs are increased in granulosa cells of 1 day old CL in rabbits ¹⁸². Similarly, treatment of rhesus macaques with LH or hCG can induce LD-associated proteins in granulosa cells within 12 hours ²³. Additionally, transcripts of PLIN2 increase significantly in LH treated bovine granulosa and theca cells ¹⁸³ and unpublished data.

2.4.3. *Lipid composition of LDs*

Luteal LDs are composed primarily of triglycerides but have a smaller but likely significant amounts of cholesteryl esters which are greater than other bovine tissues, including adipose, granulosa, and theca. The cholesteryl esters and triglycerides of luteal cells are stored within the LDs and not elsewhere in the cells, unlike cholesterol, which is not located in LDs. Cholesteryl esters are likely substrates for steroidogenesis in bovine luteal cells. The function of the triglycerides within luteal LDs is uncertain at this time, but may be substrates for β -oxidation derived energy production to fuel the steroidogenic output of the CL ^{184,185}.

Several groups in the 1960s provided a histochemical evaluation of lipid composition throughout the estrous cycle of humans ¹⁸¹, rats ¹⁵², and rabbit ¹⁸². Despite the few studies of LD presence and amount in the bovine CL ^{147,180,186–189}, we know of no studies examining the luteal LD lipid or protein composition. Luteal LDs are also known to be regulated by diet ¹⁸⁰, LH (depletion) ^{148,190,191} and PGF2 α (increase) ^{61,62,156,192}.

In this study, only two time-points in the estrous cycle were evaluated for presence and composition of LDs. Further research examining the onset of the inclusion of LDs in luteal cells, as well as examining the presence and composition of the few LDs present in theca and granulosa cells could provide novel data on the origin and regulation of LDs within the ovary. Additional experiments examining the changes in LD size, number, and composition after luteotropic and luteolytic stimulation would benefit the field. Finally, the impact of obesity, undernutrition, and polycystic ovarian syndrome on luteal LDs may provide insights into mechanisms of infertility. We believe that luteal LDs play a critical role in progesterone production by storing cholesteryl esters in bovine luteal cells as a reservoir of substrate in preparation for progesterone synthesis.



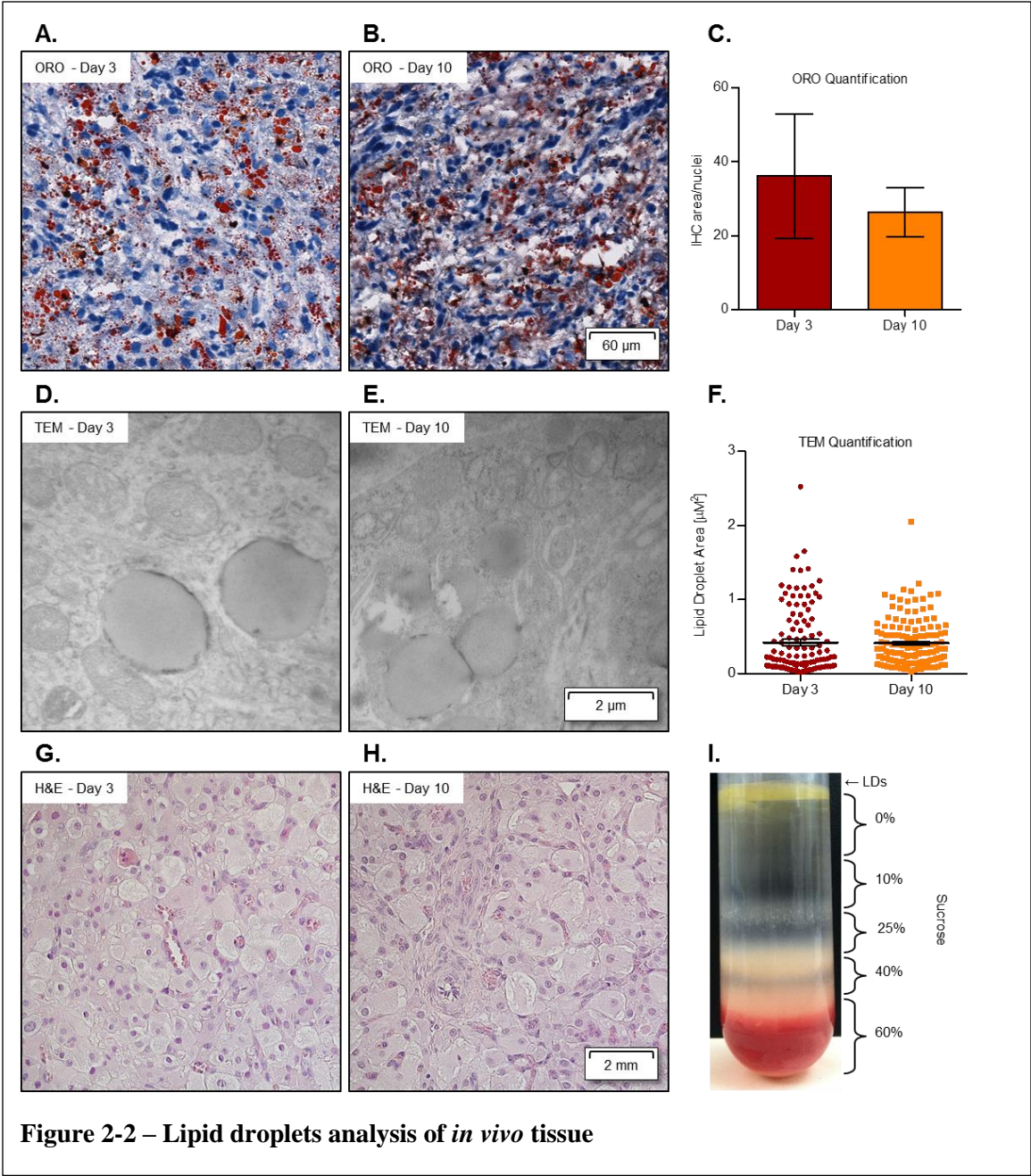


Figure 2-2 – Lipid droplets analysis of *in vivo* tissue

(A & B) Representative images of oil red O (ORO) staining of LDs in frozen tissue sections of the CL from Day 3 (A, red, $n = 4$) and Day 10 (B, yellow, $n = 3$) post-ovulation. The images were acquired using Ventana's Coreo Au Slide Scanner at 40x, scale bar for both images appears in (B). C) Quantification of the IHC area (in μm^2)/nuclei performed using Definiens Tissue Studio, bars represent mean \pm SEM. $P = 0.65$, non-significant. D & E) Representative images of transmission electron micrographs (TEM) of Day 3 (D, red, $n = 3$) and Day 10 (E, yellow, $n = 3$) bovine CL demonstrating LD presence using a magnification of 8,000x, scale bar for both images appears in (E). F) Each point demonstrates the area (μm^2) occupied by individual lipid droplets in three randomly chosen images from at $n = 3$ for each condition, mean \pm SEM is overlayed in black. $P = 0.84$, non-significant. G & H) Representative images of hematoxylin and eosin (H&E) stained Day 3 (G) and Day 10 (H) paraffin embedded sections. Large luteal cells, small luteal cells, and endothelial cells of blood vessels are readily apparent at both stages and no morphological differences are apparent. I) Representative image of a discontinuous sucrose gradient (steps are labeled with % sucross) used to isolate luteal LDs, the LDs form a distinct yellow band at the top of the gradient.

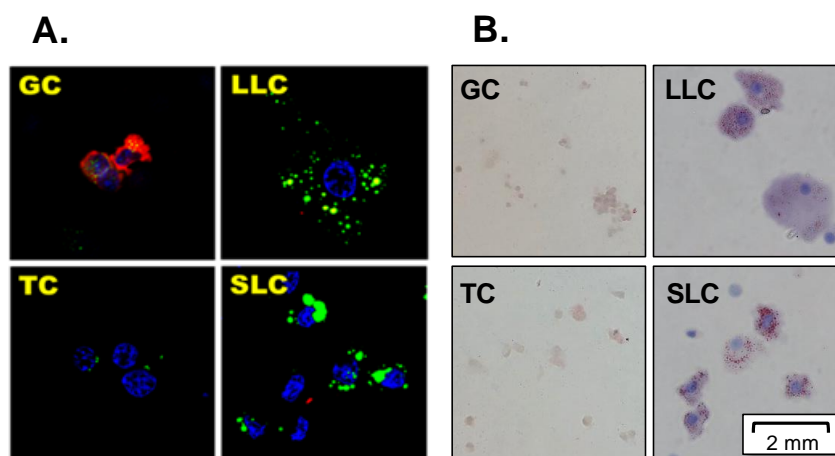
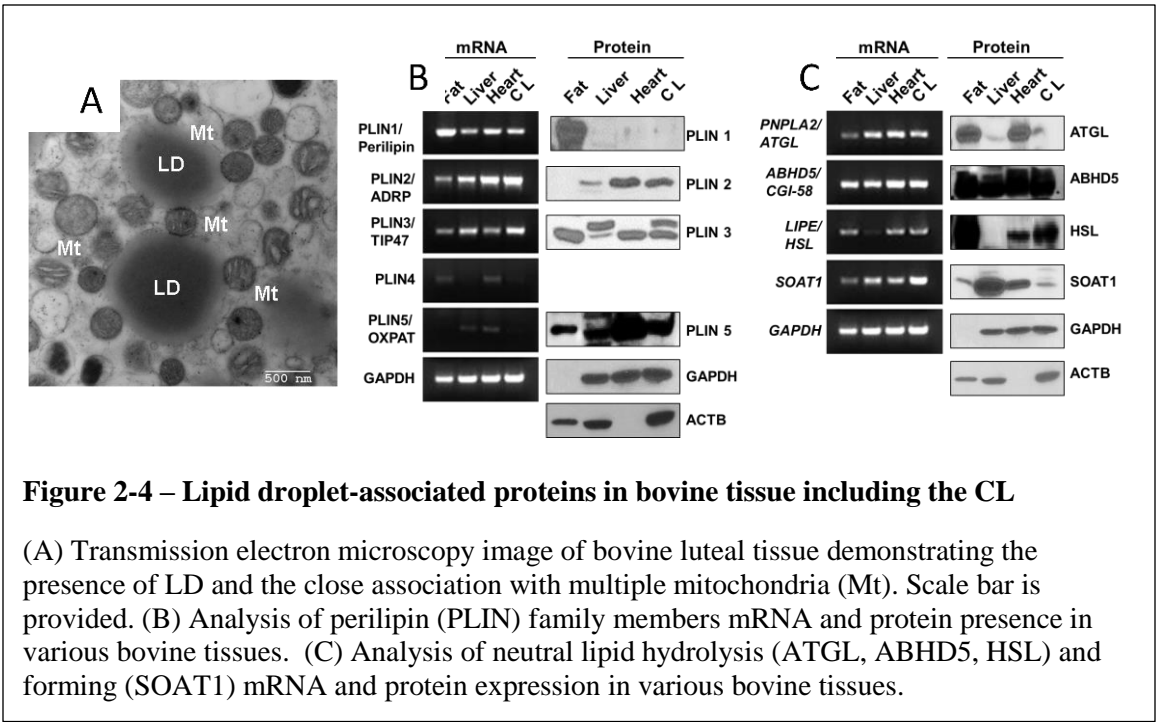


Figure 2-3 – Lipid droplets of isolated cells

A) Confocal fluorescent image showing LD staining in freshly isolated bovine granulosa (GC), theca (TC) and the steroidogenic luteal cell types: large (LLC) and small luteal cells (SLC). LDs were stained with the neutral lipid dye BODIPY 493/503 (green), and cells were immuno-labeled using an aromatase antibody to specifically label granulosa cells (red), and the nuclei are counter-stained with DAPI (blue). All images are equal magnification. B) Light microscope image showing LD staining in freshly isolated GC, TC, LLC, and SLC. LDs were labeled with the neutral lipid dye oil red O (ORO) and nuclei are counter-stained with Harris' hematoxylin. All images are equal magnification and a scale bar is provided.



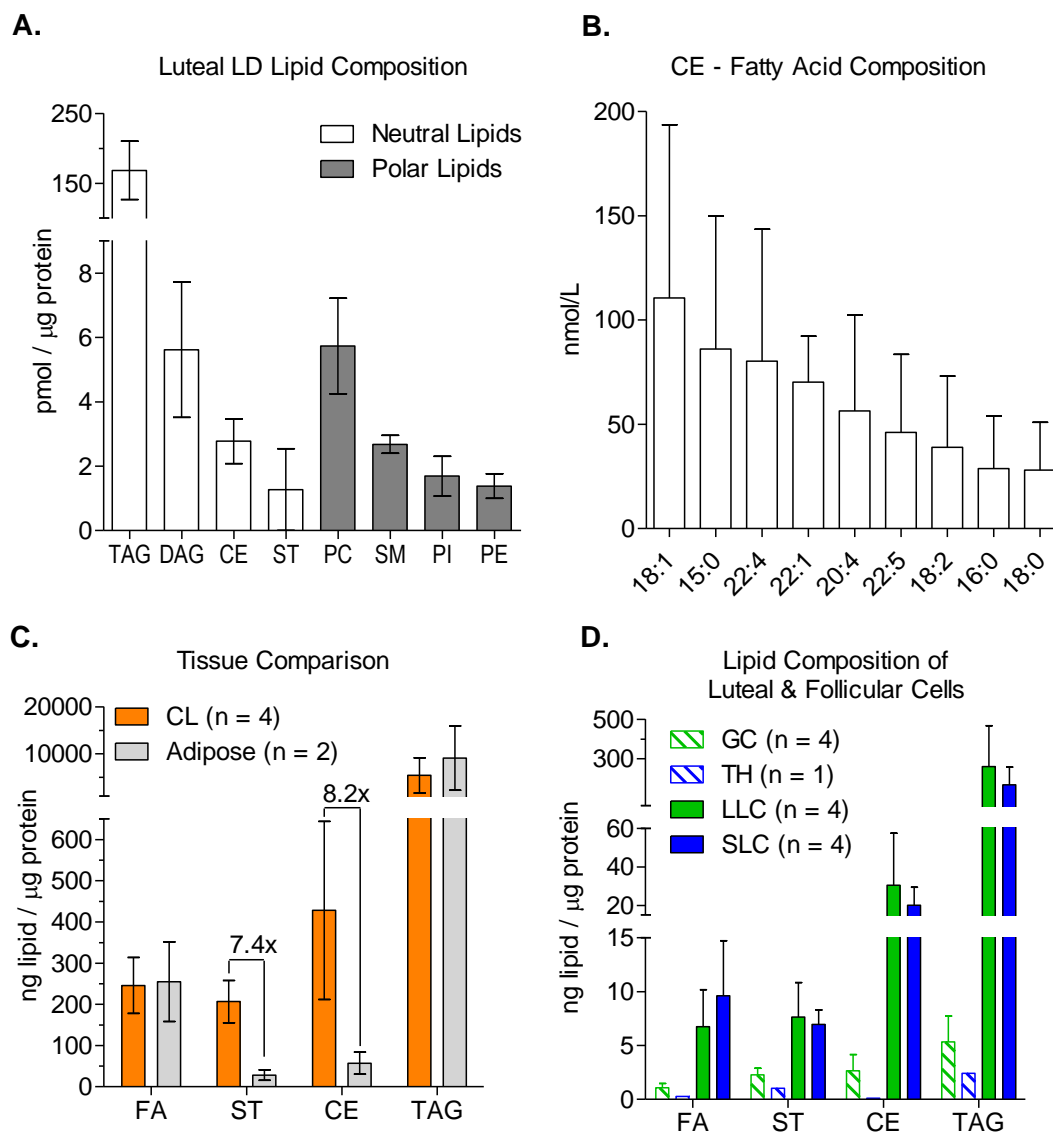


Figure 2-5 – Lipid composition of luteal LDs

(A) Analysis of purified LDs from bovine CL of early pregnancy by ultra-performance liquid chromatography system coupled with tandem quadrupole mass spectrometry. $n = 3$. TAG-triacylglycerol; DAG-diacylglycerol; CE-cholesteryl esters; ST-sterols; PC-phosphatidylcholine; SM-sphingomyelins; PI-phosphatidylinositol; PE-phosphatidylethanolamine. (B) Lipidomics determined fatty acid composition of cholesteryl esters, X:X - number of carbons in the fatty acid: number of double bounds in the fatty acid. High performance thin layer chromatography (HPTLC) analysis of whole bovine CL versus adipose tissue FA, free fatty acids. (C) HPTLC analysis of freshly-isolated LLC, SLC, GC, and TH cells. Bars represent means \pm SEM

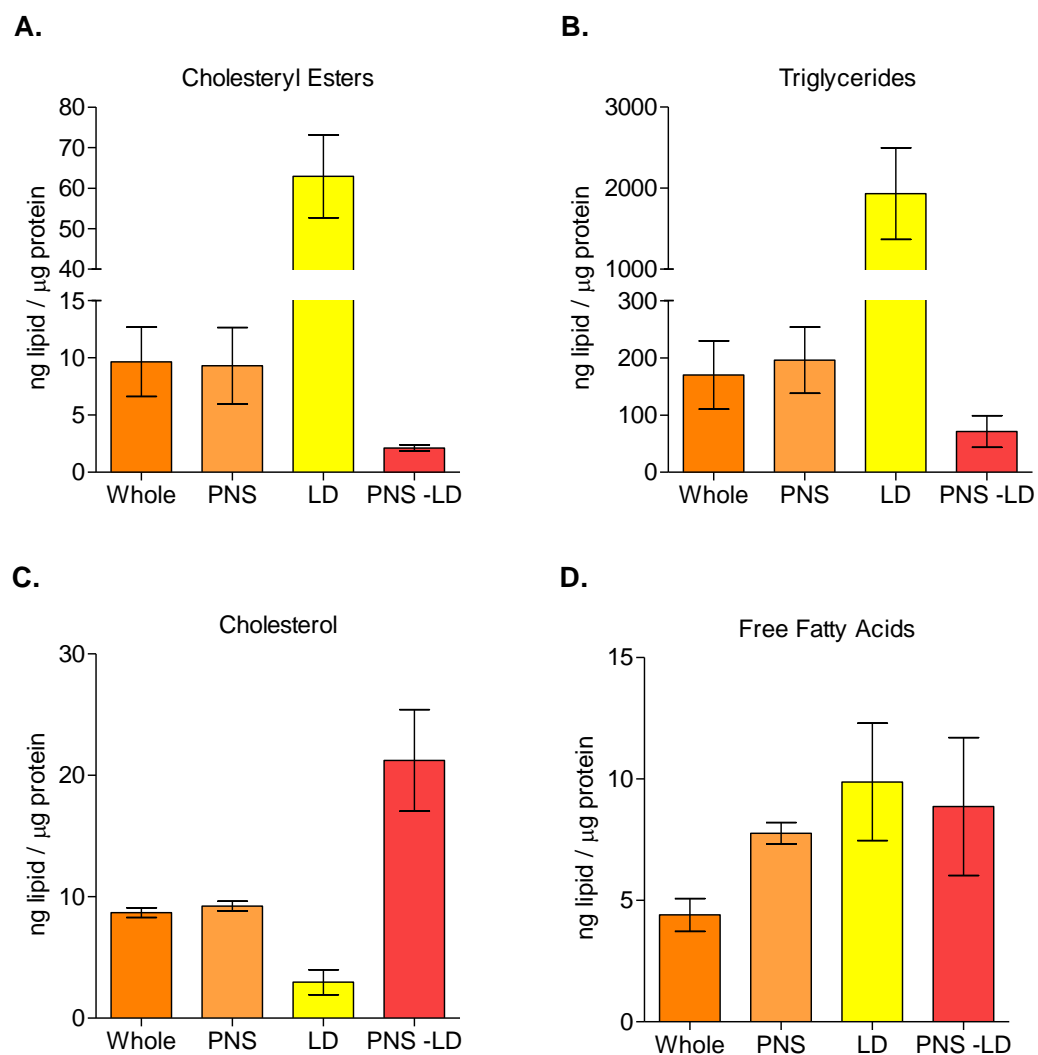


Figure 2-6 – Lipid composition of subcellular compartments of luteal tissue

Lipid analysis by HPTLC of whole tissue lysate, post-nuclear supernatant (PNS), lipid droplet fraction (LD), and post-nuclear supernatant minus LD fraction (PNS-LD). Lipid content of each fraction was normalized to protein content. Bars indicate means \pm S.E.M, $n = 2$.

CHAPTER 3: LIPID DROPLETS ARE DYNAMICALLY REGULATED BY LUTEINIZING HORMONE SIGNALING IN THE BOVINE CORPUS LUTEUM ‡

Abstract

Growth and maturation of the corpus luteum is accompanied by accumulation of cytoplasmic lipid droplets (LDs). These LDs are proposed to store cholesteryl esters for progesterone synthesis. LDs in other tissue can be dynamically regulated, but it is unclear how luteal cells regulate LDs. Hormone-sensitive lipase (HSL) and other LD-associated proteins including perilipin2 (PLIN2) were assessed during *in vivo* and *in vitro* differentiation of luteal cells from follicular cell types. In luteal cell cultures, the activation and localization of HSL after hormone stimulation and the impact of an HSL inhibitor on progesterone secretion were assessed. Finally, the luteal LD proteome was assessed by both proteomics and Western blot. HSL and PLIN2 increased during *in vivo* and *in vitro* differentiation to luteal cell phenotypes. Dose-dependent inhibition of HSL activity inhibits luteinizing hormone (LH)- and HDL-stimulated progesterone secretion. Stimulation with LH, forskolin, and 8-br-cAMP phosphorylated HSL at the PKA-sensitive Ser563, which is selectively associated with luteal LDs. Proteomics analysis revealed 469 bovine-specific proteins which included steroidogenic enzymes StAR, P450_{scc}, and 3B-HSD, which was confirmed by Western blot analysis of *in vivo* luteal tissue. The surface of LDs may serve as a novel platform for steroidogenesis through the intimate association and potential tethering of steroidogenic enzymes present in the mitochondria and endoplasmic reticulum to the coat proteins of the LDs to facilitate the handoff of steroid precursors at each step to efficiently produce steroids, such as progesterone.

‡ The material presented in this chapter is in preparation to be as submitted as a manuscript: Talbott *et al.* Lipid Droplets are dynamically regulated by luteinizing hormone signaling in the bovine corpus luteum .

3.1. Introduction

Understanding the regulation of luteal function will allow for the development of advanced treatment techniques for improving female fertility. We have demonstrated that the corpus luteum (CL) has numerous lipid droplets (LDs) within the steroidogenic cells (manuscript in preparation, Chapter 2), which are thought to store the steroid precursor cholesterol as cholesteryl esters. The formation and breakdown of LDs is known in fat and liver tissue to be regulated by LD-associated proteins which include perilipins (PLINs) and hormone-sensitive lipase (HSL) ^{10,160,193}. PLIN proteins are embedded within the LD surface and stabilize the organelle and facilitate interactions with transient LD proteins. Whereas, HSL is an enzyme that can liberate cholesterol from cholesteryl esters after protein kinase A (PKA) stimulation.

3.1.1. Regulation of CL formation

The CL is responsible for synthesizing the progesterone that supports early pregnancy in most mammals ¹³⁴ and progesterone deficits are associated with early embryonic loss in women ^{194–196} and female livestock ^{197–199}. Early embryonic loss of pregnancies is commonly associated with luteal insufficiency, which is characterized by deficiencies in progesterone secretion, either in amount or duration ²⁰⁰. Luteal insufficiency results in a failure to develop a mature secretory endometrium, preventing embryo implantation, and has been found in 3-10% of infertile women and up to 35% of women with recurrent abortion ^{201,202}. In cattle, early embryonic loss accounts for 30% of infertility cases ^{197–199}, of which, many are believed to be due to a deficiency in progesterone secretion ²⁰⁰. Improvement of the understanding of CL function and the biosynthesis of the critical steroid hormone, progesterone, could lead to infertility management strategies for successful intervention in human and livestock fertility outcomes.

CL formation begins with the luteinizing hormone (LH) surge, which causes ovulation and initiates the differentiation of follicular granulosa and theca cells into progesterone-secreting luteal cells. Secretion of progesterone by luteal cells requires direct action of three proteins, 1)

steroidogenic acute regulatory protein (StAR), which facilitates transport of cholesterol to the mitochondrial matrix, 2) P450 side-chain cleavage (P450_{scc}) which removes the side-chain from cholesterol to form pregnenolone, and 3) 3- β hydroxysteroid dehydrogenase (3 β HSD) which dehydrogenates pregnenolone to form progesterone. Key features of CL development include the development of an extensive vascular bed^{203,204}, recruitment of neutrophils,^{205–207} and monocytes^{208,209}. Additionally, CL development and function are metabolically regulated both systemically^{210,211}, and intracellularly by key regulators such as insulin^{212,213}, insulin-like growth factors^{212,214}, leptin^{210,215,216}, and adenosine monophosphate-activated protein kinase (AMPK)^{88,91,94}. In addition to overall metabolic status, both dietary lipids^{158,180,211,217,218} and tissue lipid contents^{73,219} can impact ovarian function.

3.1.2. *Lipid droplets in the CL*

For over 40 years, luteal cells have been noted as containing LDs^{145,146}. One report determined that LDs made up 1.6-9.2% of identifiable subcellular components (mitochondria, granules, etc.) during the functional life span of the CL¹⁴⁷. LDs have been postulated to store cholesteryl esters that could be used for steroidogenesis¹⁵⁹. Armstrong *et al.* demonstrated that in rats and rabbits these LDs were primarily composed of cholesteryl esters and that treatment with LH reduced the total amount of cholesteryl esters present¹⁴⁸. As well, several research groups showed cholesterol and cholesteryl ester storage using the cholesterol sensing Schultz reagent^{149–154}. Reports by Armstrong, Claesson, Gurarya, and others indicated that luteal LDs in various species could be altered by treatment with LH and prostaglandin F2 α , which is important in the involution of the CL^{148,155–157}.

Guraya *et al.* who described that granulosa cells in humans developed fine “lipid granules” and “heterogeneous lipid bodies” within newly ruptured follicles, and that the theca interna cells of newly ruptured follicles are filled with sudanophilic lipids, including cholesterol and its esters¹⁸¹. Additionally LDs are increased in granulosa cells of 1 day old CL in rabbits¹⁸². Similarly,

treatment of primates with LH or hCG can induce LD-associated proteins in granulosa cells within 12 hours ²³. Transcripts of PLIN2 increase significantly in LH treated bovine granulosa and theca cells ¹⁸³ and unpublished data.

3.1.3. *Regulation of LDs*

Neutral lipids, such as triglycerides and cholesteryl esters, can be stored intracellularly in specialized LD organelles. These unique organelles store neutral lipids (including cholesteryl esters) within a phospholipid monolayer, as opposed to the bilayer surrounding most other organelles. Embedded and associated with the monolayer are LD-associated proteins. The major LD-associated proteins are the PLIN family which includes, PLIN1 (perilipin), PLIN2 (adipophilin/ADRP/ADFP), and PLIN3 (previously Tip47/M6PRBP1). The PLIN family of proteins can stabilize the lipid droplet surface and can serve as a platform for recruitment or sequestration of proteins that insert new lipids into the LD core, as well as exporting and modifying the neutral lipids for use in the cell. Additional proteins associated with the LD surface regulate the trafficking of LDs throughout the cell (e.g. Rab) and facilitate LD interaction with other organelles (PLIN5, vimentin). The LD proteome has been characterized to varying degrees in steroidogenic tissues and cell lines including, mouse testes ⁵⁷, the MLTC1 Leydig cell line ⁵⁶, and rat granulosa cells ⁵⁵. Studies in the ovary have indicated that LD-associated PLIN coat proteins ^{38,220,221} and HSL, a key enzyme for hormonally-stimulated lipolysis ^{39,220,221}, are expressed.

3.1.4. *Hormone-sensitive lipase*

Lipolysis of LD-stored triglycerides and cholesteryl esters can be stimulated by catecholamines in adipocytes through the action of HSL, which upon activation, translocates to the LD surface ^{26–28}. The proposed mechanism of HSL translocation to the LD involves PKA-dependent phosphorylation of PLIN1 and HSL, which allows the proteins to interact on the LD surface ³¹. The phosphorylation of HSL facilitates its association with PLIN1 on the LD and the

stored lipid substrates³², permitting lipid hydrolysis to proceed. Stimulation of HSL catalytic activity and translocation to LDs occurs by phosphorylation at both Ser-563 and Ser-660 by PKA^{33–36}. Negative regulation of HSL activity is accomplished by AMPK dependent phosphorylation of HSL at Ser-565³⁷. In adipose tissue, HSL contributes to energy homeostasis through lipolysis of LD-stored substrates after hormonal stimulation of PKA. HSL-null mice have aberrant steroid production in both the testes and adrenal glands^{40,41}. Together, these findings suggest that the intracellular processing and availability of cholesterol for steroidogenesis may include an HSL-dependent step. Therefore, we hypothesized that LDs are dynamically regulated in luteal cells, particularly by activation of PKA downstream of LH signaling.

3.2. Materials and Methods

3.2.1. Isolation and culture of human granulosa cells

Human granulosa cells were isolated from follicular aspirates of reproductive-age patients undergoing oocyte retrieval for *in vitro* fertilization. This study was approved by the Ethics Review Board of the University of Nebraska Medical Center. Tissue was collected through the obstetrical and gynecological tissue and fluid bank under an approved Institutional Review Board. Signed consent forms were obtained from each patient for use of discarded granulosa cells. Tissue was subsequently acquired from the tissue bank under an exemption from IRB Review. Ovarian stimulation was induced by treatment with recombinant human follicle stimulating hormone (FSH), followed by administration of hCG. Oocyte retrieval was performed 35 h after hCG administration by aspirating follicular fluid under ultrasound guidance. After removal of the oocyte-cumulus complex, all of the follicular aspirates donated from a single patient were pooled and centrifuged at 400 g for 10 min. Cells were resuspended in M199, layered onto 40% Percoll, and centrifuged at $200 \times g$ for 20 min. Granulosa cells were collected from the interphase of the Percoll gradient, washed with M199, and seeded into 24-well plates at a density of 100,000/well in M199 containing 10% fetal bovine serum (FBS) for overnight

plating. After overnight plating, cells were washed and then cultured and luteinized in M199 containing PenStrep, 0.1% BSA, 1 $\mu\text{g/mL}$ insulin, 2% FBS, and 10 μM forskolin or 1 IU/mL hCG. Culture media were changed every 2 d.

3.2.2. *Isolation of large and small luteal cells*

For luteal cell preparations, bovine ovaries were collected during early pregnancy (fetal crown-rump length < 12 cm) from a local abattoir (JBS USA, Omaha, NE) and transported to the laboratory on a cold pack. The luteal tissue was dissociated with collagenase as described previously¹⁷³. The cell viability was determined by the trypan blue exclusion test, and luteal cell preparations with more than 90% viability were used. Small luteal cells (SLC) and large luteal cells (LLC) were separated, essentially as previously described¹⁰⁴. Briefly, the mixed luteal cells were resuspended in elutriation medium (calcium-free Dulbecco's modified eagle medium (DMEM) [US Biological D9800-10], supplemented with 25 mM HEPES, 3.89 g/L sodium bicarbonate, and 3 mg/mL glucose). Resuspended cells were subjected to centrifugal elutriation with continuous flow using a Beckman Coulter Avanti J-20 XP centrifuge equipped with a Beckman JE-5.0 elutriator rotor. The fractions containing SLC and LLC were pelleted and resuspended in basal M199 (0.1% BSA, 100 U/ml penicillin-G-sodium, 100 $\mu\text{g/mL}$ streptomycin sulfate, and 10 $\mu\text{g/mL}$ gentamicin sulfate). The average purity of SLC was 90% and LLC in F4 were >50%.

3.2.3. *Isolation of granulosa and theca cells*

Follicular granulosa and theca cells were prepared from bovine ovaries collected from a local abattoir (JBS USA, Omaha, NE). Large follicles (> 0.8 cm) were punctured with a 20-gauge needle and follicular fluid was removed, the needle was reinserted and the granulosa cells were resuspended in an equal volume of elutriation medium containing 20 $\mu\text{g/mL}$ DNase (Worthington). After the granulosa cells were removed, the follicle was opened and the theca was removed from the surrounding stroma and stored in elutriation medium. Small antral follicles (<

0.8 cm) were opened with a scalpel and the granulosa cells were gently scraped from the follicle wall using the blunt side of the scalpel and resuspended in elutriation medium. Theca were removed from surrounding stroma and placed in Elutriation Medium. Granulosa cells were washed by centrifugation three times at 150 rcf for 5-10 min and filtration through a 70 μ m mesh. Theca cells were resuspended in 0.2 mg/mL Collagenase 2 (Atlanta Biologicals) in elutriation medium and dispersed using constant agitation at 37 °C for 1 h. Dispersed theca were removed from the undigested tissue by filtration through a 70 μ m mesh then washed by centrifugation three times at 150 rcf for 5-10 min. Red blood cells were removed by resuspending theca cells in dH₂O and immediate addition of 2x phosphate-buffered saline (PBS). Granulosa and theca cell viability and concentration were determined by trypan blue exclusion test.

3.2.4. *Luteal cell culture*

Bovine SLC and LLC were plated (SLC: 1×10^5 , LLC: 4×10^4 cells/cm²) in basal M199 with 5% FBS for 18 h at 37 °C in a humidified atmosphere of 5% CO₂. Cells were washed with PBS and the medium was replaced with serum-free M199 2 h prior to the experiment (treatment specifics are described in corresponding figure legends).

3.2.5. *Differentiation of granulosa and theca cells to luteal cell types*

Bovine granulosa and theca cells were plated (2×10^5 and 4×10^4 cells/cm², respectively) in basal DMEM:Ham's F-12 (F12) (1:1) [100 U/mL penicillin, 100 μ g/mL streptomycin, 10 μ g/mL gentamycin, and 0.1% BSA] containing 10% FBS for 36 h at 37 °C in a humidified chamber with 5% CO₂. Cells were washed with PBS and medium was replaced with basal DMEM : F12 containing 1% FBS. Cells were treated with either 1% insulin-transferrin-selenium (ITS) or 1% ITS + 10 μ M forskolin to induce differentiation, controls were unstimulated or treated with 5 ng/mL FSH, as described in the figure legends. All wells received equal amounts of dimethyl sulfoxide (DMSO) and the medium was changed every two days.

3.2.6. *Western blots*

Tissue samples were weighed and homogenized (~100 mg/mL) in cell lysis buffer (20mM Tris [pH 7.4], 150 mM NaCl, 1 mM EDTA, 1 mM EGTA, 1% Triton x-100, protease and phosphatase inhibitor cocktails) using OMNI Tissue homogenizer then sonicated for 3 s. Lysates were centrifuged at 18,350 x g for 15 min at 4 °C and the supernatant was collected for SDS-PAGE analysis. Protein concentration was determined by Bradford reaction (Bio-Rad 500-0006). Aliquots of samples (10-30 µg protein) were suspended in protein loading buffer (50 mM Tris pH 6.8, 300 mM glycerol, 25 mM SDS, 45 mM DTT, 260 mM 2-mercaptoethanol, bromophenol) separated on 10% SDS-PAGE gel and transferred to nitrocellulose membranes. Membranes were blocked in 0.1% Tween 20 in Tris-buffered saline (TBST) (10 mM Tris-HCl, 150 mM NaCl, 0.1% Tween 20; pH 7.5) with 5% fat-free milk for 1 h at room temperature. Membranes were incubated either overnight at 4 °C or for 2 h at room temperature with primary antibody diluted in TBST with 1% non-fat milk or 5% BSA. After washing, membranes were incubated for 1 h at room temperature with 1:20,000 anti-rabbit or anti-mouse HRP-conjugated IgG diluted in TBST with 1% non-fat milk. After washing, protein bands were detected with SuperSignal West Femto (Thermo 34095).

3.2.7. *Progesterone assay*

Media from luteal cells was diluted in water (1:150) and assayed for progesterone concentration using either RIA (Siemens TKPG1) or ELISA kit (DRG EIA-1561) following manufacturers' instructions and using a 4-parameter regression to interpolate unknowns from the standard curve.

3.2.8. *Lipid droplet isolation from cells*

Cells from 6-100 mm² dishes were washed twice with PBS and then scraped into PBS combined and centrifuged for 10 min at 1000 x g, 4 °C. Cells were resuspended in hypotonic lysis medium (20 mM Tris [pH 7.4], 1 mM EDTA, 10 mM NaF) and homogenized using a Parr cell

disruption bomb at 300 psi for 12 minutes. The post-nuclear supernatant was obtained by centrifuging the cell lysate for 10 min at 1,000 x g at 4 °C. The supernatant was mixed with an equal volume of hypotonic lysis medium containing 60% sucrose and loaded into a 30 mL polypropylene thick-walled ultracentrifuge tube, overlaid sequentially with 5% and 0% sucrose in HLM buffer. Samples were centrifuged at 110,000 x g (r_{avg}) for 30 min at 4 °C with no brake in Beckman Coulter Avanti J-20 XP and SW 32 Ti rotor. The LDs concentrated in a yellow/white band at the top of the gradient were harvested and concentrated by centrifugation at 2000 rcf for 10 min at 4 °C with no brake. The protocol was derived from ¹⁷⁵.

3.2.9. Proteomics

Acetone-precipitated LD proteins were suspended in 2x protein loading buffer (100 mM Tris pH 6.8, 600 mM glycerol, 50 mM SDS, 90 mM DTT, 525 mM 2-mercaptoethanol, and bromophenol blue) and boiled for 5 min at 100 °C. A 10% SDS-PAGE gel was used to separate LD proteins. Coomassie blue-stained gel pieces were manually cut into two pieces using a sterile scalpel and kept in sterile microcentrifuge tubes. Gel pieces were washed with HPLC water and shrunk by removing all liquid using 100% acetonitrile (ACN). Proteins were reduced using 2 mM tris(2-carboxyethyl)phosphine (TCEP) in 50 mM ammonium bicarbonate (AmBic) for 1 h at 37 °C. After incubation, ACN was added to TCEP to destain gel pieces. After gel pieces were dried by adding additional portion of ACN, thiol groups of proteins were alkylated with 55 mM iodoacetamide (IAA) in 50 mM AmBic for 20 min in dark. Samples were dried again with ACN and 10 nM MS-grade trypsin (Thermo Scientific, Rockford, IL, USA) was added for protein digestion. Samples were incubated with trypsin for 30 min on ice. After the excess of trypsin was removed from tubes, 25 mM AmBic was added to the gel pieces. Tryptic digestion continued overnight at 37 °C. Digested peptides were then extracted from gel with 50% ACN/0.1%

trifluoroacetic acid solution. Samples were dried in a Speedvac, dissolved in 15 μ L of 0.1% formic acid (FA) and submitted for LC-MS/MS analysis.

In-gel digested peptide samples were analyzed using high-resolution mass spectrometry LC-MS/MS system (LTQ Orbitrap Elite Velos Pro, Thermo Scientific, West Palm Beach, FL, USA), coupled with an Eksigent NanoLC-Ultra 1D plus (Eksigent, Dublin, CA, US) and nanoFlex cHiPLC system (Eksigent), equipped with two alternating peptide traps. 10 μ L of each sample were loaded onto the peptide trap using 0.1% FA solvent. The samples were eluted using a 1 hour linear gradient of 0–60% of ACN in 0.1% FA. The nanospray needle voltage was set to 2400 V in HPLC MS mode and linear ion trap scan mode was used for MS/MS. Resolution of the full scan in the Orbitrap was set to 120,000 m/z with a range from 300 to 2000 Da. The collision energy was set to 35 kV.

The MS/MS spectra from the peptides were analyzed by assigning the fragments to the candidate sequence using MASCOT search engine (Matrix Science, London, UK, version 2.5.1) with a Swissprot database (Taxonomy: Mammalia). Parameters on MASCOT were set as follows: Enzyme: trypsin, Max missed cleavage: 2, Peptide charge: 1+, 2+ and 3+, Peptide tolerance: ± 0.8 Da, Fixed modifications: carbamidomethyl (C), Variable modifications: oxidation (M), phospho (ST) and phospho (Y), MS/MS tolerance: ± 0.6 Da, Instrument: ESI-TRAP. MASCOT results for different gel cuts of the same sample were combined and analyzed using Scaffold (Proteome Software, Inc., Portland, OR, version 4.4.5), which allows multiple search results to be condensed into a single result file. Peptide identifications were accepted if they were established at greater than 95.0% probability by the Peptide Prophet algorithm²²² Scaffold delta-mass

correction. Protein identifications were accepted if they were established at greater than 95.0% Protein probabilities were assigned by the Protein Prophet algorithm²²³. Proteins that contained similar peptides and could not be differentiated based on MS/MS analysis alone were grouped to satisfy the principles of parsimony. Proteins sharing significant peptide evidence were grouped into clusters.

3.2.10. *Animals*

Post-pubertal multiparous female cattle (n = 15) of composite breeding (½ Red Angus, Pinzgauer, Red Poll, Hereford and ½ Red Angus and Gelbvieh) were synchronized using two intramuscular injections of PGF2 α (25mg; Lutalyse®, Zoetis Inc., Kalamazoo Michigan, MI) 11 days apart. A bilateral ovariectomy, between 3 and 10 days post-ovulation, was performed through a right flank approach under local anesthesia^{277,278}. The CL was removed from the ovary, weighed and 2.5 g was used for LD isolation (Section 3.2.11). All animal procedures were completed under an IACUC-approved protocol and performed at the University of Nebraska—Lincoln, Animal Sciences Department (Lincoln, NE). Statistical differences in animal characteristics were determined using one-way analysis of variance in GraphPad Prism (La Jolla, CA).

3.2.11. *Lipid droplet isolation from tissue*

Tissue (~2.5 g) was washed thoroughly in TE buffer (10 mM Tris, 1 mM EDTA, pH 7.4). Minced tissue was resuspended in 10 mL tissue homogenate buffer (60% sucrose w/v in TE buffer containing protease and phosphatase inhibitor cocktail) and homogenized with a Teflon Dounce homogenizer in a glass vessel. The post-nuclear supernatant fraction was obtained after centrifugation at 2000 rcf for 10min. The supernatant was loaded into a 30 mL ultracentrifuge tube and overlaid sequentially with 40%, 25%, 10%, and 0% sucrose (w/v) in TE buffer containing protease and phosphatase inhibitor cocktails. Samples were centrifuged at 111,000 x g (r_{avg}) for 30 min at 4 °C with no brake in a Beckman Coulter Avanti J-20 XP ultracentrifuge using

an SW 32 Ti rotor. The LDs concentrated in a yellow/white band at the top of the gradient were harvested and concentrated by centrifugation at 2000 rcf for 10 min at 4 °C, the protocol was modified from ^{174,175}.

3.2.12. Western blots of LDs

Acetone-precipitated LD proteins were suspended in 2x protein loading buffer (100 mM Tris pH 6.8, 600 mM glycerol, 50 mM SDS, 90 mM DTT, 525 mM 2-mercaptoethanol, and bromophenol blue) and boiled for 5 min at 100 °C, separated on a 10% SDS-PAGE gel, and transferred to nitrocellulose membranes. Membranes were blocked in TBST (10 mM Tris-HCl, 150 mM NaCl, 0.1% Tween 20; pH 7.5) with 5% fat-free milk for 1 h at room temperature. Membranes were incubated either overnight at 4 °C or for 2 h at room temperature with primary antibody diluted in TBST with 1% non-fat milk or 5% BSA. After washing, membranes were incubated for 1 h at room temperature with 1:20,000 anti-rabbit or anti-mouse HRP-conjugated IgG diluted in TBST with 1% non-fat milk. After washing, protein bands were detected with SuperSignal West Femto (Thermo 34095).

3.3. Results

3.3.1. Formation of LDs during differentiation

Previously we identified LD-associated protein transcripts for *PLIN2*, *PLIN3*, and *LIPE* (the gene encoding HSL) were increased in both steroidogenic luteal cell types over their follicular counterparts, as assessed by microarray (GSE83524) (Figure 3-1 A) ²²⁰. The protein abundance of *PLIN2* and HSL was increased in luteal tissue as assessed by Western blot (Figure 3-1 B). *In vitro* differentiation of granulosa cells with 1% ITS + 10 μM forskolin, increased the amounts of HSL, *PLIN2*, *StAR*, *P450scc*, and *3βHSD* that were intermediate to levels seen in luteal cells (Figure 3-2 A). As well, progesterone secretion gradually increased over 7 days in culture with treatment of ITS + 10 μM forskolin, whereas control treated cells maintained a low level of progesterone

secretion (B). The differentiation protocol of 1% ITS + 10 μ M forskolin increased LD formation in both bovine and human granulosa cells (C & D).

3.3.2. *Phosphorylation of HSL at Ser563 by LH and LH signaling intermediates*

Luteal cells were treated with LH, forskolin (an adenylate cyclase activator), and 8-bromo cyclic AMP (a protein kinase A activator) to determine whether LH and LH signaling pathways phosphorylated HSL at its activation site Ser563. Treatment of mixed luteal cells with LH, forskolin or 8-Br cAMP increased phosphorylation of the PKA-sensitive site Ser563 on HSL within 5 minutes and was sustained for 4 h (Figure 3-3).

3.3.3. *Regulation of LDs*

Luteal cells were pretreated with an HSL inhibitor, CAY10499, before stimulation with LH and/or high-density lipoprotein (HDL) as an exogenous cholesterol source. CAY10499 inhibited LH-induced progesterone secretion by bovine luteal cells with pretreatment of 10 and 20 μ M CAY10499 (Figure 3-4 A). Treatment with LH stimulated progesterone synthesis (SLC: 6-fold, LLC: 3.6-fold) which was increased with co-incubation with HDL (SLC: 11.3-fold, LLC: 5-fold). CAY10499 pretreatment prevented both the LH- and HDL + LH-induced progesterone secretion but had no effect on basal progesterone secretion in either SLC or LLC (Figure 3-4 C & D). The influence of off-target effects of CAY10499 was excluded because inclusion of hydroxylated cholesterol could still increase luteal progesterone secretion [Appendix A-2]

3.3.4. *PKA stimulation promotes alterations in the luteal LD proteome*

Stimulation of luteal tissue punches with the PKA activator 8-br-cAMP resulted in phosphorylation of HSL at Ser563 and an increased HSL localization on luteal LDs (Figure 3-5). The LDs isolated from untreated and 8-Br cAMP-treated luteal cells were acetone-precipitated and the protein content was analyzed by proteomics. LC-MS/MS analysis determined 469 bovine-specific proteins were present in bovine LDs isolated from cultured mixed luteal cells; of these, 85 proteins were increased in 8-Br cAMP-treated samples, and 48 were decreased. The top

ten most abundant proteins in both treated and untreated LDs included 3 β HSD, PLIN2, vimentin, and P450scc. Proteins with increased abundance on luteal lipid droplets following 8-bromo cAMP treatment included LD coat protein PLIN2, trafficking (Rab8A, Rab14), and steroidogenesis (StAR, 3 β HSD) [Appendix A-3].

3.3.5. *Luteal LDs are associated with steroidogenic enzymes*

Confirmation of proteomics results was achieved by Western blot analysis of purified LDs from functional bovine CLs obtained by ovariectomy. PLIN3, vimentin, P450scc, and 3 β HSD were all significantly enriched in luteal LDs compared to whole luteal tissue. However, mitochondrial marker COX IV and endoplasmic reticulum marker HSP47 were nearly absent from luteal LDs (Figure 3-6). Quantification of immunodetection by Western blot is available in [Appendix A-5].

3.4. Discussion

Lipid droplets and LD-associated proteins are under regulation by LH signaling in the bovine CL. As granulosa cells differentiate to form luteal cells, increases in both LDs and LD-associated proteins, HSL and PLIN2 are seen which correlate with luteal differentiation markers and progesterone secretion. Signaling by LH causes phosphorylation of HSL at Ser563 and translocation of HSL to the LD surface (these changes activate HSL). Furthermore, chemical inhibition of HSL by CAY10499 prevents LH-induced progesterone secretion even in the presence of HDL-supplied cholesterol indicating that cholesteryl esters originating either in LDs or delivered by HDL are processed by an HSL-dependent step. Finally, luteal LDs have a high content of steroidogenic enzymes including, 3 β HSD and P450scc. Furthermore, LD-associated StAR can increase by 14-fold after treatment with 8-br cAMP. These data lead us to hypothesize that the surface of LDs may serve as a novel platform for steroidogenesis through the intimate association and potential tethering of steroidogenic enzymes to the coat proteins of the LD

facilitating the handoff of steroid precursors at each step to produce steroids, like progesterone (Figure 3-7).

Differentiation of granulosa cells occurs after ovulation and is accompanied by increases in steroidogenic enzymes 3β HSD, P450_{scc}, and StAR, which promote an increase in progesterone secretion. As bovine granulosa cells differentiate, LDs form and LD-associated proteins increase in correspondence with standard differentiation markers. This is confirmed by the previous work of Meidan *et al.* which examined the *in vitro* differentiation of theca and granulosa cells into luteal-like cells¹⁸⁹. This indicates that LD accumulation may be a natural consequence of granulosa to luteal cell differentiation.

HSL is a key regulator of lipolysis in adipose tissue. In fat tissue, HSL is phosphorylated by PKA on Ser563 that is correlated with translocation of HSL to LDs and activation of its lipase activities. Activated HSL results in the release of cholesterol and free fatty acids from neutral lipid stores within LDs for cellular use. We have shown that HSL can be phosphorylated at S563 after treatment with LH, forskolin, or 8-bromo cAMP. Pretreatment of luteal cell cultures with a chemical inhibitor of HSL activity, CAY10499, could prevent LH- and LH+HDL-stimulated progesterone secretion. LH may regulate the phosphorylation of PLINs and HSL via a cAMP/PKA signaling pathway allowing for hydrolysis of cholesteryl esters stored in luteal LDs to produce substrate for progesterone synthesis. This indicates that stimulated but not basal progesterone is processed through an HSL-dependent and likely LD-dependent step.

Isolated luteal LDs were examined using both a non-targeted and targeted approaches. It was determined that the steroidogenic enzymes StAR, P450_{scc}, and 3β HSD were found in the LDs fraction in addition to known LD markers such as PLIN2, PLIN3, vimentin, and HSL. However, other mitochondrial and endoplasmic reticulum markers were not abundant, indicating a selective association with steroidogenic enzymes. Taken together, these data indicate that the surface of LDs may serve as a novel platform for steroidogenesis by an intimate association with

steroidogenic enzymes, allowing for the handoff of steroid precursors from the LD to the mitochondria and endoplasmic reticulum for steroidogenic modifications of cholesterol. Possible interactions between LDs, mitochondria, and the endoplasmic reticulum could involve physical tethering of the membranes similar to mitochondrial associated membranes, whereby the mitochondria and endoplasmic reticulum have microdomains of highly associated membranes to facilitate lipid transfer ²²⁴.

We found evidence for enrichment of known LD-associated proteins on luteal LDs including HSL, PLIN3, and vimentin. Additionally the steroidogenic enzymes P450scc and 3 β HSD were enriched in the LD fraction. This is similar for the LD proteome determined for other steroidogenic cells including the MLTC-1 Leydig cell line (analogous to the granulosa cells of the female reproductive tract), ⁵⁶ LDs purified from mouse testes, ⁵⁷ and lipid-loaded rat granulosa cells⁵⁵. The finding of steroidogenic enzymes within the LD proteome by four separate groups indicate this is an important feature of LDs within steroidogenic cells and is not simply a matter of contamination. Ultrastructural studies have often noted the close proximity of mitochondria with LDs ²²⁵, and the emerging field of mitochondrial associated membranes offers the possibility that there are regionalized areas of contact between mitochondria and LDs ²²⁶.

Khor *et al.* compared the proteome of LDs from rat granulosa cells treated *in vitro* with either HDLs or fatty acids to enrich cytoplasmic LDs with cholesteryl esters or triacylglycerides, respectively ⁵⁵. When comparing the LD proteomes, a large number of proteins (278) were common to the LDs prepared from either treatment. These proteins included PLIN2 and were similar to other studies on LD proteomes. They also identified 61 proteins unique to the cholesteryl ester-rich LDs and 40 proteins unique to triacylglycerol-rich LDs. Notably, they identified 3 β HSD, vimentin, and voltage-dependent anion channel proteins enriched in the cholesteryl ester-rich LDs. Recent reports on the proteomic analysis of LD isolated from the

mouse Leydig tumor cell line MLTC-1⁵⁶, and mouse testes⁵⁷ also revealed the presence of PLIN family proteins and enzymes involved in the synthesis of steroid hormones.

Previous studies that have examined the LD proteome in steroidogenic tissues have also found steroidogenic enzymes^{55,57}. Reports in the monkey²³ and mouse²⁴ indicate that the ovary expresses PLIN2, a LD coat protein associated with cholesteryl ester storage²⁵. Manna *et al.* recently reported that activation of the PKA pathway in MA-10 mouse Leydig cells enhanced expression of HSL and its phosphorylation at Ser-563 and Ser-660. Additionally, inhibition of HSL activity suppressed cAMP-induced progesterone synthesis and resulted in increased cholesteryl ester levels in MA-10 cells⁴². The data presented herein complements these observations and provides mechanisms for regulation of LD-associated proteins in luteal cells.

Also of interest is a report⁴³ demonstrating an interaction between StAR and HSL in the rat adrenal following treatment with adrenocorticotrophic hormone. Furthermore, the co-expression of StAR and HSL resulted in elevated HSL activity and mitochondrial cholesterol content⁴³. These observations, suggest that the proteins involved in production and transport of cholesterol may co-localize in LDs and mitochondria. We have observed that mitochondria are closely associated with cytoplasmic LDs in bovine luteal cells (Figure 1-1 B)¹⁶¹. These observations, in combination with this study, indicate that luteal LDs and mitochondria may interact to facilitate steroidogenesis.

These data improve our understanding of the biochemistry of steroidogenesis. As we learn more about how cholesterol is stored and utilized, particularly during steroidogenesis we can gain insight into how to manipulate steroidogenesis to either increase or decrease steroid production. Our study has focused on non-pathological conditions to gain a clear insight into the role of LDs in highly steroidogenic tissues. Future studies into how LDs and flux of cholesterol through cells is altered in obesity and polycystic ovarian syndrome could indicate mechanisms by which those conditions impair fertility, specifically if steroid production or LD formation is altered.

Additionally, further analysis of the additional cholesteryl esterases and activity will clarify how the pathways of steroidogenesis within the luteal tissue are regulated. Furthermore, a direct investigation into the presence of mitochondrial and endoplasmic reticulum tethering to the LD surface is ongoing.

Formation of LDs during granulosa to luteal cell differentiation appears to be a normal, and potentially necessary accumulation. Stimulated, but not basal, progesterone is processed through an HSL-dependent, and likely LD-dependent step. The surface of LDs may serve as a novel platform for steroidogenesis by an intimate association with steroidogenic enzymes. The close proximity of mitochondria and the endoplasmic reticulum may facilitate the handoff of steroid precursors at each step to efficiently produce steroids such as progesterone. We postulate that progesterone synthesis is enhanced by physical tethering of mitochondria and the endoplasmic reticulum to the LD surface using a similar mechanism to mitochondrial associated membranes, which tether microdomains of the endoplasmic reticulum to mitochondria to facilitate lipid transfer ²²⁴. Our results support a growing body of research indicating that LDs play a critical role in steroid production and may provide novel biomarkers of infertility and therapeutic targets for altering fertility status of humans and other mammals.

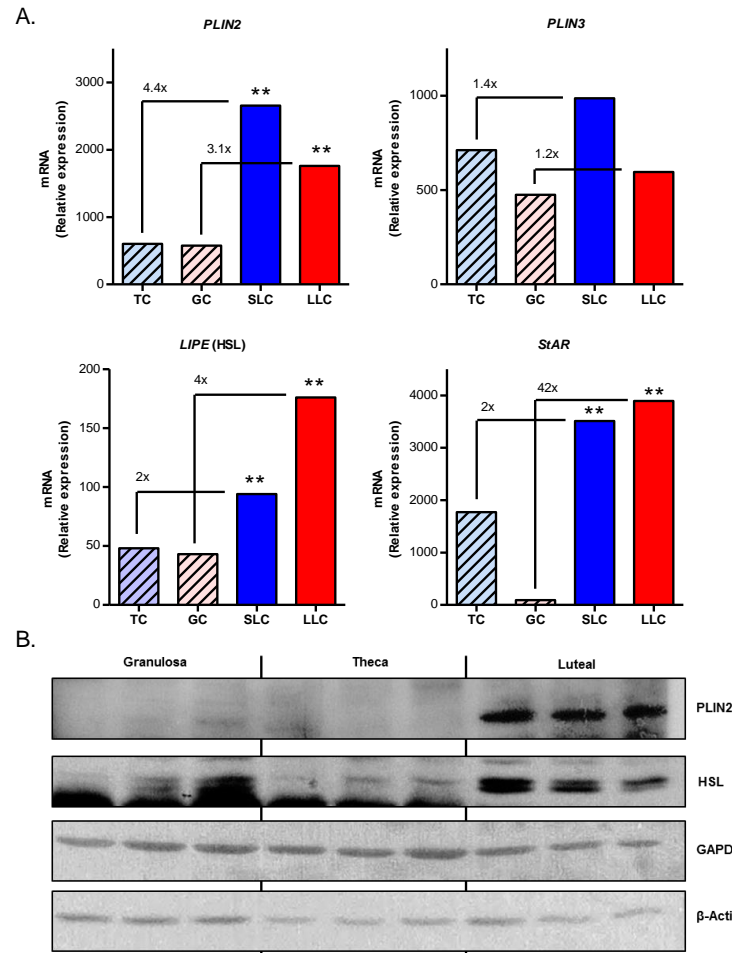


Figure 3-1 – Lipid droplet-associated proteins were expressed at greater amounts in luteal cells at both transcriptional and protein levels

(A) Microarray-determined relative transcription expression levels of key LD-associated coat proteins perilipins 2 and 3 (*PLIN2* and *PLIN3*, respectively), hormone sensitive lipase (HSL, gene name *LIPE*), and luteal differentiation marker steroidogenic acute regulatory protein (*StAR*) fold changes from precursor follicular cells to luteal cell types is written above brackets. Gene expression data was generated in a previous study and is publically available (GSE83524)²²⁰. (B) Western blot analysis of freshly-isolated granulosa, theca, or luteal tissue for expression of *PLIN2*, *HSL* with *GAPDH* and β -actin as loading controls. ** $P \leq 0.01$

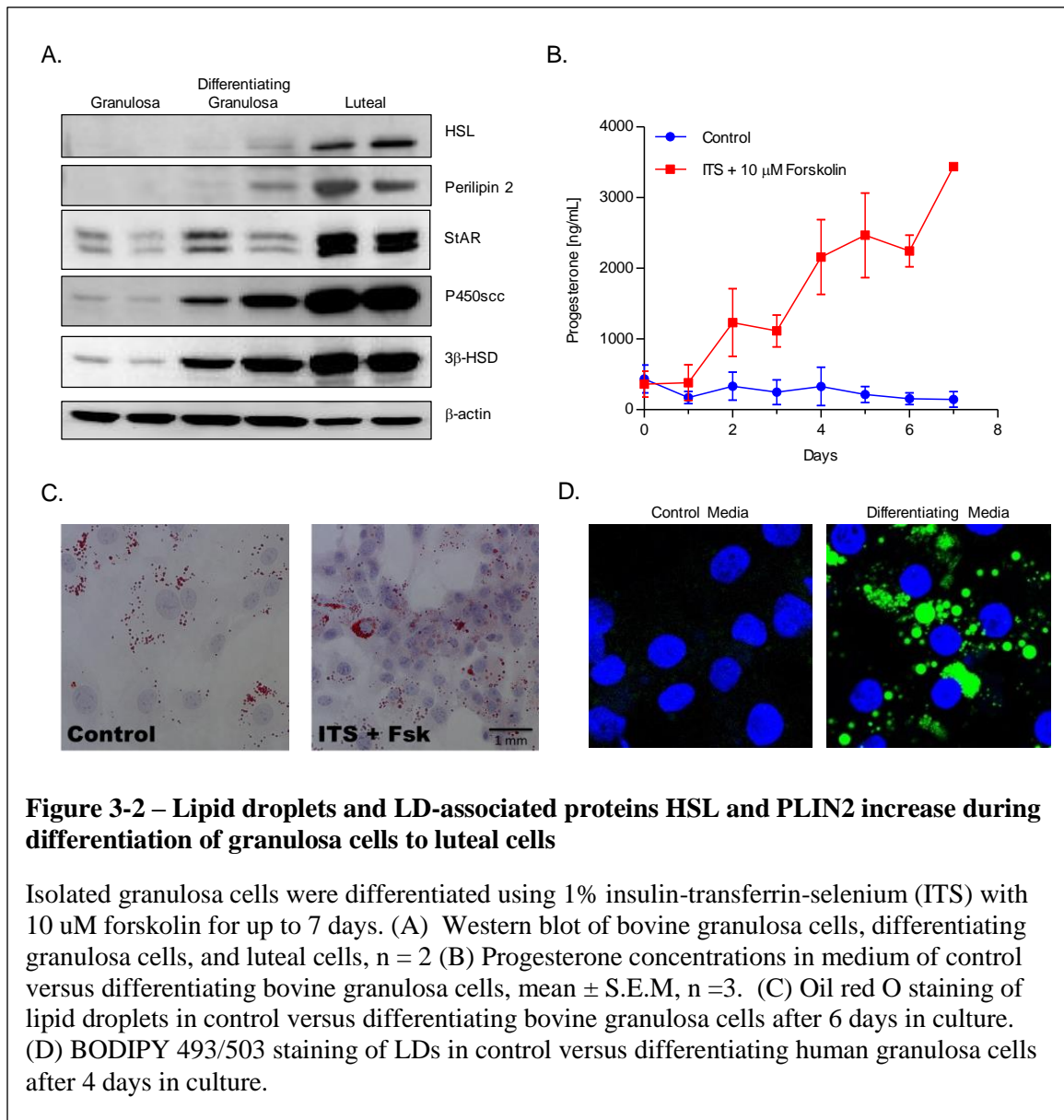
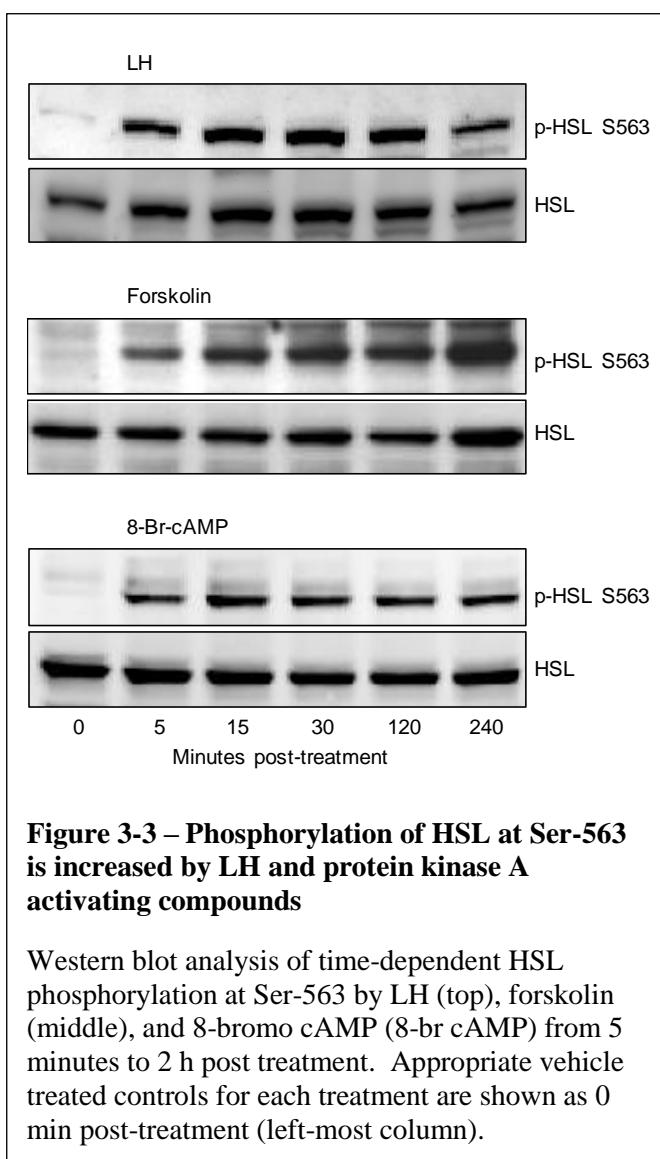
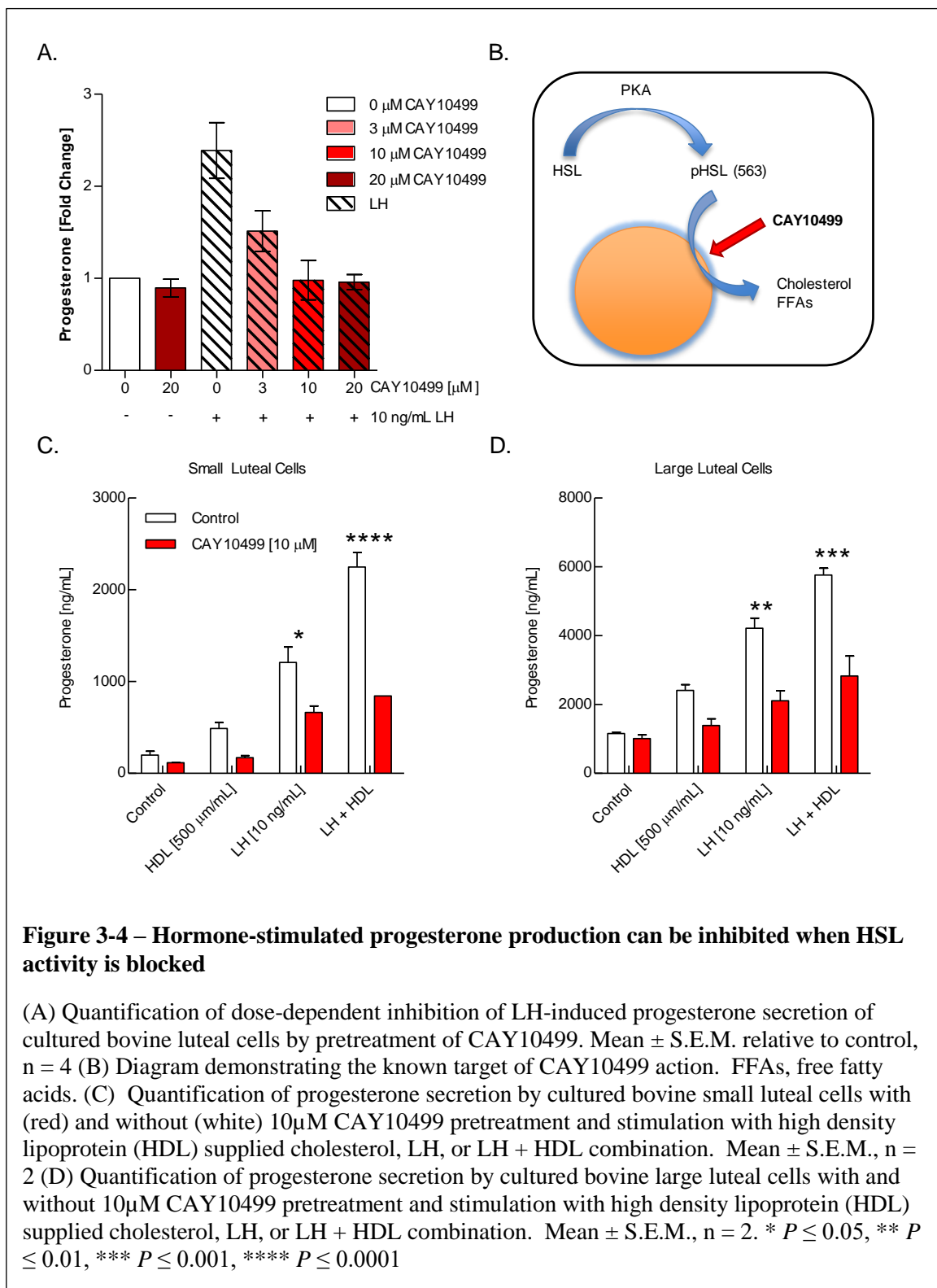
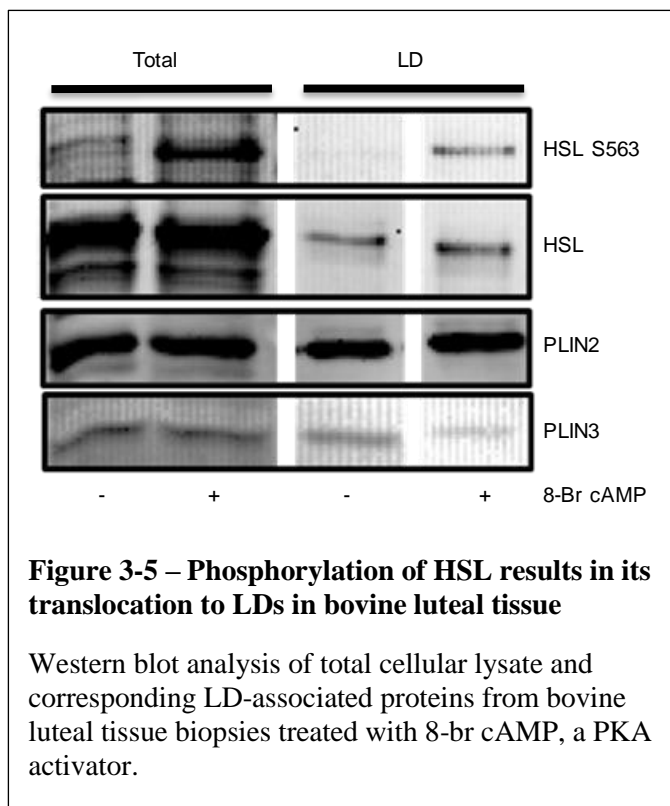


Figure 3-2 – Lipid droplets and LD-associated proteins HSL and PLIN2 increase during differentiation of granulosa cells to luteal cells

Isolated granulosa cells were differentiated using 1% insulin-transferrin-selenium (ITS) with 10 μ M forskolin for up to 7 days. (A) Western blot of bovine granulosa cells, differentiating granulosa cells, and luteal cells, $n = 2$ (B) Progesterone concentrations in medium of control versus differentiating bovine granulosa cells, mean \pm S.E.M, $n = 3$. (C) Oil red O staining of lipid droplets in control versus differentiating bovine granulosa cells after 6 days in culture. (D) BODIPY 493/503 staining of LDs in control versus differentiating human granulosa cells after 4 days in culture.







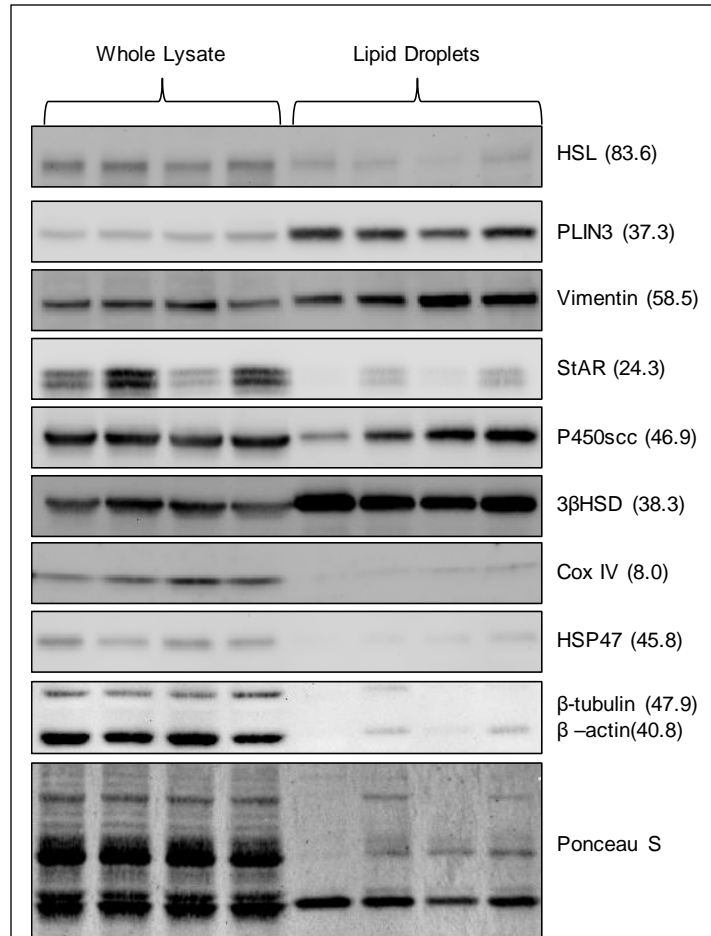
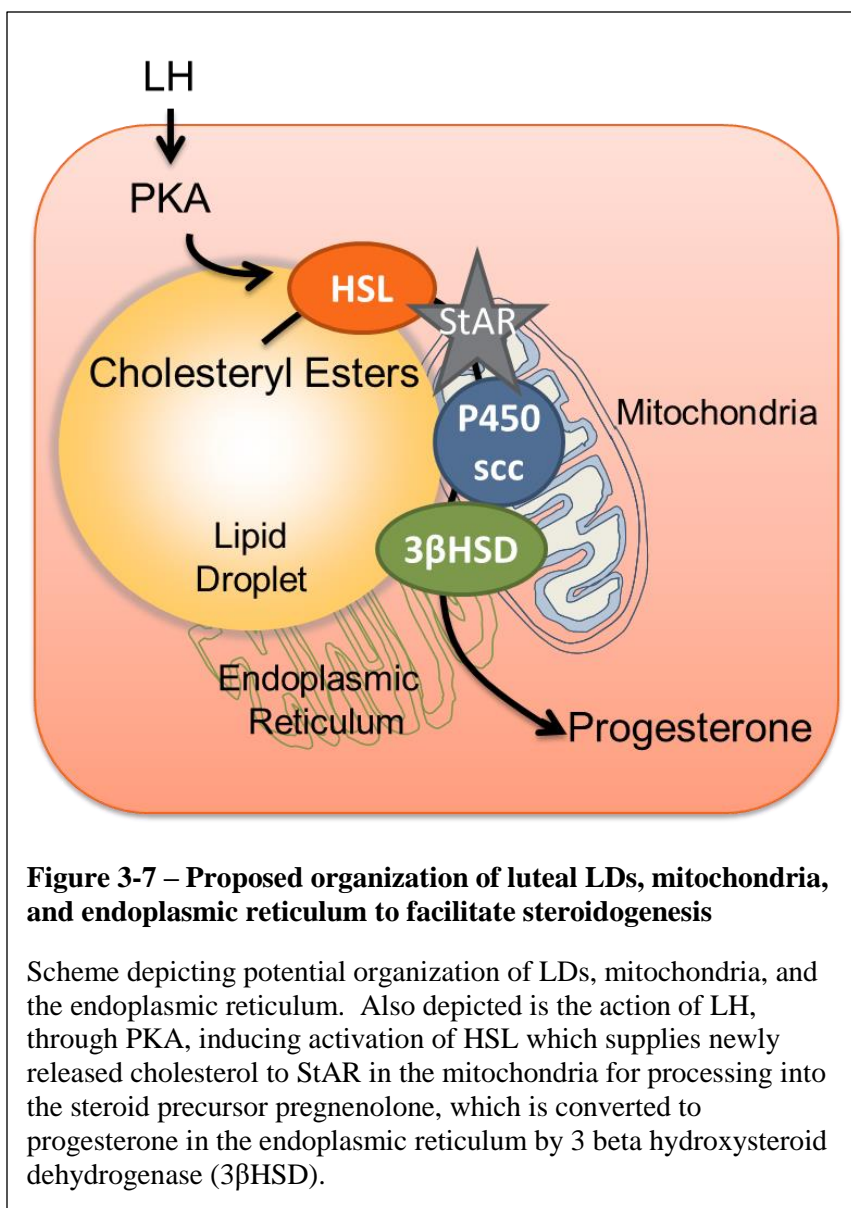


Figure 3-6 – Western blot analysis of LD associated proteins from functional bovine CL confirms proteomic identification of LD-associated steroidogenic enzymes

Western blot analysis of total cellular lysate and corresponding LD-associated proteins from fully functional bovine luteal tissue. Each panel is labeled with the examined protein and the apparent molecular weight of the band based on simultaneously run markers follows each protein in parentheses (kDa).



CHAPTER 4: EARLY TRANSCRIPTOME RESPONSES OF THE BOVINE MID-CYCLE CORPUS LUTEUM TO PROSTAGLANDIN F2 ALPHA INCLUDES CYTOKINE SIGNALING §

Abstract

In ruminants, prostaglandin F2alpha (PGF2α)-mediated luteolysis is essential for initiation of the estrous cycle and is a target for improving fertility. To deduce early PGF2α-provoked changes in the corpus luteum a short time-course (0.5–4 h) was performed on cows at mid-cycle. A microarray-determined transcriptome was established and examined by bioinformatic pathway analysis. Classic PGF2α effects were evident by changes in early response genes (FOS, JUN) and prediction of active pathways (PKC, MAPK). Several cytokine transcripts were elevated and NF-κB and STAT activation were predicted by pathway analysis. Self-organizing map analysis (SOMs) grouped differentially expressed transcripts into ten mRNA expression patterns indicative of temporal signaling cascades. Comparison with two analogous datasets revealed a conserved group of 124 transcripts similarly altered by PGF2α treatment, which both, directly and indirectly, indicated cytokine activation. Elevated levels of cytokine transcripts after PGF2α and predicted activation of cytokine pathways implicate inflammatory reactions early in PGF2α-mediated luteolysis.

§ The material presented in this chapter was submitted as a manuscript: Talbott *et al.* Early transcriptome responses of the bovine mid-cycle corpus luteum to prostaglandin F2α includes cytokine signaling. *Molecular and Cellular Endocrinology* 2017 ²²¹.

4.1. Introduction

In mammals, multiple fertile cycles depend on the formation and regression of a transient endocrine structure in the ovary termed the corpus luteum (CL) ^{134,227}. The CL forms at the beginning of each estrous cycle and synthesizes progesterone, a hormone critical for early embryonic survival during pregnancy ^{135–137,228}. However, before the next follicle can develop, the steroidogenic luteal cells of the CL must cease the production of progesterone—contingent on the absence of a pregnancy—and ultimately undergo apoptosis ^{123,229}. Prostaglandin F_{2α} (PGF_{2α}) is a recognized lipid mediator that triggers CL regression after an unsuccessful reproductive cycle or at parturition in mammals ^{65,134,230}. Thus, PGF_{2α}-mediated luteolysis is a key checkpoint in the reproductive cycle and is a useful target for controlling the estrous cycle and fertility.

Signaling by PGF_{2α} has been studied extensively *in vitro*, and the classic signaling pathway involves the binding of PGF_{2α} to its G-protein-coupled receptor and activating Gα_{q/11} ^{231–233}. The early intracellular signaling events initiated by PGF_{2α} in luteal cells include the activation of phospholipase C ^{234,235}, phospholipase A₂ ^{236,237}, an increase in intracellular Ca²⁺ ²³⁵, activation of protein kinase C (PKC) ¹⁰⁵ and activation of mitogen-activated protein kinase (MAPK) signaling cascades including extracellular signal-regulated kinase (ERK) ^{105,238–241}. These signaling cascades are responsible for the transcriptional and translational induction of several early response genes including transcription factors such as, Finkel-Biskis-Jenkins murine osteosarcoma viral oncogene homolog (*FOS*) ¹⁰⁵, Jun proto-oncogene (*JUN*) ¹⁰⁵, early growth response 1 (*EGR1*) ¹⁰⁶, and activating transcription factor 3 (*ATF3*) ¹⁰⁴. The transcription factors induced by PGF_{2α} control the abundance of target messenger RNAs (mRNAs) which, when translated, alter the luteal proteome enabling luteolysis to proceed. For example, sustained ATF3 expression can inhibit luteinizing hormone-induced progesterone production by bovine luteal cells ¹⁰⁴. As well, EGR1 expression stimulates the synthesis of transforming growth factor beta (TGFβ) ¹⁰⁶, which coordinates the activities of a number of cell types during luteal regression.

Specifically, TGF β inhibits luteal progesterone secretion^{106,242,243}, acts on luteal endothelial cells to disrupt the microvasculature²⁴⁴, and stimulates the profibrotic activity of luteal fibroblasts²⁴⁵.

The luteolytic process is a well-coordinated series of events similar to an acute inflammatory response consisting of a sequential time-dependent infiltration of neutrophils^{205,207,246,247}, macrophages^{205,209,248–250}, and T lymphocytes^{205,209,248,251}. Accordingly, there is likely time-dependent secretion of cytokines to recruit and activate the various leukocytes^{203,252–254}. Several cytokine transcripts are induced by PGF2 α in the mid- to late-stage CL including tumor necrosis factor alpha (*TNF*)^{255,256}, interleukin 1 beta (*IL1B*)^{108,255,257}, interferon gamma²⁵⁵, *TGFB1*^{106,256,257}, and the chemokines; C-C motif chemokine ligand 2 (*CCL2*, previously known as *MCPI*)^{257–259} and C-X-C motif 8 (*CXCL8*, previously known as *CXCL8*)^{108,207,246,256,257,260}. These cytokines have pleiotropic effects on luteal cells, including inhibition of progesterone secretion^{261–266}, stimulation of PGF2 α secretion^{263–267}, and stimulation of apoptosis of multiple luteal cell types^{262,263,268–272}. The production of luteolytic factors, decrease in progesterone secretion, recruitment of immune cells, the release of pro-inflammatory cytokines, reduction in blood supply, and the creation of a hypoxic environment^{273,274} likely act in concert within the CL to cause the functional and structural regression of the CL.

The purpose of this study was to understand the early PGF2 α -elicited changes in the CL based on temporal patterns of early transcript expression following *in vivo* treatment with PGF2 α . While many studies have examined luteolytic alterations both *in vivo* and *in vitro*, most studies have focused on changes 3-24 hours after PGF2 α administration^{256,257} or used targeted rather than global approaches^{108,275,276}. Therefore, little is known about the very early temporal changes in global mRNA expression elicited in response to PGF2 α treatment *in vivo*. Examination of the early transcriptional responses to PGF2 α will provide a context for understanding the events responsible for orchestrating the cascade of events required for functional and eventual structural regression of the CL. In the present study, a systems biology approach using Affymetrix Bovine

Arrays was employed to evaluate gene expression at 0.5 - 4 hours post-PGF2; followed by bioinformatics analysis of PGF2 α -mediated signals. We hypothesized that the sequence of events after *in vivo* PGF2 α administration would include early changes of classical targets of PGF2 α signaling pathways followed by fluctuations in targets of cytokine signaling at later time-points.

4.2. Materials and Methods

4.2.1. Animals

Post-pubertal multiparous female cattle (n = 15) of composite breeding (½ Red Angus, Pinzgauer, Red Poll, Hereford and ½ Red Angus and Gelbvieh) were synchronized using two intramuscular injections of PGF2 α (25mg; Lutalyse®, Zoetis Inc., Kalamazoo Michigan, MI) 11 days apart. At mid-cycle (days 9-10), cows were treated with an intramuscular injection of saline (n = 3) or PGF2 α (n = 12). At each of four time-points post-injection (0.5, 1, 2, and 4 h) three cows per treatment were subjected to a bilateral ovariectomy through a right flank approach under local anesthesia^{277,278}. The CL was removed from each ovary, weighed and < 5 mm³ sections were snap-frozen in liquid N₂ for subsequent protein and ribonucleic acid (RNA) analysis. Plasma progesterone concentrations were determined using the ImmuChem Progesterone Coated Tube radioimmunoassay kit (MP Biomedicals, Santa Ana, CA) with an intra-assay coefficient of variation of 9.13% and inter-assay coefficient of variation of 7.99%. The University of Nebraska-Lincoln Institutional Animal Care and Use Committee approved all procedures and facilities used in this animal experiment and animal procedures were performed at the University of Nebraska—Lincoln, Animal Science Department. Statistical differences in animal characteristics were determined using Kruskal-Wallis test followed by Dunn's post-test or one-way analysis of variance followed by Bonferroni's multiple comparison test as appropriate (GraphPad Prism, La Jolla, CA).

4.2.2. *Steroidogenic luteal cell culture*

Bovine ovaries were collected during mid-cycle or early pregnancy from a local slaughterhouse (JBS® USA, Omaha, NE). Steroidogenic cells were prepared from luteal slices by enzymatic digestion with type II collagenase (103 IU/mL) as described previously¹⁰⁶. Enriched fractions of small luteal cells (SLC) and large luteal cells (LLC) were prepared from CLs of early pregnancy using centrifugal elutriation similar to a previous study¹⁰⁴. The unseparated luteal cells were resuspended in elutriation medium (calcium-free Dulbecco's modified eagle medium (DMEM) [D9800-10 US Biological, Salem, MA], supplemented with 25 mM 4-(2-hydroxyethyl)-1-piperazineethanesulfonic acid (HEPES), 3.89 g/L sodium bicarbonate, and 3 mg/mL glucose). Resuspended cells were subjected to centrifugal elutriation with continuous flow using a Beckman Coulter Avanti J-20 XP centrifuge equipped with a Beckman JE-5.0 elutriator rotor. The first 100 mL fraction containing primarily erythrocytes and endothelial cells was collected using 1800 rpm and 16 mL/min flow rate, the next 100 mL were discarded. The second 100 mL fraction contained endothelial and SLC (1400 rpm and 16 mL/min). The third 100 mL fraction contained primarily SLC (1200 rpm, 24 mL/min), and the next 100 mL were discarded. The fourth fraction contained primarily LLC (680 rpm and 30 mL/min). The fractions containing SLC and LLC were pelleted and resuspended in basal M199 (0.1% bovine serum albumin (BSA), 100 U/ml penicillin, 100 µg/ml streptomycin, and 10 µg/ml gentamycin). The average purity of SLC was ~90% and LLC was > 50%.

Cells were seeded at a density of 1×10^5 cells/cm² for mid-cycle mixed luteal cells, 1×10^5 cells/cm² for SLC and a density of 4×10^4 cells/cm² for LLC. Cells were allowed to attach in a 5% CO₂ incubator at 37 °C in basal M199 medium containing 5% fetal bovine serum. The next day, the medium was removed and cells washed with phosphate-buffered saline. The cells were incubated in serum-free medium for 3 hours before applying treatments as described in the legends to the figures [PGF2α (in ethanol, #16010, Cayman Chemical, Ann Arbor, MI), TNFα (210-TA, R&D, Minneapolis, MN), IL-1β (RP0106B), IL-6 (RP0014B), IL-17A (RP0056B,

Kingfisher Biotech, Saint Paul, MN)]. Luteal cell cultures were harvested into lysis buffer (20 mM Tris [pH 7.5], 150 mM NaCl, 1 mM EDTA (ethylenediaminetetraacetic acid), 0.2 mM EGTA, 1% Triton X-100, protease and phosphatase inhibitor cocktails) and lysed by sonication.

Lysates were centrifuged at 18,000 g for 15 minutes at 4 °C and the supernatant collected for suspension in sodium dodecyl sulfate (SDS) loading buffer (50 mM Tris [pH 6.8], 300 mM glycerol, 25 mM SDS, 45 mM dithiothreitol, 260 mM 2-mercaptoethanol, bromophenol blue). Proteins were separated by electrophoresis using 10% SDS-polyacrylamide gels and transferred to nitrocellulose membranes. Membranes were blocked with 5% non-fat milk in 0.1% Tween 20 in Tris-buffered saline (TBST) then incubated overnight with the primary antibody diluted in 1% non-fat milk or BSA in TBST at 4 °C. After three, 5-minute washes with TBST, membranes were incubated for 1 hour at room temperature with anti-rabbit or mouse (1:20,000) horseradish peroxidase-conjugated IgG diluted in TBST with 1% non-fat milk. After three 5-minute washes, protein bands were detected with ECL reagent (SuperSignal West Femto Thermo Science, Miami, OK, or PerkinElmer, Waltham, MA). Signals were visualized on FluorChem M (ProteinSimple, San Jose, CA) or UVP (UVP, LLC, Upland, CA) systems. Phosphorylated nuclear factor kappa B (NF- κ B) subunit P65 (phospho-P65, 3031 AB_330559) and phosphorylated ERK1/2 P44/P42 (phospho-P44/P42, 9101, AB_331646) antibodies were from Cell Signaling Technology (Danvers, MA); β -actin (A5441, AB_476744) and β -tubulin (T4026, AB_477577) antibodies were from Sigma (St. Louis, MO); and anti-mouse (115-035-205, AB_2338513) and anti-rabbit (111-035-003, AB_2313567) HRP-conjugated IgG from Jackson (West Grove, PA). Protein band density was analyzed using UVP software (Version 6.7.4), using area density of equally sized rectangles encompassing the bands at the appropriate molecular weight, normalized to the corresponding β -actin density and compared to control treatment by fold change.

4.2.3. *Affymetrix bovine gene chip microarray*

Each CL from the *in vivo* experiment described in *Section 2.1* was homogenized and RNA was extracted using a Stratagene RNA Isolation Kit (Santa Clara, CA) following manufacturer's instructions. Transcriptional changes were analyzed by hybridization of 500 ng biotinylated cDNA using Affymetrix (Santa Clara, CA) bovine whole-transcript microarray (Bovine Gene v1 Array [BovGene-1_0-v1]; GPL17645) at the University of Nebraska Medical Center Microarray Core Facility. Validation of target transcripts was performed after reverse transcription of 1 µg RNA using SuperScript II Reverse Transcriptase (Invitrogen, Grand Island, NY) followed by quantitative real-time PCR (qPCR) using gene-specific primers (Appendix B-1) on a CFX96 Touch™ Real-Time PCR Cycler (Bio-Rad, Hercules, CA) with SsoFast™ EvaGreen® Supermix (Bio-Rad, Hercules, CA). Comprehensive microarray methods and data are available in the Gene Expression Omnibus (GEO) database under accession GSE94069 and are described in the accompanying Data in Brief article ²⁷⁹.

4.2.4. *Microarray statistics*

The microarray data were preprocessed using the robust multi-array average (RMA) method from Affymetrix expression console software (Affymetrix Inc., Santa Clara, CA) to normalize data at the exon level. The mean intensities of multiple probe sets of the same gene were calculated under each array to obtain the corresponding gene expression intensities. The data was filtered to keep the genes with a raw expression value after preprocessing to be 10 or more for at least three of the 15 samples. Linear Models for Microarray Analysis ²⁸⁰ in the Bioconductor suite ²⁸¹ under the statistical program R ²⁸² was applied to compare the log ratio between each of the PGF2α time-points and the saline control after adjusting for the box effect. R code used to process the data is available in ²⁷⁹. Transcripts with a fold change of at least 1.5 and a Benjamini-Hochberg adjusted *P*-value of less than 0.05 for each treatment condition versus control were identified as differentially expressed genes.

4.2.5. Self-organizing maps and statistics

Microarray data was filtered to keep genes with a raw expression value after preprocessing to be 30 or more for at least three of the 15 samples. The log ratio between each of the time-points and the saline control were compared using Linear Models of Microarray Analysis in the Bioconductor suite in R. The self-organizing map (SOM) clustering algorithm GeneCluster 2.0²⁸³ was applied to differentially expressed genes that had a greater than 1.5-fold change in expression and $P\text{-value} \leq 0.05$ between PGF2 α -treated samples and the saline control. The mean normalized log₂ intensity values from each of the five examined biological conditions were used as transcript expression profiles in the clustering analysis. The number of iterations in SOM clustering was set to 500,000 to generate SOMs and hierarchical clustering (correlation-based distance, average link).

4.2.6. Dataset comparisons

Two previously published microarray datasets, GSE23348²⁵⁷ and GSE27961²⁵⁶ examined the effect of *in vivo* PGF2 α or analog treatment on the bovine luteal transcriptome using Affymetrix Bovine Whole Genome Gene Chips (GPL 2112). These datasets were chosen for comparison to the transcriptome dataset presented herein based on similarities in the experimental protocol comparing mid-cycle control CL expression profiles to CL profiles after treatment with PGF2 α or analog for 4 hours (GSE23348) or 6 hours (GSE27961). Original.CEL and.CHP files were downloaded from the GEO database and processed as described in *Section 4.2.4 Microarray statistics*. The differentially expressed mRNAs at 4 or 6 hours were compared between the three microarray datasets to determine the similarities among the datasets.

4.2.7. Pathway analysis

Pathway analysis was evaluated using Ingenuity Pathway Analysis (IPA) [Application: Build: 430520M Copyright 2017 QIAGEN (Redwood City, CA)]. Transcripts found to be differentially expressed compared to saline-injected controls with ≥ 1.5 -fold change and $P \leq 0.05$ were input

into IPA for core analysis using Entrez gene IDs for evaluations of the time-course and comparison datasets. Unmapped genes ranged from 6.5-20.7% per individual time-points or datasets. Datasets were assessed for prediction of upstream regulators and signaling pathways. Additional pathway analysis was completed using DAVID (Version 6.8, released: Oct 2016)^{284,285}, PANTHER Database (Version 11.1, released: Oct 2016)²⁸⁶⁻²⁸⁸, and STRING Database (Version 10.0, released: Apr 16, 2016)²⁸⁹ to validate IPA findings and provide unique perspectives based on each tool's functionality. Functional categorization of genes common to all three datasets examined was done by manual annotation of a single major functional category for each gene based on National Center for Biotechnology Information and GeneCardsSuite descriptions and gene ontology annotations of genes.

4.3. Results

4.3.1. *Bovine microarray*

The analysis of the Affymetrix gene arrays revealed 1654 gene transcripts that were differentially expressed. The number of differentially expressed genes increased throughout the time-course (Figure 4-1 A). Up-regulated transcripts predominated at early time-points in response to PGF2 α (89.6% and 97.1% up-regulated, 0.5 and 1 h, respectively). Similar numbers of up-regulated and down-regulated transcripts were observed at 2 hours post-PGF2 α (53.4% up-regulated genes). Conversely, at 4 hours post-PGF2 α , 58.2% of differentially regulated transcripts were down-regulated. The overlap of altered transcripts among time-points is shown in a Venn diagram in Figure 4-1 B. Of note, 14 of the 29 differentially expressed mRNAs detected at 0.5 hours post-PGF2 α were differentially expressed at all 4 time-points. Additionally, at 4 hours post-PGF2 α , there were 1,507 differentially expressed transcripts unique to that time-point. Comprehensive microarray data is found in the GEO database under accession GSE94069. A full list of differentially expressed genes, fold changes and *P*-values is provided in Appendix B-2.

The top 10 up-regulated and down-regulated transcripts (by fold-change) at each time-point along with their fold change and *P*-values are listed in Table 4-1 & Table 4-2, respectively. Transcription factors were particularly prominent early in the time-course response to PGF2 α and although the number of transcription factors continued to increase, they made up a lower proportion of differentially expressed genes as the time-course proceeded. One-half hour after PGF2 α treatment, 34.5% of the mapped differentially expressed genes had a transcription factor classification using DAVID molecular function analysis and at 4 hours post-PGF2 α , only 1.9% of the differentially expressed genes were classified as transcription factors [Appendix B-4]. Transcription factors that were up-regulated at all time-points investigated included *ATF3*, *BTG2*, *FOS*, *FOSB*, *EGR3*, *JUNB*, *NR4A1*, *NR4A2*, *NR4A3*, and *ZFP36*. Verification of microarray results was completed using qPCR to verify the stimulation of several immediate-early response genes (*ATF3*, *FOS*, *JUN*, *JUNB*) which peaked between 1-2 hours (Figure 4-1 C).

Several cytokine and cytokine-related transcripts were up-regulated in response to PGF2 α . At 2 hours post-PGF2 α , up-regulated cytokine transcripts included *CCL8*, *IL1A*, *IL1B*, and *IL33*. Lastly, at 4 hours, 25 cytokine-related transcripts were up-regulated including all of the up-regulated cytokines at 2 hours and additionally including, *CCL2*, *CCL3*, *CCL4*, *CXCL2*, *CXCL5*, *CXCL8*, *CXCL13*, and *IL18*. Validation of selected cytokine transcripts was performed by qPCR (Figure 4-1 D) and described by ²⁶⁰. Suppressor of cytokine signaling 3 (*SOCS3*), which encodes a protein important in preventing over-activation of inflammatory conditions, was the first inflammation/cytokine-related transcript significantly up-regulated at 1 hour. At the 2- and 4-hour time-points, both *SOCS3* and *SOCS1* were up-regulated [Appendix B-2].

Down-regulated genes included *NF5A2* (also known as *LRH1*); however, many of the down-regulated genes have no known role in CL function or luteolysis. Analysis by IPA of down-regulated genes indicated activation of ‘decreased size of body’ (z-scores; -4.029 and -8.795 at 2 and 4 hours, respectively). Upstream regulators included activation of NUPR1 (z-scores; 2.53,

4.01 at 2 and 4 hours, respectively) and inhibition of vascular endothelial growth factor (VEGF), upstream transcription factor 1 (USF1), and endothelin 1 (EDN1) (z-scores at 4 hours; -4.55, -2.58, -2.43, respectively). Functional analysis by DAVID of down-regulated genes at 4 hours indicated an enrichment in insulin signaling and cyclic adenosine monophosphate signaling and metabolic processes.

4.3.2. *Functional luteolysis*

Serum progesterone was significantly decreased by PGF2 α treatment at 2 and 4 hours (51% and 54%, respectively) compared to saline-treated mid-cycle cows (Figure 4-2 A). Cows from different treatment groups were not different in age, weight or number of calves produced. There were no significant differences among groups in CL weight, ovary dimensions, and antral follicle counts [Appendix B-5].

Despite the decrease in progesterone secretion by 2 hours post-PGF2 α , there were no changes within our time-course in the transcripts that directly control progesterone synthesis (Figure 4-2 B). The proteins encoded by *StAR*, *CYP11A1*, and *HSD3B1* (steroidogenic acute regulatory protein, cytochrome P450 family 11 subfamily A member 1, and hydroxyl- δ -5-steroid dehydrogenase, 3 β and steroid δ -isomerase 1, respectively) are directly responsible for the modification of cholesterol to progesterone, but the abundance of the transcripts were not changed following PGF2 α treatment. Additionally, no changes were observed in the luteinizing hormone/chorionic gonadotropin receptor (*LHCGR*) or lipoprotein receptors: *SCARB1*, and *LDLR* (scavenger receptor class B member 1, and low-density lipoprotein receptor).

Conversely, several transcripts associated with cholesterol availability were differentially regulated. Transcript abundance of lipase E, hormone-sensitive type (*LIPE*), was decreased at 2 and 4 hours; *LIPE* encodes the cholesteryl esterase hormone-sensitive lipase (HSL). As well, the LDLR adaptor protein (*LDLRAP1*) transcript abundance decreased beginning at 2 hours. Other genes that have products influencing cholesterol availability that increased during the time-course

included insulin induced gene 1 (*INSIG1*) and cholesterol 25-hydroxylase (*CH25H*) transcripts. Genes encoding members of the lipid droplet coat protein family, perilipin (PLINs), were also altered after PGF2 α treatment including a 2.6 fold increase in *PLIN2* transcript levels, and -1.9 fold decrease in *PLIN3*. Finally, there were no changes observed in transcript abundance of genes for reverse cholesterol transport proteins (*ABCA1*, *ABCG1*, *NR1H2*, *NF1H3*, *APOA1*, and *APOE*) except *ABCA1*, which was reduced at 4 hours.

4.3.3. Pathway analysis of short time-course

Ingenuity Pathway Analysis identified known PGF2 α mediators including PGF2 α itself (identified in IPA as the synthetic PGF2 α , dinoprost), PKC group¹⁰⁵, ERK/MAPK^{105,238–241}, and Ca²⁺²⁹⁰. All of these known PGF2 α signaling intermediates were predicted as activated by IPA and the activation z-scores for each of these mediators are graphically represented in Figure 4-3 A. Most of these upstream regulators were predicted to have the greatest effect at 2 hours. Upstream regulator analysis predicted TNF α , IL-1 β , IL-6 and IL-17A as active upstream regulators during the short time-course. Figure 4-3 B displays the activation z-scores of several inflammatory cytokines during the 4-hour time-course demonstrating that activation scores for these inflammatory cytokines increased throughout the study. Inflammatory cytokine signaling often involves activation of NF- κ B and signal transducer and activator of transcription (STAT)^{291,292} and both NF- κ B and STAT3 were predicted to be activated during PGF2 α -induced luteal regression. Additionally, inhibitors of cytokine signaling, SOCS1 and SOCS3 were predicted to be inhibited (Figure 4-3 C).

To test whether PGF2 α or the predicted cytokines were capable of activating NF- κ B, dispersed luteal cells from mid-cycle CL or enriched preparations of SLCs and LLCs were treated with PGF2 α or select cytokines and acute activation of NF- κ B and ERK pathways were examined. Figure 4-3 D & E shows that PGF2 α rapidly stimulated ERK phosphorylation but did not alter phosphorylation of the NF- κ B subunit P65 in a 5-120 minute timecourse. Figure 4-3 D

illustrates that TNF α , IL-1 β , and IL-17A consistently stimulated the phosphorylation of NF- κ B P65 in dispersed mid-cycle luteal cells. The cytokines, TNF α , IL-1 β , and IL-17A stimulated phosphorylation of P65 in both SLC and LLC, and PGF2 α selectively stimulated ERK phosphorylation in LLC but had no effect on P65 (Figure 4-3 F). Interleukin-6 did not stimulate phosphorylation of ERK or P65 NF- κ B as it is known to activate the JAK/STAT signaling pathway²⁹³.

Ingenuity Pathway Analysis highlighted canonical pathways predicted to be activated or inhibited within this dataset based on the downstream targets' differential expression (P -value) and direction of change (z-score). The top five canonical pathways identified from each time-point are listed in Table 4-3. At 0.5 hours post-PGF2 α , no pathways had a z-score $\geq |2|$, likely due to the small number of differentially expressed genes. However, several pathways had P -values ≤ 0.05 , including 'NRF2-mediated Oxidative Stress Response'. A total of seven pathways were predicted as activated at the 1-hour time-point. At 2 hours post-PGF2 α , five pathways were predicted as activated and at 4 hours post-PGF2 α , 20 pathways were identified (5 activated and 15 inhibited). Two canonical pathways were predicted to be activated in 2 of the 4 time-points examined, 'cholecystokinin/gastrin-mediated signaling', and 'Toll-like receptor signaling'. Several additional canonical pathways including, 'Acute Phase Response Signaling', 'ILK Signaling', and 'TGF- β Signaling' were identified that had z-scores $\geq |1|$ in at least two time-points.

4.3.4. PGF2 α activates well-organized transcriptional cascades

Ten SOMs were generated based on transcripts that had similar changes in their expression profiles relative to control throughout all four time-points. The differentially expressed transcripts included in each SOM are found in Appendix B-6. Of these, two SOMs reflected the expression patterns of early response genes (Figure 4-4 A & F) and reached peak levels in 1-2 hours and then returned toward baseline. Four SOMs corresponded to early and delayed-early responsive

transcripts with changes in mRNA abundance early in the time-course (but less rapid than the immediate-early response genes) which either plateaued (Figure 4-4 B & G) or continued to change throughout the examined time frame (Figure 4-4 C & H). Finally, there were two SOMs where changes in transcript abundance did not begin until the 2-hour time-point indicative of late-response genes (Figure 4-4 D & I). Two additional SOMs had biphasic transcript profiles, which changed early (either up- or down-regulated), returned to baseline and then rebounded at later time-points (Figure 4-4 E & J).

Up-regulated SOMs had several common IPA-predicted upstream regulators such as TNF α , TGF β , IL-1 β , and NF- κ B. Down-regulated SOMs had common inhibition predictions of VEGF, peroxisome proliferator-activated receptors ligands, and T3 (the thyroid hormone, triiodothyronine). Functional analysis by IPA of the genes in each SOM predicted activated ‘migration of cells’ and inhibition of organismal death in immediately-early up-regulated genes. Early and delayed-early up-regulated gene patterns had functional predictions of ‘cell survival’. Late up-regulated gene patterns were consistent with increases in ‘migration of cells’ and biphasic up-regulated genes had functional predictions of inhibited ‘organismal death’. Down-regulated SOMs had functional predictions of ‘organismal death’ for immediate-early and down-regulated gene patterns. Functional annotations predicted activation of ‘organismal death’ in delayed-early down-regulated SOM, increased ‘morbidity or mortality’ in late down-regulated genes, and death and increased ‘organismal death’ in biphasic down-regulated genes.

Functional annotations of each SOM revealed that SOMs, which peaked early, had a greater proportion of genes with a ‘regulation of gene expression’ biological process annotation by DAVID; including, within the immediate-early categories 47.2% of up- and 18.2% of down-regulated genes. In the early responses, ‘regulation of gene expression’ composed of 31.4% of up-regulated and 22.9% of down-regulated genes. Within the delayed-early SOMs, 19.2% of up- and 22.3% of down-regulated genes were also annotated with ‘regulation of gene expression’.

Whereas, late-response gene patterns had fewer genes classified as ‘regulation of gene expression’ compared to earlier gene profiles (18.2% up- and 19.6% down-regulated). Instead, delayed-early and late up-regulated SOMs had 7.1% of genes associated with “inflammatory reactions” (*P*-values: 1.50E-05, 9.50E-08, DAVID). Biphasic up-regulated genes had biological process annotations including immune response-activating signal transduction. Finally, biphasic down-regulated genes had annotations related to fibrosis. Of the down-regulated SOMs, several contained components of peroxisome proliferator-activated receptor signaling and VEGF signaling.

4.3.5. Dataset comparisons

Two previously published microarray datasets examined the effect of *in vivo* PGF2 α treatment on mid-cycle bovine CL. The similarities in experimental design allowed direct comparison of the microarray data at 4 hours post-PGF2 α to the previously published microarray analyses from GSE23348²⁵⁷ and GSE27961²⁵⁶. Mondal *et al.* collected luteal tissue from Angus crossbred heifers 4 hours after giving an intramuscular injection of 25 mg Lutalyse at day 11 of the estrous cycle. Shah *et al.* treated non-lactating *Bubalus bubalis* (water buffalo) cows with a 500 μ g dose of Juramate (equivalent to 25 mg of Lutalyse²⁹⁴) and collected luteal tissue at 6 hours post-PGF2 α . The overlap of differentially expressed transcripts between the three datasets is visually represented in a Venn diagram in Figure 4-5 A. Comparison of the three datasets revealed 515 genes found by at least 2 of the 3 studies, and 124 genes that were similarly altered in all the datasets including 43 up-regulated genes and 81 down-regulated genes. A full list of the genes common to all three datasets is available in Table 4-4.

Independent bioinformatics analysis of each dataset revealed common regulatory elements. First, IPA predicted similar upstream regulators in each dataset such as PKC, MAPK/ERK, TNF α , IL-1 α/β , and IL-17. Canonical pathway analysis of each of the three datasets commonly predicted activation of triggering receptor expressed on myeloid cells 1 (TREM1) signaling, an

important pathway for activation of macrophages and neutrophils²⁹⁵. Bioinformatic analysis of the 124 genes common to all 3 datasets indicated activation of FOS, JUNB, MAPK/ERK, IL-1 β , TNF α , TGF β , IL-6 (Figure 4-5 B) as well as canonical pathways like IL-6 Signaling, Acute Phase Response Signaling, and NF- κ B Signaling. Pathway analysis of the 124 common genes by IPA, DAVID, PANTHER, and STRING consistently reported enrichment of TGF β signaling (4 of 4) and p53 signaling (3 of 4). Finally, the functional analysis indicated groups of genes involved in cell-cell interaction (12.9%), cytokine signaling (8.9%), and transcriptional regulation (8.1%) in Figure 4-5 C. The genes in each functional category are listed in Table 4-4.

4.4. Discussion

4.4.1. Overview of study

This study uses a systems biology approach to provide a detailed understanding of the early (0.5 – 4 h) transcriptional effects that occur during PGF2 α -induced luteolysis *in vivo*. Our analysis predicts activation of cytokines (TNF α , IL-1 β , IL-6, IL-17A, & IL-33) and cytokine signaling intermediates (NF- κ B, STAT) early in the time-course. However, changes in cytokine transcripts are not apparent until 2 - 4 hours post-PGF2 α . The effects of PGF2 α *in vivo* may require the activation of secondary mediators, such as cytokines, which activate NF- κ B and STAT signaling because PGF2 α is unable to stimulate phosphorylation of NF- κ B P65 in isolated luteal cells. The rapid influx of various immune cells in response to the initiation of luteolysis^{207,209,246} and the release of pre-formed cytokines could explain the prediction of cytokine signaling effects very early in the PGF2 α response. As well, the activation of NF- κ B signaling could contribute to later responses seen after PGF2 α administration.

Analysis of gene expression changes also confirms changes in the transcriptome that are consistent with PGF2 α signaling. Evidence of classical PGF2 α signaling activation is seen directly in the rapid induction of immediate-early response genes (*ATF3*, *EGRI*, *FOS*, *JUN*, and *NR4A2*), consistent with changes in genes documented to be direct targets of PGF2 α signaling

^{92,104,105,108,296,297}. Bioinformatics analysis also identifies upstream regulators consistent with known PGF2 α signaling mediators such as dinoprost (PGF2 α), PKC, Ca²⁺, and ERK. The bioinformatics findings indicating activation of classical PGF2 α signaling pathways after *in vivo* treatment are an important validation of the predictive power of the bioinformatics tools used in this study. Comparison with similar datasets ^{256,257} yields comparable results, predicting both PGF2 α signaling and cytokine signaling in the CL after PGF2 α treatment.

4.4.2. Induction of functional luteolysis

In this study, *in vivo* administration of PGF2 α decreases serum progesterone within 2 hours of treatment. However, serum progesterone concentrations are not under 1 ng/mL, a cutoff that indicates irreversible functional regression, which typically occurs 18-24 hours after the onset of luteolysis ²⁹⁸⁻³⁰¹. Additionally, there are no changes in CL weight, indicating that structural regression of the CL has not yet begun. The reduction in serum progesterone concentrations is not accompanied by reductions in the expression of the steroidogenic enzymes: *StAR*, *CYP11A1*, and *HSD3B1*. Furthermore, transcripts for key receptors (*LHCGR*, *SCARB1*, or *LDLR*) intimately involved in progesterone synthesis are also unchanged. These findings showing a marked reduction in serum progesterone prior to changes in steroidogenic gene transcript abundance are similar to other studies ^{108,255-257}. However, it is possible that changes in abundance or function of specific proteins may occur prior to down-regulation of the corresponding mRNA ^{256,302}.

These observations suggest that alternate pathways could contribute to the early reduction in luteal progesterone synthesis. Based on our findings, it seems possible that the decrease in *LIPE* could contribute to the decrease in progesterone production because its protein product, HSL, interacts directly with lipid droplets to hydrolyze cholesteryl esters to liberate cholesterol for steroidogenesis ^{8,40,42,43}. The reduction in *LIPE* expression together with alterations in *LDLRAP1*, *INSIG1*, and *CH25H* transcript abundance could have a combined negative effect on intracellular cholesterol availability. Decreases in *LDLRAP1* could inhibit progesterone production by

reducing the cholesterol available for use in the cell since endocytosis of low-density lipoprotein particles requires the LDLRAP1 cofactor^{303,304}. An increase in INSIG1 concentrations could affect steroidogenesis through suppressing transcription of *de novo* cholesterol synthesis and uptake proteins,^{305,306}; however, *de novo* synthesis is not a primary source of cholesterol for steroidogenesis in the CL^{143,307,308}. Finally, increases in CH25H could catalyze the hydroxylation of cholesterol to 25-hydroxycholesterol which is a potent inhibitor of *de novo* cholesterol synthesis³⁰⁹. However, 25-hydroxycholesterol can also act as a substrate for steroidogenesis³¹⁰ although it is unclear how physiological concentrations of this oxysterol would act on bovine luteal cells or neighboring cells.

Activation of reverse cholesterol transport could also effectively reduce intracellular cholesterol availability for progesterone synthesis. Other studies have reported an increase in reverse cholesterol transport transcripts such as *ABCA1*, *ABCG1*, *NR1H2*, *NF1H3*, *APOA1*, and *APOE* during luteolysis^{311–313}. However, in this dataset, only a single transcript of the reverse cholesterol transport process, *ABCA1*, changes compared to control, and it decreases. Thus, changes in transcript abundance that contribute to increases in reverse cholesterol transport do not appear to contribute to the early reductions in circulating progesterone.

4.4.3. Cytokine signaling

The present study implicates IL-33 and IL-17 cytokines as potential regulators of luteal regression, although neither have previously been proposed to have a role in luteolysis. Nevertheless, transcripts abundance of *IL33* increase 17-fold over controls and up-regulated in all three datasets. Two recent reports indicate that IL-33 may play a role in follicular atresia^{314,315} and we propose that IL-33 may play a similar role in luteal regression. Preliminary data in our laboratory indicates that IL-33 does not have a direct effect on *in vitro* primary luteal cell cultures, presumably because luteal cells lack or have a low representation of components of the IL-33 receptor complex^{220,279}. In the regressing CL, IL-33 could play a role in macrophage

recruitment^{314,315}, mast cell activation³¹⁶, and is likely derived from the endothelial cells rather than the steroidogenic cells of the CL^{315,316}.

Another novel cytokine highlighted in this dataset is IL-17A, which is identified as an activated upstream regulator in three of the time-points examined. There are no reports of a role for IL-17 in the CL, however, a recent study by Ozkan *et al.* demonstrated that elevated serum IL-17 concentrations predicted infertility and poor responsiveness to *in vitro* fertilization³¹⁷. Analysis of this dataset using a more robust method of calling differentially expressed transcripts increased z-score predicted activation of IL-17 signaling³¹⁸, and our data indicate that IL-17 can directly activate NF- κ B and ERK1/2 signaling in luteal cell cultures. How IL-33 and IL-17 contribute to luteal regression is a subject of future investigations.

Cytokine signaling intermediates such as NF- κ B and STAT3 are predicted by IPA to be activated in response to PGF2 α throughout the time-course. Activation of NF- κ B or prediction of NF- κ B activation is consistently reported after PGF2 α treatment *in vivo*^{256,257,319,320}. However, *in vitro* PGF2 α does not phosphorylate NF- κ B in luteal cells (present study) or endometrial adenocarcinoma cells³²¹. Thus, *in vivo* PGF2 α may use secondary mediators, such as cytokines, which would activate NF- κ B and STAT signaling. This prediction is supported by significant increases in expression of SOCS3 transcripts within 1 hour (4-fold) and SOCS1 at 4 hours (1.7-fold), findings consistent with a well-controlled tissue-specific inflammatory response. However, IPA predicts the inhibition of SOCS1 and SOCS3 during the PGF2 α time-course, which could be. This expands on work by ourselves and others that previously proposed a role for cytokines and immune cells in PGF2 α -induced luteolysis at 3 or more hours after PGF2 α treatment

106,207,244,246,256,257,260,322.

We found both direct and indirect evidence for increases in expression of pro-inflammatory cytokines and signaling during the early responses to PGF2 α . Changes in cytokine-related transcripts do not occur until 2-4 hours post-PGF2 α treatment; although, IPA predicts upstream

cytokine activation and signaling at all 4 time-points. Secretion of cytokines (TNF α , TGF β , and CXCL8) can be stimulated by PGF2 α treatment in the ovary^{106,207,323}, and other tissues^{321,324}. For example, PGF2 α treatment *in vivo* and *in vitro* induces CXCL8^{108,207,246,260,325}, a cytokine which potentially serves to recruit neutrophils and macrophages to the CL^{207,260,326,327}. The recruitment and activation of immune cells along with the actions of pre-formed cytokines could be responsible for the very early gene expression changes that are indicative of cytokine signaling. Both neutrophils and mast cells can store and release large amounts of cytokines and other bioactive proteins immediately after activation without the need for *de novo* synthesis of proteins^{328–330}. This would allow for immediate responses without requiring transcription or translation; therefore, these genes would not be identified in transcriptome-based studies.

4.4.4. PGF2 α activates well-organized signaling cascades

Analysis of SOMs demonstrates that a coordinated cascade of transcription occurs after PGF2 α administration and includes immediate-early, early, delayed-early, late, and biphasic transcriptional responses. This suggests that a carefully orchestrated succession of gene expression changes occurs during PGF2 α -induced luteolysis. Our analysis clarifies the early temporal responses required for PGF2 α -induced luteolysis. As expected, the immediate-early up-regulated and early down-regulated responses are composed primarily of transcription factors. Later signaling waves contain a greater proportion of genes that are non-transcription factors suggesting that genes with an immediate-early expression profile could trigger transcription of early, and delayed-early type genes which could then alter transcription of late-type genes in a transcriptional cascade³³¹.

Up-regulated gene patterns are consistent with inflammatory response and activation of immune cells. The common upstream regulators TNF α , TGF β , IL-1 β , and NF- κ B support this prediction. Down-regulated SOMs correspond with the activation of death pathways and inhibition of cellular proliferation. Interestingly, up-regulated SOMs had functional annotations

such as decreased organismal death whereas down-regulated SOMs noted increased organismal death, which highlights that during a complex event such as luteolysis, there are populations of cells, which are activated and proliferating (potentially immune cells), and other cell types that will be inhibited and primed for apoptosis such as endothelial and steroidogenic luteal cells. Notably, the common upstream regulators EDN1 and VEGF support the idea that CL regression involves early changes in the vasculature, which has been previously suggested^{332–334}. Moreover, several studies indicate that biphasic transcriptional responses are correlated with fluctuations in activation of NF- κ B in response to cytokines like TNF α ^{335–337}. These biphasic, oscillatory responses that can activate both acute and chronic changes within the target tissues are characteristic of cytokine and NF- κ B signaling^{335–339}. In accordance, the cytokines IL-1 β , and TNF α are predicted as upstream regulators of the up-regulated biphasic response SOM. Additionally, Mondal *et al.* proposed that sustained activation of NF- κ B signaling only occurred in PGF2 α -sensitive luteal tissues, and the biphasic patterns of gene expression could reflect both acute activation and the beginning of a chronic activation of target genes. Together these SOMs indicate a cascade of events, whereby immediate-early response genes, composed mostly of transcription factors alters early and delayed-early gene expressions, which contribute to changes in the expression of late-response genes.

4.4.5. Dataset comparison and relationship to previous studies

Comparison of our dataset to two other studies, GSE23348²⁵⁷ and GSE27961²⁵⁶ that used microarray analysis to determine the bovine luteal transcriptome after PGF2 α treatment. Our dataset comparison reveals 124 differentially expressed transcripts common to all three datasets, including *BCL6*, *BMP2*, *FOSL1*, *IL33*, *INHBA*, and *NR5A2*. Bioinformatics analysis of the common transcripts predicts activation of cytokine signaling and includes the upstream regulators IL-1 β , TNF α , and TGF β . This comparison provides several high confidence transcriptome changes that occur in the bovine CL after PGF2 α treatment, which vary minimally across study

sites and investigation groups, providing an important resource for future studies. Importantly, our analysis of the differentially expressed genes common to all three datasets as well as each independent dataset are consistent with the activation of both PGF2 α and cytokine signaling. Additionally, functional annotations of common genes indicate a large proportion of gene products function in cytokine signaling and cell-cell interaction, which both play critical roles in luteolysis. These findings validate the predictions based on the short time-course and support a growing body of literature that suggests that immune cells and cytokines play a key role in CL regression.

4.4.6. *Conclusions from the study*

Shortly after PGF2 α administration, phospholipase C, PKC, Ca²⁺, and ERK trigger a variety of signaling cascades to begin the luteolytic process. Our data suggests that *in vivo*, PGF2 α administration stimulates a series of transcriptional waves likely as a result of classical PGF2 α and cytokine signaling events, as early as 30 minutes post-PGF2 α treatment. This is the beginning of a cascade of events that will initiate decreases in progesterone secretion (2-12 hours post-PGF2 α) and result in the structural regression of the CL 12-18 hours post-PGF2 α ^{240,340}. The earliest decreases in progesterone secretion during luteolysis may be due to changes in protein function and in *LIPE*/HSL expression and other transcripts which regulate cholesterol availability rather than changes in the expression of mRNA encoding the primary steroidogenic enzymes. We propose that during the early stages of functional regression in combination with PGF2 α , the reduction in progesterone, and increase in inflammatory cytokines (potentially including IL-33 and IL-17) contribute to luteal regression. As the intra-luteal concentrations of PGF2 α and inflammatory cytokines increase they may act within an auto-amplification loop eventually reaching a critical point from which there is no rescue from the luteolytic cascade^{67,341–344}. Future studies to identify the specific transcriptional changes occurring in steroidogenic

cells, endothelial cells, immune cells, and fibroblasts is needed to better understand the dynamic network of changes that enable functional and structural luteal regression.

Figure 4-1 - Time-course of the transcriptomic response to PGF2 α

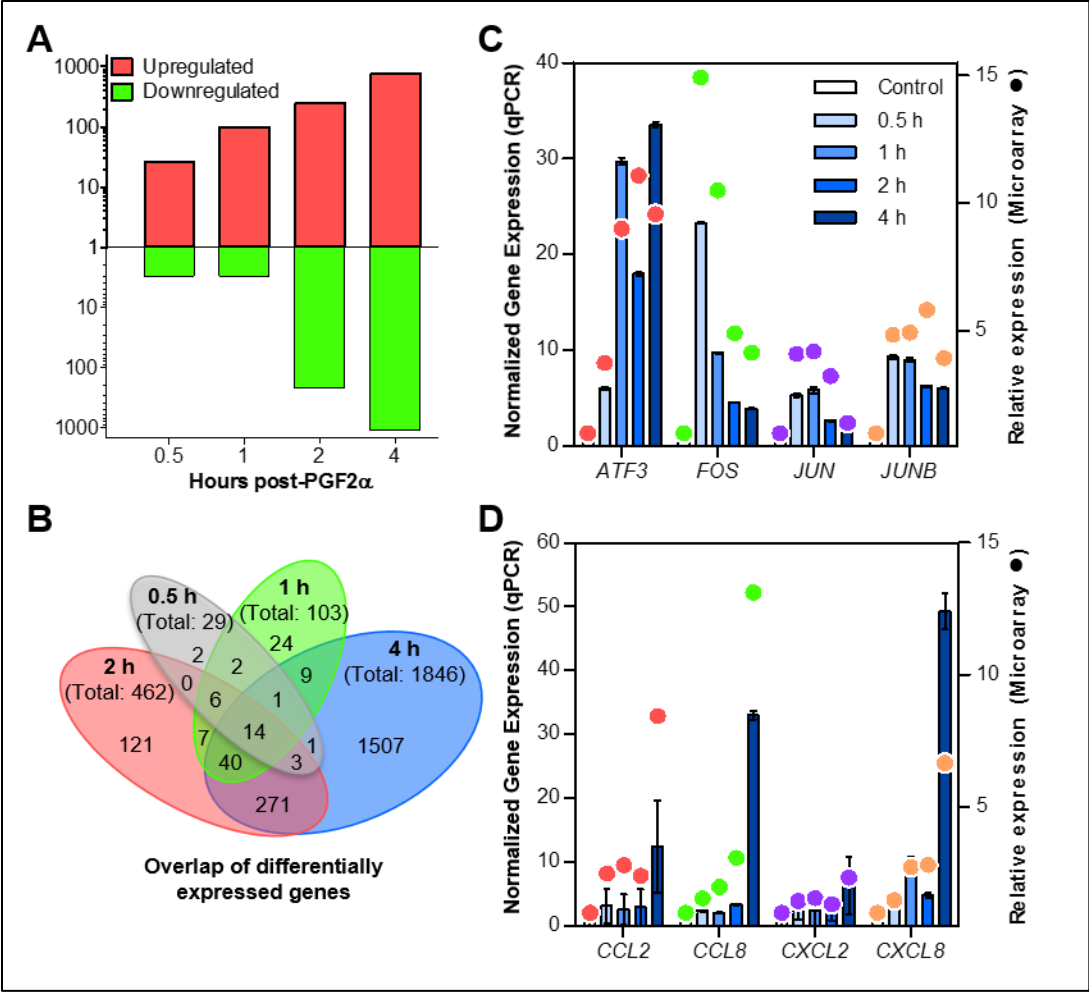


Figure 4-1 – Time-course of the transcriptomic response to PGF2 α

Mid-cycle cows ($n = 3$ /time-point) were treated with 25 mg PGF2 α for 0.5, 1, 2, and 4 hours and control saline injections ($n = 3$). Samples were analyzed by Affymetrix bovine whole transcript microarray (Bovine Gene v1 Array [BovGene-1_0-v1]; GPL17645) and differentially expressed transcripts were identified based on fold change $\geq |1.5|$ and Benjamini-Hochberg adjusted P -value ≤ 0.05 compared to saline controls ($n = 3$). **(A)** Number of upregulated and downregulated differentially expressed transcripts at each time-point graphed on a log scale, upregulated transcripts appear in red above the central axis, and downregulated transcripts appear in green below the axis. **(B)** Venn diagram of the number of differentially expressed genes that overlapped between the four time-points examined. Each oval is labeled with the time-point and the total number of differentially expressed genes in the time-point. Overlapping parts of the ovals are labeled with the number of transcripts that were differentially expressed at the corresponding time-points. **(C & D)**. Quantitative PCR (qPCR) analysis of target genes normalized to *ACTB* and *GAPDH* expression and compared to saline controls using fold-change are displayed using bar graphs to represent mean \pm SEM and plotted on the left Y-axis. Microarray determined fold-change of the target genes compared to control are overlaid using filled circles \bullet to represent the mean ($n = 3$) and plotted on the right Y-axis. **(C)** Selected transcription factor genes (*ATF3*, *FOS*, *JUN*, and *JUNB*) were significantly different from control values ($P < 0.0001$) as determined by qPCR and determined as differentially expressed in the microarray (except *JUN* at 4 h). **(D)**. Target cytokine transcripts (*CCL2*, *CCL8*, *CXCL2*, and *CXCL8*) were all upregulated at 4 h ($P < 0.01$). Additionally, *CXCL8* was significantly upregulated at 1 and 2 hours ($P < 0.0001$, $P < 0.05$, respectively) as determined by qPCR. Determination of differentially expressed transcripts by microarray indicated significant upregulation of *CXCL2* and *CXCL8* at 4 hours and *CCL8* at both 2 and 4 hours. Submitted for publication as part of ²²¹.

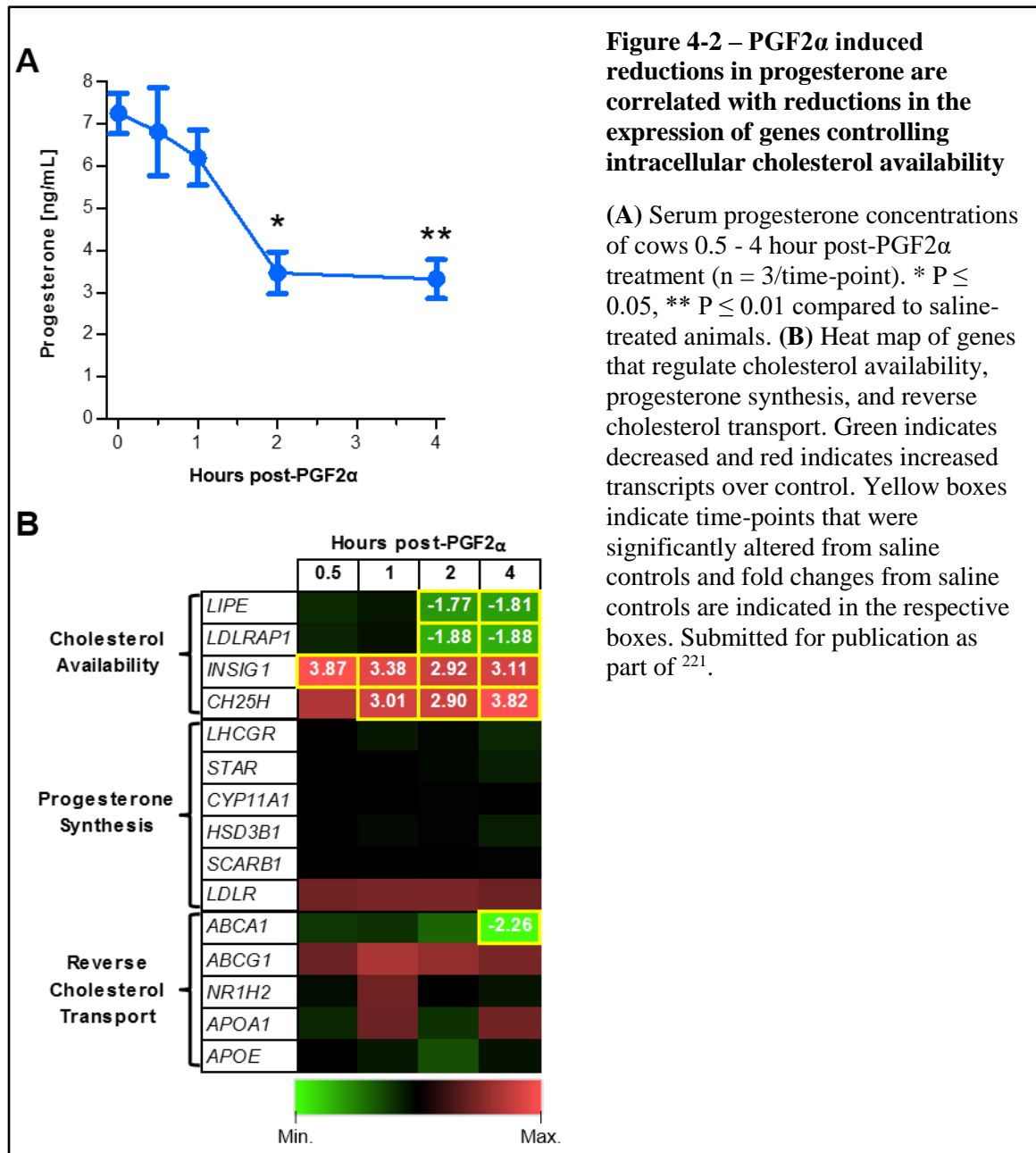


Figure 4-3 – *In vivo* treatment with PGF2 α predicts classical PGF2 α and cytokine signaling

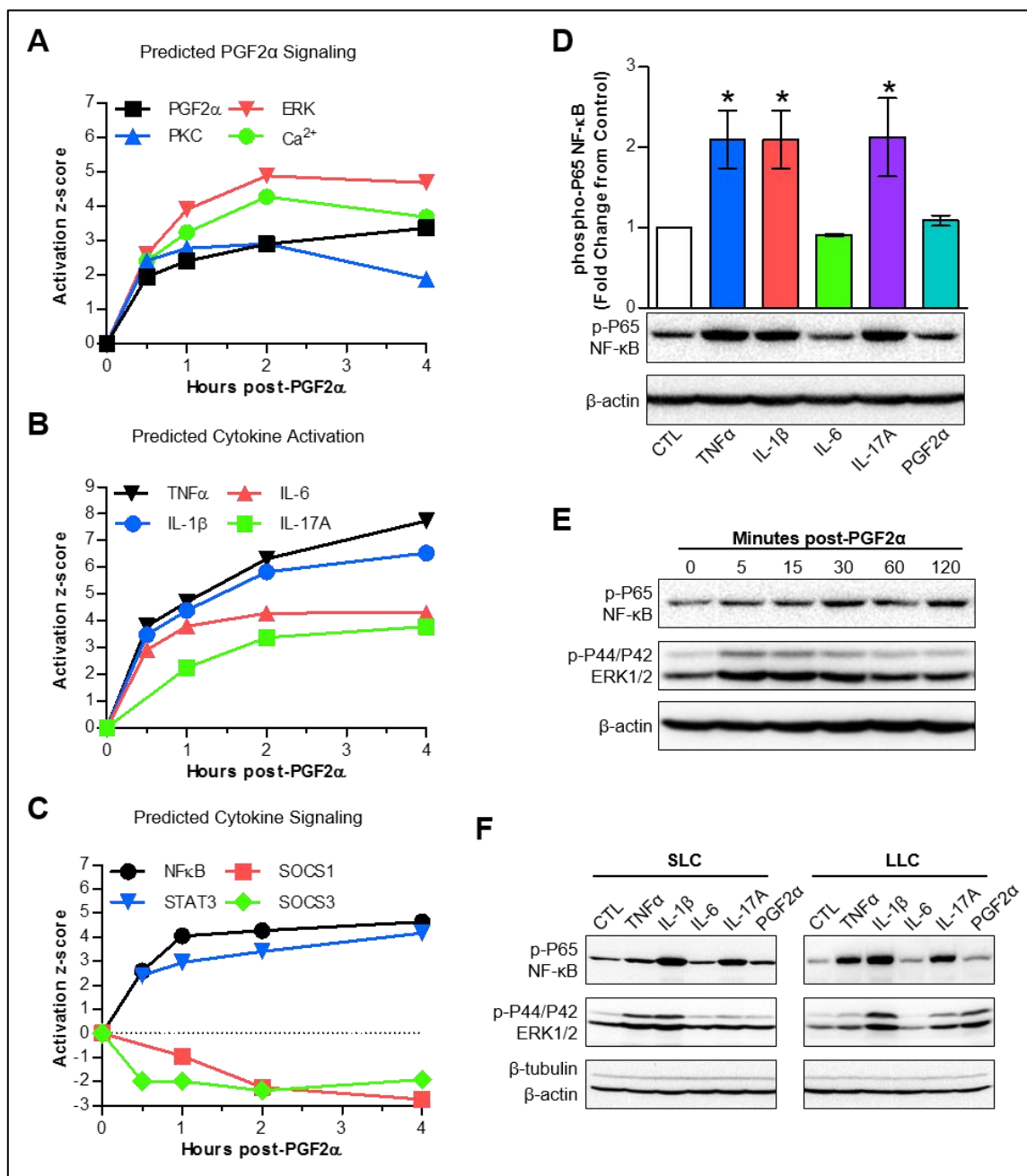


Figure 4-3 – *In vivo* treatment with PGF2 α predicts classical PGF2 α and cytokine signaling

(A, B & C) The activation z-score of specific upstream regulators, determined by IPA, graphed against time. (A) Classic mediators of PGF2 α signaling including, PGF2 α itself (dinoprost, black), protein kinase C (PKC group, blue), ERK (red), and Ca²⁺ (green). (B) Cytokine activation scores including, TNF α (black), IL-1 β (blue), IL-6 (red), and IL-17 (green). (C) Cytokine signaling molecules: NF- κ B (black), STAT3 (blue), and suppressors of cytokine signaling, SOCS1 (red) and SOCS3 (green). (D) Phospho-P65 quantification (mean \pm SEM) of non-pregnant mid-cycle luteal cells (n = 3) treated with TNF α , IL-1 β , IL-17A and PGF2 α for 30 minutes followed by Western blot analysis, normalized to β -actin and compared to untreated controls, representative immunoblots are shown below the bar graph. * $P \leq 0.05$ compared to control. (E) Western blot of non-pregnant mid-cycle luteal cells treated with PGF2 α for the indicated times immunoblotted for phospho-P65, phospho-ERK1/2, β -tubulin, and β -actin. (F) Western blot of small luteal cells (SLC) and large luteal cells (LLC) treated with TNF α , IL-1 β , IL-6, IL-17A (10 ng/mL each) and PGF2 α (100 nM) for 30 minutes and immunoblotted for phospho-P65, phospho-ERK1/2, β -tubulin, and β -actin. Submitted for publication as part of ²²¹.

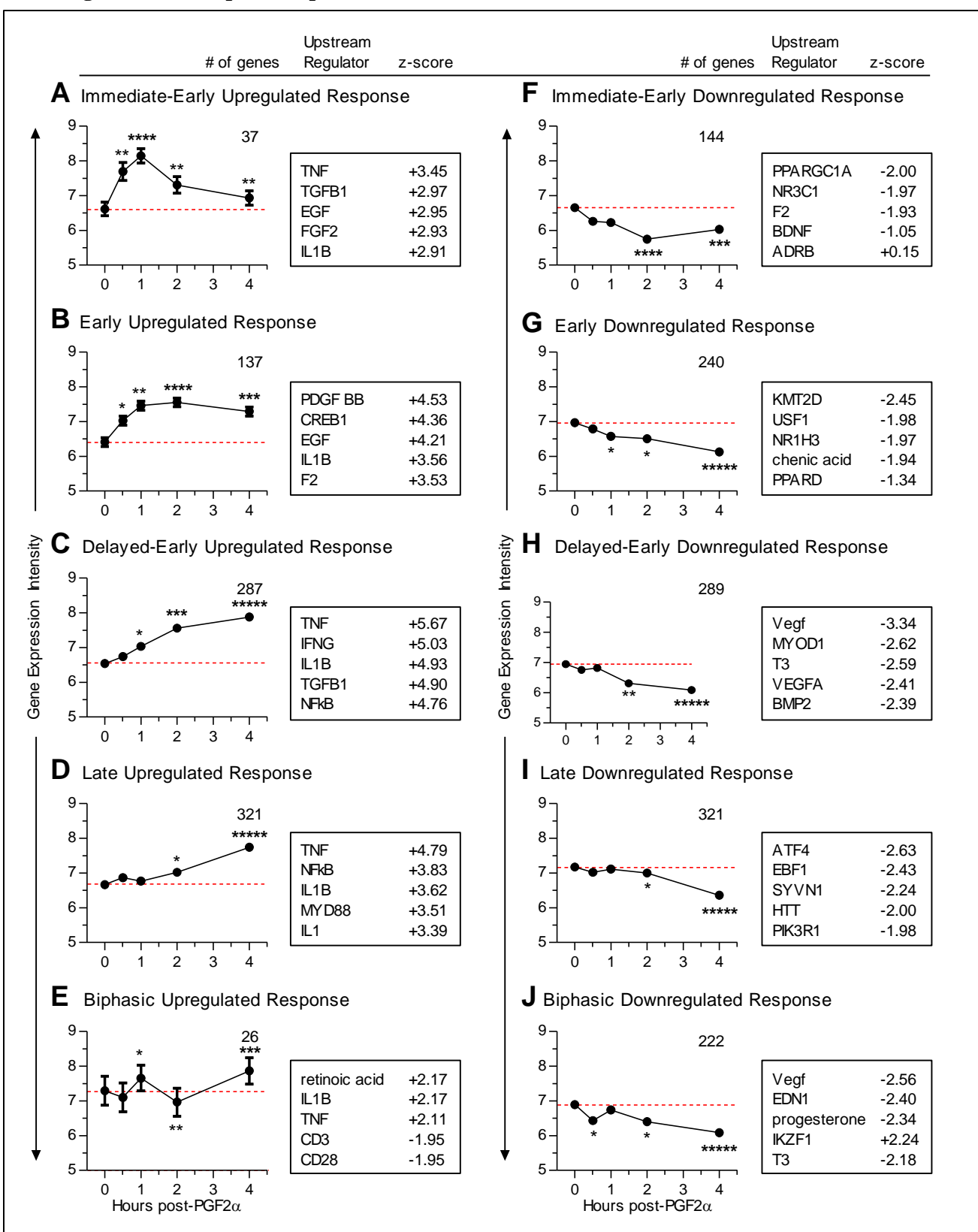
Figure 4-4 – Temporal response waves to PGF2 α 

Figure 4-4 – Temporal response waves to PGF2 α

Self-organizing maps (SOMs) graphs were generated as detailed in Methods. Each graph shows the average log₂ transcript expression intensity \pm SEM of the transcripts grouped into each SOM. Red dashed lines demonstrate the average transcript expression intensity at baseline. Numbers in the upper right of the individual graphs represent the number of transcripts within each SOM. Groups of transcripts that were upregulated during the PGF2 α time-course are shown on the left (**A, B, C, D, & E**) and downregulated transcripts on the right (**F, G, H, I, & J**). (**A & F**) SOMs showed responses typical of immediate-early response genes, peaked between 1-2 hour and returned to baseline. (**B & G**) SOMs demonstrated early response genes, peaked at 2 hours and maintained through the 4-hour time-point. (**C & H**) SOMs demonstrated delayed-early response genes, which gradually moved away from baseline throughout the time-course. (**D & I**) SOMs showed late-response genes, which stayed near the baseline and then began changing at 2-4 hour. (**E & J**) Biphasic SOMs, which had an early change in transcript expression, returned to baseline and then had a second change in transcription levels. Boxes to the right of the graphs include the top upstream regulators predicted to be involved using IPA at the peak of change from controls,

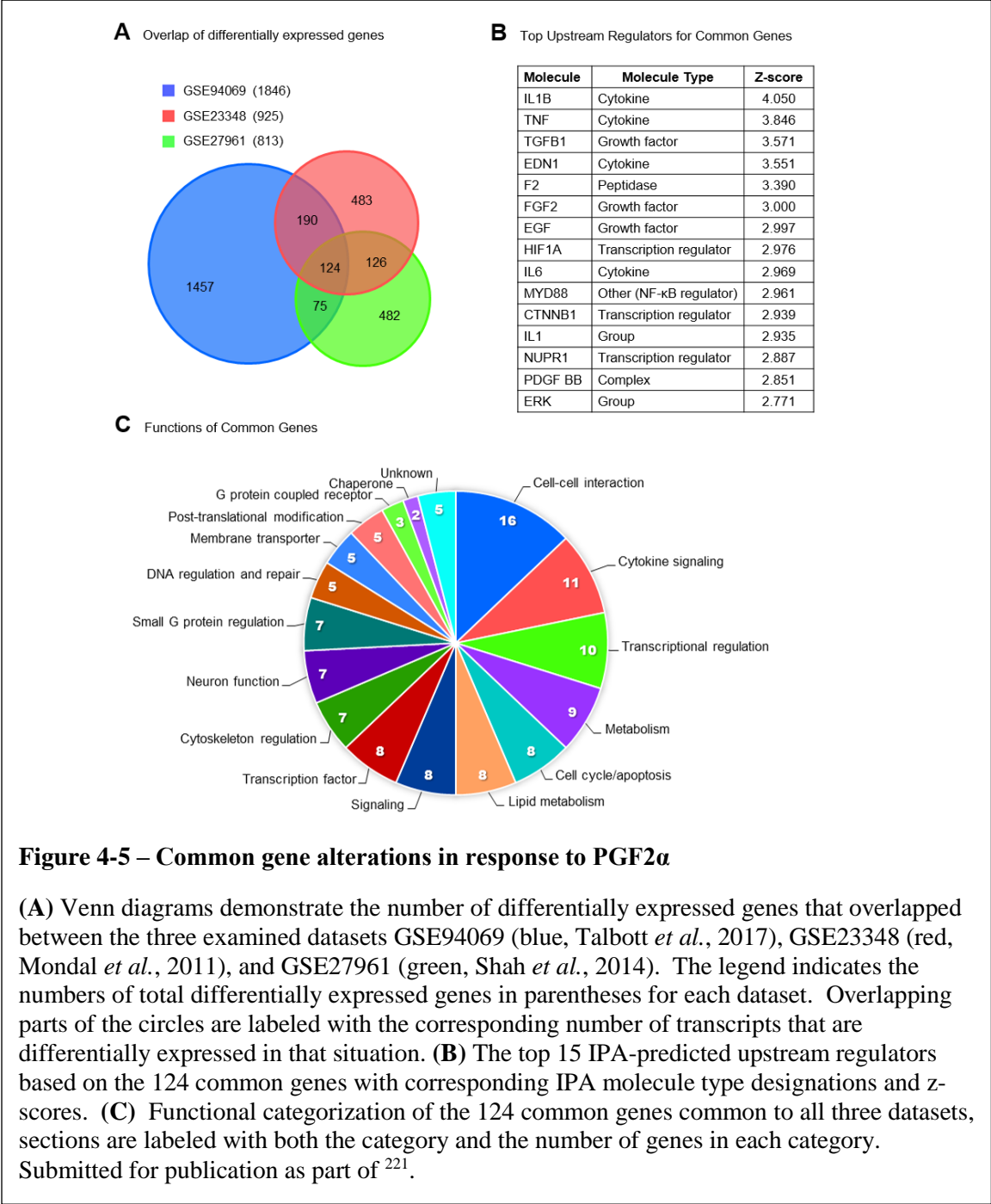


Table 4-1 – Top ten up-regulated genes at each time-point

	Gene Symbol	Entrez ID	Gene Name	Fold Change	P-value
0.5 h	<i>FOS</i>	280795	Fos proto-oncogene, AP-1 transcription factor subunit	14.94	8.22E-04
	<i>NR4A1</i>	528390	nuclear receptor subfamily 4 group A member 1	8.56	1.30E-05
	<i>NR4A2</i>	540245	nuclear receptor subfamily 4 group A member 2	7.34	4.94E-06
	<i>NR4A3</i>	528877	nuclear receptor subfamily 4 group A member 3	7.15	2.67E-04
	<i>FOSB</i>	540819	FosB proto-oncogene, AP-1 transcription factor subunit	6.74	2.40E-04
	<i>APOLD1</i>	538827	apolipoprotein L domain containing 1	6.57	8.33E-04
	<i>IER2</i>	525380	immediate early response 2	6.04	4.50E-05
	<i>EGR1</i>	407125	early growth response 1	5.57	2.40E-04
	<i>JUNB</i>	514246	JunB proto-oncogene, AP-1 transcription factor subunit	4.86	1.79E-06
1 h	<i>CYR61</i>	508941	cysteine rich angiogenic inducer 61	4.61	3.03E-03
	<i>NR4A3</i>	528877	nuclear receptor subfamily 4 group A member 3	27.85	7.81E-07
	<i>FOSB</i>	540819	FosB proto-oncogene, AP-1 transcription factor subunit	16.65	1.38E-06
	<i>DUSP2</i>	539140	dual specificity phosphatase 2	13.06	7.27E-05
	<i>NR4A1</i>	528390	nuclear receptor subfamily 4 group A member 1	11.36	1.38E-06
	<i>EGR4</i>	407155	early growth response 4	10.81	1.26E-04
	<i>FOS</i>	280795	Fos proto-oncogene, AP-1 transcription factor subunit	10.50	1.38E-03
	<i>ATF3</i>	515266	activating transcription factor 3	9.00	1.22E-05
	<i>NR4A2</i>	540245	nuclear receptor subfamily 4 group A member 2	8.84	9.30E-07
2 h	<i>ARC</i>	519403	activity regulated cytoskeleton associated protein	7.06	4.02E-04
	<i>DUSP5</i>	507061	dual specificity phosphatase 5	6.55	9.51E-06
	<i>EGR4</i>	407155	early growth response 4	20.38	1.44E-05
	<i>FOSB</i>	540819	FosB proto-oncogene, AP-1 transcription factor subunit	15.13	2.80E-06
	<i>SERPINE2</i>	505184	serpin peptidase inhibitor, clade B (ovalbumin), member 2	14.42	1.74E-04
	<i>ARC</i>	519403	activity regulated cytoskeleton associated protein	13.90	1.79E-05
	<i>DUSP5</i>	507061	dual specificity phosphatase 5	12.31	4.85E-07
	<i>NR4A3</i>	528877	nuclear receptor subfamily 4 group A member 3	11.77	1.49E-05
	<i>F3</i>	280686	coagulation factor III, tissue factor	11.10	1.89E-02
4 h	<i>ATF3</i>	515266	activating transcription factor 3	11.09	4.85E-06
	<i>INA</i>	532236	internexin neuronal intermediate filament protein alpha	10.41	2.25E-03
	<i>MMP12</i>	526981	matrix metalloproteinase 12	10.26	2.11E-03
	<i>MMP12</i>	526981	matrix metalloproteinase 12	41.71	1.06E-05
	<i>SERPINE2</i>	505184	serpin peptidase inhibitor, clade B (ovalbumin), member 2	25.49	1.31E-05
	<i>SERPINE1</i>	281375	serpin family E member 1	17.87	1.01E-06
	<i>CSRP3</i>	540407	cysteine and glycine rich protein 3	17.82	2.31E-04
	<i>SERPINA14</i>	286871	serpin peptidase inhibitor, clade A (alpha-1 antitrypsin), member 14	17.57	2.58E-04
	<i>IL33</i>	507054	interleukin 33	17.46	1.76E-07
	<i>IL1A</i>	281250	interleukin 1 alpha	16.65	1.77E-05
	<i>TNFSF18</i>	768081	tumor necrosis factor superfamily member 18	15.38	1.60E-06
	<i>DUSP5</i>	507061	dual specificity phosphatase 5	14.52	1.23E-07
	<i>INHBA</i>	281867	inhibin beta A subunit	13.57	1.23E-07

Submitted for publication as part of ²²¹.

Table 4-2 – Top ten down-regulated genes at each time-point

	Gene Symbol	Entrez ID	Gene Name	Fold Change	P-value
0.5 h	<i>LOC100337120</i>	100337120	T-cell activation Rho GTPase-activating protein-like	-3.81	4.47E-03
	<i>LOC783362</i>	783362	uncharacterized LOC783362	-3.81	3.25E-03
	<i>MIR2450B</i>	100313224	microRNA 2450b	-3.46	8.13E-03
1 h	<i>GBP4</i>	100298387	guanylate binding protein 4	-2.56	3.74E-02
	<i>ARHGAP25</i>	534994	Rho GTPase activating protein 25	-2.06	8.59E-03
	<i>CARD6</i>	520291	caspase recruitment domain family member 6	-1.75	3.74E-02
2 h	<i>GRIA1</i>	529618	glutamate ionotropic receptor AMPA type subunit 1	-4.57	3.26E-02
	<i>LOC783362</i>	783362	uncharacterized LOC783362	-4.24	7.48E-04
	<i>CEP295NL</i>	100125412	CEP295 N-terminal like	-3.95	3.30E-02
	<i>CALB2</i>	513947	calbindin 2	-3.57	1.63E-02
	<i>LOC510193</i>	527460	apolipoprotein L3	-3.41	4.43E-02
	<i>LOC100337457</i>	100337457	solute carrier family 23 member 2	-3.23	3.33E-02
	<i>FAM13C</i>	540918	family with sequence similarity 13 member C	-3.20	2.88E-03
	<i>LOC100337120</i>	100337120	T-cell activation Rho GTPase-activating protein-like	-3.04	6.89E-03
	<i>RUNDC3B</i>	525116	RUN domain containing 3B	-2.82	7.69E-03
4 h	<i>SDPR</i>	532333	serum deprivation response	-2.78	7.24E-03
	<i>LOC783362</i>	783362	uncharacterized LOC783362	-4.77	1.44E-04
	<i>APLNR</i>	615435	apelin receptor	-4.20	5.10E-04
	<i>FOXL2</i>	281770	forkhead box L2	-4.16	3.35E-06
	<i>ARHGAP20</i>	515501	Rho GTPase activating protein 20	-4.05	3.06E-04
	<i>PIEZO2</i>	522631	piezo type mechanosensitive ion channel component 2	-3.80	2.39E-04
	<i>NPNT</i>	513362	nephronectin	-3.69	8.59E-04
	<i>GPAM</i>	497202	glycerol-3-phosphate acyltransferase, mitochondrial	-3.55	7.42E-03
	<i>LRIG3</i>	506574	leucine rich repeats and immunoglobulin like domains 3	-3.50	5.31E-04
	<i>MAMSTR</i>	505540	MEF2 activating motif and SAP domain containing transcriptional regulator	-3.38	9.54E-04
	<i>TNS3</i>	516555	tensin 3	-3.31	8.60E-05

Submitted for publication as part of ²²¹.

Table 4-3 – Top five canonical pathways predictions during each timepoint during the early response to PGF2 α treatment

	Ingenuity Canonical Pathways	z-score	P-value	Molecules
0.5 h	NRF2-mediated Oxidative Stress Response		1.41E-02	<i>FOS, JUN, DNAJB1, JUNB</i>
	Corticotropin Releasing Hormone Signaling		1.41E-02	<i>FOS, JUN, NR4A1</i>
	IGF-1 Signaling		1.41E-02	<i>FOS, JUN, CYR61</i>
	IL-17A Signaling in Gastric Cells		1.41E-02	<i>FOS, JUN</i>
	PI3K Signaling in B Lymphocytes		1.41E-02	<i>FOS, JUN, ATF3</i>
1 h	ILK Signaling	2.449	2.34E-02	<i>FOS, JUN, SNAI1, MYC, SNAI2, RND3</i>
	Cholecystokinin/Gastrin-mediated Signaling	2	3.89E-02	<i>FOS, JUN, SRF, RND3</i>
	HMGB1 Signaling	2	2.45E-02	<i>FOS, JUN, SERPINE1, PLAT, RND3</i>
	Endothelin-1 Signaling	2	8.71E-02	<i>FOS, JUN, MYC, EDNRB</i>
	IL-8 Signaling	2	1.08E-01	<i>FOS, JUN, ANGPT2, RND3</i>
2 h	Cholecystokinin/Gastrin-mediated Signaling	2.646	2.99E-01	<i>FOS, JUN, SRF, IL1B, IL1A, RND3, IL33</i>
	Acute Phase Response Signaling	2.121	4.81E-01	<i>FOS, JUN, IL1B, JAK2, SOCS3, IL1A, SERPINE1, IL33</i>
	Toll-like Receptor Signaling	2	2.99E-01	<i>FOS, JUN, IL1B, IL1A, TRAF1, IL33</i>
	TGF- β Signaling	2	5.45E-01	<i>FOS, JUN, INHBA, SERPINE1</i>
	LPS/IL-1 Mediated Inhibition of RXR Function	2	7.43E-01	<i>JUN, IL1B, PPARGC1B, IL1A, NR5A2, IL33</i>
4 h	Death Receptor Signaling	-2.714	3.23E-01	<i>IKBKG, TANK, CFLAR, NFKB1, PARP1, PARP4, CASP9, NFKBIA, ACIN1, TNKS, BIRC3, SPTAN1</i>
	Integrin Signaling	-2.683	4.69E-01	<i>ASAP1, TLN1, RRAS2, ITGAV, ITGA2, CAPN1, TSPAN4, PXN, PIK3C2B, MYL9, PIK3R1, GAB1, ITGA9, SOS1, PIK3CG, RHOG, PIK3CA, ARHGEF7, MAP2K2, TSPAN5, PPP1CB, PLCG1, ACTN4</i>
	UVA-Induced MAPK Signaling	-2.496	1.64E-01	<i>SMPD2, MTOR, PARP4, RRAS2, CASP9, PIK3C2B, PIK3R1, GAB1, TP53, TNKS, PIK3CG, FOS, RPS6KA5, PARP1, PIK3CA, PLCG1</i>
	Retinoic acid Mediated Apoptosis Signaling	-2.449	1.78E-01	<i>CFLAR, PARP1, PARP4, CASP9, RXRB, CRABP2, RARG, TNKS</i>
	MIF Regulation of Innate Immunity	2.449	3.44E-01	<i>FOS, LY96, NFKB1, CD14, NFKBIA, TP53</i>

Submitted for publication as part of ²²¹.

Table 4-4 – Common transcripts differentially expressed in response to PGF2 α treatment

		Fold Change		
Gene	Entrez Gene ID	GSE94069	GSE23348	GSE27961
Cell-cell interaction				
SERPINB2	505184	25.49	5.27	5.10
SERPINE1	281375	17.87	28.96	31.00
AMIGO2	514273	8.27	8.65	8.09
PLAUR	281983	6.83	5.92	7.39
SDC4	508133	6.59	8.44	19.13
HS3ST5	540355	4.77	7.73	9.33
MMP1	281308	4.11	12.26	6.44
THBS1	281530	2.89	2.02	3.90
CLDN1	414922	2.65	3.52	3.23
CD44	281057	2.49	3.44	8.22
CLDND1	515537	2.45	1.55	1.79
ITGAV	281875	1.75	1.93	2.79
EMCN	616367	-2.05	-1.55	-2.74
CLIC5	281696	-2.41	-1.69	-2.19
TMEM204	615464	-2.83	-1.72	-1.89
NPNT	513362	-3.69	-2.33	-2.51
Cytokine signaling				
IL33	507054	17.46	6.92	2.96
INHBA	281867	13.57	19.69	27.25
SPP1	281499	5.73	7.55	4.65
MT2A	404070	3.56	4.65	3.99
BAMBI	530147	3.41	1.57	2.99
NRG1	281361	3.14	2.15	8.78
IL18	281249	3.08	2.53	2.50
BMP2	615037	3.02	5.47	3.92
STAMBP	532672	1.82	1.98	3.19
CD14	281048	1.81	2.48	3.68
PDGFC	613787	1.70	1.77	1.78
Transcriptional Regulation				
ELL2	782605	2.30	2.15	4.06
HMGA1	618849	1.86	4.11	3.71
AGO2	404130	1.75	2.03	2.41
RPF2	511294	1.59	1.62	1.50
EIF4A1	504958	1.56	1.53	1.71
CPEB2	538880	-1.63	-1.95	-1.67
POLR1E	511587	-1.65	-1.90	-2.53
DCP1B	514548	-1.71	-1.54	-1.95
HEXIM1	539696	-2.88	-2.24	-2.37
ZMYM3	522721	-3.11	-2.18	-2.62
Metabolism				
ARG2	518752	5.95	2.56	3.95
GCNT4	782825	4.47	2.84	3.18
HK2	788926	3.50	3.61	4.24
LDHA	281274	1.77	1.54	2.32
PDP1	280891	1.64	1.50	2.02
RPIA	613376	1.52	1.68	2.04
METRNL	534297	1.52	1.89	2.11
PGM5	785045	-1.68	-1.73	-2.02
MPPED2	540914	-2.35	-1.60	-2.33

Table 4-4 – Common transcripts differentially expressed in response to PGF2 α treatment (continued)

		Fold Change		
Gene	Entrez Gene ID	GSE94069	GSE23348	GSE27961
Transcription factor				
FOSL1	531389	2.85	2.80	3.19
BCL6	539020	2.69	3.49	2.23
SRF	533039	2.58	2.42	2.75
TGIF1	510050	2.29	2.50	1.90
BZW2	326579	2.11	1.85	2.19
NR5A2	541305	-1.79	-2.27	-2.58
ZNF22	768051	-2.29	-1.68	-1.73
ZNF827	104974573	-2.30	-1.53	-1.67
Signaling				
PDE8A	506787	1.97	2.31	4.12
PDE4B	100124505	1.76	2.22	3.60
PPP4R4	537521	1.72	3.59	10.10
TMEM64	536822	1.62	1.70	1.69
PIK3CA	282306	1.54	1.57	1.80
EVC2	280834	-1.70	-1.52	-1.78
DACT1	538778	-2.18	-1.90	-1.75
TMEM88	507172	-2.76	-1.78	-2.75
Lipid metabolism				
OLR1	281368	9.18	14.54	15.84
SRD5A1	614612	2.43	2.31	4.57
SPHK1	618605	2.18	2.27	2.04
PITPNC1	782067	1.53	1.57	1.55
ABCD4	515848	-1.80	-1.80	-1.80
OXSM	513530	-1.86	-2.40	-2.14
MID1IP1	615572	-1.90	-1.89	-2.68
GPAM	497202	-3.55	-2.86	-2.34
Cell cycle/apoptosis				
CDKN1A	513497	4.16	3.67	2.55
TNFRSF12A	617439	2.63	2.45	4.22
BTG1	281032	2.58	1.80	2.29
CCNG2	512960	2.18	1.59	1.90
STK17A	513665	2.05	1.81	1.90
BTG3	541054	1.89	1.53	2.11
CCNYL1	538167	1.70	1.69	1.97
IFT122	536731	-1.53	-1.71	-1.64
Small G-protein regulation				
RASA2	533491	3.21	1.74	1.70
TIAM1	536517	2.28	3.43	2.38
RHOBTB1	540513	-1.85	-1.57	-2.49
WIPF3	786606	-1.90	-1.55	-2.13
AGFG2	510361	-2.08	-2.01	-1.93
RGL1	522344	-2.23	-1.58	-1.73
ARHGAP19	526945	-2.34	-2.02	-2.08
Neuron function				
GAL	280799	10.15	55.44	11.39
CA8	515918	2.97	3.60	6.36
STK38L	514787	2.05	1.54	1.85
SLITRK2	540117	2.01	4.08	6.64
PNMA1	538718	-1.98	-3.18	-1.83
SEMA6D	518458	-2.28	-2.05	-1.95
PTHLH	286767	-2.49	-3.91	-4.55

Table 4-4 – Common transcripts differentially expressed in response to PGF2 α treatment (continued)

		Fold Change		
Gene	Entrez Gene ID	GSE94069	GSE23348	GSE27961
Cytoskeleton regulation				
Cnn1	534583	5.19	6.55	5.80
MICAL2	534041	3.39	3.45	7.05
TPM4	535277	2.63	1.66	2.56
MARCKSL1	539555	2.19	2.84	1.95
RAI14	525869	1.89	2.24	2.24
MYO18A	519634	-1.98	-1.51	-1.61
TNS3	516555	-3.31	-3.03	-3.13
Post-translational modification				
UFM1	530547	2.63	1.72	1.92
DPH3	511579	2.62	1.84	1.57
RWDD3	614557	-1.62	-2.22	-2.16
KBTD4	617482	-1.74	-1.52	-1.59
TRIM68	538657	-2.30	-1.64	-1.54
Membrane transporter				
TRPC4	282102	4.33	3.33	3.50
SLC39A8	508193	2.86	2.58	3.73
SLC20A2	518905	2.79	1.89	1.53
SLC2A1	282356	2.44	2.43	4.71
SLC12A2	286845	1.78	2.69	1.57
DNA regulation and repair				
RBBP8	512977	4.08	1.99	3.10
H2AFZ	287016	1.61	1.54	1.55
PAPD7	523016	1.50	1.86	3.36
ZRANB3	529922	-1.88	-1.82	-1.53
MUM1	513471	-2.16	-1.71	-1.55
G-protein coupled receptor				
F2RL2	512581	2.17	1.82	3.34
AGTR1	281607	-2.16	-2.07	-1.95
APLNR	615435	-4.20	-2.76	-1.83
Chaperone				
DNAJA1	528862	2.31	1.60	1.51
HSPA2	281827	-1.96	-1.65	-1.57
Unknown				
C23H6orf141	100271839	2.45	1.98	6.27
LHFPL2	616131	2.35	3.32	2.16
LOC540312	540312	-1.81	-1.84	-4.54
CYYR1	768230	-1.98	-1.51	-2.08
LOC511229	511229	-2.33	-2.08	-1.77

Submitted for publication as part of ²²¹.

CHAPTER 5: EFFECTS OF CXCL8 AND IMMUNE CELLS ON THE REGULATION OF LUTEAL PROGESTERONE SECRETION **

Abstract

Recent studies suggest that chemokines may mediate the luteolytic action of prostaglandin F2 α (PGF2 α). Our objective was to identify chemokines induced by PGF2 α *in vivo* and to determine the effects of CXCL8 on specific luteal cell types *in vitro*. Mid-cycle cows were injected with saline or PGF2 α , ovaries were removed after 0.5 - 4 h and chemokine expression was analyzed by qPCR. *In vitro* expression of CXCL8 was analyzed after PGF2 α administration and with cell signaling inhibitors to determine the mechanism of PGF2 α -induced chemokine expression. Purified neutrophils were analyzed for migration and activation in response to CXCL8 and PGF2 α . Purified luteal cell types (steroidogenic, endothelial and fibroblast cells) were used to identify which cells respond to chemokines. Neutrophils and peripheral blood mononuclear cells (PBMCs) were co-cultured with steroidogenic cells to determine their effect on progesterone production. *CXCL8*, *CXCL2*, *CCL2*, and *CCL8* transcripts were rapidly increased following PGF2 α treatment *in vivo*. The stimulatory action of PGF2 α on *CXCL8* mRNA expression *in vitro* was prevented by inhibition of p38 and JNK signaling. CXCL8, but not PGF2 α , TNF α , or TGF β , stimulated neutrophil migration. CXCL8 had no apparent action in purified luteal steroidogenic, endothelial, or fibroblast cells, but CXCL8 stimulated extracellular signal-regulated kinase (ERK) phosphorylation in neutrophils. In co-culture experiments neither CXCL8 nor activated neutrophils altered basal or luteinizing hormone (LH)-stimulated luteal cell progesterone synthesis. In contrast, activated PBMCs inhibited LH-stimulated progesterone synthesis from cultured luteal cells. These data implicate a complex cascade of events during luteolysis involving chemokine signaling, neutrophil recruitment, and immune cell action within the corpus luteum.

** The material presented in this chapter was previously published: Talbott *et al.* Effects of IL8 and immune cells on the regulation of luteal progesterone secretion. *Reproduction* 2014 ²⁶⁰.

5.1. Introduction

The corpus luteum develops after ovulation and secretes progesterone, a steroid hormone essential for the establishment and maintenance of early pregnancy^{134,230}. In the absence of hormonal cues or pregnancy the corpus luteum will regress in a process termed luteolysis. In many species, luteolysis is mediated by uterine and/or intra-luteal release of prostaglandin F2 alpha (PGF2 α)^{65,67,343,345}. PGF2 α has been shown to act indirectly at the vascular level to cause disruption of luteal capillaries²⁴⁴ and apoptosis of capillary endothelial cells³⁴⁶. PGF2 α has also been implicated in the initiation of luteal cell apoptosis *in vivo*^{65,347}; however, PGF2 α alone cannot directly reduce the viability of luteal cells *in vitro*^{65,348}. Thus, other mechanisms must be activated for luteolysis to proceed through both the functional (loss of progesterone secretion) and structural (apoptosis and tissue remodeling) stages of regression.

Immune cells and their effector cytokines participate in various reproductive processes^{203,246,349,350} including: ovulation^{351,352}, endometrial function^{353,354}, as well as corpus luteum formation and regression^{203,246,349,354–357}. CXCL8 (previously known as IL-8) is a known chemotactic cytokine secreted by a variety of cells in response to inflammatory stimuli. CXCL8 secretion is implicated in the recruitment and activation of neutrophils^{358,359}, including within the corpus luteum^{207,246,360}. In rabbits, neutralization of CXCL8 suppresses neutrophil activation and ovulation³⁵². Recent studies also indicate that neutrophils and CXCL8 are involved in establishment of the corpus luteum following ovulation. CXCL8 and neutrophils are known to promote angiogenesis^{361,362} findings which have been recently extended to the developing corpus luteum^{207,246,363}. CXCL8 is also capable of stimulating progesterone secretion by luteinizing granulosa³²⁶ and theca cells³⁶⁴.

Our objective was to identify chemokines induced by PGF2 α *in vivo* and to determine the effect of CXCL8 on specific luteal cell types *in vitro*. We employed co-cultures to evaluate the effects of immune cells on luteal progesterone synthesis. The present study demonstrates that

PGF2 α stimulates the transcription of *CXCL8*, *CCL8*, *CCL2* and *CXCL2*. While *CXCL8* was effective at recruitment of neutrophils, neither *CXCL8* nor activated neutrophils reduced luteinizing hormone (LH)-stimulated luteal progesterone synthesis. In contrast, activated polymorphic mononuclear cells (PBMCs) inhibited LH-stimulated progesterone by luteal cells *in vitro*. Indicating that the activation of immune cells during luteolysis may be involved in the regression of the bovine corpus luteum.

5.2. Materials and Methods

5.2.1. *In vivo studies*

All animal procedures were conducted under an IACUC-approved protocol and performed at the University of Nebraska-Lincoln, Animal Sciences Department. Post-pubertal female cattle of composite breeding age were given an intramuscular injection at mid-cycle (days 9-10) with saline (n = 3) or 25 mg of the PGF2 α analog, Lutalyse (Pharmacia & Upjohn Company, New York, NY, n = 12). Ovariectomies were performed at 0.5, 1, 2, and 4 h after treatment and RNA was isolated from the corpora lutea using an Absolutely mRNA Purification Kit (Agilent Technologies Inc., Santa Clara, CA.) according to the manufacturer's instructions. RNA yields were measured using a fluorescence detection kit (RiboGreen; Invitrogen, Carlsbad, CA). Screening with whole-transcript bovine microarray (Affymetrix, Santa Clara, CA) revealed several chemokines that were induced following treatment with PGF2 α . Quantitative real-time polymerase chain reaction (qPCR) was used to validate changes in *CXCL8*, *CCL2*, *CCL8*, and *CXCL2* mRNA using the primers provided in Table 5-1. First-strand cDNA was synthesized from 1 μ g total RNA using iScriptTM cDNA synthesis kit (Bio-Rad, Hercules, CA) according to the manufacturers' instructions. qPCR was performed using the CFX96TM Real-Time PCR Detection System (Bio-Rad, Hercules, CA) with ssoFastTM EvaGreen[®] Supermix (Bio-Rad, Hercules, CA) with the following parameters: 95 °C for 30 s followed by 40 cycles of: 95 °C for 5 s, and 55 °C for 5 s. β -actin (*ACTB*) or glyceraldehyde 3-phosphate dehydrogenase (*GADPH*)

were used as internal standards of mRNA expression. The authenticity of the PCR signal was verified by reactions containing no RNA or reactions omitting reverse transcriptase. Melt curve analysis was performed to ensure amplification of a single product at the predicted melting temperature.

5.2.2. *In vitro studies*

All cell culture experiments described below were done in tissue culture plastic (Corning CoStar, Corning, NY) and included penicillin (100 IU/ml, Gibco Life Technologies, Carlesbad, CA) streptomycin (100 µg/ml, Gibco Life Technologies, Carlesbad, CA), and amphotericin (50 µg/ml, MP Biomedicals, Santa Ana, CA) in cell culture medium to prevent bacterial and fungal growth.

5.2.3. *Isolation of bovine luteal cells*

Bovine ovaries were collected from a local abattoir (JBS, Omaha, NE). The tissue was obtained from cows during early pregnancy (fetal crown-rump length < 10 cm) to assure luteal function³⁶⁵. The luteal tissue was dissected from the ovary and dissociated with 103 IU/mL collagenase (Atlanta Biologicals, Norcross, GA) as described previously³⁶⁶. Luteal cell viability was determined using trypan blue exclusion, and luteal cell preparations with more than 90% viability were used. Enriched bovine steroidogenic luteal cells (1×10^5 cells/cm²) were plated as previously described⁹⁴. Cells were incubated overnight in medium 199 (M199, Lonza, Basel, Switzerland) supplemented with 5% fetal bovine serum (FBS, Valley Biomedical, Winchester, VA). The next day the medium was changed and the incubations were continued for 1 day in FBS-free media. On the day of the experiment, the medium was replaced with fresh FBS-free medium for 2-3 h to pre-equilibrate before applying the treatments detailed in the figure legends.

5.2.4. *Isolation of bovine endothelial and fibroblast cells*

Endothelial cells were isolated from bovine corpus luteum of early pregnancy and purified as described before²⁴⁵. Endothelial cells were positive for vascular endothelial cell cadherin (VE-

cadherin) and negative for steroidogenic enzymes and prolyl 4-hydroxylase (antibodies are listed in Table 5-2). Cells were grown to ~80% confluence in Dulbecco's Modified Eagle Medium (DMEM, Corning CellGro, Corning, NY) containing 10% FBS and 20 µg/ml endothelial cell growth supplement (ECGS, Millipore, Bedford, MA). The medium was changed to serum-free DMEM containing 20 µg/ml ECGS for 2 h prior to treatment as described in the figure legends.

Fibroblasts were isolated from the bovine corpus luteum and characterized as previously described²⁴⁵. The fibroblasts were positive for prolyl 4-hydroxylase and collagen 1 and negative for steroidogenic enzymes and VE-cadherin (antibodies listed in Table 5-2). Luteal fibroblasts were grown to ~80% confluence and changed to serum-free DMEM for 2 h prior to treatment with CXCL8 as described in the figure legends.

5.2.5. *Isolation of bovine neutrophils and migration assays*

Potassium ethylenediaminetetraacetic acid (Sigma-Aldrich, St. Louis, MO)-anticoagulated bovine blood samples were collected from a local abattoir (JBS, Omaha, NE), centrifuged, and subjected to Percoll gradient (Sigma-Aldrich, St. Louis, MO) separation to isolate neutrophils. The remaining erythrocytes were lysed by rapid treatment with dH₂O and the remaining cells were resuspended in Roswell Park Memorial Institute 1640 medium (RPMI, Thermo Fisher Scientific HyClone, Waltham, MA). Cell migration was assayed using the Boyden chamber method. Bovine neutrophils (2.5×10^5) were seeded in transparent polyethylene terephthalate membrane cell culture inserts with 3 µm pores (B&D Falcon, Franklin Lakes, NJ) placed in 24-well plates. The lower chamber was filled with 500 µl RPMI with or without 30 ng/mL CXCL8 (R&D Systems, Minneapolis, MN), 100 nM PGF₂α, 10 ng/ml tumor necrosis factor alpha (TNFα, R&D Systems, Minneapolis, MN) or 1 ng/ml transforming growth factor beta 1 (TGFβ). Cell migration was carried out for up to 24 h at 37 °C. Migrated cells were counted with a hemacytometer.

To determine the signaling pathways used by CXCL8 in bovine neutrophils, we treated neutrophils with CXCL8 or TNF α (R&D Systems, Minneapolis, MN), a modulator of immune function and activator of multiple signaling pathways. Western blot analysis was performed to examine the mitogen-activated protein kinase (ERK1/2, p38 and JNK), AKT and NF- κ B signaling pathways using phospho-specific antibodies. See Table 5-2 for a complete list of antibodies used.

5.2.6. *Isolation of human neutrophils and degranulation assays*

Human neutrophils were isolated from peripheral blood of healthy donors by density gradient centrifugation under an approved IRB at the University of Nebraska Medical Center, using polymorphprep (Axis-Shield, Oslo, Norway) in accordance with manufacturer's instruction. Purified neutrophils were resuspended in RPMI + 5% FBS. Neutrophils (3×10^5 cells) were incubated with different concentrations of CXCL8 at 37 °C for 1 h. Neutrophil degranulation was examined by fluorescence-activated cell sorting for increased cell surface expression of granule molecules carcinoembryonic antigen-related cell adhesion molecule 8 (CD66b); and integrin alpha M (ITGAM, also known as CD11b). Cells were stained with fluorescein isothiocyanate (FITC)-conjugated mouse anti-human CD66b antibody and allophycocyanin (APC)-conjugated mouse anti-human CD11b antibody on ice for 30 min. After rinsing, cells were fixed with phosphate-buffered saline plus 2% formaldehyde. Flow cytometry analysis was done using a Becton Dickinson (Franklin Lakes, NJ) FACSCaliber flow cytometer and was performed at the University of Nebraska Medical Center Cell and Tissue Analysis Facility.

5.2.7. *Isolation of bovine peripheral blood mononuclear cells (PBMC)*

Acid citrate dextrose-anticoagulated blood samples from cows were collected from a local abattoir (JBS, Omaha, NE). Blood was then diluted 1:2 in cold Hank's Balance Salt Solution (HBSS, Corning CellGro, Corning, NY) with 2 mM EDTA (Sigma-Aldrich, St. Louis, MO) and 5% FBS. Diluted blood was underlayered with an equal volume of Histopaque (specific gravity =

1.083, Sigma-Aldrich, St. Louis, MO) and centrifuged at 900 x g for 30 min. PBMCs were collected from interface between the plasma and Histopaque. The cells were then washed in HBSS three times before use.

5.2.8. *Co-culture experiments*

Enriched bovine steroidogenic luteal cells were plated ($\sim 1 \times 10^5$ cells/cm²) in basal M199 medium containing 5% FBS in 48-well plates overnight as described above.

5.2.9. *Neutrophil-luteal cell co-culture:*

Neutrophils were isolated on the same day that luteal cells were prepared. Purified neutrophils were then cultured in RPMI (10% FBS) with or without 30 ng/ml CXCL8 and 20 nM phorbol myristate acetate (PMA, EMD Millipore Calbiochem, Billerica, MA) overnight. After 24 h the medium was replaced on the luteal cell cultures. Neutrophils (250,000 cells/ml) were then added to the luteal cells in M199 and RPMI (1:1) with 10% FBS for 2 h before adding control media or 10 ng/ml bLH (Tucker Endocrine Research Institute, Atlanta, GA). Medium from each well was collected 6 hours after LH or control treatments for progesterone analysis.

5.2.10. *PBMC-luteal cell co-culture:*

Twenty-four hours after plating the luteal cells, the medium was removed from the culture wells and replaced with fresh M199. Then an equal volume of newly isolated bovine PBMCs in RPMI (100,000 cells/ml) were added to the luteal cell culture. Co-cultures were incubated for 24 h in M199 and RPMI (1:1 ratio) + 10% FBS, and with or without 10 µg/ml concavalin A (Sigma, St. Louis, MO) to activate the PBMCs. After 24 h of co-culture, medium was replaced with M199:RPMI + 10% FBS for 2 h to pre-equilibrate the cells before the addition of control media or 10 ng/ml LH. Medium was removed from each well after 6 h of control or LH treatment for progesterone analysis.

5.2.11. Western blot analysis

Cultures of neutrophils, steroidogenic cells, luteal endothelial cells, and luteal fibroblasts were harvested with ice cold cell lysis buffer [20 mM Tris-HCl (pH = 7), 150 mM NaCl, 1 mM Na₂EDTA, 1 mM EGTA, 1% Triton X-100 and protease and phosphatase inhibitor cocktails (Sigma-Aldrich, St. Louis, MO)]. Protein concentration was determined and 40-60 µg protein was subjected to 10% SDS-PAGE. After transfer to polyvinylidene fluoride (PVDF) membranes, the membranes were probed with appropriate amounts of primary antibodies and bound antibodies were detected with a horse radish peroxidase-conjugated secondary antibody and the Femto Western Blotting Detection Kit (GE Healthcare Amersham, Cleveland, OH). Signals were visualized using a Digital Sciences Image Station 440 (Kodak, Rochester, NY).

5.2.12. Progesterone analysis

Conditioned media were collected for progesterone determination using Coat-A-Count progesterone radioimmunoassay kit (Siemens, Deerfield, IL) according to the manufacturer's instructions and as previously reported ⁹⁴.

5.2.13. Statistical analysis

All experiments were performed at least two times using different cell preparations with qualitatively comparable results. The data are presented as representative experiments or as the means \pm SEM of the averages from multiple experiments. The differences in means were analyzed by t test or analysis of variance followed by multiple range testing. $P \leq 0.05$ was considered statistically significant.

5.3. Results

5.3.1. PGF2 α stimulates chemokine gene expression *in vivo*

Treatment with PGF2 α *in vivo* resulted in a 4.3-fold increase in CXCL8 mRNA within 30 min and a 9-fold increase in CXCL8 mRNA within 1 h of administration (Figure 5-1 A). Treatment with PGF2 α also increased CCL8, CXCL2, and CCL2 mRNA after 1 h (fold increases of 2.5 \pm

0.6; 2.9 ± 0.7 and 3.1 ± 0.6 , respectively). After a brief lag the expression of chemokine mRNA increased dramatically after 4 h of treatment with PGF2 α . A 35 ± 4 fold increase in *CXCL8* mRNA expression was observed in response to a 4 h treatment with PGF2 α . At the 4 h mark PGF2 α also stimulated significant ($P \leq 0.05$) increases in *CCL8*, *CCL2* and *CXCL2* mRNA expression (29 ± 3.8 , 12 ± 1.5 and 6.4 ± 1 fold, respectively).

5.3.2. PGF2 α stimulates *CXCL8* expression *in vitro*

Treatment of steroidogenic luteal cells with PGF2 α for 1 h *in vitro* also increased *CXCL8* mRNA expression (3-fold increase, $P \leq 0.05$; (Figure 5-1 B). Luteal steroidogenic cells were pretreated in the presence or absence of specific inhibitors of the mitogen-activated protein kinase (MAPK) signaling cascade to determine which intracellular signals contribute to the stimulatory effect of PGF2 α on the induction of *CXCL8* gene expression (Figure 5-1 B). Pretreatment with the ERK1/2 inhibitor U0126 (Enzo Life Sciences, Farmingdale, NY) failed to prevent the stimulatory effect of PGF2 α on *CXCL8* mRNA (Figure 5-1 B). In contrast, inhibition of the stress-activated protein kinase p38 MAPK with SB2037580 resulted in a complete inhibition of the response to PGF2 α . Treatment with the JNK inhibitor SP600125 also resulted in a significant inhibition (77%, $P \leq 0.05$) of the PGF2 α -induced increase in *CXCL8* mRNA.

5.3.3. *CXCL8* induces migration of bovine neutrophils

To determine whether *CXCL8* would affect the function of bovine neutrophils, we purified neutrophils from blood collected at slaughter from non-pregnant cows. As shown in Figure 5-2 A neutrophils stained with hematoxylin and eosin had distinct multi-lobular nuclei, a characteristic of neutrophils. A Boyden chamber assay (Figure 5-2 A) was used to determine whether *CXCL8* or other factors produced during luteolysis could increase migration of bovine neutrophils. We observed that treatment for 18 h with 30 ng/ml *CXCL8* caused a 20-fold ($P \leq 0.05$) increase in neutrophil migration. However, treatment of neutrophils with 100 nM PGF2 α under identical conditions had no effect on neutrophil migration (Figure 5-2 B). Migration assays were also

performed with other chemokines that have been implicated in luteal regression; namely TNF α ^{346,367} and TGF β ^{244,245}. In experiments evaluating neutrophil migration during a 3 h treatment period, we found that 30 ng/ml CXCL8, but not 100 nM PGF2 α , 10 ng/ml TNF α , or 1 ng/ml TGF β , was capable of stimulating migration of neutrophils (Figure 5-2 C).

Activation of neutrophils results in the rapid cell surface expression of molecules that allows for endothelium attachment for extravasation. Treatment of human neutrophils with increasing concentrations of human CXCL8 (0-100 ng/ml) resulted in the rapid expression of the cell adhesion molecules ITGAM and as determined by flow cytometry (not shown).

5.3.4. *CXCL8 selectively stimulates signaling in bovine neutrophils*

Treatment with CXCL8 for 15 min stimulated an increase (5-fold, $P \leq 0.05$) in ERK1/2 phosphorylation (Figure 5-3 A). The response was transient and returned to control levels within 120 min following CXCL8 treatment (Figure 5-3 A & Figure 5-4A). CXCL8 did not stimulate either the p38 or the JNK MAPK signaling pathways (Figure 5-3). In contrast to CXCL8, TNF α provoked sustained ERK phosphorylation, as well as p38 and JNK phosphorylation in bovine neutrophils throughout the 120 min investigated (Figure 5-3). CXCL8 exerted a slight, but consistent, increase in the phosphorylation of p65-NF- κ B and AKT; whereas, TNF α stimulated a robust increase in p65-NF- κ B and AKT phosphorylation in neutrophils. To determine whether CXCL8 could similarly stimulate other cells of the corpus luteum, we treated bovine luteal fibroblasts, endothelial cells and steroidogenic cells with CXCL8 under a various treatment times and concentrations. CXCL8 did not stimulate the phosphorylation of AKT, ERK or NF- κ B in any other cell type examined. As a positive control we observed that TNF α stimulated MAPK and NF- κ B signaling in each cell type examined; whereas PGF2 α only stimulated MAPK signaling in luteal steroidogenic cells (data not shown).

In view of the very prominent effect of CXCL8 on ERK signaling in neutrophils, we tested whether the CXCL8-induced increase in ERK phosphorylation was associated with the effect of

CXCL8 on neutrophil migration. Pretreatment with 5 μ M of U0126, completely blocked the induction of ERK phosphorylation (Figure 5-4 A), but did not prevent the stimulatory effect of CXCL8 on bovine neutrophil migration (Figure 5-4 B).

5.3.5. *Effect of CXCL8 and immune cells on progesterone secretion*

Experiments were performed to determine whether CXCL8 altered progesterone secretion. Pretreatment of steroidogenic luteal cells with increasing amounts of CXCL8 (0-30 ng/ml) did not alter basal or LH-simulated progesterone production in luteal cells (Figure 5-3 A). Next, we co-cultured neutrophils with steroidogenic cells and evaluated the ability of LH to stimulate progesterone secretion. We observed that co-cultures of steroidogenic cells and neutrophils had no effect on the ability of LH to increase progesterone (Figure 5-3 B). Furthermore, co-cultures of steroidogenic cells and activated neutrophils had no effect on basal or LH-stimulated progesterone production.

Co-cultures of steroidogenic cells and PBMCs had no effect on the ability of LH to secrete progesterone (Figure 5-6). However, LH-stimulated progesterone production was completely abrogated ($P \leq 0.05$) in cultures of activated PBMCs and steroidogenic luteal cells (Figure 5-6).

5.4. Discussion

For over 30 years the immune system has been postulated as essential for fertility³⁶⁸. The present study provides additional insight into the expression and function of chemokines during luteal regression. We observed that induction of luteal regression in cows with a bolus of PGF2 α *in vivo* resulted in a rapid increase in the expression of CXCL8, CCL8, CCL2, and CXCL2. Our findings confirm recent findings by Shirasuna *et al.*, 2012²⁴⁶ that PGF2 α treatment of dairy cattle increased luteal CXCL8 mRNA by approximately 4-fold within 30 min. In that study, the fold increase in CXCL8 mRNA remained constant over 4-hr of treatment with PGF2 α . In the present study using beef cattle we observed more robust increases in luteal CXCL8 mRNA expression; 9-fold increases within 1 h and 35-fold increases after 4 h of PGF2 α treatment. At present it is not

clear whether the differences in the magnitude of the responses are due to differences in the cattle breeds since there are reported differences in the responses of beef and dairy cattle to synchronization protocols using PGF2 α ³⁶⁹ or other factors. Based on the pronounced increase in CXCL8 expression, it was selected for further analysis. We found that CXCL8 acted directly on neutrophils but had little effect on other cell types in the mid-cycle corpus luteum. Furthermore, co-cultures of luteal cells with activated neutrophils did not alter LH-stimulated progesterone synthesis; whereas co-cultures with activated PBMCs suppressed LH-stimulated progesterone synthesis.

Activation of the PGF2 α receptor rapidly induces calcium mobilization and activation of PKC²³⁵. These initial signaling events lead to the activation of ERK1/2^{238,239}, p38, and JNK^{104,240,241} *in vivo* and *in vitro*, with subsequent activation of multiple transcription factors. The MAPK signaling family induces early response genes such as FOS and JUN¹⁰⁵, NR4A1^{108,134}, EGR1^{106,108}, and ATF3¹⁰⁴ in the corpus luteum. To determine which intracellular signals contribute to the stimulatory effect of PGF2 α on CXCL8 gene expression, luteal cells were treated with specific inhibitors of ERK1/2, p38, and JNK. We observed that the ERK1/2 inhibitor U0126 had no effect on CXCL8 mRNA expression in response to PGF2 α , while the p38 MAPK inhibitor SB2037580 and the JNK inhibitor SP600125 significantly inhibited the PGF2 α -mediated upregulation of CXCL8 mRNA. The results indicate that the stress-activated MAPKs: p38 and JNK play an important and perhaps overlapping role in the induction of CXCL8 mRNA in response to PGF2 α .

Chemokines like CXCL8 are responsible for the recruitment of immune cells to chemokine-producing tissues. Our findings demonstrate that CXCL8 is chemotactic for bovine neutrophils, in agreement with previous literature^{207,246,358,359}. CXCL8 stimulated a 6-fold increase in neutrophil migration within 3 h and after 24 h CXCL8-treatment increased neutrophil migration nearly 20-fold. In contrast, treatment with PGF2 α had no effect on neutrophil migration at either time-point.

These findings are consistent the studies by ^{246,370} showing that immune cells are unresponsive to PGF2 α because they do not express the PGF2 α receptor. In the present study we also report that TNF α and TGF β , two cytokines induced rapidly in the bovine corpus luteum in response to PGF2 α and implicated in events associated with luteal regression ^{106,245,257,346}, did not increase the migration of bovine neutrophils in the Boyden chamber assay. Our observations support the recent reports ^{108,246,257,321} showing that PGF2 α induces *CXCL8* mRNA and that the expression of *CXCL8* is associated with the appearance of neutrophils in the bovine corpus luteum ^{203,207,246}. In addition, our studies indicate that *CXCL8* stimulates the degranulation of human neutrophils which supports the studies of Shirasuna *et al.*, 2012 ²⁴⁶ indicating that the rapid appearance of E-selectin on neutrophils follows treatment with *CXCL8*. Since other chemokines (*CCL8*, *CCL2*, and *CXCL2*) are induced concomitantly with *CXCL8*, it will be important to evaluate the contributions of each individual chemokine to the recruitment of specific immune cells into the regressing corpus luteum. Future experiments should also address how combinations of these chemokines signal the recruitment and activation of immune cells within the corpus luteum ³⁷¹.

Treatment of neutrophils with *CXCL8* stimulated a robust increase in ERK phosphorylation, a slight increase in AKT and NF- κ B phosphorylation, and had no effect on p38 and JNK signaling. In contrast, TNF α activated all of these pathways simultaneously in neutrophils. Since ERK signaling was the most prominent pathway activated following *CXCL8* treatment of bovine neutrophils, we determined whether neutrophil migration could be blocked by treatment with the ERK1/2 inhibitor U0126. Interestingly, we found that inhibition of ERK signaling with U0126 had no inhibitory effect on *CXCL8*-stimulated neutrophil migration. These results suggest that another signaling pathway is responsible for *CXCL8*-stimulated chemotaxis, likely the PI3K and Rac signaling pathway ^{372,373}. Further studies are required to determine the contributions of other signaling pathways to neutrophil activation and migration.

CXCL8 has been shown to induce diverse cellular responses in cells other than neutrophils³⁵⁸. Recent studies suggest that CXCL8 may contribute the angiogenesis in the newly forming corpus luteum²⁰⁷ and progesterone secretion by granulosa³²⁶ and theca³⁶⁴ cells. Treatment with various CXCL8 concentrations and treatment times revealed no changes in cell signaling in steroidogenic cells, endothelial cells, or fibroblasts isolated from the bovine corpus luteum. However, CXCL8 stimulated a robust increase in ERK phosphorylation in neutrophils. Furthermore, CXCL8 did not affect basal or LH-stimulated progesterone secretion from cultured luteal cells. In contrast to the findings by Shimizu *et al.*, 2012³²⁶, we found no evidence suggesting that CXCL8 acted directly on bovine luteal cells types that are involved in luteal regression (e.g., endothelial cells, fibroblasts and steroidogenic cells). Based on these findings it appears that CXCL8 exerts specific effects on ovarian cell types depending on their stage of differentiation. Given that the corpus luteum is highly differentiated and undergoes regression in response to PGF2 α , the lack of a stimulatory effect of CXCL8 on angiogenesis and steroidogenesis may be expected since the vasculature and steroid secretion are disrupted during regression^{65,134,245,374}. It is possible that during luteal regression CXCL8-activated neutrophils contribute to phagocytosis during structural regression of the corpus luteum.

The increase observed in multiple chemokines suggests that immune cells other than neutrophils could be recruited in to the corpus luteum following administration of PGF2 α . In fact, studies from multiple laboratories have demonstrated an increase in neutrophils, T cells, or macrophages during the regression of the corpus luteum in rodents³⁷⁵, rabbits³⁷⁶, ruminants^{209,377}, primates³⁵³, and women^{205,249,378,379}. A previous report indicated that co-culture of rat neutrophils with luteal cells resulted in a decrease in progesterone secretion, presumably as a result of oxidative stress³⁸⁰. However, under our experimental conditions co-cultures of bovine neutrophils and steroidogenic luteal cells did not alter basal or LH-stimulated progesterone synthesis. Treatment of neutrophils with CXCL8 and PMA, alone or in combination, to activate

neutrophils was not sufficient to reduce progesterone secretion under co-culture conditions. In addition to neutrophils, monocytes are immune effector cells that are also equipped with chemokine receptors and adhesion receptors that mediate migration from blood to tissues ³⁸¹. Since we observed that PGF2 α rapidly induced the expression of other chemokines (*CCL8*, *CCL2*, and *CXCL2*), which could recruit other types of immune cells, we established a co-culture system with PBMCs and luteal cells. Although, un-activated PBMCs did not reduce progesterone secretion, we observed that activated PBMCs effectively reduced LH-driven progesterone secretion. These observations support our earlier findings ³⁷⁰ that activated immune cells may contribute a factor (or factors) that impair steroidogenesis in response to LH. It is known that activated monocytes produce inflammatory cytokines, nitric oxide, and reactive oxygen species ^{381,382} all of which may contribute individually or in combination to the inhibition of progesterone synthesis ^{347,383,384}. In the *in vivo* setting, activated monocytes may also secrete matrix metalloproteinases that contribute to the degradation of the extracellular matrix ³⁸¹, which could facilitate the recruitment of additional inflammatory cells to the regressing corpus luteum.

A complex interaction of endocrine and immune cells appears to be required to mediate the structural and functional regression of the bovine corpus luteum. Since chemokines act synergistically to activate their target cells ³⁷¹, additional studies are needed to examine the actions of chemokines as a complex cocktail rather in isolation as performed in the present study. The current findings complement a recent review ³⁸⁵ that postulates that immune cells in the developing and functional corpus luteum play a supportive role, but once corpus luteum regression is triggered, the immune cells promote apoptosis, debris clearance and tissue remodeling. Understanding these endocrine and immune events is important for increasing our ability to control reproductive function to facilitate full-term pregnancies in both humans and livestock.

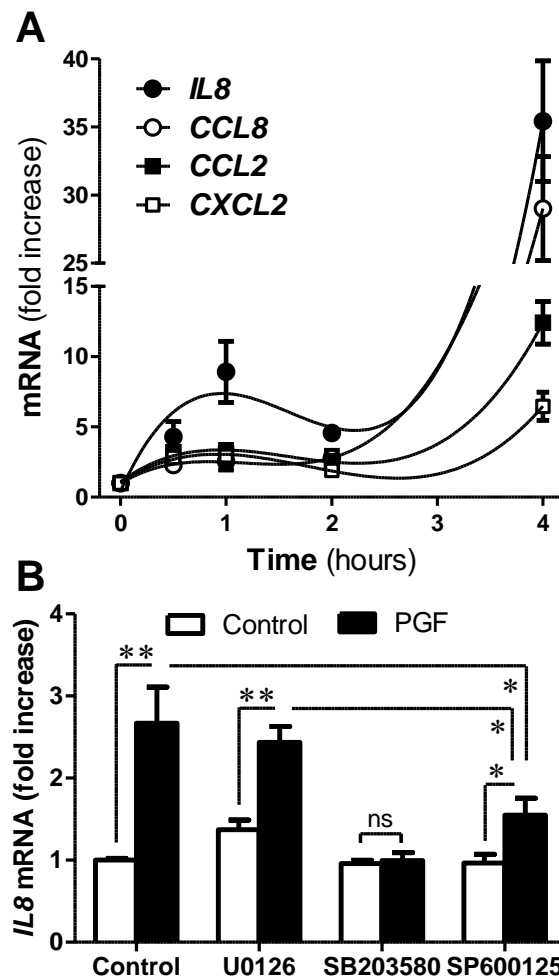


Figure 5-1 – Induction of chemokines following treatment with PGF in vivo and in vitro

A) Midluteal phase cows were treated with saline or the PGF analog Lutalyse (25 mg) for up to 4 h. Ovaries were surgically removed and RNA was isolated from corpora lutea. Quantitative real-time PCR was carried out. Results are shown as means \pm S.E.M., $n=3$. (B) To determine the cellular signaling pathway leading to the induction of IL8 mRNA, bovine steroidogenic luteal cells were pretreated for 60 min with vehicle, the ERK1/2 inhibitor U0126 (20 mM), the p38 MAPK inhibitor SB207580 (10 mM), or the JNK inhibitor SP600125 (20 mM). Luteal cells were then treated with control media (open bars) or PGF (100 nM, solid bars) for 60 min. Quantitative real-time PCR for IL8 mRNA was carried out. Results are shown as means S.E.M., $n=3$. * $P \leq 0.05$; ** $P \leq 0.01$; NS, not significant. Previously published in ²⁶⁰.

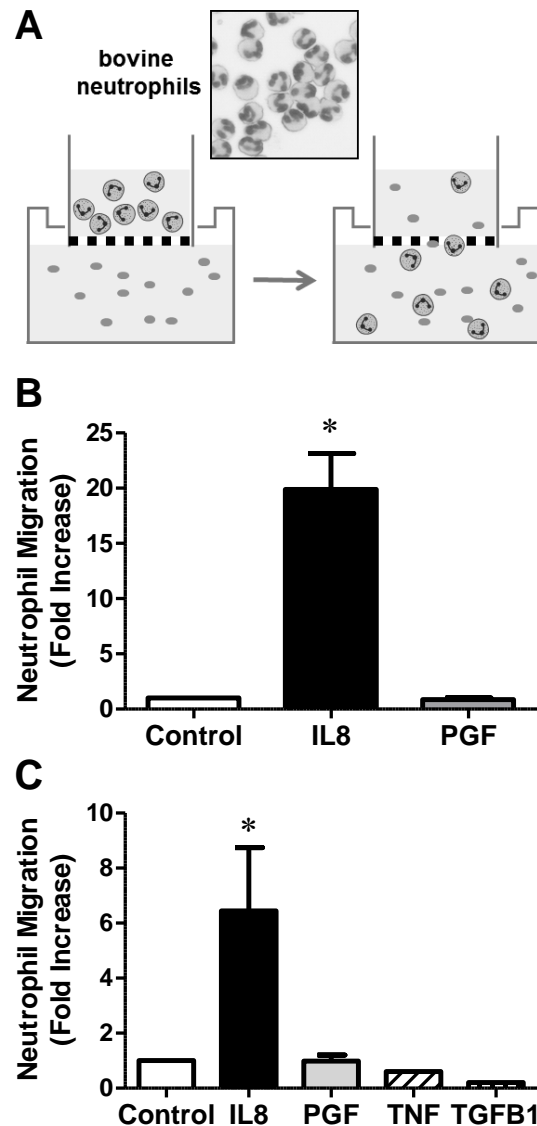
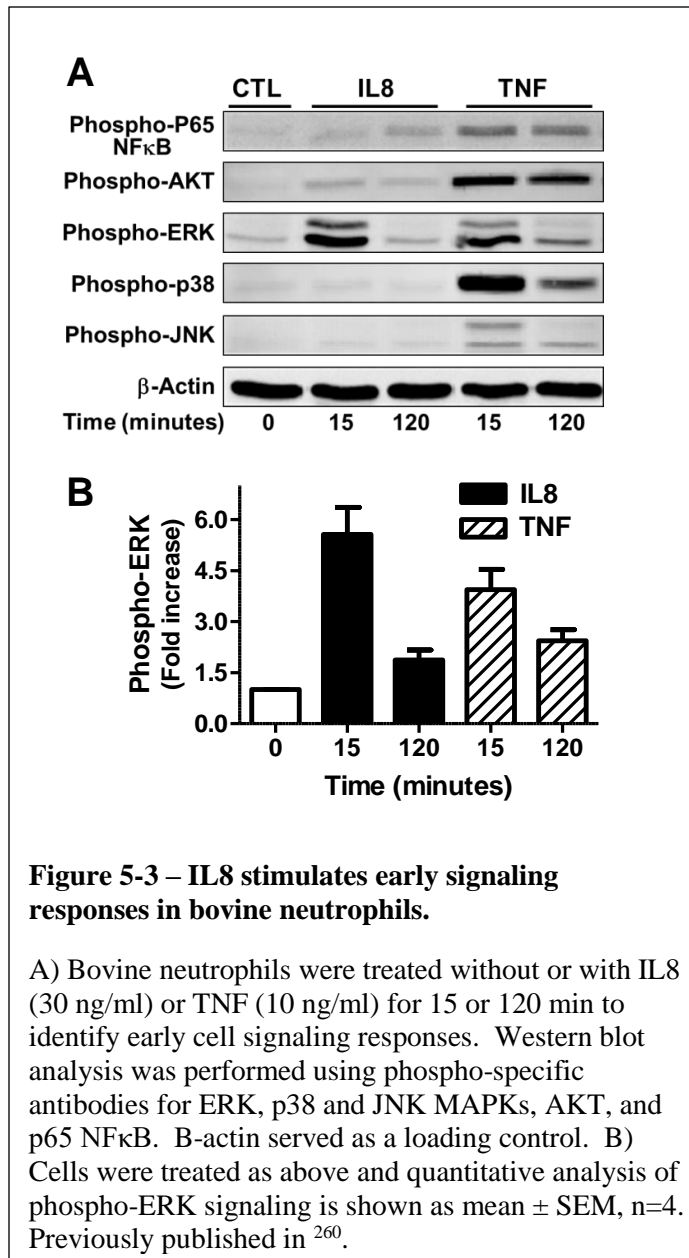
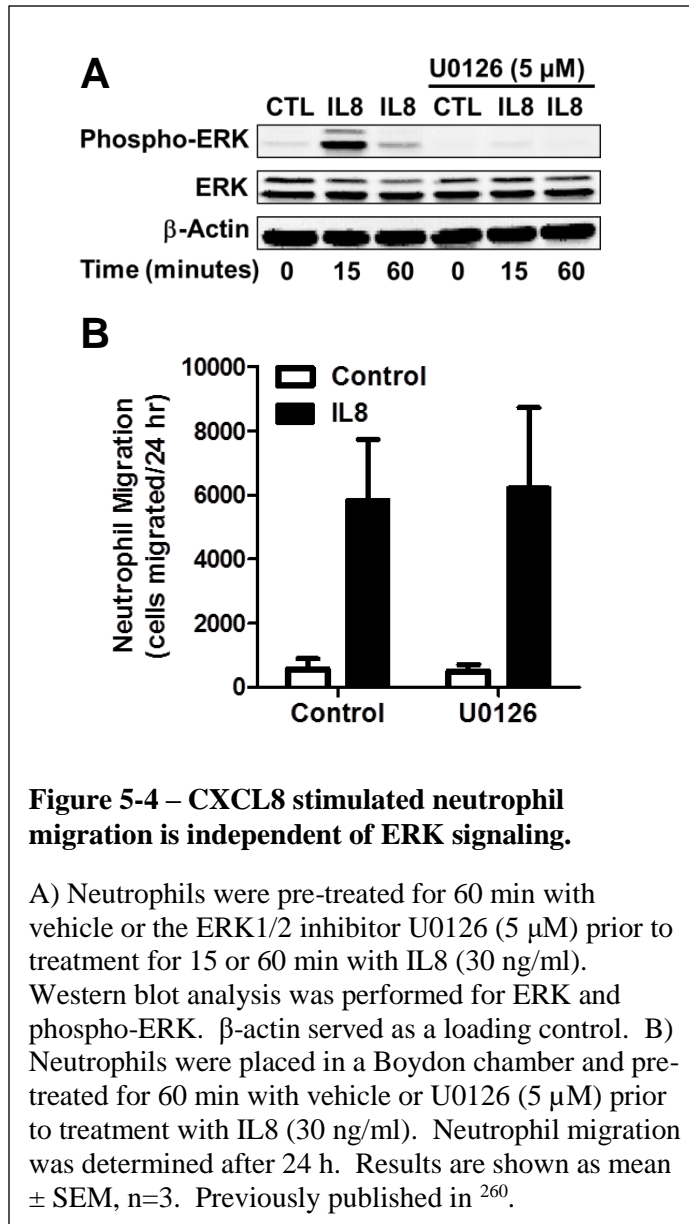


Figure 5-2 – Stimulatory effects of CXCL8 on neutrophils.

(A) Bovine neutrophils were isolated as described in the Materials and Methods. Hematoxylin and eosin stain of the purified bovine neutrophils used in the chemotaxis assay is shown in the figure. Neutrophils (105 cells) were placed in the upper chamber of a Boyden apparatus and control media or CXCL8 (30 ng/ml) was placed in the lower chamber. Cell numbers in the lower chamber were quantified at various intervals. (B) Control media (Control), CXCL8 (30 ng/ml) or PGF (100 nM) was added to the lower chamber and migration of bovine neutrophils was determined after 18 h. Results are shown as mean±S.E.M., n=3. *P≤0.05, vs control. (C) Control media (Control), CXCL8 (30 ng/ml), PGF (100 nM), TNF (10 ng/ml), or TGFB1 (1 ng/ml) was added to the lower chamber and migration of bovine neutrophils was determined after 3 h. Results are shown as mean±S.E.M., n=4 for CTL, CXCL8, PGF, and n=2 for TNF and TGFB1. *P≤0.05 vs control. Previously published in ²⁶⁰.





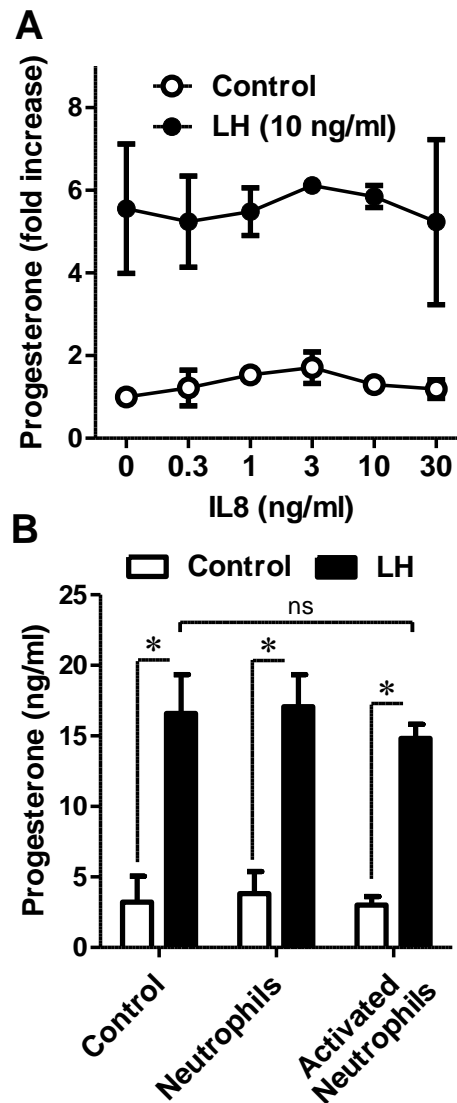


Figure 5-5 – CXCL8 and neutrophils do not inhibit luteal progesterone production.

(A) Steroidogenic luteal cells were pretreated with increasing amounts of CXCL8 (0–30 ng/ml) for 30 min and then treated without (Control) or with LH (10 ng/ml) for 4 h. Progesterone in the media was measured by radioimmunoassay (RIA). Results are shown as mean \pm S.E.M., $n=4$. (B) Steroidogenic luteal cells were co-cultured with bovine neutrophils or activated bovine neutrophils as described in the Materials and Methods. Cells were then treated without (Control) or with LH (10 ng/ml) for 4 h. Progesterone in the media was measured by RIA. Results are shown as mean \pm S.E.M., $n=3$. * $P \leq 0.05$ vs control; not significant (NS). Previously published in ²⁶⁰.

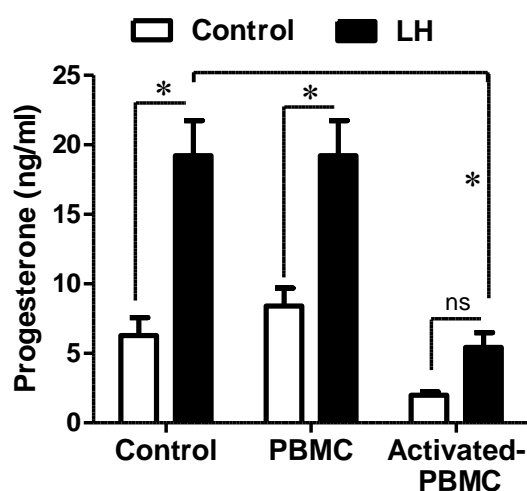


Figure 5-6 – Cocultures of luteal cells with activated peripheral blood mononuclear cells (PBMCs) inhibit luteal progesterone production.

Steroidogenic luteal cells were cocultured with bovine PBMCs or activated PBMCs as described in the Materials and methods. Cells were then treated without (Control) or with LH (10 ng/ml) for 4 h. Progesterone in the media was measured by RIA. Results are shown as mean \pm S.E.M., $n=4$. * $P \leq 0.05$; NS, not significant. Previously published in ²⁶⁰.

Table 5-1 – Bovine primers for qPCR

Gene Name	Primers for qPCR
CXCL8	F: TGTGAAGCTGCAGTTCTGTCAAG R: TGCACCCACTTTTCCTTGGGGT
CCL2	F: TGCTCGCTCAGCCAGATGCAAT R: GGACACTTGCTGCTGGTGACTCT
CCL8	F: TCTCAGGCTGAAGCCCCCGT R: ACTGAATCTGGCTGAGCGAGCA
CXCL2	F: GCGCCCCGTGGTCAACGAACT R: AGACTGGCTATGACTTCGGTTTGGT
ACTB	F: ACACCGCAACCAGTTCGCCAT R: AAGACGGCCCCGGGAGCATC
GAPDH	F: AGATGGTGAAGGTCGGAGTG R: GATCTCGCTCCTGGAAGATG

Previously published in ²⁶⁰.

Table 5-2 – Antibodies used for cell signaling, Western blots, and flow analysis

Antibody	Vendor
VE-cadherin	Pierce (Rockford, IL, USA)
StAR	Douglas Stocco, Ph.D. (Texas Tech Univ)
3β-HSD	Ian Mason, Ph.D. (Dallas, TX, USA)
P450scc	Millipore (Danvers, MA, USA)
Prolyl 4-hydroxylase	Acris (Brisbane, QLD, Australia)
Collagen 1	Rockland Monoclonal (Gilbertsville, PA, USA)
Phospho ERK1/2	Cell Signaling (Danvers, MA, USA)
Phospho p38	Cell Signaling (Danvers, MA, USA)
Phospho JNK	Santa Cruz (Santa Cruz, CA, USA)
Phospho AKT	Cell Signaling (Danvers, MA, USA)
Phospho P65-NF-κB	Cell Signaling (Danvers, MA, USA)
IκBα	Santa Cruz (Santa Cruz, CA, USA)
β-Actin	Sigma-Aldrich (St. Louis, MO, USA)
FITC mouse anti-human CD66b	AbD Serotec (Raleigh, NC, USA)
APC mouse anti-human CD11b	BD Biosciences (Franklin Lakes, NJ, USA)

Previously published in ²⁶⁰.

CHAPTER 6: DISCUSSION

6.1. Overview

This dissertation describes a study of the mechanisms regulating the genesis and involution of the temporary endocrine structure, the corpus luteum (CL), through use of a bovine model. During the rise of the CL, the composition and regulation of lipid droplets (LDs) were studied and it was determined that LDs comprise a substantial proportion of luteal cell structures, and store cholesteryl esters and triglycerides. As well, the LD-associated proteome was assessed and established that steroidogenic enzymes are enriched in purified luteal LD fractions. Demonstrating that luteal LDs may serve as critical mediators of steroidogenesis by storing substrates for steroidogenesis and a close association with steroidogenic enzymes. At the fall of the CL alterations in the luteal transcriptome were determined and revealed changes consistent with early activation of cytokine signaling. One target, C-X-C motif chemokine ligand 8 (previously IL-8), was assessed for its ability to regulate luteal cell function. CXCL8 expression was determined to be induced via p38 and JNK signaling and could induce bovine neutrophil migration however, only activated peripheral blood mononuclear cells (PBMC) could inhibit luteal cell progesterone secretion. Together, these data indicate that LDs and cytokines can play important roles in CL development, function, and regression.

6.2. Composition of the lipid droplets of the bovine corpus luteum

Within the bovine CL LDs are a prominent feature which are established by day 3 post-ovulation and maintained at mid-cycle (day 10). Lipid droplets are a large component of both early (day 3) and mid-cycle CL (day 10) comprising 26 - 36 $\mu\text{m}^2/\text{nuclei}$, which amounts to 5-16% of luteal cell area. These LDs are enriched in several classic LD-associated proteins as assessed by mRNA and protein abundance. Although the major constituent of bovine LDs is triglyceride, cholesteryl esters constitute $2.78 \pm 0.70 \text{ pmol}/\mu\text{g}$ protein. Luteal cells are enriched in cholesterol and cholesteryl esters compared to adipose tissue, likely for use in steroidogenesis. In contrast, the granulosa and theca cells of the follicle have few lipid droplets, and have reduced lipid

content (of all major classes) compared to the steroidogenic luteal cells. There does not appear to be a difference in lipid composition of granulosa versus theca cells or of the large luteal cells (LLC) versus small luteal cells (SLC). We propose that luteal LDs play a critical role in progesterone production by storing cholesteryl esters, and interacting with steroidogenic proteins to efficiently produce steroids.

6.3. Lipid droplets are dynamically regulated by luteinizing hormone signaling in the bovine corpus luteum

Lipid droplets and LD-associated proteins are under regulation by luteinizing hormone (LH) signaling in the bovine corpus luteum. As granulosa cells differentiate to form luteal cells increases in both LDs and LD-associated proteins, hormone sensitive lipase (HSL) and PLIN2 are seen which correlate with luteal differentiation markers and progesterone secretion. Signaling by LH causes phosphorylation at S563 and translocation of HSL, which are associated with an activated state of HSL. Furthermore, chemical inhibition of HSL prevents LH-induced progesterone secretion even in the presence of HDL-supplied cholesterol indicating that cholesteryl esters are processed by an HSL-dependent step. Finally, luteal lipid droplets have a high content of steroidogenic enzymes, 3β HSD and P450_{scc}, and LD-associated steroidogenic acute regulatory protein (StAR) can increase by 14-fold after activation of protein kinase A (PKA). These data lead us to believe that the surface of lipid droplets may serve as a novel platform for steroidogenesis through the intimate association and potential tethering of steroidogenic enzymes to the coat proteins of the lipid droplet to facilitate the handoff of steroid precursors at each step to produce efficiently steroids like progesterone (Figure 3-7).

These data have implications for our understanding of the biochemistry of steroidogenesis. As we learn more about how cholesterol is stored and utilized, particularly during steroidogenesis we can gain insight into how to manipulate the system to either increase or decrease steroid production. Our study has focused on non-pathological conditions to gain a clear insight into the role of LDs in highly steroidogenic tissues. Future studies into how LDs and flux of cholesterol

through cells is altered in obesity, and polycystic ovarian syndrome could indicate mechanisms by which those conditions impair fertility.

LDs are a natural consequence of granulosa-to-luteal cell differentiation. Stimulated but not basal progesterone is processed through an HSL-dependent and likely LD-dependent step. The surface of lipid droplets may serve as a novel platform for steroidogenesis by an intimate association with steroidogenic enzymes. The close proximity of mitochondria and the endoplasmic reticulum facilitates the handoff of steroid precursors at each step to efficiently produce steroids such as progesterone. Potentially this could involve physical tethering of mitochondria and the endoplasmic reticulum to the LD surface using a similar mechanism to mitochondrial associated membranes, which tether microdomains of the endoplasmic reticulum to mitochondria to facilitate lipid transfer ²²⁴.

6.4. Early transcriptome responses of the bovine mid-cycle corpus luteum to prostaglandin F2 alpha includes cytokine signaling

This study uses a systems biology approach to provide a detailed understanding of the early (0.5 – 4 h) mRNA changes that occur during PGF2 α -induced luteolysis *in vivo*. Our analysis predicts activation of cytokines (TNF α , IL-1 β , IL-6, IL-17A, & IL-33) and cytokine signaling intermediates (NF- κ B, signal transducer and activator of transcription (STAT)) early in the time-course. However, changes in cytokine transcripts are not apparent until 2 - 4 hours post-PGF2 α . The effects of PGF2 α *in vivo* may require the activation of secondary mediators, such as cytokines, which activate NF- κ B and STAT signaling because PGF2 α is unable to stimulate NF- κ B P65 phosphorylation in isolated luteal cells. The rapid influx of various immune cells in response to the initiation of luteolysis ^{207,209,246} and the release of pre-formed cytokines could explain the prediction of cytokine signaling effects very early in the PGF2 α response. As well, the activation of NF- κ B signaling could contribute to later responses seen after PGF2 α administration.

Shortly after PGF2 α administration, phospholipase C, PKC, Ca²⁺, and extracellular signal-regulated kinase (ERK) trigger a variety of signaling cascades to begin the luteolytic process. Our data suggests that *in vivo*, PGF2 α administration stimulates a series of transcriptional waves likely as a result of classical PGF2 α and cytokine signaling events, as early as 30 minutes post-PGF2 α treatment. This is the beginning of a cascade of events that will initiate decreases in progesterone secretion (2-12 hours post-PGF2 α) and result in the structural regression of the CL 12-18 hours post-PGF2 α ^{240,340}. The earliest decreases in progesterone secretion during luteolysis may be due to changes *LIPE*/HSL expression and other transcripts which regulate cholesterol availability rather than changes in the primary steroidogenic enzymes. We propose that during the early stages of functional regression in combination with PGF2 α , the reduction in progesterone, and increase in inflammatory cytokines (potentially including IL-33 and IL-17) contribute to luteal regression. As the intra-luteal concentrations of PGF2 α and inflammatory cytokines increase they may act within an auto-amplification loop eventually reaching a critical point from which there is no rescue from the luteolytic cascade ^{67,341–344}. Future studies to identify the specific transcriptional changes occurring in steroidogenic cells, endothelial cells, immune cells, and fibroblasts is needed to better understand the dynamic network of changes that enable functional and structural luteal regression.

6.5. Effects of CXCL8 and immune cells on the regulation of luteal progesterone secretion

For over thirty years the immune system has been postulated as essential for fertility ³⁶⁸. The present study provides additional insight into the expression and function of chemokines during luteal regression. We observed that induction of luteal regression in cows with a bolus of PGF2 α *in vivo* resulted in a rapid increase in the expression of *CXCL8*, *CCL8*, *CCL2*, and *CXCL2*. Our findings confirm recent findings by Shirasuna *et al.*, 2012 ²⁴⁶ that PGF2 α treatment of dairy cattle increased luteal *CXCL8* mRNA by approximately 4-fold within 30 min. In that study, the fold increase in *CXCL8* mRNA remained constant over 4-hr of treatment with PGF2 α . In the present

study using beef cattle, we observed more robust increases in luteal CXCL8 mRNA expression; a 9-fold increase within 1 h and 35-fold increases after 4 h of PGF2 α treatment. At present, it is not clear whether the differences in the magnitude of the responses are due to differences in the cattle breeds since there are reported differences in the responses of beef and dairy cattle to synchronization protocols using PGF2 α ³⁶⁹ or other factors. Based on the pronounced increase in CXCL8 expression, it was selected for further analysis. We found that CXCL8 acted directly on neutrophils but had little effect on other cell types in the mid-cycle corpus luteum. Furthermore, co-cultures of luteal cells with activated neutrophils did not alter LH-stimulated progesterone synthesis; whereas co-cultures with activated PBMCs suppressed LH-stimulated progesterone synthesis.

A complex interaction of endocrine and immune cells appears to be required to mediate the structural and functional regression of the bovine corpus luteum. Since chemokines act synergistically to activate their target cells³⁷¹, additional studies are needed to examine the actions of chemokines as a complex cocktail rather in isolation as performed in the present study. The current findings complement a recent review³⁸⁵ that postulates that immune cells in the developing and functional corpus luteum play a supportive role, but once corpus luteum regression has been triggered, the immune cells promote apoptosis, clearance of debris and tissue remodeling. Understanding these endocrine and immune events is important for increasing our ability to control reproductive function to facilitate full-term pregnancies in both humans and livestock.

6.6. Conclusions

This dissertation describes a study of the mechanisms regulating the genesis and involution of the temporary endocrine structure, the corpus luteum, using a bovine model. During the rise of the CL, the composition and regulation of LDs were studied and it was determined that LDs comprise a substantial proportion of luteal cell structures, and store cholesteryl esters and

triglycerides. Finally, the LD-associated proteome was determined and established that steroidogenic enzymes are enriched in purified LD fractions. This demonstrates that luteal LDs may serve as critical mediators of steroidogenesis by storing substrate and a close association with steroidogenic machinery. At the fall of the CL alterations in the luteal transcriptome were determined and revealed decreased *LIPE* levels as well as changes consistent with early activation of cytokine signaling. One target, C-X-C motif chemokine ligand 8 (previously IL-8), was assessed for its ability to regulate luteal cell function. CXCL8 expression was determined to be induced via p38 and JNK signaling and could induce bovine neutrophil migration, however, only activated PBMCs could inhibit luteal cell progesterone secretion. Together, these indicate that LDs and cytokines can play important roles in CL development, function, and regression.

BIBLIOGRAPHY

1. Greenberg, A. S. *et al.* The role of lipid droplets in metabolic disease in rodents and humans. *J. Clin. Invest.* **121**, 2102–10 (2011).
2. Thiam, A. R., Farese, R. V & Walther, T. C. The biophysics and cell biology of lipid droplets. *Nat. Rev. Mol. Cell Biol.* **14**, 775–86 (2013).
3. Wältermann, M. & Steinbüchel, A. Neutral lipid bodies in prokaryotes: recent insights into structure, formation, and relationship to eukaryotic lipid depots. *J. Bacteriol.* **187**, 3607–19 (2005).
4. Natarajan, S. K. *et al.* Structure, function and metabolism of hepatic and adipose tissue lipid droplets: implications in alcoholic liver disease. *Curr. Mol. Pharmacol.* (2015).
5. D’Souza, K., Nziroera, C. & Kienesberger, P. C. Lipid metabolism and signaling in cardiac lipotoxicity. *Biochim. Biophys. Acta* (2016). doi:10.1016/j.bbalip.2016.02.016
6. Yuan, Y., Li, P. & Ye, J. Lipid homeostasis and the formation of macrophage-derived foam cells in atherosclerosis. *Protein Cell* **3**, 173–81 (2012).
7. Servetnick, D. A. *et al.* Perilipins are associated with cholesteryl ester droplets in steroidogenic adrenal cortical and Leydig cells. *J. Biol. Chem.* **270**, 16970–3 (1995).
8. Shen, W.-J., Azhar, S. & Kraemer, F. B. Lipid droplets and steroidogenic cells. *Exp. Cell Res.* **340**, 209–14 (2016).
9. Konige, M., Wang, H. & Sztalryd, C. Role of adipose specific lipid droplet proteins in maintaining whole body energy homeostasis. *Biochim. Biophys. Acta* **1842**, 393–401 (2014).
10. Zechner, R. *et al.* FAT SIGNALS--lipases and lipolysis in lipid metabolism and signaling. *Cell Metab.* **15**, 279–91 (2012).
11. Beller, M., Thiel, K., Thul, P. J. & Jäckle, H. Lipid droplets: a dynamic organelle moves into

- focus. *FEBS Lett.* **584**, 2176–82 (2010).
12. Brasaemle, D. L. & Wolins, N. E. Packaging of fat: an evolving model of lipid droplet assembly and expansion. *J. Biol. Chem.* **287**, 2273–9 (2012).
 13. Farese, R. V & Walther, T. C. Lipid droplets finally get a little R-E-S-P-E-C-T. *Cell* **139**, 855–60 (2009).
 14. Yang, H., Galea, A., Sytnyk, V. & Crossley, M. Controlling the size of lipid droplets: lipid and protein factors. *Curr. Opin. Cell Biol.* **24**, 509–16 (2012).
 15. Olofsson, S.-O. *et al.* Lipid droplets as dynamic organelles connecting storage and efflux of lipids. *Biochim. Biophys. Acta* **1791**, 448–58 (2009).
 16. Brasaemle, D. L. Thematic review series: adipocyte biology. The perilipin family of structural lipid droplet proteins: stabilization of lipid droplets and control of lipolysis. *J. Lipid Res.* **48**, 2547–2559 (2007).
 17. Kimmel, A. R., Brasaemle, D. L., McAndrews-Hill, M., Sztalryd, C. & Londos, C. Adoption of PERILIPIN as a unifying nomenclature for the mammalian PAT-family of intracellular lipid storage droplet proteins. *J. Lipid Res.* **51**, 468–71 (2010).
 18. Paul, A., Chan, L. & Bickel, P. E. The PAT family of lipid droplet proteins in heart and vascular cells. *Curr. Hypertens. Rep.* **10**, 461–6 (2008).
 19. Nishino, N. *et al.* FSP27 contributes to efficient energy storage in murine white adipocytes by promoting the formation of unilocular lipid droplets. *J. Clin. Invest.* **118**, 2808–21 (2008).
 20. McManaman, J. L. *et al.* Perilipin-2-null mice are protected against diet-induced obesity, adipose inflammation, and fatty liver disease. *J. Lipid Res.* **54**, 1346–59 (2013).
 21. Sztalryd, C. *et al.* Functional compensation for adipose differentiation-related protein (ADFP) by Tip47 in an ADFP null embryonic cell line. *J. Biol. Chem.* **281**, 34341–8 (2006).

22. Chen, W. *et al.* Inactivation of Plin4 downregulates Plin5 and reduces cardiac lipid accumulation in mice. *Am. J. Physiol. Endocrinol. Metab.* **304**, E770-9 (2013).
23. Seachord, C. L., VandeVoort, C. a & Duffy, D. M. Adipose differentiation-related protein: a gonadotropin- and prostaglandin-regulated protein in primate periovulatory follicles. *Biol. Reprod.* **72**, 1305–14 (2005).
24. Yang, X. *et al.* Identification of perilipin-2 as a lipid droplet protein regulated in oocytes during maturation. *Reprod. Fertil. Dev.* **22**, 1262–71 (2010).
25. Feingold, K. R. *et al.* ADRP/ADFP and Mal1 expression are increased in macrophages treated with TLR agonists. *Atherosclerosis* **209**, 81–8 (2010).
26. Holm, C. Molecular mechanisms regulating hormone-sensitive lipase and lipolysis. *Biochem. Soc. Trans.* **31**, 1120–4 (2003).
27. Kraemer, F. B. Adrenal cholesterol utilization. *Mol. Cell. Endocrinol.* **265–266**, 42–5 (2007).
28. Osterlund, T. Structure-function relationships of hormone-sensitive lipase. *Eur. J. Biochem.* **268**, 1899–907 (2001).
29. Bickel, P. E., Tansey, J. T. & Welte, M. A. PAT proteins, an ancient family of lipid droplet proteins that regulate cellular lipid stores. *Biochim. Biophys. Acta* **1791**, 419–40 (2009).
30. Lampidonis, A. D., Rogdakis, E., Voutsinas, G. E. & Stravopodis, D. J. The resurgence of Hormone-Sensitive Lipase (HSL) in mammalian lipolysis. *Gene* **477**, 1–11 (2011).
31. Lafontan, M. & Langin, D. Lipolysis and lipid mobilization in human adipose tissue. *Prog. Lipid Res.* **48**, 275–97 (2009).
32. Krintel, C., Mörgelin, M., Logan, D. T. & Holm, C. Phosphorylation of hormone-sensitive lipase by protein kinase A in vitro promotes an increase in its hydrophobic surface area. *FEBS J.* **276**, 4752–62 (2009).

33. Su, C.-L. *et al.* Mutational analysis of the hormone-sensitive lipase translocation reaction in adipocytes. *J. Biol. Chem.* **278**, 43615–9 (2003).
34. Shen, W.-J., Patel, S., Natsu, V. & Kraemer, F. B. Mutational analysis of structural features of rat hormone-sensitive lipase. *Biochemistry* **37**, 8973–9 (1998).
35. Anthonsen, M. W., Rönstrand, L., Wernstedt, C., Degerman, E. & Holm, C. Identification of novel phosphorylation sites in hormone-sensitive lipase that are phosphorylated in response to isoproterenol and govern activation properties in vitro. *J. Biol. Chem.* **273**, 215–21 (1998).
36. Miyoshi, H. *et al.* Perilipin promotes hormone-sensitive lipase-mediated adipocyte lipolysis via phosphorylation-dependent and -independent mechanisms. *J. Biol. Chem.* **281**, 15837–44 (2006).
37. Watt, M. J. *et al.* Regulation of HSL serine phosphorylation in skeletal muscle and adipose tissue. *Am. J. Physiol. Endocrinol. Metab.* **290**, E500–8 (2006).
38. Londos, C. *et al.* Perilipin: unique proteins associated with intracellular neutral lipid droplets in adipocytes and steroidogenic cells. *Biochem. Soc. Trans.* **23**, 611–5 (1995).
39. Lobo, M. V. T. *et al.* Hormone-sensitive lipase expression and IHC localization in the rat ovary, oviduct, and uterus. *J. Histochem. Cytochem.* **57**, 51–60 (2009).
40. Kraemer, F. B. *et al.* Hormone-sensitive lipase is required for high-density lipoprotein cholesteryl ester-supported adrenal steroidogenesis. *Mol. Endocrinol.* **18**, 549–57 (2004).
41. Kraemer, F. B. *et al.* Adrenal neutral cholesteryl ester hydrolase: identification, subcellular distribution, and sex differences. *Endocrinology* **143**, 801–6 (2002).
42. Manna, P. R. *et al.* Mechanisms of action of hormone-sensitive lipase in mouse Leydig cells: its role in the regulation of the steroidogenic acute regulatory protein. *J. Biol. Chem.* **288**,

8505–18 (2013).

43. Shen, W.-J. *et al.* Interaction of hormone-sensitive lipase with steroidogenic acute regulatory protein: facilitation of cholesterol transfer in adrenal. *J. Biol. Chem.* **278**, 43870–6 (2003).
44. Rone, M. B., Fan, J. & Papadopoulos, V. Cholesterol transport in steroid biosynthesis: role of protein-protein interactions and implications in disease states. *Biochim. Biophys. Acta* **1791**, 646–58 (2009).
45. Arrese, E. L., Saudale, F. Z. & Soulages, J. L. Lipid Droplets as Signaling Platforms Linking Metabolic and Cellular Functions. *Lipid Insights* **7**, 7–16 (2014).
46. Murphy, S., Martin, S. & Parton, R. G. Lipid droplet-organelle interactions; sharing the fats. *Biochim. Biophys. Acta* **1791**, 441–7 (2009).
47. Wu, C. C., Howell, K. E., Neville, M. C., Yates, J. R. & McManaman, J. L. Proteomics reveal a link between the endoplasmic reticulum and lipid secretory mechanisms in mammary epithelial cells. *Electrophoresis* **21**, 3470–82 (2000).
48. Brasaemle, D. L., Dolios, G., Shapiro, L. & Wang, R. Proteomic analysis of proteins associated with lipid droplets of basal and lipolytically stimulated 3T3-L1 adipocytes. *J. Biol. Chem.* **279**, 46835–42 (2004).
49. Cho, S. Y. *et al.* Identification of mouse Prp19p as a lipid droplet-associated protein and its possible involvement in the biogenesis of lipid droplets. *J. Biol. Chem.* **282**, 2456–65 (2007).
50. Turró, S. *et al.* Identification and characterization of associated with lipid droplet protein 1: A novel membrane-associated protein that resides on hepatic lipid droplets. *Traffic* **7**, 1254–69 (2006).
51. Zhang, H. *et al.* Proteome of skeletal muscle lipid droplet reveals association with

- mitochondria and apolipoprotein a-I. *J. Proteome Res.* **10**, 4757–68 (2011).
52. Umlauf, E. *et al.* Association of stomatin with lipid bodies. *J. Biol. Chem.* **279**, 23699–709 (2004).
 53. Fujimoto, Y. *et al.* Identification of major proteins in the lipid droplet-enriched fraction isolated from the human hepatocyte cell line HuH7. *Biochim. Biophys. Acta* **1644**, 47–59 (2004).
 54. Sato, S. *et al.* Proteomic profiling of lipid droplet proteins in hepatoma cell lines expressing hepatitis C virus core protein. *J. Biochem.* **139**, 921–30 (2006).
 55. Khor, V. K. *et al.* The proteome of cholesteryl-ester-enriched versus triacylglycerol-enriched lipid droplets. *PLoS One* **9**, e105047 (2014).
 56. Yamaguchi, T. *et al.* Characterization of lipid droplets in steroidogenic MLTC-1 Leydig cells: Protein profiles and the morphological change induced by hormone stimulation. *Biochim. Biophys. Acta* **1851**, 1285–95 (2015).
 57. Wang, W. *et al.* Proteomic analysis of murine testes lipid droplets. *Sci. Rep.* **5**, 12070 (2015).
 58. Chitraju, C. *et al.* Lipidomic analysis of lipid droplets from murine hepatocytes reveals distinct signatures for nutritional stress. *J. Lipid Res.* **53**, 2141–52 (2012).
 59. Xu, L., Zhou, L. & Li, P. CIDE proteins and lipid metabolism. *Arterioscler. Thromb. Vasc. Biol.* **32**, 1094–8 (2012).
 60. Strauss, J. F., Seifter, E., Lien, E. L., Goodman, D. B. & Stambaugh, R. L. Lipid metabolism in regressing rat corpora lutea of pregnancy. *J. Lipid Res.* **18**, 246–58 (1977).
 61. Waterman, R. A. Lipid and arachidonic acid accumulation in naturally regressing porcine corpora lutea. *Prostaglandins* **20**, 57–71 (1980).
 62. Waterman, R. A. & Guthrie, H. D. Effects of Cloprostenol administration on neutral lipid and

- prostaglandin F metabolism by porcine luteal tissue. - PubMed - NCBI. *Prostaglandins* **27**, 131–46 (1984).
63. Waterman, R. A. Changes in lipid contents and fatty acid compositions in ovine corpora lutea during the estrous cycle and early pregnancy. *Biol. Reprod.* **38**, 605–15 (1988).
64. Weinhouse, S. & Brewer, J. I. Cyclic variations in the lipids of the corpus luteum. *J. Biol. Chem.* **143**, 617–623 (1942).
65. Davis, J. S. & Rueda, B. R. The corpus luteum: an ovarian structure with maternal instincts and suicidal tendencies. *Front. Biosci.* **7**, d1949-78 (2002).
66. Alila, H. W., Dowd, J. P., Corradino, R. A., Harris, W. V & Hansel, W. Control of progesterone production in small and large bovine luteal cells separated by flow cytometry. *J. Reprod. Fertil.* **82**, 645–55 (1988).
67. Niswender, G. D. *et al.* Judge, jury and executioner: the auto-regulation of luteal function. *Soc. Reprod. Fertil. Suppl.* **64**, 191–206 (2007).
68. Wiltbank, M. C. *et al.* Comparison of endocrine and cellular mechanisms regulating the corpus luteum of primates and ruminants. *Anim. Reprod.* **9**, 242–259 (2012).
69. Marcinkiewicz, A., Gauthier, D., Garcia, A. & Brasaemle, D. L. The phosphorylation of serine 492 of perilipin a directs lipid droplet fragmentation and dispersion. *J. Biol. Chem.* **281**, 11901–9 (2006).
70. Orlicky, D. J., Monks, J., Stefanski, A. L. & McManaman, J. L. Dynamics and molecular determinants of cytoplasmic lipid droplet clustering and dispersion. *PLoS One* **8**, e66837 (2013).
71. Bogan, R. L. & Niswender, G. D. Constitutive steroidogenesis in ovine large luteal cells may be mediated by tonically active protein kinase A. *Biol. Reprod.* **77**, 209–16 (2007).

72. O'Neill, H. M., Holloway, G. P. & Steinberg, G. R. AMPK regulation of fatty acid metabolism and mitochondrial biogenesis: implications for obesity. *Mol. Cell. Endocrinol.* **366**, 135–51 (2013).
73. Dunning, K. R., Russell, D. L. & Robker, R. L. Lipids and oocyte developmental competence: The role of fatty acids and β -oxidation. *Reproduction* **148**, (2014).
74. Paczkowski, M., Schoolcraft, W. B. & Krisher, R. L. Fatty acid metabolism during maturation affects glucose uptake and is essential to oocyte competence. *Reproduction* **148**, 429–39 (2014).
75. Midzak, A. S., Chen, H., Aon, M. A., Papadopoulos, V. & Zirkin, B. R. ATP synthesis, mitochondrial function, and steroid biosynthesis in rodent primary and tumor Leydig cells. *Biol. Reprod.* **84**, 976–85 (2011).
76. Brown, K. A., Samarajeewa, N. U. & Simpson, E. R. Endocrine-related cancers and the role of AMPK. *Mol. Cell. Endocrinol.* **366**, 170–9 (2013).
77. Ross, F. A., MacKintosh, C. & Hardie, D. G. AMP-activated protein kinase: a cellular energy sensor that comes in 12 flavours. *FEBS J.* **283**, 2987–3001 (2016).
78. Bertoldo, M. J., Faure, M., Dupont, J. & Froment, P. AMPK: a master energy regulator for gonadal function. *Front. Neurosci.* **9**, 1–11 (2015).
79. Hardie, D. G. AMPK: positive and negative regulation, and its role in whole-body energy homeostasis. *Curr. Opin. Cell Biol.* **33**, 1–7 (2015).
80. Hardie, D. G. Regulation of AMP-activated protein kinase by natural and synthetic activators. *Acta Pharm. Sin. B* **6**, 1–19 (2016).
81. Hardie, D. G., Schaffer, B. E. & Brunet, A. AMPK: An Energy-Sensing Pathway with Multiple Inputs and Outputs. *Trends Cell Biol.* **26**, 190–201 (2015).

82. Daval, M. *et al.* Anti-lipolytic action of AMP-activated protein kinase in rodent adipocytes. - PubMed - NCBI. *J. Biol. Chem.* 25250–25257 (2005).
83. Kraemer, F. B., Khor, V. K., Shen, W.-J. & Azhar, S. Cholesterol ester droplets and steroidogenesis. *Mol. Cell. Endocrinol.* **371**, 15–19 (2013).
84. Dupont, J., Chabrolle, C., Ramé, C., Tosca, L. & Coyral-Castel, S. Role of the peroxisome proliferator-activated receptors, adenosine monophosphate-activated kinase, and adiponectin in the ovary. *PPAR Res.* **2008**, 176275 (2008).
85. Tosca, L., Chabrolle, C., Uzbekova, S. & Dupont, J. Effects of metformin on bovine granulosa cells steroidogenesis: possible involvement of adenosine 5' monophosphate-activated protein kinase (AMPK). *Biol. Reprod.* **76**, 368–78 (2007).
86. Tosca, L., Chabrolle, C., Crochet, S., Tesseraud, S. & Dupont, J. IGF-1 receptor signaling pathways and effects of AMPK activation on IGF-1-induced progesterone secretion in hen granulosa cells. *Domest. Anim. Endocrinol.* **34**, 204–16 (2008).
87. Tosca, L. *et al.* Adenosine 5'-monophosphate-activated protein kinase regulates progesterone secretion in rat granulosa cells. *Endocrinology* **146**, 4500–13 (2005).
88. Tosca, L., Ramé, C., Chabrolle, C., Tesseraud, S. & Dupont, J. Metformin decreases IGF1-induced cell proliferation and protein synthesis through AMP-activated protein kinase in cultured bovine granulosa cells. *Reproduction* **139**, 409–18 (2010).
89. Will, M. A., Palaniappan, M., Peegel, H., Kayampilly, P. & Menon, K. M. J. Metformin: direct inhibition of rat ovarian theca-interstitial cell proliferation. *Fertil. Steril.* **98**, 207–14 (2012).
90. Palaniappan, M., Menon, B. & Menon, K. M. J. Stimulatory effect of insulin on theca-interstitial cell proliferation and cell cycle regulatory proteins through MTORC1 dependent pathway. *Mol. Cell. Endocrinol.* **366**, 81–9 (2013).

91. Bowdridge, E. C., Goravanahally, M. P., Inskip, E. K. & Flores, J. A. Activation of Adenosine Monophosphate-Activated Protein Kinase Is an Additional Mechanism That Participates in Mediating Inhibitory Actions of Prostaglandin F₂α in Mature, but Not Developing, Bovine Corpora Lutea. *Biol. Reprod.* **93**, 7 (2015).
92. Wright, M. F. *et al.* Mechanisms of intracellular calcium homeostasis in developing and mature bovine corpora lutea. *Biol. Reprod.* **90**, 55 (2014).
93. Goravanahally, M. P., Salem, M., Yao, J., Inskip, E. K. & Flores, J. A. Differential gene expression in the bovine corpus luteum during transition from early phase to midphase and its potential role in acquisition of luteolytic sensitivity to prostaglandin F₂ α. *Biol. Reprod.* **80**, 980–8 (2009).
94. Hou, X., Arvisais, E. & Davis, J. Luteinizing hormone stimulates mammalian target of rapamycin signaling in bovine luteal cells via pathways independent of AKT and mitogen-activated protein kinase. *Endocrinology* **151**, 2846–2857 (2010).
95. Hawley, S. A. *et al.* Phosphorylation by Akt within the ST loop of AMPK-α1 down-regulates its activation in tumour cells. *Biochem. J.* **459**, 275–87 (2014).
96. Hurley, R. L. *et al.* Regulation of AMP-activated protein kinase by multisite phosphorylation in response to agents that elevate cellular cAMP. *J. Biol. Chem.* **281**, 36662–72 (2006).
97. Horman, S. *et al.* Insulin antagonizes ischemia-induced Thr172 phosphorylation of AMP-activated protein kinase α-subunits in heart via hierarchical phosphorylation of Ser485/491. *J. Biol. Chem.* **281**, 5335–40 (2006).
98. Djouder, N. *et al.* PKA phosphorylates and inactivates AMPKα to promote efficient lipolysis. *EMBO J.* **29**, 469–81 (2010).
99. Alila, H. W., Davis, J. S., Dowd, J. P., Corradino, R. A. & Hansel, W. Differential effects of calcium on progesterone production in small and large bovine luteal cells. *J. Steroid*

- Biochem.* **36**, 687–93 (1990).
100. Davis, J. S. *et al.* Second messenger systems and progesterone secretion in the small cells of the bovine corpus luteum: effects of gonadotropins and prostaglandin F2a. *J. Steroid Biochem.* **32**, 643–9 (1989).
 101. Davis, J. S., Weakland, L. L., Farese, R. V & West, L. A. Luteinizing hormone increases inositol trisphosphate and cytosolic free Ca²⁺ in isolated bovine luteal cells. *J. Biol. Chem.* **262**, 8515–8521 (1987).
 102. Roy, L. *et al.* Convergence of 3',5'-Cyclic Adenosine 5'-Monophosphate/Protein Kinase A and Glycogen Synthase Kinase-3b/b-Catenin Signaling in Corpus Luteum Progesterone Synthesis. *Endocrinology* **150**, 5036–5045 (2009).
 103. Kahn, B. B., Alquier, T., Carling, D. & Hardie, D. G. AMP-activated protein kinase: ancient energy gauge provides clues to modern understanding of metabolism. *Cell Metab.* **1**, 15–25 (2005).
 104. Mao, D. *et al.* ATF3 expression in the corpus luteum: possible role in luteal regression. *Mol. Endocrinol.* **27**, 2066–79 (2013).
 105. Chen, D., Fong, H. W. & Davis, J. S. Induction of c-fos and c-jun messenger ribonucleic acid expression by prostaglandin F2alpha is mediated by a protein kinase C-dependent extracellular signal-regulated kinase mitogen-activated protein kinase pathway in bovine luteal cells. *Endocrinology* **142**, 887–95 (2001).
 106. Hou, X. *et al.* Prostaglandin F2alpha stimulates the expression and secretion of transforming growth factor B1 via induction of the early growth response 1 gene (EGR1) in the bovine corpus luteum. *Mol. Endocrinol.* **22**, 403–14 (2008).
 107. Guo, N. *et al.* Prostaglandin F2 α induces expression of activating transcription factor 3 (ATF3) and activates MAPK signaling in the rat corpus luteum. *Acta Histochem.* **117**,

- 211–8 (2015).
108. Atli, M. O. *et al.* Patterns of gene expression in the bovine corpus luteum following repeated intrauterine infusions of low doses of prostaglandin F2alpha. *Biol. Reprod.* **86**, 130 (2012).
 109. Sen, A., Browning, J., Inskeep, E. K., Lewis, P. & Flores, J. A. Expression and activation of protein kinase C isozymes by prostaglandin F(2alpha) in the early- and mid-luteal phase bovine corpus luteum. *Biol. Reprod.* **70**, 379–84 (2004).
 110. Arvisais, E. W., Romanelli, A., Hou, X. & Davis, J. S. AKT-independent phosphorylation of TSC2 and activation of mTOR and ribosomal protein S6 kinase signaling by prostaglandin F2alpha. *J. Biol. Chem.* **281**, 26904–26913 (2006).
 111. Yoon, M.-S. Vps34 and PLD1 take center stage in nutrient signaling: their dual roles in regulating autophagy. *Cell Commun. Signal.* **13**, 44 (2015).
 112. Mizushima, N. & Komatsu, M. Autophagy: renovation of cells and tissues. *Cell* **147**, 728–41 (2011).
 113. Dall’Armi, C., Devereaux, K. A. & Di Paolo, G. The role of lipids in the control of autophagy. *Curr. Biol.* **23**, R33–45 (2013).
 114. Gawriluk, T. R. *et al.* Autophagy is a cell survival program for female germ cells in the murine ovary. *Reproduction* **141**, 759–65 (2011).
 115. Song, Z.-H. *et al.* Germ cell-specific Atg7 knockout results in primary ovarian insufficiency in female mice. *Cell Death Dis.* **6**, e1589 (2015).
 116. Choi, J., Jo, M., Lee, E. & Choi, D. AKT is involved in granulosa cell autophagy regulation via mTOR signaling during rat follicular development and atresia. *Reproduction* **147**, 73–80 (2014).

117. Morais, R. D. V. S., Thomé, R. G., Lemos, F. S., Bazzoli, N. & Rizzo, E. Autophagy and apoptosis interplay during follicular atresia in fish ovary: a morphological and immunocytochemical study. *Cell Tissue Res.* **347**, 467–78 (2012).
118. Quatacker, J. R. Formation of autophagic vacuoles during human corpus luteum involution. *Z. Zellforsch. Mikrosk. Anat.* **122**, 479–87 (1971).
119. Paavola, L. G. The corpus luteum of the guinea pig. II. Cytochemical studies on the Golgi complex, GERL, and lysosomes in luteal cells during maximal progesterone secretion. *J. Cell Biol.* **79**, 45–58 (1978).
120. Stacy, B. D., Gemmell, R. T. & Thorburn, G. D. Morphology of the corpus luteum in the sheep during regression induced by prostaglandin F₂ALPHA. *Biol. Reprod.* **14**, 280–91 (1976).
121. McClellan, M. C., Abel, J. H. & Niswender, G. D. Function of lysosomes during luteal regression in normally cycling and PGF alpha-treated ewes. *Biol. Reprod.* **16**, 499–512 (1977).
122. Gawriluk, T. R., Ko, C., Hong, X., Christenson, L. K. & Rucker, E. B. Beclin-1 deficiency in the murine ovary results in the reduction of progesterone production to promote preterm labor. *Proc. Natl. Acad. Sci. U. S. A.* **111**, E4194-203 (2014).
123. Aboelenain, M. *et al.* Status of autophagy, lysosome activity and apoptosis during corpus luteum regression in cattle. *J. Reprod. Dev.* **61**, 229–36 (2015).
124. Gaytán, M., Morales, C., Sánchez-Criado, J. E. & Gaytán, F. Immunolocalization of beclin 1, a bcl-2-binding, autophagy-related protein, in the human ovary: possible relation to life span of corpus luteum. *Cell Tissue Res.* **331**, 509–17 (2008).
125. Choi, J., Jo, M., Lee, E. & Choi, D. The role of autophagy in corpus luteum regression in the rat. *Biol. Reprod.* **85**, 465–72 (2011).

126. Choi, J., Jo, M., Lee, E. & Choi, D. ERK1/2 is involved in luteal cell autophagy regulation during corpus luteum regression via an mTOR-independent pathway. *Mol. Hum. Reprod.* **20**, 972–80 (2014).
127. Maejima, Y., Isobe, M. & Sadoshima, J. Regulation of autophagy by Beclin 1 in the heart. *J. Mol. Cell. Cardiol.* **95**, 19–25 (2016).
128. Lin, H. *et al.* Activating transcription factor 3 protects against pressure-overload heart failure via the autophagy molecule Beclin-1 pathway. *Mol. Pharmacol.* **85**, 682–91 (2014).
129. Yuan, J. *et al.* MYBL2 guides autophagy suppressor VDAC2 in the developing ovary to inhibit autophagy through a complex of VDAC2-BECN1-BCL2L1 in mammals. *Autophagy* **11**, 1081–98 (2015).
130. Martinez-Lopez, N. & Singh, R. Autophagy and Lipid Droplets in the Liver. *Annu. Rev. Nutr.* **35**, 215–37 (2015).
131. Shibata, M. *et al.* LC3, a microtubule-associated protein1A/B light chain3, is involved in cytoplasmic lipid droplet formation. *Biochem. Biophys. Res. Commun.* **393**, 274–9 (2010).
132. Shpilka, T. *et al.* Lipid droplets and their component triglycerides and sterol esters regulate autophagosome biogenesis. *EMBO J.* **34**, e201490315 (2015).
133. Velikkakath, A. K. G., Nishimura, T., Oita, E., Ishihara, N. & Mizushima, N. Mammalian Atg2 proteins are essential for autophagosome formation and important for regulation of size and distribution of lipid droplets. *Mol. Biol. Cell* **23**, 896–909 (2012).
134. Stocco, C., Telleria, C. & Gibori, G. The molecular control of corpus luteum formation, function, and regression. *Endocr. Rev.* **28**, 117–149 (2007).
135. Micks, E., Raglan, G. B. & Schulkin, J. Bridging progestogens in pregnancy and

- pregnancy prevention. *Endocr. Connect.* **4**, R81-92 (2015).
136. Wiltbank, M. C. *et al.* Physiological and practical effects of progesterone on reproduction in dairy cattle. *Animal* **8 Suppl 1**, 70–81 (2014).
 137. Spencer, T. E., Forde, N. & Lonergan, P. The role of progesterone and conceptus-derived factors in uterine biology during early pregnancy in ruminants. *J. Dairy Sci.* **99**, 5941–50 (2016).
 138. Sudhindra Mohan, B. Mid-luteal phase plasma progesterone levels in spontaneous and clomiphene citrate induced conception cycles. *J. Obstet. Gynecol. India* **55**, 350–352 (2005).
 139. Stricker, R. *et al.* Establishment of detailed reference values for luteinizing hormone, follicle stimulating hormone, estradiol, and progesterone during different phases of the menstrual cycle on the Abbott ARCHITECT analyzer. *Clin. Chem. Lab. Med.* **44**, 883–7 (2006).
 140. Sartori, R., Haughian, J. M., Shaver, R. D., Rosa, G. J. M. & Wiltbank, M. C. Comparison of ovarian function and circulating steroids in estrous cycles of Holstein heifers and lactating cows. *J. Dairy Sci.* **87**, 905–20 (2004).
 141. Carroll, D. J., Grummer, R. R. & Clayton, M. K. Stimulation of luteal cell progesterone production by lipoproteins from cows fed control or fat-supplemented diets. *J. Dairy Sci.* **75**, 2205–14 (1992).
 142. Bao, B., Thomas, M. G. & Williams, G. L. Regulatory roles of high-density and low-density lipoproteins in cellular proliferation and secretion of progesterone and insulin-like growth factor I by enriched cultures of bovine small and large luteal cells. *J. Anim. Sci.* **75**, 3235–45 (1997).
 143. O'Shaughnessy, P. J. & Wathes, D. C. Role of lipoproteins and de-novo cholesterol

- synthesis in progesterone production by cultured bovine luteal cells. *Reproduction* **74**, 425–432 (1985).
144. Grummer, R. R. & Carroll, D. J. A review of lipoprotein cholesterol metabolism: importance to ovarian function. *J. Anim. Sci.* **66**, 3160–73 (1988).
 145. Adams, E. C. & Hertig, A. T. Studies on the human corpus luteum. I. Observations on the ultrastructure of development and regression of the luteal cells during the menstrual cycle. *J. Cell Biol.* **41**, 696–715 (1969).
 146. Blanchette, E. J. Ovarian steroid cells. II. The lutein cell. *J. Cell Biol.* **31**, 517–42 (1966).
 147. Parry, D. M., Willcox, D. L. & Thorburn, G. D. Ultrastructural and cytochemical study of the bovine corpus luteum. *J. Reprod. Fertil.* **60**, 349–57 (1980).
 148. Armstrong, D. T. & Flint, A. P. Isolation and properties of cholesterol ester storage granules from ovarian tissues. *Biochem. J.* **134**, 399–406 (1973).
 149. Blanchette, E. J. Ovarian steroid cells. I. Differentiation of the lutein cell from the granulosa follicle cell during the preovulatory stage and under the influence of exogenous gonadotrophins. *J. Cell Biol.* **31**, 501–16 (1966).
 150. Foley, R. C., Reece, R. P. & Leathem, J. H. Histochemical Observations of the Bovine Uterus, Placenta, and Corpus Luteum during early Pregnancy. *J. Anim. Sci.* **13**, 131 (1954).
 151. Leckie, F. H. A histochemical study of the human ovary; preliminary report. *J. Obstet. Gynaecol. Br. Emp.* **61**, 772–6 (1954).
 152. Guraya, S. S. Histochemical observations on the lipid changes in the rat corpus luteum during various reproductive states. *J. Reprod. Fertil.* **42**, 59–65 (1975).
 153. Guraya, S. S. Some observations on the histochemical features of developing follicle and

- corpus luteum in the cat and dog ovary. *Acta Vet. Acad. Sci. Hung.* **19**, 351–62 (1969).
154. Sangha, G. K., Sharma, R. K. & Guraya, S. S. Biology of corpus luteum in small ruminants. *Small Rumin. Res.* **43**, 53–64 (2002).
 155. Guraya, S. S. Histochemical observations on the lipid changes in rat corpora lutea during various reproductive states after treatment with exogenous hormones. *J. Reprod. Fertil.* **43**, 67–75 (1975).
 156. Heath, E., Weinstein, P., Merritt, B., Shanks, R. & Hixon, J. Effects of prostaglandins on the bovine corpus luteum: granules, lipid inclusions and progesterone secretion. *Biol. Reprod.* **29**, 977–85 (1983).
 157. Armstong, D. T. & Black, D. L. Influence of luteinizing hormone on corpus luteum metabolism and progesterone biosynthesis throughout the bovine estrous cycle. *Endocrinology* **78**, 937–44 (1966).
 158. Khanthusaeng, V. *et al.* Lipid droplets in cultured luteal cells in non-pregnant sheep fed different planes of nutrition. *Acta Histochem.* **118**, 553–9 (2016).
 159. Deane, H. W., Hay, M. F., Moor, R. M., Rowson, L. E. & Short, R. V. The corpus luteum of the sheep: relationships between morphology and function during the oestrous cycle. *Acta Endocrinol. (Copenh).* **51**, 245–63 (1966).
 160. Hashemi, H. F. & Goodman, J. M. The life cycle of lipid droplets. *Curr. Opin. Cell Biol.* **33**, 119–24 (2015).
 161. Talbott, H. A. & Davis, J. S. in *The Life Cycle of the Corpus Luteum* (ed. Meidan, R.) 57–78 (Springer International Publishing, 2017). doi:10.1007/978-3-319-43238-0_4
 162. Gross, D. A. & Silver, D. L. Cytosolic lipid droplets: from mechanisms of fat storage to disease. *Crit. Rev. Biochem. Mol. Biol.* **49**, 304–26

163. Najt, C. P. *et al.* Structural and functional assessment of perilipin 2 lipid binding domain(s). *Biochemistry* **53**, 7051–66 (2014).
164. Hickenbottom, S. J., Kimmel, A. R., Londos, C. & Hurley, J. H. Structure of a lipid droplet protein; the PAT family member TIP47. *Structure* **12**, 1199–207 (2004).
165. Yu, J. *et al.* Lipid droplet remodeling and interaction with mitochondria in mouse brown adipose tissue during cold treatment. *Biochim. Biophys. Acta* **1853**, 918–28 (2015).
166. Pu, J. *et al.* Interactomic study on interaction between lipid droplets and mitochondria. *Protein Cell* **2**, 487–96 (2011).
167. Robenek, H. *et al.* Adipophilin-enriched domains in the ER membrane are sites of lipid droplet biogenesis. *J. Cell Sci.* **119**, 4215–24 (2006).
168. Velázquez, A. P., Tatsuta, T., Ghillebert, R., Drescher, I. & Graef, M. Lipid droplet-mediated ER homeostasis regulates autophagy and cell survival during starvation. *J. Cell Biol.* **212**, 621–31 (2016).
169. Barneda, D. *et al.* The brown adipocyte protein CIDEA promotes lipid droplet fusion via a phosphatidic acid-binding amphipathic helix. *Elife* **4**, e07485 (2015).
170. Zhang, X., Wang, Y. & Liu, P. Omic studies reveal the pathogenic lipid droplet proteins in non-alcoholic fatty liver disease. *Protein Cell* **8**, 4–13 (2017).
171. Lang, P. D. & Insull, W. Lipid droplets in atherosclerotic fatty streaks of human aorta. *J. Clin. Invest.* **49**, 1479–88 (1970).
172. Schneider, C. A., Rasband, W. S. & Eliceiri, K. W. NIH Image to ImageJ: 25 years of image analysis. *Nat. Methods* **9**, 671–5 (2012).
173. Davis, J. S., Farese, R. V & Marsh, J. M. Stimulation of phospholipid labeling and steroidogenesis by luteinizing hormone in isolated bovine luteal cells. *Endocrinology* **109**,

- 469–475 (1981).
174. Ding, Y., Wu, Y., Zeng, R. & Liao, K. Proteomic profiling of lipid droplet-associated proteins in primary adipocytes of normal and obese mouse. *Acta Biochim. Biophys. Sin. (Shanghai)*. **44**, 394–406 (2012).
 175. Brasaemle, D. L. & Wolins, N. E. Isolation of lipid droplets from cells by density gradient centrifugation. *Curr. Protoc. Cell Biol.* **Chapter 3**, Unit 3.15 (2006).
 176. Bligh, E. G. & Dyer, W. J. A rapid method of total lipid extraction and purification. *Can. J. Biochem. Physiol.* **37**, 911–7 (1959).
 177. Folch, J., Lees, M. & Sloane Stanley, G. H. A simple method for the isolation and purification of total lipides from animal tissues. *J. Biol. Chem.* **226**, 497–509 (1957).
 178. Mangold, H. K. & Malins, D. C. Fractionation of fats, oils, and waxes on thin layers of silicic acid. *J. Am. Oil Chem. Soc.* **37**, 383–385 (1960).
 179. Rizzo, W. B. *et al.* Abnormal fatty alcohol metabolism in cultured keratinocytes from patients with Sjögren-Larsson syndrome. *J. Lipid Res.* **49**, 410–419 (2008).
 180. Hawkins, D. E. *et al.* An increase in serum lipids increases luteal lipid content and alters the disappearance rate of progesterone in cows. *J. Anim. Sci.* **73**, 541–5 (1995).
 181. Guraya, S. S. Histochemical study of granulosa and theca interna during follicular development, ovulation, and corpus luteum formation and regression in the human ovary. *Am. J. Obstet. Gynecol.* **101**, 448–57 (1968).
 182. Guraya, S. S. A histochemical study of pre-ovulatory and post-ovulatory follicles in the rabbit ovary. *J. Reprod. Fertil.* **15**, 381–387 (1968).
 183. Christenson, L. K. *et al.* Research resource: preovulatory LH surge effects on follicular theca and granulosa transcriptomes. *Mol. Endocrinol.* **27**, 1153–71 (2013).

184. Jansen, H., de Greef, W. J. & Uilenbroek, J. T. Localization of liver-type lipase in rat ovaries and its activity during the estrous cycle and lactation. *Mol. Cell. Endocrinol.* **42**, 253–8 (1985).
185. Shemesh, M., Bensadoun, A. & Hansel, W. Lipoprotein lipase activity in the bovine corpus luteum during the estrous cycle and early pregnancy. *Proc. Soc. Exp. Biol. Med.* **151**, 667–9 (1976).
186. Paciga, M., McCudden, C. R., Londos, C., DiMattia, G. E. & Wagner, G. F. Targeting of big stanniocalcin and its receptor to lipid storage droplets of ovarian steroidogenic cells. *J. Biol. Chem.* **278**, 49549–54 (2003).
187. Chegini, N., Ramani, N. & Rao, C. V. Morphological and biochemical characterization of small and large bovine luteal cells during pregnancy. *Mol. Cell. Endocrinol.* **37**, 89–102 (1984).
188. Fields, M. J., Barros, C. M., Watkins, W. B. & Fields, P. A. Characterization of large luteal cells and their secretory granules during the estrous cycle of the cow. *Biol. Reprod.* **46**, 535–45 (1992).
189. Meidan, R., Girsh, E., Blum, O. & Aberdam, E. In vitro differentiation of bovine theca and granulosa cells into small and large luteal-like cells: morphological and functional characteristics. *Biol. Reprod.* **43**, 913–21 (1990).
190. Claesson, L. Quantitative relationship between gonadotrophic stimulation and lipid changes in the interstitial gland of the rabbit ovary. *Acta Physiol. Scand. Suppl.* **31**, 23–51 (1954).
191. Guraya, S. S. Cytochemical observations concerning the formation, release, and transport of lipid secretory products in the interstitial (thecal) cells of the rabbit ovary. *Z. Zellforsch. Mikrosk. Anat.* **83**, 187–95 (1967).

192. Waterman, R. A. Lipid metabolism and in vitro production of progesterone and prostaglandin F during induced regression of porcine corpora lutea. *Prostaglandins* **20**, 73–85 (1980).
193. Welte, M. A. Expanding roles for lipid droplets. *Curr. Biol.* **25**, R470-81 (2015).
194. Hartwig, I. R., Pincus, M. K., Diemert, A., Hecher, K. & Arck, P. C. Sex-specific effect of first-trimester maternal progesterone on birthweight. *Hum. Reprod.* **28**, 77–86 (2013).
195. Jayasooriya, G. S. & Lamont, R. F. The use of progesterone and other progestational agents to prevent spontaneous preterm labour and preterm birth. *Expert Opin. Pharmacother.* **10**, 1007–1016 (2009).
196. Chang, H. H. *et al.* Preventing preterm births: analysis of trends and potential reductions with interventions in 39 countries with very high human development index. *Lancet* **381**, 223–234 (2013).
197. Lucy, M. C. Reproductive loss in high-producing dairy cattle: where will it end? *J. Dairy Sci.* **84**, 1277–1293 (2001).
198. Geary, T. Management strategies to reduce embryonic loss. in *Range Beef Cow Symposium* 36 (2005).
199. Humblot, P. Use of pregnancy specific proteins and progesterone assays to monitor pregnancy and determine the timing, frequencies and sources of embryonic mortality in ruminants. *Theriogenology* **56**, 1417–1433 (2001).
200. Mann, G. E. & Lamming, G. E. The Influence of Progesterone During Early Pregnancy in Cattle. *Reprod. Domest. Anim.* **34**, 269–274 (1999).
201. Devoto, L., Kohen, P., Muñoz, A. & Strauss, J. F. Human corpus luteum physiology and the luteal-phase dysfunction associated with ovarian stimulation. *Reprod. Biomed. Online*

- 18 Suppl 2**, 19–24 (2009).
202. Bukulmez, O. & Arici, A. Luteal phase defect: myth or reality. *Obstet. Gynecol. Clin. North Am.* **31**, 727–744 (2004).
 203. Shirasuna, K. *et al.* Vascular and immune regulation of corpus luteum development, maintenance, and regression in the cow. *Domest. Anim. Endocrinol.* **43**, 198–211 (2012).
 204. Woad, K. J. & Robinson, R. S. Luteal angiogenesis and its control. *Theriogenology* **86**, 221–8 (2016).
 205. Best, C. L., Pudney, J., Welch, W. R., Burger, N. & Hill, J. A. Localization and characterization of white blood cell populations within the human ovary throughout the menstrual cycle and menopause. *Hum. Reprod.* **11**, 790–797 (1996).
 206. Brännström, M., Pascoe, V., Norman, R. J. & McClure, N. Localization of leukocyte subsets in the follicle wall and in the corpus luteum throughout the human menstrual cycle. *Fertil. Steril.* **61**, 488–95 (1994).
 207. Jientaweewoon, S. *et al.* Evidence that polymorphonuclear neutrophils infiltrate into the developing corpus luteum and promote angiogenesis with interleukin-8 in the cow. *Reprod. Biol. Endocrinol.* **9**, 79 (2011).
 208. Dahm-Kähler, P., Ghahremani, M., Lind, A.-K., Sundfeldt, K. & Brännström, M. Monocyte chemotactic protein-1 (MCP-1), its receptor, and macrophages in the perifollicular stroma during the human ovulatory process. *Fertil. Steril.* **91**, 231–9 (2009).
 209. Penny, L. A. *et al.* Immune cells and cytokine production in the bovine corpus luteum throughout the oestrous cycle and after induced luteolysis. *J. Reprod. Fertil.* **115**, 87–96 (1999).
 210. Hausman, G. J., Barb, C. R. & Lents, C. A. Leptin and reproductive function. *Biochimie*

- 94**, 2075–81 (2012).
211. Wehrman, M. E., Welsh, T. H. & Williams, G. L. Diet-induced hyperlipidemia in cattle modifies the intrafollicular cholesterol environment, modulates ovarian follicular dynamics, and hastens the onset of postpartum luteal activity. *Biol. Reprod.* **45**, 514–22 (1991).
 212. Spicer, L. J. & Echternkamp, S. E. The ovarian insulin and insulin-like growth factor system with an emphasis on domestic animals. *Domest. Anim. Endocrinol.* **12**, 223–45 (1995).
 213. Neuvians, T. P., Pfaffl, M. W., Berisha, B. & Schams, D. The mRNA expression of insulin receptor isoforms (IR-A and IR-B) and IGFR-2 in the bovine corpus luteum during the estrous cycle, pregnancy, and induced luteolysis. *Endocrine* **22**, 93–100 (2003).
 214. Zhou, P. *et al.* IGF-I Signaling Is Essential for FSH Stimulation of AKT and Steroidogenic Genes in Granulosa Cells. *Mol. Endocrinol.* (2013). doi:10.1210/me.2012-1307
 215. Smith, G. D., Jackson, L. M. & Foster, D. L. Leptin regulation of reproductive function and fertility. *Theriogenology* **57**, 73–86 (2002).
 216. Barb, C. R., Hausman, G. J. & Lents, C. A. Energy metabolism and leptin: effects on neuroendocrine regulation of reproduction in the gilt and sow. *Reprod. Domest. Anim.* **43 Suppl 2**, 324–30 (2008).
 217. Kuokkanen, S. *et al.* Corpus luteum as a novel target of weight changes that contribute to impaired female reproductive physiology and function. *Syst. Biol. Reprod. Med.* **62**, 227–42 (2016).
 218. Talavera, F., Park, C. S. & Williams, G. L. Relationships among dietary lipid intake, serum cholesterol and ovarian function in Holstein heifers. *J. Anim. Sci.* **60**, 1045–51

- (1985).
219. Silva, R. C., B  o, S. N., Jivago, J. L. P. R. R. & Lucci, C. M. Ultrastructural characterization of porcine oocytes and adjacent follicular cells during follicle development: lipid component evolution. *Theriogenology* **76**, 1647–57 (2011).
 220. Romereim, S. M. *et al.* Gene expression profiling of bovine ovarian follicular and luteal cells provides insight into cellular identities and functions. *Mol. Cell. Endocrinol.* **439**, 379–394 (2017).
 221. Talbott, H. A. *et al.* Early transcriptome responses of the bovine mid-cycle corpus luteum to prostaglandin F2 alpha includes cytokine signaling. *Mol. Cell. Endocrinol.* **Submitted**, (2017).
 222. Keller, A., Nesvizhskii, A. I., Kolker, E. & Aebersold, R. Empirical statistical model to estimate the accuracy of peptide identifications made by MS/MS and database search. *Anal. Chem.* **74**, 5383–92 (2002).
 223. Nesvizhskii, A. I., Keller, A., Kolker, E. & Aebersold, R. A statistical model for identifying proteins by tandem mass spectrometry. *Anal. Chem.* **75**, 4646–58 (2003).
 224. Prasad, M. *et al.* Mitochondria-associated endoplasmic reticulum membrane (MAM) regulates steroidogenic activity via steroidogenic acute regulatory protein (StAR)-voltage-dependent anion channel 2 (VDAC2) interaction. *J. Biol. Chem.* **290**, 2604–16 (2015).
 225. Green, J. A. & Maqueo, M. Ultrastructure of the human ovary. I. The luteal cell during the menstrual cycle. *Am. J. Obstet. Gynecol.* **92**, 946–57 (1965).
 226. Vance, J. E. MAM (mitochondria-associated membranes) in mammalian cells: lipids and beyond. *Biochim. Biophys. Acta* **1841**, 595–609 (2014).
 227. *The Life Cycle of the Corpus Luteum.* (Springer International Publishing, 2017).

doi:10.1007/978-3-319-43238-0

228. Wetendorf, M. & DeMayo, F. J. Progesterone receptor signaling in the initiation of pregnancy and preservation of a healthy uterus. *Int. J. Dev. Biol.* **58**, 95–106 (2014).
229. Del Canto, F. *et al.* Features of natural and gonadotropin-releasing hormone antagonist-induced corpus luteum regression and effects of in vivo human chorionic gonadotropin. *J. Clin. Endocrinol. Metab.* **92**, 4436–43 (2007).
230. Niswender, G. D., Juengel, J. L., Silva, P. J., Rollyson, M. K. & McIntush, E. W. Mechanisms controlling the function and life span of the corpus luteum. *Physiol. Rev.* **80**, 1–29 (2000).
231. Väänänen, J. E., Lee, S., Väänänen, C. C., Yuen, B. H. & Leung, P. C. Stepwise activation of the gonadotropic signal transduction pathway, and the ability of prostaglandin F2alpha to inhibit this activated pathway. *Endocrine* **8**, 301–7 (1998).
232. Mejia, R., Waite, C. & Ascoli, M. Activation of Gq/11 in the mouse corpus luteum is required for parturition. *Mol. Endocrinol.* **29**, 238–46 (2015).
233. McCann, T. J. & Flint, A. P. Use of pertussis toxin to investigate the mechanism of action of prostaglandin F2 alpha on the corpus luteum in sheep. *J. Mol. Endocrinol.* **10**, 79–85 (1993).
234. Lahav, M., Davis, J. S. & Rennert, H. Mechanism of the luteolytic action of prostaglandin F-2 alpha in the rat. *J. Reprod. Fertil.* **37**, 233–40 (1989).
235. Davis, J. S., Weakland, L. L., Weiland, D. A., Farese, R. V & West, L. A. Prostaglandin F2 alpha stimulates phosphatidylinositol 4,5-bisphosphate hydrolysis and mobilizes intracellular Ca²⁺ in bovine luteal cells. *Proc. Natl. Acad. Sci. U. S. A.* **84**, 3728–32 (1987).

236. Kurusu, S., Iwao, M., Kawaminami, M. & Hashimoto, I. Involvement of cytosolic phospholipase A2 in the ovulatory process in gonadotropin-primed immature rats. *Prostaglandins. Leukot. Essent. Fatty Acids* **58**, 405–11 (1998).
237. Kurusu, S., Sapirstein, A. & Bonventre, J. V. Group IVA phospholipase A2 optimizes ovulation and fertilization in rodents through induction of and metabolic coupling with prostaglandin endoperoxide synthase 2. *FASEB J.* **26**, 3800–3810 (2012).
238. Chen, D. B., Westfall, S. D., Fong, H. W., Roberson, M. S. & Davis, J. S. Prostaglandin F2alpha stimulates the Raf/MEK1/mitogen-activated protein kinase signaling cascade in bovine luteal cells. *Endocrinology* **139**, 3876–85 (1998).
239. Arvisais, E. *et al.* Prostaglandin F2alpha represses IGF-I-stimulated IRS1/phosphatidylinositol-3-kinase/AKT signaling in the corpus luteum: role of ERK and P70 ribosomal S6 kinase. *Mol. Endocrinol.* **24**, 632–43 (2010).
240. Yadav, V. K., Sudhagar, R. R. & Medhamurthy, R. Apoptosis during spontaneous and prostaglandin F(2alpha)-induced luteal regression in the buffalo cow (*Bubalus bubalis*): involvement of mitogen-activated protein kinases. *Biol. Reprod.* **67**, 752–9 (2002).
241. Yadav, V. K. & Medhamurthy, R. Dynamic changes in mitogen-activated protein kinase (MAPK) activities in the corpus luteum of the bonnet monkey (*Macaca radiata*) during development, induced luteolysis, and simulated early pregnancy: a role for p38 MAPK in the regulation of luteal functio. *Endocrinology* **147**, 2018–27 (2006).
242. Miyamoto, A., Okuda, K., Schweigert, F. J. & Schams, D. Effects of basic fibroblast growth factor, transforming growth factor-beta and nerve growth factor on the secretory function of the bovine corpus luteum in vitro. *J. Endocrinol.* **135**, 103–14 (1992).
243. Zheng, X., Price, C. A., Tremblay, Y., Lussier, J. G. & Carrière, P. D. Role of transforming growth factor-beta1 in gene expression and activity of estradiol and

- progesterone-generating enzymes in FSH-stimulated bovine granulosa cells. *Reproduction* **136**, 447–57 (2008).
244. Maroni, D. & Davis, J. S. TGFB1 disrupts the angiogenic potential of microvascular endothelial cells of the corpus luteum. *J. Cell Sci.* **124**, 2501–2510 (2011).
 245. Maroni, D. & Davis, J. S. Transforming Growth Factor Beta 1 Stimulates Profibrotic Activities of Luteal Fibroblasts in Cows. *Biol. Reprod.* **87**, 1–11 (2012).
 246. Shirasuna, K. *et al.* Rapid accumulation of polymorphonuclear neutrophils in the corpus luteum during prostaglandin F(2 α)-induced luteolysis in the cow. *PLoS One* **7**, e29054 (2012).
 247. Brännström, M., Giesecke, L., Moore, I. C., van den Heuvel, C. J. & Robertson, S. A. Leukocyte subpopulations in the rat corpus luteum during pregnancy and pseudopregnancy. *Biol. Reprod.* **50**, 1161–7 (1994).
 248. Bauer, M., Reibiger, I. & Spaniel-Borowski, K. Leucocyte proliferation in the bovine corpus luteum. *Reproduction* **121**, 297–305 (2001).
 249. Gaytán, F. *et al.* Macrophages, cell proliferation, and cell death in the human menstrual corpus luteum. *Biol. Reprod.* **59**, 417–425 (1998).
 250. Wu, R., Van der Hoek, K. H., Ryan, N. K., Norman, R. J. & Robker, R. L. Macrophage contributions to ovarian function. *Hum. Reprod. Update* **10**, 119–133 (2004).
 251. Duncan, W. C., Rodger, F. E. & Illingworth, P. J. The human corpus luteum: reduction in macrophages during simulated maternal recognition of pregnancy. *Hum. Reprod.* **13**, 2435–42 (1998).
 252. Pate, J. L., Johnson-Larson, C. J. & Ottobre, J. S. Life or death decisions in the corpus luteum. *Reprod. Domest. Anim.* **47 Suppl 4**, 297–303 (2012).

253. Townson, D. H. & Liptak, A. R. Chemokines in the corpus luteum: implications of leukocyte chemotaxis. *Reprod. Biol. Endocrinol.* **1**, 94 (2003).
254. Henkes, L. E., Davis, J. S. & Rueda, B. R. Mutant mouse models and their contribution to our knowledge of corpus luteum development, function and regression. *Reprod. Biol. Endocrinol.* **1**, 87 (2003).
255. Neuvians, T. P., Schams, D., Berisha, B. & Pfaffl, M. W. Involvement of pro-inflammatory cytokines, mediators of inflammation, and basic fibroblast growth factor in prostaglandin F₂α-induced luteolysis in bovine corpus luteum. *Biol. Reprod.* **70**, 473–80 (2004).
256. Shah, K. B., Tripathy, S., Suganthi, H. & Rudraiah, M. Profiling of luteal transcriptome during prostaglandin F₂-α treatment in buffalo cows: analysis of signaling pathways associated with luteolysis. *PLoS One* **9**, e104127 (2014).
257. Mondal, M. *et al.* Deciphering the luteal transcriptome: potential mechanisms mediating stage-specific luteolytic response of the corpus luteum to prostaglandin F₂α. *Physiol. Genomics* **43**, 447–56 (2011).
258. Penny, L. A. *et al.* Expression of monocyte chemoattractant protein-1 in the bovine corpus luteum around the time of natural luteolysis. *Biol. Reprod.* **59**, 1464–9 (1998).
259. Townson, D. H., O'Connor, C. L. & Pru, J. K. Expression of monocyte chemoattractant protein-1 and distribution of immune cell populations in the bovine corpus luteum throughout the estrous cycle. *Biol. Reprod.* **66**, 361–6 (2002).
260. Talbott, H. A. *et al.* Effects of IL8 and immune cells on the regulation of luteal progesterone secretion. *Reproduction* **148**, 21–31 (2014).
261. Pitzel, L., Jarry, H. & Wuttke, W. Effects and interactions of prostaglandin F₂ α, oxytocin, and cytokines on steroidogenesis of porcine luteal cells. *Endocrinology* **132**,

- 751–6 (1993).
262. Wuttke, W., Pitzel, L., Knoke, I., Theiling, K. & Jarry, H. Immune-endocrine interactions affecting luteal function in pigs. *J. Reprod. Fertil. Suppl.* **52**, 19–29 (1997).
 263. Benyo, D. F. & Pate, J. L. Tumor necrosis factor-alpha alters bovine luteal cell synthetic capacity and viability. *Endocrinology* **130**, 854–60 (1992).
 264. Fairchild, D. L. & Pate, J. L. Modulation of bovine luteal cell synthetic capacity by interferon-gamma. *Biol. Reprod.* **44**, 357–63 (1991).
 265. Estevez, A., Tognetti, T., Luchetti, C. G., Sander, V. & Motta, A. B. Sequence of interleukin 1beta actions on corpus luteum regression: relationship with inducible cyclooxygenase and nitric oxide synthase expression. *Reproduction* **126**, 639–45 (2003).
 266. Hurwitz, A. *et al.* Interleukin-1 beta inhibits progesterone accumulation in rat corpora luteal cell cultures in a mechanism dissociated from its effects on nitric oxide and prostaglandin E accumulation. *Mol. Cell. Endocrinol.* **133**, 41–8 (1997).
 267. Nothnick, W. B. & Pate, J. L. Interleukin-1 beta is a potent stimulator of prostaglandin synthesis in bovine luteal cells. *Biol. Reprod.* **43**, 898–903 (1990).
 268. Hojo, T., Oda, A., Lee, S.-H., Acosta, T. J. & Okuda, K. Effects of tumor necrosis factor α and Interferon γ on the viability and mRNA expression of TNF receptor type I in endothelial cells from the bovine corpus luteum. *J. Reprod. Dev.* **56**, 515–9 (2010).
 269. Pru, J. K., Lynch, M. P., Davis, J. S. & Rueda, B. R. Signaling mechanisms in tumor necrosis factor alpha-induced death of microvascular endothelial cells of the corpus luteum. *Reprod. Biol. Endocrinol.* **1**, 17 (2003).
 270. Taniguchi, H., Yokomizo, Y. & Okuda, K. Fas-Fas ligand system mediates luteal cell death in bovine corpus luteum. *Biol. Reprod.* **66**, 754–9 (2002).

271. Jo, T. *et al.* Apoptosis of cultured mouse luteal cells induced by tumor necrosis factor- α and interferon- γ . *Anat. Rec.* **241**, 70–6 (1995).
272. Petroff, M. G., Petroff, B. K. & Pate, J. L. Mechanisms of cytokine-induced death of cultured bovine luteal cells. *Reproduction* **121**, 753–760 (2001).
273. Nishimura, R. & Okuda, K. Multiple roles of hypoxia in ovarian function: roles of hypoxia-inducible factor-related and -unrelated signals during the luteal phase. *Reprod. Fertil. Dev.* (2015). doi:10.1071/RD15010
274. Nishimura, R., Komiyama, J., Tasaki, Y., Acosta, T. J. & Okuda, K. Hypoxia promotes luteal cell death in bovine corpus luteum. *Biol. Reprod.* **78**, 529–36 (2008).
275. Shirasuna, K., Sasahara, K., Matsui, M., Shimizu, T. & Miyamoto, A. Prostaglandin F $_{2\alpha}$ differentially affects mRNA expression relating to angiogenesis, vasoactivation and prostaglandins in the early and mid corpus luteum in the cow. *J. Reprod. Dev.* **56**, 428–36 (2010).
276. Shirasuna, K. *et al.* Expression of prostaglandin F $_{2\alpha}$ (PGF $_{2\alpha}$) receptor and its isoforms in the bovine corpus luteum during the estrous cycle and PGF $_{2\alpha}$ -induced luteolysis. *Domest. Anim. Endocrinol.* **43**, 227–38 (2012).
277. Youngquist, R. S., Garverick, H. A. & Keisler, D. H. Use of umbilical cord clamps for ovariectomy in cows. *J. Am. Vet. Med. Assoc.* **207**, 474–5 (1995).
278. Summers, A. F. *et al.* Altered theca and cumulus oocyte complex gene expression, follicular arrest and reduced fertility in cows with dominant follicle follicular fluid androgen excess. *PLoS One* **9**, e110683 (2014).
279. Talbott, H. A. *et al.* Transcriptomic and bioinformatic analysis of short prostaglandin F $_{2\alpha}$ time-course in bovine corpus luteum. *Data Br.* **in press**, (2017).

280. Smyth, G. K. Linear models and empirical bayes methods for assessing differential expression in microarray experiments. *Stat. Appl. Genet. Mol. Biol.* **3**, Article3 (2004).
281. Gentleman, R. C. *et al.* Bioconductor: open software development for computational biology and bioinformatics. *Genome Biol.* **5**, R80 (2004).
282. R Core Team. R: A Language and Environment for Statistical Computing.
283. Tamayo, P. *et al.* Interpreting patterns of gene expression with self-organizing maps: methods and application to hematopoietic differentiation. *Proc. Natl. Acad. Sci. U. S. A.* **96**, 2907–2912 (1999).
284. Huang, D. W., Sherman, B. T. & Lempicki, R. A. Bioinformatics enrichment tools: paths toward the comprehensive functional analysis of large gene lists. *Nucleic Acids Res.* **37**, 1–13 (2009).
285. Huang, D. W., Sherman, B. T. & Lempicki, R. A. Systematic and integrative analysis of large gene lists using DAVID bioinformatics resources. *Nat. Protoc.* **4**, 44–57 (2009).
286. Mi, H., Muruganujan, A., Casagrande, J. T. & Thomas, P. D. Large-scale gene function analysis with the PANTHER classification system. *Nat. Protoc.* **8**, 1551–66 (2013).
287. Mi, H., Poudel, S., Muruganujan, A., Casagrande, J. T. & Thomas, P. D. PANTHER version 10: expanded protein families and functions, and analysis tools. *Nucleic Acids Res.* **44**, D336–42 (2016).
288. Thomas, P. D. *et al.* Applications for protein sequence-function evolution data: mRNA/protein expression analysis and coding SNP scoring tools. *Nucleic Acids Res.* **34**, W645–50 (2006).
289. Szklarczyk, D. *et al.* STRING v10: protein-protein interaction networks, integrated over the tree of life. *Nucleic Acids Res.* **43**, D447–52 (2015).

290. Davis, J. S. Stimulation of intracellular free Ca^{2+} by luteinizing hormone in isolated bovine luteal cells. *Adv. Exp. Med. Biol.* **219**, 671–675 (1987).
291. Leonard, W. J. & Lin, J. X. Cytokine receptor signaling pathways. *J. Allergy Clin. Immunol.* **105**, 877–88 (2000).
292. Lawrence, T. The nuclear factor NF-kappaB pathway in inflammation. *Cold Spring Harb. Perspect. Biol.* **1**, a001651 (2009).
293. Schaper, F. & Rose-John, S. Interleukin-6: Biology, signaling and strategies of blockade. *Cytokine Growth Factor Rev.* **26**, 475–87 (2015).
294. Salverson, R. R., DeJarnette, J. M., Marshall, C. E. & Wallace, R. A. Synchronization of estrus in virgin beef heifers using melengestrol acetate and PGF $_{2\alpha}$: an efficacy comparison of cloprostenol and dinoprost tromethamine. *Theriogenology* **57**, 853–8 (2002).
295. Arts, R. J. W., Joosten, L. A. B., van der Meer, J. W. M. & Netea, M. G. TREM-1: intracellular signaling pathways and interaction with pattern recognition receptors. *J. Leukoc. Biol.* **93**, 209–15 (2013).
296. Abayasekara, D. R., Jones, P. M., Persaud, S. J., Michael, A. E. & Flint, A. P. Prostaglandin F $_{2\alpha}$ activates protein kinase C in human ovarian cells. *Mol. Cell. Endocrinol.* **91**, 51–7 (1993).
297. Skarzynski, D. J., Kobayashi, S. & Okuda, K. Influence of nitric oxide and noradrenaline on prostaglandin F $_{2\alpha}$ -induced oxytocin secretion and intracellular calcium mobilization in cultured bovine luteal cells. *Biol. Reprod.* **63**, 1000–5 (2000).
298. Dobson, H., Midmer, S. E. & Fitzpatrick, R. J. Relationship between progesterone concentrations in milk and plasma during the bovine oestrous cycle. *Vet. Rec.* **96**, 222–3 (1975).

299. Broes, A. & LeBlanc, S. J. Comparison of commercial progesterone assays for evaluation of luteal status in dairy cows. *Can. Vet. J. = La Rev. Vet. Can.* **55**, 582–4 (2014).
300. Levy, N. *et al.* Administration of prostaglandin f(2 alpha) during the early bovine luteal phase does not alter the expression of ET-1 and of its type A receptor: a possible cause for corpus luteum refractoriness. *Biol. Reprod.* **63**, 377–382 (2000).
301. Acosta, T. J., Yoshizawa, N., Ohtani, M. & Miyamoto, A. Local changes in blood flow within the early and midcycle corpus luteum after prostaglandin F(2 alpha) injection in the cow. *Biol. Reprod.* **66**, 651–8 (2002).
302. Fiedler, E. P., Plouffe, L., Hales, D. B., Hales, K. H. & Khan, I. Prostaglandin F(2alpha) induces a rapid decline in progesterone production and steroidogenic acute regulatory protein expression in isolated rat corpus luteum without altering messenger ribonucleic acid expression. *Biol. Reprod.* **61**, 643–50 (1999).
303. Sirinian, M. I. *et al.* Adaptor protein ARH is recruited to the plasma membrane by low density lipoprotein (LDL) binding and modulates endocytosis of the LDL/LDL receptor complex in hepatocytes. *J. Biol. Chem.* **280**, 38416–23 (2005).
304. Garcia, C. K. *et al.* Autosomal recessive hypercholesterolemia caused by mutations in a putative LDL receptor adaptor protein. *Science* **292**, 1394–8 (2001).
305. Yang, T. *et al.* Crucial step in cholesterol homeostasis: sterols promote binding of SCAP to INSIG-1, a membrane protein that facilitates retention of SREBPs in ER. *Cell* **110**, 489–500 (2002).
306. Sun, L.-P., Li, L., Goldstein, J. L. & Brown, M. S. Insig required for sterol-mediated inhibition of Scap/SREBP binding to COPII proteins in vitro. *J. Biol. Chem.* **280**, 26483–90 (2005).
307. Savion, N., Laherty, R., Cohen, D., Lui, G. M. & Gospodarowicz, D. Role of lipoproteins

- and 3-hydroxy-3-methylglutaryl coenzyme A reductase in progesterone production by cultured bovine granulosa cells. *Endocrinology* **110**, 13–22 (1982).
308. Pate, J. L. & Condon, W. A. Effects of serum and lipoproteins on steroidogenesis in cultured bovine luteal cells. *Mol. Cell. Endocrinol.* **28**, 551–62 (1982).
 309. Lund, E. G., Kerr, T. A., Sakai, J., Li, W. P. & Russell, D. W. cDNA cloning of mouse and human cholesterol 25-hydroxylases, polytopic membrane proteins that synthesize a potent oxysterol regulator of lipid metabolism. *J. Biol. Chem.* **273**, 34316–27 (1998).
 310. Toaff, M. E., Schleyer, H. & Strauss, J. F. Metabolism of 25-hydroxycholesterol by rat luteal mitochondria and dispersed cells. *Endocrinology* **111**, 1785–90 (1982).
 311. Bogan, R. L. & Hennebold, J. D. The reverse cholesterol transport system as a potential mediator of luteolysis in the primate corpus luteum. *Reproduction* **139**, 163–76 (2010).
 312. Seto, N. L. & Bogan, R. L. Decreased cholesterol uptake and increased liver x receptor-mediated cholesterol efflux pathways during prostaglandin F2 alpha-induced and spontaneous luteolysis in sheep. *Biol. Reprod.* **92**, 128 (2015).
 313. Bishop, C. V, Bogan, R. L., Hennebold, J. D. & Stouffer, R. L. Analysis of microarray data from the macaque corpus luteum; the search for common themes in primate luteal regression. *Mol. Hum. Reprod.* **17**, 143–151 (2011).
 314. Wu, J. *et al.* IL-33 is required for disposal of unnecessary cells during ovarian atresia through regulation of autophagy and macrophage migration. *J. Immunol.* **194**, 2140–7 (2015).
 315. Carlock, C. I. *et al.* Unique temporal and spatial expression patterns of IL-33 in ovaries during ovulation and estrous cycle are associated with ovarian tissue homeostasis. *J. Immunol.* **193**, 161–9 (2014).

316. Lott, J. M., Sumpter, T. L. & Turnquist, H. R. New dog and new tricks: evolving roles for IL-33 in type 2 immunity. *J. Leukoc. Biol.* **97**, 1037–48 (2015).
317. Ozkan, Z. S. *et al.* What is the impact of Th1/Th2 ratio, SOCS3, IL17, and IL35 levels in unexplained infertility? *J. Reprod. Immunol.* **103**, 53–8 (2014).
318. Yu, F., Chen, M.-H. M.-H., Kuo, L., Talbott, H. A. & Davis, J. S. J. S. Confident difference criterion: a new Bayesian differentially expressed gene selection algorithm with applications. *BMC Bioinformatics* **16**, 245 (2015).
319. Taniguchi, K. *et al.* Prostaglandin F2 α (PGF2 α) stimulates PTGS2 expression and PGF2 α synthesis through NF κ B activation via reactive oxygen species in the corpus luteum of pseudopregnant rats. *Reproduction* **140**, 885–92 (2010).
320. Luo, W., Diaz, F. J. & Wiltbank, M. C. Induction of mRNA for chemokines and chemokine receptors by prostaglandin F2 α is dependent upon stage of the porcine corpus luteum and intraluteal progesterone. *Endocrinology* **152**, 2797–805 (2011).
321. Sales, K. J. *et al.* Prostaglandin F(2 α)-F-prostanoid receptor regulates CXCL8 expression in endometrial adenocarcinoma cells via the calcium-calcineurin-NFAT pathway. *Biochim. Biophys. Acta* **1793**, 1917–28 (2009).
322. Pate, J. L., Toyokawa, K., Walusimbi, S. & Brzezicka, E. The interface of the immune and reproductive systems in the ovary: lessons learned from the corpus luteum of domestic animal models. *Am. J. Reprod. Immunol.* **64**, 275–286 (2010).
323. Shaw, D. W. & Britt, J. H. Concentrations of tumor necrosis factor alpha and progesterone within the bovine corpus luteum sampled by continuous-flow microdialysis during luteolysis in vivo. *Biol. Reprod.* **53**, 847–54 (1995).
324. Xu, C. *et al.* PGF2 α modulates the output of chemokines and pro-inflammatory cytokines in myometrial cells from term pregnant women through divergent signaling pathways.

- Mol. Hum. Reprod.* **21**, 603–14 (2015).
325. Luo, W., Salih, S. M., Bormann, C. L. & Wiltbank, M. C. Induction of chemokines and prostaglandin synthesis pathways in luteinized human granulosa cells: potential role of luteotropin withdrawal and prostaglandin F₂ α in regression of the human corpus luteum. *Reprod. Biol.* **15**, 247–56 (2015).
 326. Shimizu, T. *et al.* Effects of interleukin-8 on estradiol and progesterone production by bovine granulosa cells from large follicles and progesterone production by luteinizing granulosa cells in culture. *Cytokine* **57**, 175–81 (2012).
 327. Nio-Kobayashi, J. *et al.* Regulated C-C motif ligand 2 (CCL2) in luteal cells contributes to macrophage infiltration into the human corpus luteum during luteolysis. *Mol. Hum. Reprod.* **21**, 645–54 (2015).
 328. Sheshachalam, A., Srivastava, N., Mitchell, T., Lacy, P. & Eitzen, G. Granule protein processing and regulated secretion in neutrophils. *Front. Immunol.* **5**, 448 (2014).
 329. Wernersson, S. & Pejler, G. Mast cell secretory granules: armed for battle. *Nat. Rev. Immunol.* **14**, 478–94 (2014).
 330. Kaneko, I. *et al.* Prostaglandin F(2 α) regulates cytokine responses of mast cells through the receptors for prostaglandin E. *Biochem. Biophys. Res. Commun.* **367**, 590–6 (2008).
 331. Jothi, R. *et al.* Genomic analysis reveals a tight link between transcription factor dynamics and regulatory network architecture. *Mol. Syst. Biol.* **5**, 294 (2009).
 332. Miyamoto, A., Shirasuna, K. & Sasahara, K. Local regulation of corpus luteum development and regression in the cow: Impact of angiogenic and vasoactive factors. *Domest. Anim. Endocrinol.* **37**, 159–69 (2009).

333. Stouffer, R. L., Bishop, C. V., Bogan, R. L., Xu, F. & Hennebold, J. D. Endocrine and local control of the primate corpus luteum. *Reprod. Biol.* **13**, 259–71 (2013).
334. Meidan, R. *et al.* The yin and yang of corpus luteum-derived endothelial cells: balancing life and death. *Domest. Anim. Endocrinol.* **29**, 318–28 (2005).
335. Zambrano, S., De Toma, I., Piffer, A., Bianchi, M. E. & Agresti, A. NF- κ B oscillations translate into functionally related patterns of gene expression. *Elife* **5**, e09100 (2016).
336. Tian, B., Nowak, D. E. & Brasier, A. R. A TNF-induced gene expression program under oscillatory NF-kappaB control. *BMC Genomics* **6**, 137 (2005).
337. Schmidt, C. *et al.* Mechanisms of proinflammatory cytokine-induced biphasic NF-kappaB activation. *Mol. Cell* **12**, 1287–300 (2003).
338. Tian, B., Nowak, D. E., Jamaluddin, M., Wang, S. & Brasier, A. R. Identification of direct genomic targets downstream of the nuclear factor-kappaB transcription factor mediating tumor necrosis factor signaling. *J. Biol. Chem.* **280**, 17435–48 (2005).
339. Kleinschmidt, S. *et al.* Proinflammatory cytokine gene expression in whole blood from patients undergoing coronary artery bypass surgery and its modulation by pentoxifylline. *Shock* **9**, 12–20 (1998).
340. Sawyer, H. R., Niswender, K. D., Braden, T. D. & Niswender, G. D. Nuclear changes in ovine luteal cells in response to PGF2 alpha. *Domest. Anim. Endocrinol.* **7**, 229–37 (1990).
341. Townson, D. H. & Pate, J. L. Regulation of prostaglandin synthesis by interleukin-1 beta in cultured bovine luteal cells. *Biol. Reprod.* **51**, 480–485 (1994).
342. Tsai, S. J., Juengel, J. L. & Wiltbank, M. C. Hormonal regulation of monocyte chemoattractant protein-1 messenger ribonucleic acid expression in corpora lutea.

- Endocrinology* **138**, 4517–4520 (1997).
343. Wiltbank, M. C. & Ottobre, J. S. Regulation of intraluteal production of prostaglandins. *Reprod. Biol. Endocrinol.* **2**, 1–11 (2003).
 344. Kumagai, A., Yoshioka, S., Sakumoto, R. & Okuda, K. Auto-amplification system for prostaglandin F2 α in bovine corpus luteum. *Mol. Reprod. Dev.* **81**, 646–54 (2014).
 345. Bogan, R. L., Murphy, M. J., Stouffer, R. L. & Hennebold, J. D. Prostaglandin synthesis, metabolism, and signaling potential in the rhesus macaque corpus luteum throughout the luteal phase of the menstrual cycle. *Endocrinology* **149**, 5861–71 (2008).
 346. Henkes, L. E. *et al.* Acid sphingomyelinase involvement in tumor necrosis factor alpha-regulated vascular and steroid disruption during luteolysis in vivo. *Proc. Natl. Acad. Sci. U. S. A.* **105**, 7670–5 (2008).
 347. Quirk, S. M., Cowan, R. G. & Harman, R. M. Role of the cell cycle in regression of the corpus luteum. *Reproduction* **145**, 161–75 (2013).
 348. Kawaguchi, S., Bowolaksono, A., Yoshioka, S., Sakumoto, R. & Okuda, K. Luteoprotective mechanisms of prostaglandin F2 α stimulated by luteinizing hormone in the bovine corpus luteum. *J. Reprod. Dev.* **59**, 225–30 (2013).
 349. Skarzynski, D. J., Ferreira-Dias, G. M. & Okuda, K. Regulation of luteal function and corpus luteum regression in cows: hormonal control, immune mechanisms and intercellular communication. *Reprod. Domest. Anim.* **43 Suppl 2**, 57–65 (2008).
 350. Pate, J. L. & Keyes, P. L. Immune cells in the corpus luteum: friends or foes? *Reproduction* **122**, 665–676 (2001).
 351. Vinatier, D. *et al.* Immunological aspects of ovarian function: role of the cytokines. *Eur. J. Obstet. Gynecol. Reprod. Biol.* **63**, 155–168 (1995).

- 352. Ujioka, T. *et al.* Interleukin-8 as an essential factor in the human chorionic gonadotropin-induced rabbit ovulatory process: interleukin-8 induces neutrophil accumulation and activation in ovulation. *Biol. Reprod.* **58**, 526–30 (1998).
- 353. Braundmeier, A. *et al.* Induction of endometriosis alters the peripheral and endometrial regulatory T cell population in the non-human primate. *Hum. Reprod.* **27**, 1712–1722 (2012).
- 354. Care, A. S. *et al.* Macrophages regulate corpus luteum development during embryo implantation in mice. *J. Clin. Invest.* **123**, 3472–87 (2013).
- 355. Erlebacher, A., Zhang, D., Parlow, A. F. & Glimcher, L. H. Ovarian insufficiency and early pregnancy loss induced by activation of the innate immune system. *J. Clin. Invest.* **114**, 39–48 (2004).
- 356. Shirasuna, K. *et al.* Possible action of vasohibin-1 as an inhibitor in the regulation of vascularization of the bovine corpus luteum. *Reproduction* **143**, 491–500 (2012).
- 357. Shirasuna, K., Shimizu, T., Matsui, M. & Miyamoto, A. Emerging roles of immune cells in luteal angiogenesis. *Reprod. Fertil. Dev.* **25**, 351–61 (2013).
- 358. Mukaida, N. Pathophysiological roles of interleukin-8/CXCL8 in pulmonary diseases. *Am. J. Physiol. Lung Cell. Mol. Physiol.* **284**, 566–577 (2003).
- 359. Mukaida, N. Interleukin-8: an expanding universe beyond neutrophil chemotaxis and activation. *Int. J. Hematol.* **72**, 391–398 (2000).
- 360. Połec, A., Tanbo, T. & Fedorcsák, P. Cellular interaction regulates interleukin-8 secretion by granulosa-lutein cells and monocytes/macrophages. *Am. J. Reprod. Immunol.* **61**, 85–94 (2009).
- 361. Heidemann, J. *et al.* Angiogenic effects of interleukin 8 (CXCL8) in human intestinal

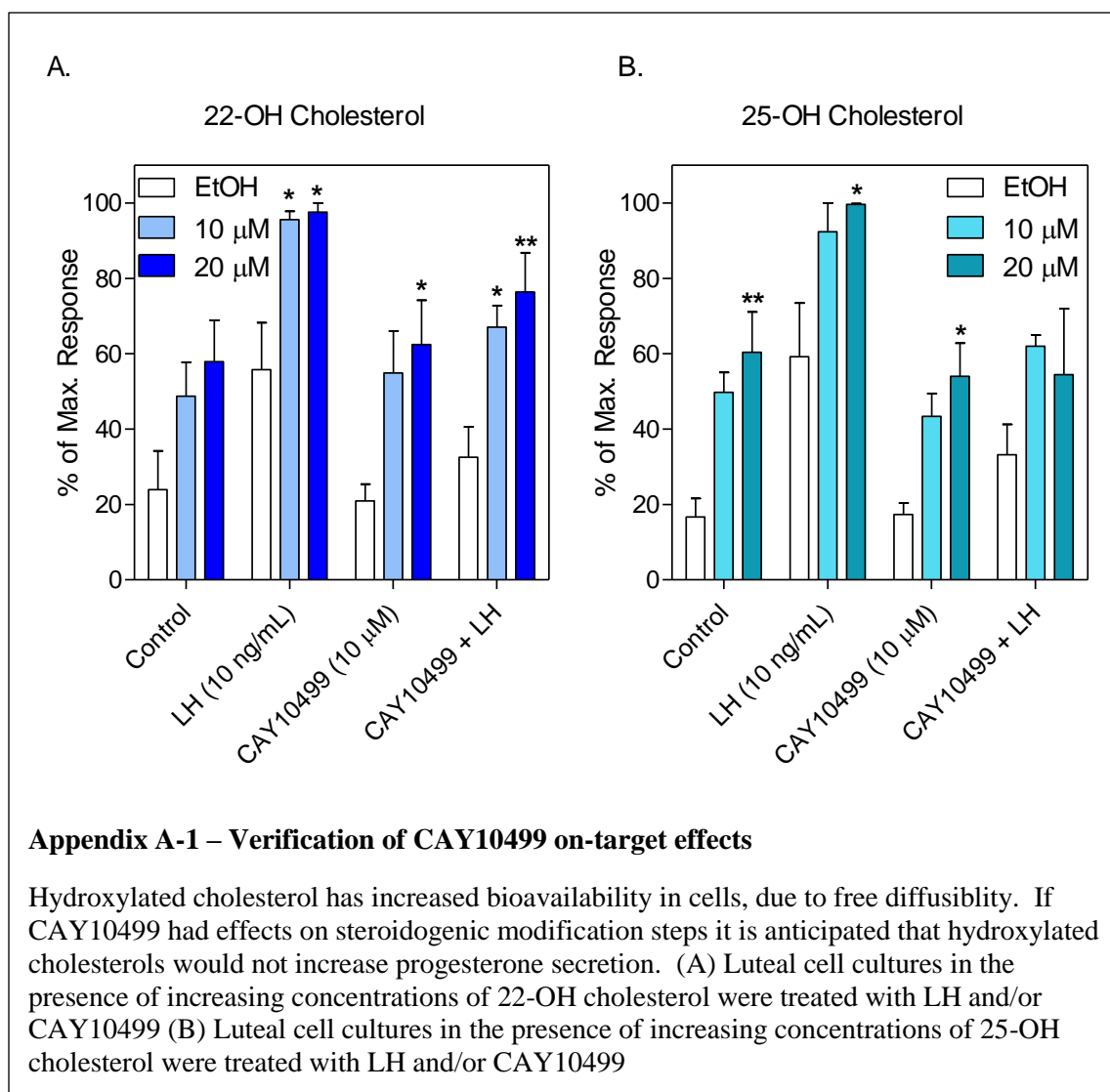
- microvascular endothelial cells are mediated by CXCR2. *J. Biol. Chem.* **278**, 8508–8515 (2003).
362. Li, A., Dubey, S., Varney, M. L., Dave, B. J. & Singh, R. K. IL-8 directly enhanced endothelial cell survival, proliferation, and matrix metalloproteinases production and regulated angiogenesis. *J. Immunol.* **170**, 3369–76 (2003).
 363. Nitta, A. *et al.* Possible involvement of IFNT in lymphangiogenesis in the corpus luteum during the maternal recognition period in the cow. *Reproduction* **142**, 879–92 (2011).
 364. Shimizu, T., Imamura, E., Magata, F., Murayama, C. & Miyamoto, A. Interleukin-8 stimulates progesterone production via the MEK pathway in ovarian theca cells. *Mol. Cell. Biochem.* **374**, 157–61 (2013).
 365. Ireland, J. J., Murphee, R. L. & Coulson, P. B. Accuracy of predicting stages of bovine estrous cycle by gross appearance of the corpus luteum. *J. Dairy Sci.* **63**, 155–160 (1980).
 366. Chakravorty, A., Joslyn, M. I. & Davis, J. S. Characterization of insulin and insulin-like growth factor-I actions in the bovine luteal cell: regulation of receptor tyrosine kinase activity, phosphatidylinositol-3-kinase, and deoxyribonucleic acid synthesis. *Endocrinology* **133**, 1331–40 (1993).
 367. Skarzynski, D. & Piotrowska, K. Effects of exogenous tumour necrosis factor α on the Secretory Function of the Bovine Reproductive Tract Depend on Tumour Necrosis Factor- α Concentrations. *Reprod. Domest. Anim.* **379**, 371–379 (2009).
 368. Espey, L. L. Ovulation as an inflammatory reaction--a hypothesis. *Biol. Reprod.* **22**, 73–7106 (1980).
 369. Lucy, M. C. *et al.* Efficacy of an intravaginal progesterone insert and an injection of PGF2alpha for synchronizing estrus and shortening the interval to pregnancy in postpartum beef cows, peripubertal beef heifers, and dairy heifers. *J. Anim. Sci.* **79**, 982–

- 995 (2001).
370. Liptak, A. R. *et al.* Cooperative expression of monocyte chemoattractant protein 1 within the bovine corpus luteum: evidence of immune cell-endothelial cell interactions in a coculture system. *Biol. Reprod.* **72**, 1169–1176 (2005).
 371. Gouwy, M. *et al.* Synergy between coproduced CC and CXC chemokines in monocyte chemotaxis through receptor-mediated events. *Mol. Pharmacol.* **74**, 485–95 (2008).
 372. Neptune, E. R., Iiri, T. & Bourne, H. R. G α i is not required for chemotaxis mediated by Gi-coupled receptors. *J. Biol. Chem.* **274**, 2824–2828 (1999).
 373. Futosi, K., Fodor, S. & Mócsai, A. Neutrophil cell surface receptors and their intracellular signal transduction pathways. *Int. Immunopharmacol.* **17**, 1185–1197 (2013).
 374. Niswender, G. D. Molecular control of luteal secretion of progesterone. *Reproduction* **123**, 333–339 (2002).
 375. Kuranaga, E. *et al.* Fas/Fas ligand system in prolactin-induced apoptosis in rat corpus luteum: possible role of luteal immune cells. *Biochem. Biophys. Res. Commun.* **260**, 167–173 (1999).
 376. Krusche, C. A., Vloet, T. D., Herrler, A., Black, S. & Beier, H. M. Functional and structural regression of the rabbit corpus luteum is associated with altered luteal immune cell phenotypes and cytokine expression patterns. *Histochem. Cell Biol.* **118**, 479–89 (2002).
 377. Murdoch, W. J. Treatment of sheep with prostaglandin F₂ alpha enhances production of a luteal chemoattractant for eosinophils. *Am. J. Reprod. Immunol. Microbiol.* **15**, 52–56 (1987).
 378. Wang, L. J., Pascoe, V., Petrucco, O. M. & Norman, R. J. Distribution of leukocyte

- subpopulations in the human corpus luteum. *Hum. Reprod.* **7**, 197–202 (1992).
379. Suzuki, T. *et al.* Leukocytes in normal-cycling human ovaries: immunohistochemical distribution and characterization. *Hum. Reprod.* **13**, 2186–91 (1998).
 380. Behrman, H. R., Kodaman, P. H., Preston, S. L. & Gao, S. Oxidative stress and the ovary. *J. Soc. Gynecol. Investig.* **8**, S40-2 (2001).
 381. Murray, P. & Wynn, T. Protective and pathogenic functions of macrophage subsets. *Nat. Rev. Immunol.* **11**, 723–737 (2011).
 382. Zhou, D. *et al.* Macrophage polarization and function with emphasis on the evolving roles of coordinated regulation of cellular signaling pathways. *Cell. Signal.* **26**, 192–197 (2014).
 383. Al-Gubory, K. H., Garrel, C., Faure, P. & Sugino, N. Roles of antioxidant enzymes in corpus luteum rescue from reactive oxygen species-induced oxidative stress. *Reprod. Biomed. Online* **25**, 551–60 (2012).
 384. Skarzynski, D. J. *et al.* Growth and Regression in Bovine Corpora Lutea : Regulation by Local Survival and Death Pathways. *Reprod. Domest. Anim.* **48**, 25–37 (2013).
 385. Walusimbi, S. S. & Pate, J. L. Physiology and Endocrinology Symposium: role of immune cells in the corpus luteum. *J. Anim. Sci.* **91**, 1650–9 (2013).

APPENDIX A: SUPPLEMENTAL DATA FOR CHAPTER 3

Appendix A-1 – Verification of CAY10499 on-target effects



Appendix A-3 – Luteal lipid droplet-associated proteins determined by proteomics

Symbol	Name	Control	8-br cAMP	P-value
3BHS	3 beta-hydroxysteroid dehydrogenase/Delta 5-->4-isomerase	362	449	0.035
PLIN2	Perilipin-2	291	433	0.005
ACTC	Actin, alpha cardiac muscle 1	203	406	0.00072
VIME	Vimentin	256	344	0.46
ATPB	ATP synthase subunit beta, mitochondrial	219	331	0.0057
ACTG	Actin, cytoplasmic 2	183	363	< 0.00010
CP11A	cholesterol side-chain cleavage enzyme, mitochondrial	166	250	0.017
ATPA	ATP synthase subunit alpha, mitochondrial	145	210	0.089
CH60	60 kDa heat shock protein, mitochondrial	122	219	< 0.00010
ERG7	Lanosterol synthase	174	163	< 0.00010
GRP78	78 kDa glucose-regulated protein	128	147	0.018
ACON	Aconitate hydratase, mitochondrial	104	144	0.33
MDHM	Malate dehydrogenase, mitochondrial	96	136	0.23
PDIA1	Protein disulfide-isomerase	105	112	0.0026
NB5R3	NADH-cytochrome b5 reductase 3	79	105	0.51
BCAT2	Branched-chain-amino-acid aminotransferase, mitochondrial	56	128	< 0.00010
PDIA3	Protein disulfide-isomerase A3	89	92	0.0018
ALBU	Serum albumin	113	67	< 0.00010
NSDHL	Sterol-4-alpha-carboxylate 3-dehydrogenase, decarboxylating	80	99	0.19
ALDH2	Aldehyde dehydrogenase, mitochondrial	80	92	0.051
ENPL	Endoplasmic	67	102	0.078
AATM	Aspartate aminotransferase, mitochondrial	55	94	0.0065
ADRO	NADPH:adrenodoxin oxidoreductase, mitochondrial	58	80	0.38
ACTN4	Alpha-actinin-4	52	70	0.52
SERPH	Serpin H1	44	69	0.085
CALR	Calreticulin	58	54	0.00072
HCD2	3-hydroxyacyl-CoA dehydrogenase type-2	31	64	0.00032
HSP7C	Heat shock cognate 71 kDa protein	45	49	0.065
QCR2	Cytochrome b-c1 complex subunit 2, mitochondrial	35	58	0.047
H4	Histone H4	37	50	0.52
THIL	Acetyl-CoA acetyltransferase, mitochondrial	24	62	< 0.00010
TPM1	Tropomyosin alpha-1 chain	34	50	0.21
VDAC1	Voltage-dependent anion-selective channel protein 1	31	52	0.044
PPIB	Peptidyl-prolyl cis-trans isomerase B	36	44	0.25
ADT3	ADP/ATP translocase 3	39	41	0.029
MMSA	Methylmalonate-semialdehyde dehydrogenase [acylating], mitochondrial	37	41	0.099
PTGIS	Prostacyclin synthase	35	41	0.17
ECHB	Trifunctional enzyme subunit beta, mitochondrial	17	58	< 0.00010
ACTN1	Alpha-actinin-1	32	43	0.45
VDAC2	Voltage-dependent anion-selective channel protein 2	29	46	0.089
TBB5	Tubulin beta-5 chain	37	38	0.23
G3P	Glyceraldehyde-3-phosphate dehydrogenase	29	42	0.33
ODO2	Dihydrolipoyllysine-residue succinyltransferase component of 2-oxoglutarate dehydrogenase complex, mitochondrial	29	41	0.39
TBA4A	Tubulin alpha-4A chain	36	32	0.024
PRDX3	Thioredoxin-dependent peroxide reductase, mitochondrial	29	39	0.49
THIM	3-ketoacyl-CoA thiolase, mitochondrial	25	42	0.07
OAT	Ornithine aminotransferase, mitochondrial	16	49	< 0.00010
PYGL	Glycogen phosphorylase, liver form	33	31	0.0076
EFTU	Elongation factor Tu, mitochondrial	20	44	0.00035
AL7A1	Alpha-aminoacidic semialdehyde dehydrogenase	22	40	0.034
SDHA	Succinate dehydrogenase [ubiquinone] flavoprotein subunit, mitochondrial	23	39	0.06
ATPO	ATP synthase subunit O, mitochondrial	21	40	0.012

ODPB	Pyruvate dehydrogenase E1 component subunit beta, mitochondrial	22	38	0.038
SODM	Superoxide dismutase [Mn], mitochondrial	16	43	< 0.00010
ETFA	Electron transfer flavoprotein subunit alpha, mitochondrial	25	33	0.44
HS71A	Heat shock 70 kDa protein 1A	31	27	0.0032
ADT1	ADP/ATP translocase 1	26	31	0.28
RAB1B	Ras-related protein Rab-1B	20	35	0.046
ODO1	2-oxoglutarate dehydrogenase, mitochondrial	16	39	< 0.00010
QCR1	Cytochrome b-c1 complex subunit 1, mitochondrial	22	32	0.33
A2MG	Alpha-2-macroglobulin	27	25	0.0093
ACADV	Very long-chain specific acyl-CoA dehydrogenase, mitochondrial	21	31	0.24
ODPA	Pyruvate dehydrogenase E1 component subunit alpha, somatic form, mitochondrial	19	33	0.059
PDIA4	Protein disulfide-isomerase A4	22	28	0.38
CISY	Citrate synthase, mitochondrial	21	29	0.44
MPCP	Phosphate carrier protein, mitochondrial	17	32	0.021
AT1A1	Sodium/potassium-transporting ATPase subunit alpha-1	25	23	0.011
VDAC3	Voltage-dependent anion-selective channel protein 3	20	28	0.35
NDUS1	NADH-ubiquinone oxidoreductase 75 kDa subunit, mitochondrial	20	28	0.41
AT5F1	ATP synthase F(0) complex subunit B1, mitochondrial	19	28	0.25
TBB4B	Tubulin beta-4B chain	22	24	0.13
ATP5H	ATP synthase subunit d, mitochondrial	14	32	0.0012
LONM	Lon protease homolog, mitochondrial	21	25	0.26
PHB	Prohibitin	18	26	0.33
CATD	Cathepsin D	18	25	0.45
ECHM	Enoyl-CoA hydratase, mitochondrial	12	31	0.0004
ITAV	Integrin alpha-V	24	18	0.0012
H2B1N	Histone H2B type 1-N	16	26	0.13
HSP72	Heat shock-related 70 kDa protein 2	20	21	0.092
ETFB	Electron transfer flavoprotein subunit beta	15	27	0.057
PHB2	Prohibitin-2	14	27	0.027
5NTD	5'-nucleotidase	15	24	0.22
PCCB	Propionyl-CoA carboxylase beta chain, mitochondrial	16	23	0.45
TMEDA	Transmembrane emp24 domain-containing protein 10	16	23	0.34
ANXA1	Annexin A1	17	21	0.41
TPM2	Tropomyosin beta chain	15	24	0.18
LETM1	LETM1 and EF-hand domain-containing protein 1, mitochondrial	15	21	0.45
CASA1	Alpha-S1-casein	29	8	< 0.00010
RAB5C	Ras-related protein Rab-5C	18	18	0.18
EF1A1	Elongation factor 1-alpha 1	12	23	0.05
HSPB1	Heat shock protein beta-1	14	22	0.26
3HIDH	3-hydroxyisobutyrate dehydrogenase, mitochondrial	9	26	0.00033
SUCB2	Succinyl-CoA ligase [GDP-forming] subunit beta, mitochondrial	13	21	0.21
SCRB1	Scavenger receptor class B member 1	15	19	0.39
TSP1	Thrombospondin-1	14	20	0.45
SCPDL	Saccharopine dehydrogenase-like oxidoreductase	14	20	0.45
GNS	N-acetylglucosamine-6-sulfatase	16	18	0.22
FDFT	Squalene synthase	14	20	0.33
RPN2	Dolichyl-diphosphooligosaccharide--protein glycosyltransferase subunit 2	13	20	0.35
CY1	Cytochrome c1, heme protein, mitochondrial	14	19	0.46
APOA1	Apolipoprotein A-I	6	27	< 0.00010
HBB	Hemoglobin subunit beta	19	14	0.0023
FINC	Fibronectin	9	23	0.00099
CPT2	Carnitine O-palmitoyltransferase 2, mitochondrial	14	18	0.53
TRAP1	Heat shock protein 75 kDa, mitochondrial	16	16	0.066

NNTM	NAD(P) transhydrogenase, mitochondrial	21	11	< 0.00010
IDHP	Isocitrate dehydrogenase [NADP], mitochondrial	9	22	0.0052
M2OM	Mitochondrial 2-oxoglutarate/malate carrier protein	12	18	0.3
HS90A	Heat shock protein HSP 90- α	18	12	0.00037
DHE3	Glutamate dehydrogenase 1, mitochondrial	9	20	0.018
SFXN1	Sideroflexin-1	11	18	0.24
OST48	Dolichyl-diphosphooligosaccharide--protein glycosyltransferase 48 kDa subunit	12	17	0.48
TXTP	Tricarboxylate transport protein, mitochondrial	15	15	0.11
IDH3A	Isocitrate dehydrogenase [NAD] subunit α , mitochondrial	7	22	0.00028
ACLY	ATP-citrate synthase	16	12	0.0059
ITB1	Integrin β -1	13	15	0.28
COX41	Cytochrome c oxidase subunit 4 isoform 1, mitochondrial	13	15	0.32
GSTA1	Glutathione S-transferase A1	12	16	0.51
COX2 (+10)	Cytochrome c oxidase subunit 2	7	20	0.00068
HA1B	BOLA class I histocompatibility antigen, α chain BL3-7	10	16	0.22
SUCA	Succinyl-CoA ligase [ADP/GDP-forming] subunit α , mitochondrial	11	15	0.49
CATA	Catalase	11	15	0.45
KAD2	Adenylate kinase 2, mitochondrial	10	16	0.24
ENOA	Alpha-enolase	13	13	0.13
GLU2B	Glucosidase 2 subunit β	14	12	0.034
PBIP1	Pre-B-cell leukemia transcription factor-interacting protein 1	12	13	0.25
RAB8A	Ras-related protein Rab-8A	5	20	< 0.00010
LG3BP	Galectin-3-binding protein	12	13	0.22
1433Z	14-3-3 protein ζ/δ	9	16	0.28
PGR1	Membrane-associated progesterone receptor component 1	10	15	0.3
ACSS3	Acyl-CoA synthetase short-chain family member 3, mitochondrial	11	13	0.3
ACDSB	Short/branched chain specific acyl-CoA dehydrogenase, mitochondrial	6	18	0.0017
RL40 (+35)	Ubiquitin-60S ribosomal protein L40	11	13	0.36
ANT3	Antithrombin-III	8	15	0.09
ACADS	Short-chain specific acyl-CoA dehydrogenase, mitochondrial	6	17	0.0038
ML12B	Myosin regulatory light chain 12B	6	17	0.005
MYL6	Myosin light polypeptide 6	4	19	< 0.00010
ATPG	ATP synthase subunit γ , mitochondrial	12	10	0.062
H2AJ	Histone H2A.J	5	17	0.00069
NDUV2	NADH dehydrogenase [ubiquinone] flavoprotein 2, mitochondrial	8	13	0.31
GLCM	Glucosylceramidase	10	10	0.16
CH10	10 kDa heat shock protein, mitochondrial	10	10	0.13
RB11B	Ras-related protein Rab-11B	9	11	0.46
ACSM1	Acyl-coenzyme A synthetase ACSM1, mitochondrial	11	9	0.067
NDKB	Nucleoside diphosphate kinase B	6	14	0.028
STAR	steroidogenic acute regulatory protein, mitochondrial	1	18	< 0.00010
NDUA9	NADH dehydrogenase [ubiquinone] 1 α subcomplex subunit 9, mitochondrial	5	14	0.0055
NDUA8	NADH dehydrogenase [ubiquinone] 1 α subcomplex subunit 8	4	15	0.00022
EF2	Elongation factor 2	7	11	0.34
RLA0	60S acidic ribosomal protein P0	7	12	0.17
ERLN2	Erlin-2	8	10	0.45
GLYM	Serine hydroxymethyltransferase, mitochondrial	8	11	0.49
ABHD6	Monoacylglycerol lipase ABHD6	7	10	0.48
NDUBA	NADH dehydrogenase [ubiquinone] 1 β subcomplex subunit 10	5	12	0.05
ANXA5	Annexin A5	5	12	0.027

COX5A	Cytochrome c oxidase subunit 5A, mitochondrial	10	7	0.016
EZRI	Ezrin	10	7	0.0075
MYO1C	Unconventional myosin-Ic	10	7	0.031
PYC	Pyruvate carboxylase, mitochondrial	7	10	0.54
NCPR	NADPH--cytochrome P450 reductase	11	6	0.00082
DHX9	ATP-dependent RNA helicase A	9	8	0.098
HNRPK	Heterogeneous nuclear ribonucleoprotein K	3	13	0.0012
RL7	60S ribosomal protein L7	4	12	0.018
RL18	60S ribosomal protein L18	4	12	0.006
RL12	60S ribosomal protein L12	6	10	0.26
SDHB	Succinate dehydrogenase [ubiquinone] iron-sulfur subunit, mitochondrial	5	10	0.17
CAZA1	F-actin-capping protein subunit alpha-1	5	11	0.058
PLBL2	Putative phospholipase B-like 2	3	12	0.0032
H2AZ	Histone H2A.Z	7	8	0.36
PRDX5	Peroxisredoxin-5, mitochondrial	4	11	0.024
TMED9	Transmembrane emp24 domain-containing protein 9	5	9	0.24
BGAL	Beta-galactosidase	8	7	0.08
RCN3	Reticulocalbin-3	7	8	0.42
RL7A	60S ribosomal protein L7a	3	11	0.006
ERP29	Endoplasmic reticulum resident protein 29	9	6	0.015
ARPC4	Actin-related protein 2/3 complex subunit 4	6	8	0.51
NDUV1	NADH dehydrogenase [ubiquinone] flavoprotein 1, mitochondrial	5	9	0.18
TRXR2	Thioredoxin reductase 2, mitochondrial	6	9	0.39
THRB	Prothrombin	1	13	< 0.00010
PGK1	Phosphoglycerate kinase 1	5	9	0.14
NDUS3	NADH dehydrogenase [ubiquinone] iron-sulfur protein 3, mitochondrial	4	10	0.041
KAD3	GTP:AMP phosphotransferase AK3, mitochondrial	3	10	0.015
02-Mar	Mitochondrial amidoxime reducing component 2	3	10	0.0082
ATP5I	ATP synthase subunit e, mitochondrial	7	6	0.062
PRDX4	Peroxisredoxin-4	3	10	0.02
SAM50	Sorting and assembly machinery component 50 homolog	5	8	0.47
LACB	Beta-lactoglobulin	6	7	0.28
PTBP1	Polypyrimidine tract-binding protein 1	0	13	< 0.00010
DHRS4	Dehydrogenase/reductase SDR family member 4	6	7	0.47
EF1G	Elongation factor 1-gamma	2	10	0.0019
C1QBP	Complement component 1 Q subcomponent-binding protein, mitochondrial	2	11	0.00013
CYC	Cytochrome c	7	5	0.088
GRPE1	GrpE protein homolog 1, mitochondrial	4	9	0.072
CATK	Cathepsin K	3	9	0.035
NDUAD	NADH dehydrogenase [ubiquinone] 1 alpha subcomplex subunit 13	5	8	0.33
ZADH2	Zinc-binding alcohol dehydrogenase domain-containing protein 2	4	9	0.072
QOR	Zeta-crystallin	5	7	0.38
TGM2	Protein-glutamine gamma-glutamyltransferase 2	8	4	0.0019
TAGL	Transgelin	4	7	0.31
ADX	Adrenodoxin, mitochondrial	6	6	0.2
DHCR7	7-dehydrocholesterol reductase	7	4	0.0085
HBA	Hemoglobin subunit alpha	8	4	0.0079
RAC1	Ras-related C3 botulinum toxin substrate 1	4	7	0.24
RS9	40S ribosomal protein S9	3	8	0.037
MTCH2	Mitochondrial carrier homolog 2	3	8	0.077
PRDX1	Peroxisredoxin-1	4	7	0.18
RAB5A	Ras-related protein Rab-5A	6	5	0.2
SUCB1	Succinyl-CoA ligase [ADP-forming] subunit beta, mitochondrial	3	8	0.049

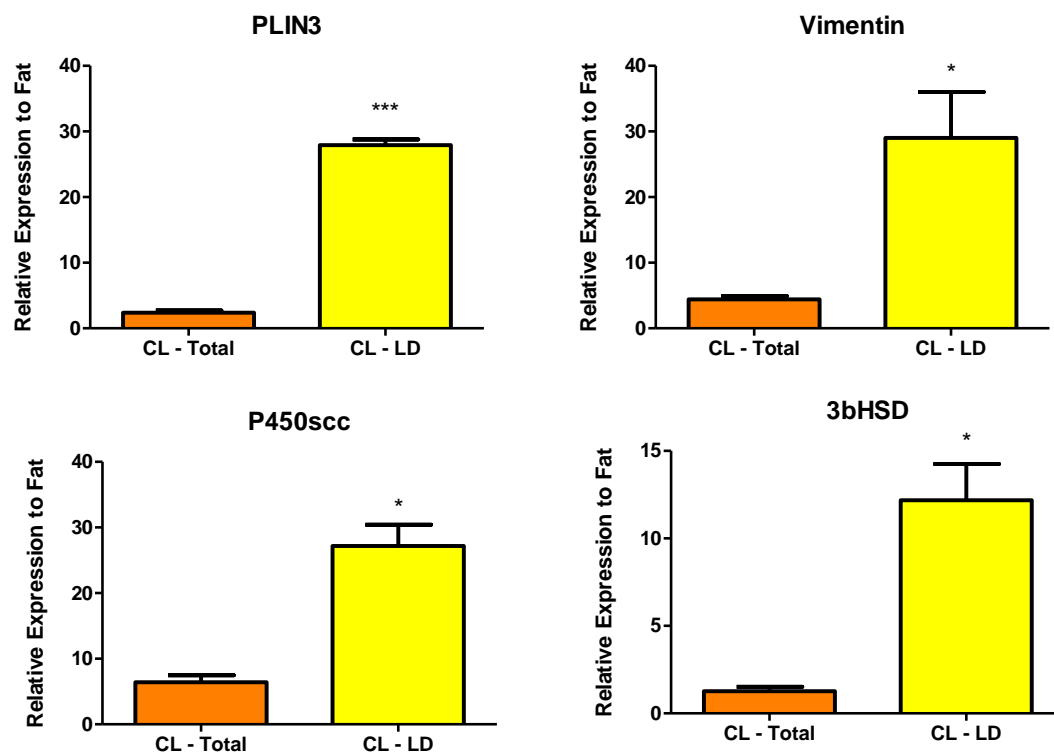
ERAP2	Endoplasmic reticulum aminopeptidase 2	8	3	0.00023
VATB2	V-type proton ATPase subunit B, brain isoform	5	6	0.39
GBB1	Guanine nucleotide-binding protein G(I)/G(S)/G(T) subunit beta-1	3	8	0.15
GELS	Gelsolin	7	4	0.02
RAP1A	Ras-related protein Rap-1A	4	7	0.21
FA5	Coagulation factor V	3	7	0.083
RS3	40S ribosomal protein S3	4	6	0.45
IDH3B	Isocitrate dehydrogenase [NAD] subunit beta, mitochondrial	1	8	0.00083
1433E	14-3-3 protein epsilon	3	7	0.068
STT3A	Dolichyl-diphosphooligosaccharide--protein glycosyltransferase subunit STT3A	6	4	0.044
UCRI	Cytochrome b-c1 complex subunit Rieske, mitochondrial	3	7	0.089
MUTA	Methylmalonyl-CoA mutase, mitochondrial	6	4	0.044
NDUS8	NADH dehydrogenase [ubiquinone] iron-sulfur protein 8, mitochondrial	3	6	0.11
RL11	60S ribosomal protein L11	3	6	0.21
RS16	40S ribosomal protein S16	5	4	0.13
MVP	Major vault protein	9	0	< 0.00010
ATPK	ATP synthase subunit f, mitochondrial	3	5	0.4
FAF2	FAS-associated factor 2	5	4	0.18
DAD1	Dolichyl-diphosphooligosaccharide--protein glycosyltransferase subunit DAD1	5	4	0.093
NDUB7	NADH dehydrogenase [ubiquinone] 1 beta subcomplex subunit 7	4	5	0.56
MMAB	Cob(I)yrinic acid a,c-diamide adenosyltransferase, mitochondrial	2	7	0.015
THTR	Thiosulfate sulfurtransferase	2	6	0.095
NDUS7	NADH dehydrogenase [ubiquinone] iron-sulfur protein 7, mitochondrial	3	5	0.47
NNRD	ATP-dependent (S)-NAD(P)H-hydrate dehydratase	1	7	0.0064
TPIS	Triosephosphate isomerase	6	2	0.00032
HSDL2	Hydroxysteroid dehydrogenase-like protein 2	2	6	0.021
RS8	40S ribosomal protein S8	2	6	0.12
HIBCH	3-hydroxyisobutyryl-CoA hydrolase, mitochondrial	2	6	0.12
SND1	Staphylococcal nuclease domain-containing protein 1	2	5	0.16
APMAP	Adipocyte plasma membrane-associated protein	2	6	0.03
NDUAA	NADH dehydrogenase [ubiquinone] 1 alpha subcomplex subunit 10, mitochondrial	1	6	0.014
TKT	Transketolase	5	2	0.015
ANXA4	Annexin A4	2	5	0.2
ODBB	2-oxoisovalerate dehydrogenase subunit beta, mitochondrial	3	5	0.35
FAHD2	Fumarylacetoacetate hydrolase domain-containing protein 2	2	5	0.1
GSTM1	Glutathione S-transferase Mu 1	3	5	0.35
SSRA	Translocon-associated protein subunit alpha	3	5	0.35
STML2	Stomatin-like protein 2, mitochondrial	0	7	< 0.00010
H31	Histone H3.1	6	1	0.00042
ANXA6	Annexin A6	2	5	0.26
VAPA	Vesicle-associated membrane protein-associated protein A	4	3	0.14
RHOA	Transforming protein RhoA	4	3	0.25
RL13	60S ribosomal protein L13	2	5	0.058
RS5	40S ribosomal protein S5	2	5	0.13
NDUB4	NADH dehydrogenase [ubiquinone] 1 beta subcomplex subunit 4	4	3	0.25
PEBP1	Phosphatidylethanolamine-binding protein 1	3	4	0.58
NPM	Nucleophosmin	0	7	< 0.00010
SSRD	Translocon-associated protein subunit delta	1	6	0.0083
TCPG	T-complex protein 1 subunit gamma	5	2	0.0037
RS18	40S ribosomal protein S18	3	3	0.34
ODB2	Lipoamide acyltransferase component of branched-chain alpha-keto acid dehydrogenase complex, mitochondrial	0	6	< 0.00010

HA1A	BOLA class I histocompatibility antigen, alpha chain BL3-6	0	6	< 0.00010
CP51A	Lanosterol 14-alpha demethylase	5	1	0.00027
QCR7	Cytochrome b-c1 complex subunit 7	5	2	0.0065
TRFE	Serotransferrin	5	1	0.00027
MTX1	Metaxin-1	2	5	0.11
1433G	14-3-3 protein gamma	2	4	0.39
ARP2	Actin-related protein 2	1	5	0.059
HTRA1	Serine protease HTRA1	3	3	0.54
EF1B	Elongation factor 1-beta	0	6	< 0.00010
PRAF3	PRA1 family protein 3	0	6	< 0.00010
NOP56	Nucleolar protein 56	2	3	0.55
ASAH1	Acid ceramidase	2	4	0.35
IDH3G	Isocitrate dehydrogenase [NAD] subunit gamma, mitochondrial	0	5	0.00013
CASA2	Alpha-S2-casein	4	1	0.002
LDHB	L-lactate dehydrogenase B chain	2	3	0.43
RSSA	40S ribosomal protein SA	2	3	0.43
PAI1	Plasminogen activator inhibitor 1	1	4	0.041
PARK7	Protein DJ-1	1	4	0.041
FAS	Fatty acid synthase	4	2	0.033
NAGAB	Alpha-N-acetylgalactosaminidase	2	3	0.43
AP1B1	AP-1 complex subunit beta-1	3	2	0.2
ERP44	Endoplasmic reticulum resident protein 44	2	3	0.57
LRC59	Leucine-rich repeat-containing protein 59	2	4	0.25
MANF	Mesencephalic astrocyte-derived neurotrophic factor	1	4	0.12
ETHE1	Persulfide dioxygenase ETHE1, mitochondrial	2	3	0.52
PABP1	Polyadenylate-binding protein 1	1	4	0.12
EMC2	ER membrane protein complex subunit 2	2	3	0.32
SRSF1	Serine/arginine-rich splicing factor 1	0	5	0.00039
ARP3	Actin-related protein 3	0	5	0.00039
APOD	Apolipoprotein D	0	5	0.00039
GT251	Procollagen galactosyltransferase 1	4	1	0.0074
ATPD	ATP synthase subunit delta, mitochondrial	3	2	0.21
ETFD	Electron transfer flavoprotein-ubiquinone oxidoreductase, mitochondrial	1	4	0.025
HEMH	Ferrochelatase, mitochondrial	1	3	0.21
SNAA	Alpha-soluble NSF attachment protein	1	4	0.085
1433T	14-3-3 protein theta	1	3	0.21
PPGB	Lysosomal protective protein	2	3	0.6
PRDX2	Peroxiredoxin-2	2	3	0.6
VPS35	Vacuolar protein sorting-associated protein 35	3	2	0.089
LUM	Lumican	0	4	0.00069
RL6	60S ribosomal protein L6	0	4	0.00069
PCBP1	Poly(rC)-binding protein 1	0	4	0.00069
AMPL	Cytosol aminopeptidase	4	1	0.0026
PPIC	Peptidyl-prolyl cis-trans isomerase C	2	3	0.49
ODPX	Pyruvate dehydrogenase protein X component	2	2	0.51
RS25	40S ribosomal protein S25	2	3	0.49
TIMP1	Metalloproteinase inhibitor 1	2	3	0.49
KRT81	Keratin, type II cuticular Hb1	0	4	0.0012
NDUB8	NADH dehydrogenase [ubiquinone] 1 beta subcomplex subunit 8, mitochondrial	0	4	0.0012
TPP1	Tripeptidyl-peptidase 1	0	4	0.0012
YBOX1	Nuclease-sensitive element-binding protein 1	0	4	0.0012
GBB2	Guanine nucleotide-binding protein G(I)/G(S)/G(T) subunit beta-2	0	4	0.0012
HNRH2	Heterogeneous nuclear ribonucleoprotein H2	0	4	0.0012
PGAM1	Phosphoglycerate mutase 1	4	0	< 0.00010
RGN	Regucalcin	3	1	0.025
NDUC2	NADH dehydrogenase [ubiquinone] 1 subunit C2	2	2	0.21

HP1B3	Heterochromatin protein 1-binding protein 3	2	2	0.59
SC11A	Signal peptidase complex catalytic subunit SEC11A	2	2	0.41
RS3A	40S ribosomal protein S3a	1	3	0.36
ODBA	2-oxoisovalerate dehydrogenase subunit alpha, mitochondrial	3	1	0.085
NLTP	Non-specific lipid-transfer protein	2	1	0.14
CN37	2',3'-cyclic-nucleotide 3'-phosphodiesterase	0	4	0.0021
TAGL2	Transgelin-2	0	4	0.0021
EF1D	Elongation factor 1-delta	0	4	0.0021
KBL	2-amino-3-ketobutyrate coenzyme A ligase, mitochondrial	0	4	0.0021
NUCB1	Nucleobindin-1	4	0	< 0.00010
VA0D1	V-type proton ATPase subunit d 1	2	2	0.31
CHP1	Calcineurin B homologous protein 1	1	2	0.45
AASS	Alpha-aminoadipic semialdehyde synthase, mitochondrial	3	1	0.045
SF3B3	Splicing factor 3B subunit 3	2	2	0.31
NNRE	NAD(P)H-hydrate epimerase	2	2	0.55
C4BPA	C4b-binding protein alpha chain	0	3	0.0037
MOES	Moesin	0	3	0.0037
TMX1	Thioredoxin-related transmembrane protein 1	0	3	0.0037
RL5	60S ribosomal protein L5	0	3	0.0037
ISOC2	Isochorismatase domain-containing protein 2, mitochondrial	0	3	0.0037
PLAK	Junction plakoglobin	3	0	0.00021
ATP5L	ATP synthase subunit g, mitochondrial	1	2	0.56
MDHC	Malate dehydrogenase, cytoplasmic	1	2	0.56
MAP4	Microtubule-associated protein 4	2	1	0.22
RL24	60S ribosomal protein L24	1	2	0.31
NDUA4	NADH dehydrogenase [ubiquinone] 1 alpha subcomplex subunit 4	2	2	0.44
DNPEP	Aspartyl aminopeptidase	2	1	0.079
CLPP	ATP-dependent Clp protease proteolytic subunit, mitochondrial	0	3	0.0065
HXK1	Hexokinase-1	3	0	0.00049
FIS1	Mitochondrial fission 1 protein	3	0	0.00049
FUCO	Tissue alpha-L-fucosidase	2	1	0.33
RL30	60S ribosomal protein L30	2	1	0.33
PP1A	Serine/threonine-protein phosphatase PP1-alpha catalytic subunit	0	3	0.011
HMGB1	High mobility group protein B1	0	3	0.011
NDUB9	NADH dehydrogenase [ubiquinone] 1 beta subcomplex subunit 9	0	3	0.011
NB5R1	NADH-cytochrome b5 reductase 1	0	3	0.011
NDUB6	NADH dehydrogenase [ubiquinone] 1 beta subcomplex subunit 6	0	3	0.011
SCO1	Protein SCO1 homolog, mitochondrial	0	3	0.011
SURF4	Surfeit locus protein 4	0	3	0.011
RBBP7	Histone-binding protein RBBP7	3	0	0.0011
CASK	Kappa-casein	3	0	0.0011
IDHC	Isocitrate dehydrogenase [NADP] cytoplasmic	1	1	0.47
PRDX6	Peroxiredoxin-6	1	2	0.26
GSTP1	Glutathione S-transferase P	1	1	0.47
NDUA2	NADH dehydrogenase [ubiquinone] 1 alpha subcomplex subunit 2	1	1	0.47
AL9A1	4-trimethylaminobutyraldehyde dehydrogenase	2	0	0.0027
WDR1	WD repeat-containing protein 1	2	0	0.0027
ITB5	Integrin beta-5	0	2	0.02
COF1	Cofilin-1	0	2	0.19
IVD	Isovaleryl-CoA dehydrogenase, mitochondrial	0	2	0.02
RT07	28S ribosomal protein S7, mitochondrial	0	2	0.02
FKB10	Peptidyl-prolyl cis-trans isomerase FKBP10	2	1	0.13
CATB	Cathepsin B	0	2	0.02
IF2A	Eukaryotic translation initiation factor 2 subunit 1	0	2	0.02

PSA6	Proteasome subunit alpha type-6	1	1	0.64
RL8	60S ribosomal protein L8	1	2	0.36
ERG24	Delta(14)-sterol reductase	2	0	0.0062
ZN326	DBIRD complex subunit ZNF326	2	0	0.0062
NCEH1	Neutral cholesteryl ester hydrolase 1	1	1	0.48
CAV1 (+27)	Caveolin-1	0	2	0.035
AOFA	Amine oxidase [flavin-containing] A	0	2	0.035
FKB11	Peptidyl-prolyl cis-trans isomerase FKBP11	0	2	0.035
SPCS3	Signal peptidase complex subunit 3	0	2	0.035
ACTN2	Alpha-actinin-2	0	2	0.035
CFDP2	Craniofacial development protein 2	0	2	0.035
DPYL2	Dihydropyrimidinase-related protein 2	2	0	0.014
PUR9	Bifunctional purine biosynthesis protein PURH	2	0	0.014
ERO1A	ERO1-like protein alpha	2	0	0.014
HEXA	Beta-hexosaminidase subunit alpha	2	0	0.014
U5S1	116 kDa U5 small nuclear ribonucleoprotein component	2	0	0.014
AP2A2	AP-2 complex subunit alpha-2	0	2	0.061
OCTC	Peroxisomal carnitine O-octanoyltransferase	0	2	0.061
CISD2	CDGSH iron-sulfur domain-containing protein 2	0	2	0.061
02-Sep	Septin-2	0	2	0.061
PSD11	26S proteasome non-ATPase regulatory subunit 11	1	1	0.37
SRSF3	Serine/arginine-rich splicing factor 3	0	2	0.061
RBM14	RNA-binding protein 14	0	2	0.061
C560	Succinate dehydrogenase cytochrome b560 subunit, mitochondrial	0	2	0.061
RM01	39S ribosomal protein L1, mitochondrial	0	2	0.061
UK114	Ribonuclease UK114	0	2	0.061
EFHD2	EF-hand domain-containing protein D2	0	2	0.061
TMED1	Transmembrane emp24 domain-containing protein 1	0	2	0.061
MPPB	Mitochondrial-processing peptidase subunit beta	0	1	0.11
F162A	Protein FAM162A	0	1	0.11
MFGM	Lactadherin	1	0	0.034
CAP1	Adenylyl cyclase-associated protein 1	1	0	0.034
DCTN2	Dynactin subunit 2	0	1	0.11
HS105	Heat shock protein 105 kDa	1	0	0.034
PARP1	Poly [ADP-ribose] polymerase 1	1	0	0.034
C1TM	Monofunctional C1-tetrahydrofolate synthase, mitochondrial	1	0	0.034
GPX1	Glutathione peroxidase 1	0	1	0.11
FUND2	FUN14 domain-containing protein 2	0	1	0.11
COF2	Cofilin-2	0	1	0.11
NUP93	Nuclear pore complex protein Nup93	1	0	0.034
PNPH	Purine nucleoside phosphorylase	0	1	0.11
TCPQ	T-complex protein 1 subunit theta	1	0	0.034
CBR4	Carbonyl reductase family member 4	0	1	0.11
TIM50	Mitochondrial import inner membrane translocase subunit TIM50	1	0	0.034
PPIA	Peptidyl-prolyl cis-trans isomerase A	1	0	0.034
1433B	14-3-3 protein beta/alpha	1	0	0.034
RS7	40S ribosomal protein S7	0	1	0.11
DHPR	Dihydropteridine reductase	1	0	0.034
PSPC1	Paraspeckle component 1	0	1	0.11
RL10A	60S ribosomal protein L10a	0	1	0.11
RL27	60S ribosomal protein L27	0	1	0.11
RS13	40S ribosomal protein S13	0	1	0.11
COX5B	Cytochrome c oxidase subunit 5B, mitochondrial	0	1	0.11
RM12	39S ribosomal protein L12, mitochondrial	1	0	0.034
ABHDB	Alpha/beta hydrolase domain-containing protein 11	0	1	0.11
ORN	Oligoribonuclease, mitochondrial	0	1	0.11
CALD1	Non-muscle caldesmon (Fragment)	0	1	0.11

GILT	Gamma-interferon-inducible lysosomal thiol reductase	0	1	0.11
ARP5L	Actin-related protein 2/3 complex subunit 5-like protein	0	1	0.19
ARPC2	Actin-related protein 2/3 complex subunit 2	0	1	0.19
KAD4	Adenylate kinase 4, mitochondrial	1	0	0.079
TMX2	Thioredoxin-related transmembrane protein 2	0	1	0.19
FRIL	Ferritin light chain	0	1	0.19
PYRD	Dihydroorotate dehydrogenase (quinone), mitochondrial	0	1	0.19
ACOX1	Peroxisomal acyl-coenzyme A oxidase 1	0	1	0.19
ESTD	S-formylglutathione hydrolase	1	0	0.079
ADPGK	ADP-dependent glucokinase	0	1	0.19
COPA	Coatomer subunit alpha	1	0	0.079
RS19	40S ribosomal protein S19	0	1	0.19
AL4A1	Delta-1-pyrroline-5-carboxylate dehydrogenase, mitochondrial	0	1	0.19
TCPD	T-complex protein 1 subunit delta	1	0	0.079
TIM21	Mitochondrial import inner membrane translocase subunit Tim21	0	1	0.19
TOM40	Mitochondrial import receptor subunit TOM40 homolog	0	1	0.19
CATZ	Cathepsin Z	0	1	0.19
MACD1	O-acetyl-ADP-ribose deacetylase MACROD1	0	1	0.19
ASPH	Aspartyl/asparaginyl beta-hydroxylase	0	1	0.19
RL35A	60S ribosomal protein L35a	0	1	0.19
TFAM	Transcription factor A, mitochondrial	0	1	0.19
RM13	39S ribosomal protein L13, mitochondrial	1	0	0.079
RM43	39S ribosomal protein L43, mitochondrial	0	1	0.19
EFTS	Elongation factor Ts, mitochondrial	0	1	0.19
ATAD3	ATPase family AAA domain-containing protein 3	1	0	0.079
MGST1	Microsomal glutathione S-transferase 1	1	0	0.079
NDUS2	NADH dehydrogenase [ubiquinone] iron-sulfur protein 2, mitochondrial	1	0	0.079
ABHGA	Abhydrolase domain-containing protein 16A	1	0	0.079
ANXA3	Annexin A3	0	1	0.19
BASP1	Brain acid soluble protein 1	0	1	0.19
CP20A	Cytochrome P450 20A1	1	0	0.079
ELMD2	ELMO domain-containing protein 2	1	0	0.079
GPX8	Probable glutathione peroxidase 8	0	1	0.19
RL9	60S ribosomal protein L9	0	1	0.19
CNN1	Calponin-1	0	1	0.33
UBXN4	UBX domain-containing protein 4	0	1	0.33
ACSF2	Acyl-CoA synthetase family member 2, mitochondrial	1	0	0.18
COPB2	Coatomer subunit beta'	1	0	0.18
LGMN	Legumain	0	1	0.33
B2MG	Beta-2-microglobulin	0	1	0.33
PSA1	Proteasome subunit alpha type-1	1	0	0.18
PSA7	Proteasome subunit alpha type-7	0	1	0.33
NDUBB	NADH dehydrogenase [ubiquinone] 1 beta subcomplex subunit 11, mitochondrial	1	0	0.18



Appendix A-4 – Quantification of LD-associated protein by Western blot

Relative expression of select proteins in total luteal lysates versus purified LD fractions. Proteins were normalized to Ponceau S signal of the corresponding lane and the expression of each protein in fat (not shown in figure) was defined as 1. Graphs display mean \pm S.E.M., $n = 4$ * $P \leq 0.05$, *** $P \leq 0.001$ as determined by two-way ANOVA.

APPENDIX B: SUPPLEMENTAL DATA FOR CHAPTER 4

Appendix B-1 – Primers used for qPCR

Gene name	Primers for qPCR
<i>ATF3</i>	F: AGCACCTCTGCCACCGGATGT R: CTTTCAGGGGCTACCTCGGCTTT
<i>FOS</i>	F: TGACACCCTCCAAGCGGAGACA R: TTGCAGGCAGGTCGGTGAGC
<i>JUN</i>	F: ACGCCGACCCCTACCCAGTTC R: GGTGGCGTAGACCGGCTGCG
<i>JUNB</i>	F: CCGGAGCCGCCTCCAGTCTA R: ATGGTGGCCGTCCGGGTACGA
<i>CCL2</i>	F: TGCTCGCTCAGCCAGATGCAAT R: GGACACTTGCTGCTGGTGACTCT
<i>CCL8</i>	F: TCTCAGGCTGAAGCCCCCGT R: ACTGAATCTGGCTGAGCGAGCA
<i>CXCL2</i>	F: GCGCCCGTGGTCAACGAAT R: AGACTGGCTATGACTTCGGTTTGGT
<i>CXCL8</i>	F: TGTGAAGCTGCAGTTCTGTCAAG R: TGCACCCACTTTTCCTTGGGGT
<i>ACTB</i>	F: ACACCGCAACCAGTTCGCCAT R: AAGACGGCCCGGGGAGCATC
<i>GAPDH</i>	F: AGATGGTGAAGGTCGGAGTG R: GATCTCGCTCCTGGAAGATG

ACTB, actin beta; *ATF3*, activating transcription factor 3; *CCL2*, C-C motif chemokine 2; *CCL8*, C-C motif chemokine 8; *CXCL8*, C-X-C motif chemokine 8; *FOS*, Finkel-Biskis-Jenkins murine osteosarcoma viral oncogene homolog; *GAPDH*, glyceraldehyde-3-phosphate dehydrogenase; *JUN*, Jun proto-oncogene; *JUNB*, Jun proto-oncogene B

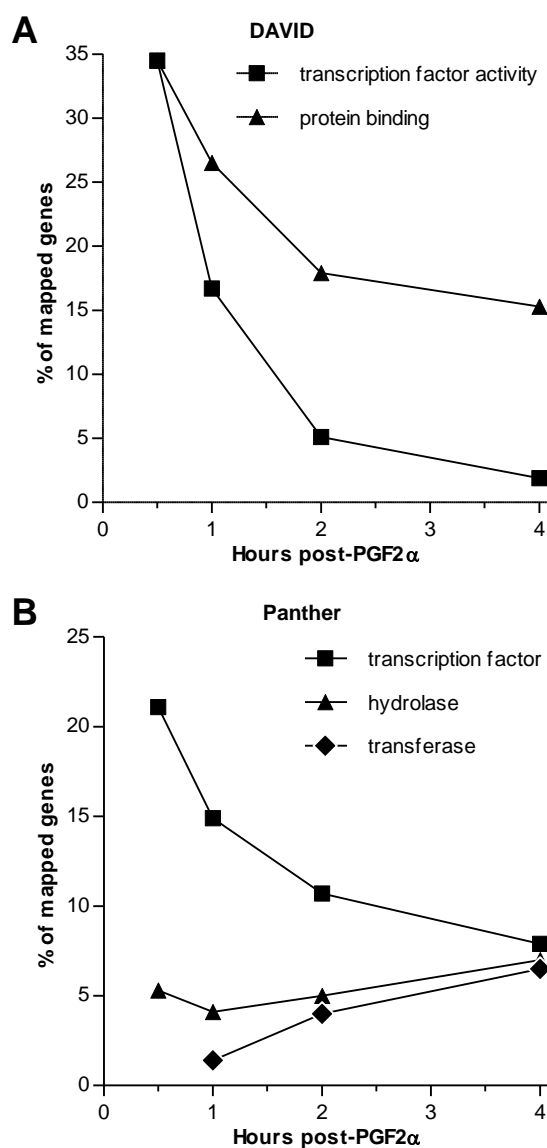
Appendix B-2 – Differentially expressed transcripts from a short PGF2 α time-course

	Up-Regulated Transcripts	Down-Regulated Transcripts
0.5 h	ADAMTS1, APOLD1, ATF3, BTG2, CYR61, DNAJB1, DUSP1, EGR1, EGR2, EGR3, FOS, FOSB, IER2, INSIG1, JUN, JUNB, LOC784931, NR4A1, NR4A2, NR4A3, PLK2, PPP1R15A, RGS2, RND1, SOWAHC, ZFP36	LOC100337120, LOC783362, MIR2450B
1 h	ABT1, ADAMTS1, ADAMTS4, ANGPT2, APOLD1, ARC, ARL5B, ATF3, BAMBI, BHLHE40, BTG1, BTG2, C15H11orf96, CCL1, CDC42EP2, CDK8, CDKN1A, CEBPD, CH25H, COQ10B, CYR61, DLL1, DNAJB1, DNAJB4, DUSP1, DUSP2, DUSP5, EDNRB, EGR1, EGR2, EGR3, EGR4, ERF, FAM43A, FAM46A, FGF18, FOS, FOSB, FOSL1, GEM, HOMER1, HSPH1, IER2, IFRD1, INSIG1, JUN, JUNB, JUND, LOC100138911, NR4A1, NR4A2, LSMEM1, MCL1, NR4A3, MXI1, MYC, NFIL3, NFKBIZ, NPAS4, PPP1R15A, RGS2, OBFC2A, PCF11, PDE4D, PER1, PEX12, PFKFB3, PHLDA1, PHLDA2, PLAT, PLK3, PLSCR4, PPP1R10, SOWAHC, PPP1R16B, RAB7B, RASD1, RCAN1, RFK, ZFP36, RND3, RNF122, SDC4, SEMA7A, SERPINE1, SIK1, SLC20A1, SLCO4A1, SNAI1, SNAI2, SOCS3, SRF, TAF4B, TMEM2, TRAF1, TRIB1, USP2, ZC3H12A, ZFAND2A, MIR2284I	ARHGAP25, CARD6, LOC100298387
2 h	RCAN1, RFK, ZFP36, RND3, RNF122, SDC4, SEMA7A, SERPINE1, SLCO4A1, SOCS3, SRF, TAF4B, TMEM2, TRAF1, TRIB1, ZC3H12A, ABL2, AMIGO2, ANGPTL5, AP1S3, AREG, ARG2, ARID5B, ATP11B, BACH1, BCL6, BDKRB1, BRIX1, BZW1, BZW2, C1H21ORF91, CBFB, CCDC41, CCDC58, CCDC85B, CCL8, CCT2, CD24, CD24, CDK17, CNN1, COPS9, CRISPLD2, CSRNP1, CSRP3, DAPP1, DCLK1, DCUN1D3, DHX15, DNAJA1, DNAJB11, DNAJC21, DPH3, EIF2C2, EIF3J, EIF4A1, ELL2, EPT1, EREG, ER11, ERICH1, F2RL1, F3, FAM71F1, FAM8A1, FBXO42, FERMT2, FGF2, FKBP5, GADD45A, GCH1, GCNT4, GJA1, GMPR, GNE, GOLM1, GPR137B, GPRC5A, HAT1, HDGFRP3, HRH1, IER3, IL1A, IL1B, IL33, INA, INHBA, JAK2, JMD1C, KDM7A, KLF5, KLF6, LDHA, LGALS1, LHFPL2, LMCD1, LOC100138700, LOC100296849, LOC100336688, LOC784931, LOC100337139, LOC286871, LOC782470, LOC788082, LONRF3, LYSMD3, MAFF, MAP3K2, MAP3K8, MAP7D2, MARCH3, MARCH5, METAP2, MMP12, MXD1, NDRG1, NET1, NKAIN2, NOP58, NPTX2, OLR1, ONECUT2, P2RY6, PDE8A, PFDN6, PIM1, PLAUR, PLPPR4, PMAIP1, PPP1C, PPP4R2, PRDM1, PSME4, PTX3, RAB20, RABEP1, RASA2, RBBP8, RDH12, RGS16, RIOK3, RNF125, RRP15, RSBN1, SAMD8, SERPINB2, SERTAD2, SETD8, SFPQ, SGMS2, SLC13A3, SLC19A2, SLC2A1, SLC2A3, SLC37A3, SLC41A2, SLC4A7, SMARCA1, SMARCA5, SNX18, SOX4, SPSB1, SPY2D1, SSFA2, STK17B, STK38L, STX11, SUB1, SUCLA2, TBC1D9, TEAD4, TFPI2, TIAM2, TIGAR, TLE3, TMEM30B, TMEM65, TNFSF18, TNFSF9, TWF1, UBALD1, UFM1, USP53, UTP15, XCL2, XIRP1, YOD1, YWHAZ, ZBTB5, ZFAND5, ZNF385B, ZNF644, ZSWIM6DAZL, LOC782090, PRRG4	ABCA7, ABCC5, ABLIM1, ADAP2, AGTR1, AHDC1, AKIP1, AMIGO1, AMOT, AOC3, ARHGAP20, ARHGEF10L, ARHGEF11, ARMCX6, ARRB1, ATAT1, ATP1B2, BCL9L, BCOR, BLES03, BORCS5, C13H20ORF27, C16H1orf115, C25H7ORF26, C28H10orf54, C5H12ORF4, CACNB2, CALB2, CAMK2G, CBX7, CCDC125, CCDC14, CD34, CEP295NL, CFAP126, CNM3, CRTCL, CTC1, CYR1, DAPK2, DISP1, DMD, DNASE1, DNM3, DPF3, EVA1B, FAM13C, FAM193B, FAM198B, FAM222B, FIS1, FLT3LG, FLVCR2, FOXL2, FSD1L, GAB1, GLTPD1, GRIA1, GRIN2A, HLX, HOXD3, HOXD4, IFT52, IRF2, ISYNA1, JUB, KANK2, KANK3, KCNN3, KIAA0232, KIAA1462, LDB1, LDLRAP1, LENG8, LIN37, LIPE, LMAN2L, LOC100335495, LOC100336724, LOC100337111, LOC100337178, LOC100337457, LOC509283, LOC510193, LOC511229, LOC514257, LOC515697, LOC787074, LRIG3, MAMSTR, MAPRE3, MFSD9, MID2, MIR2450A, MIR2475, MIR2485, MPPED2, MSRA, MSS51, MTMR11, MTP18, MTSS1, NAIF1, NFIB, NHSL1, NLRX1, NOTCH3, NPHP3, NPR3, NR1D1, NR2C2, NR2F1, NR5A2, NUMA1, OGT, PCDH12, PDRG1, PER3, PHACTR4, PHLDDB2, PIEOR2, PLEKHA2, PNMA1, PODXL, PPARGC1B, PPP1R3B, PPP2R4, PRR12, PTGDS, RAB7L1, RARG, RASGRP3, REM1, RFTN2, RFX3, RMND5B, LOC100337120, RNF113A, RNF214, RUBCN, RUNDC3B, RUSC2, RXRB, SDPR, SEPW1, SETDB1, SF4, SFRS14, SFRS8, SLC29A3, SLC39A14, SMM10, SNCAIP, LOC783362, SPRY4, ST5, ST6GAL1, STARD9, TANC1, TANC2, TBC1D13, TBC1D30, TCN2, TEK, TET1, THAP11, TM4SF1, TMEM14C, TMEM42, TNFRSF19, TNFSF10, TNRC6C, TNS3, TOR3A, TRIM62, TRIM65, TRIM68, TUBGCP5, USHBP1, VAMP2, VAMP5, VIPR1, WDR59, YPEL3, ZBTB4, ZBTB40, ZC2HC1C, ZC4H2, ZEB2, ZFP2, ZMYM3, ZMYND15, ZNF12, ZNF22, ZNF362, ZNF43, ZNF462, ZNF581, ZNF585A, ZNF629, ZNFX1APBB3, CABLES1, LOC100138414, LOC100336686, LOC616365, MIR584-7, SH3TC2, TRERF1, VSIG2, ZAR1L, ARHGAP25

4 h	<p>ARC, ARL5B, ATF3, BAMBI, BHLHE40, BTG1, BTG2, C15H11orf96, CCL1, CDK8, CDKN1A, CEBPD, CH25H, COQ10B, DNAJB1, DUSP1, DUSP2, DUSP5, EDNRB, EGR3, EGR4, FAM43A, FAM46A, FGF18, FOS, FOSB, FOSL1, GEM, HOMER1, HSPH1, IFRD1, INSIG1, JUNB, JUND, NR4A1, NR4A2, MCL1, NR4A3, NFIL3, RGS2, OBFC2A, PDE4D, PHLDA1, PHLDA2, PLK3, PLSCR4, SOWAHC, RCAN1, RFK, ZFP36, RNF122, SDC4, SERPINE1, SIK1, SLCO4A1, SOCS3, SRF, TAF4B, TMEM2, TRIB1, USP2, ZFAND2A, ABL2, AMIGO2, ABCE1, ABHD12B, AP1S3, ABTB2, AREG, AEBP2, AGFG1, ARG2, ARID5B, AH11, AHSB, AKAP4, AKIRIN1, ALCAM, BACH1, BCL6, ANKRD1, ANO6, BZW1, BZW2, C1H21ORF91, ARF4, CBFB, ARHGAP28, ARHGAP6, CCDC58, CCL8, ARL4C, CD24, ASAM, ATAD1, CD24, CDK17, ATP13A3, CNN1, ATP2A2, ATP2B1, ATP5I, ATP6V1C1, B3GALNT2, B4GALT5, COPS9, BCAP29, BCAS2, BCHE, BCL2L11, BCL3, CSRN1P1, CSRP3, DAPP1, BIRC3, BMP2, BOLA-DYA, BPIFA2A, BRINP1, BTBD10, BTG3, DNAJA1, C10H14orf119, C10H15orf65, C12H13orf27, C12H13orf30, C15H11orf46, DPH3, C16H1ORF21, C17H12orf52, C19H17orf67, EIF2C2, C23H6orf141, EIF3J, C27H8orf4, EIF4A1, C29H11orf73, C2H2orf76, C3H1orf162, ELL2, C6H4orf34, C9H6ORF115, CA8, EPT1, EREG, ERI1, CAPZA2, CBARP, ERICH1, F2RL1, F3, FAM8A1, CCDC80, FERMT2, CCK, CCL2, CCL3, CCL4, FGF2, CCNC, CCNG2, CCNYL1, CCP110, CCRN4L, CD14, GADD45A, GCH1, GCNT4, CD40, CD44, CD83, CDC42SE2, CDCP1, CDH1, GJA1, CDKL1, GMPR, CETN3, CFLAR, CGRRF1, CHIC2, CHKA, CHSY1, CLDN1, CLDND1, CLEC1A, CLEC1B, CLEC2B, GPR137B, COMMD6, GPRC5A, COX6C, CPNE8, CRABP2, CREB5, CRIPT, HAT1, CRYAB, CSF1, HRH1, CSRP2, IER3, IL1A, CTLA4, CTNNAL1, CWC22, CXCL13, CXCL2, CXCL5, CXCL8, CYB5R4, CYP3A4, CYSLTR2, IL1B, IL33, INA, INHBA, DDX3X, DDX5, DENND5A, DES, KDM7A, KLF6, LDHA, DNAJB6, DNAJB9, DNAJC12, LGALS1, LHFPL2, LMCD1, DTD1L, LOC100138700, LOC100296849, DRGX, DSTN, DTWD1, DUSP11, DUSP14, EDN2, EHBP1, EIF1AX, EIF1B, LOC100336688, LOC784931, EIF4E, LOC286871, ENTPD7, LOC782470, LOC788082, LONRF3, LYSMD3, ESYT3, MAFF, EVI2A, EXOSC1, F2RL2, MAP3K8, FAM126B, FAM148A, FAM171B, FAM18B, MARCH3, MMP12, MXD1, FAM92A1, FBXL14, NDRG1, NET1, FGF7, FGFR1OP2, FGR, NPTX2, FKBP14, OLRI, P2RY6, PDE8A, FSHR, PIM1, PLAUR, GADD45G, GAL, GAS1, GCF2C, PLPPR4, GDPD1, GLRX2, PPP4R2, GMCL1, GMFB, GMNN, PRDM1, PSME4, GNPNTAT1, PTX3, RAB20, GPR155, GPR65, GPR68, RASA2, RBBP8, GTF2E2, H2AFZ, HAS2, RDH12, HAUS3, HAUS6, HBXIP, RGS16, HGF, HIGD1D, HINT3, HK2, RIOK3, HMGA1, RNF125, RRP15, HPCA, HPCAL4, RSNB1, HS3ST5, HSPA13, IBSP, ICOSLG, SAMD8, IFT20, SERPINB2, IGF2BP2, IGFBP1, IGFBP3, IL10, IL18, IL18BP, SERTAD2, SETD8, IL1R1, IL1RN, IL21R, SFPQ, IL4R, IL7R, SGMS2, SLC13A3, INHBB, INSIG2, IPMK, IRAK2, SLC19A2, IRG1, ISCA1, ISG20, ISG20L2, SLC2A1, ITGA2, ITGAV, IVNSIABP, SLC2A3, JARID2, SLC37A3, JPH2, SLC41A2, SLC4A7, KBTBD8, KDM6B, KHDRBS3, SOX4, SPSB1, SSFA2, KLHL32, KRT18, KRT73, KRT8, KRTAP3-1, STK17B, STK38L, STX11, SUB1, TBC1D9, LIN7C, LLPH, TFP12, TIAM2, LMO7, LNP, LOC100140827, LOC100174924, LOC100294784, LOC100294785, LOC100294863, LOC100294865, LOC100295254, LOC100295381, LOC100295586, LOC100295757, LOC100295775, LOC100296441, LOC100296447, LOC100296475, LOC100296524, LOC100296684, LOC100296722, LOC100296944, LOC100297075, LOC100297413, LOC100297468, LOC100298628, LOC100300871, LOC100301462, LOC100335253, LOC100335275, LOC100335305, TMEM30B, LOC100335936, LOC100336429, LOC100336443,</p>	<p>PPP1R10, AAK1, AARS, AASDH, ABCA1, ABCF3, ABCG2, ABHD14A, ABHD14B, ACACA, ACAD10, ACAP3, ACBD4, ACD, ACIN1, ACP2, ACP5, ACTN4, ADAMTS17, ADAMTS15, ADCK2, ADCY4, ADCY9, ADD1, ADORA2A, ADPRHL2, ADRB1, AEBP1, AFF1, AFF2, AFF3, AGAP2, AGFG2, AGK, AGPAT1, AGRN, AHNAK, AKAP11, AKAP13, AKAP8L, AKR1A1, ALAD, ALDH3A2, ALDH3B1, ALG8, ANGEL1, ANKHD1, ANKLE2, ANXA11, APIB1, APEG3, APEX2, APLNR, AR, ARAP1, ARAP3, AREL1, ARFGF2, ARHGAP17, ARHGAP18, ARHGAP19, ARHGAP23, ARHGEF40, ARHGEF7, ARID1A, ARID1B, ARMCX5, ARDC1, ARSB, ARSG, ARX, ASAP1, ASXL2, ATF5, ATF6B, ATF7, ATF7IP, ATN1, ATP2C2, ATXN2, ATXN7L1, AUTS2, B3GNT3, B3GNT9, B9D2, BAT2, BAT2L1, BAZ1B, BAZ2A, BCL9, BNC2, BRPF1, C10H15orf41, C11H9orf114, C14H8ORF70, C22H3ORF37, C23H6ORF47, C28H10ORF35, C28H1orf198, C2H2orf24, C3AR1, C8H9orf23, C8H9orf91, C9H6ORF203, C9H6ORF70, CABC1, CABIN1, CAMKK2, CAPN1, CASC3, CASKIN2, CASP9, CBFA2T2, CBL, CBR4, CBX4, CBX6, CC2D1A, CC2D2A, CCDC106, CCDC6, CCDC8, CCND3, CCNJL, CCS, CDC42BPB, CDC42EP4, CDON, CEACAM8, CELSR2, CEP110, CEP68, CHD2, CHD8, CHMP1A, CHMP4C, CHRN3B, CHST7, CIITA, CIRBP, CIZ1, CKAP5, CLASP1, CLIC5, CLMN, CLN6, CMTM4, CNDP2, CNOT3, CNOT4, CNOT8, COG1, COG7, COG8, COPS7A, COQ4, CORO2B, CPEB1, CPEB2, CPSF1, CREBBP, CRT2, CRY2, CSRN3, CSTF1, CTNS, CUL7, CUL9, CUX1, CXORF36, CYB5D2, CYB5R3, DAAM2, DAB2, DAB2IP, DACT1, DAG1, DAGLA, DBP, DCAF4, DCP1B, DCTN1, DDX31, DDX42, DEF6, DENND1A, DENND4B, DEPC5, DHRS12, DHX30, DHX37, DHX57, DIP2A, DIP2B, DIS3L2, DNAJC16, DNAJC17, DNAJC30, DOCK6, DOCK9, DOPEY2, DPAGT1, DSCR3, DTNBP1, DTX2, DUSP10, DUSP15, DVL3, DYNC1H1, DYSF, EEF2K, EFTUD2, EGFLAM, EHD2, EHMT2, EIF2B4, EIF2C4, EIF4EBP2, EIF4ENIF1, ELMO1, EMC9, EMCN, EMD, EML5, ENG, EP400, EPB41, EPHB3, ERAL1, ERAP1, ERCC3, ERCC5, ERN1, EVC2, EXOC3L, EZH1, FADS6, FAM115A, FAM120B, FAM122A, FAM13A1, FAM168A, FAM171A2, FAM188B, FAM189B, FAM214B, FAM59A, FAM65A, FAM73B, FAM83H, FARP1, FASN, FBLIM1, FBLN5, FBN1, FBRS, FBXL12, FBXL6, FBXL8, FBXO10, FBXO42, FBXW12, FBXW4, FES, FGD1, FHOD1, FIGN, FITM2, FKBP15, FLAD1, FLOT2, FLYWCH2, FN3KRP, FNTB, FOXJ2, FOXN3, FOXRED1, FOXS1, FRY, FTSJD2, FUT1, FUT8, FYCO1, FZD4, FZR1, G6PD, GALNS, GALNT10, GALT, GANAB, GATA4, GATSL3, GBA2, GBF1, GCC1, GCN1L1, GEMIN4, GEMIN5, GGA3, GIPCI, GIT2, GLE1, GLG1, GLTSCR1L, GNA14, GON4L, GPAM, GPIHBP1, GPR4, GPS2, GREB1L, GRN, GTF21, GTF3C1, GTF3C4, GYS1, H1F0, H1FX, H6PD, HADH, HAUS4, HAUS5, HCFC1, HCRTR1, HDAC4, HDAC6, HDGF2, HEATR5B, HEATR7A, HECTD4, HECW2, HERC2, HEXIM1, HGS, HIG2, HIP1, HIVEP1, HLCS, HOXC6, HOXD9, HPS1, HS1BP3, HSD17B14, HSDL1, HSPA2, HSPG2, HUWE1, HYI, ICMT, ID3, IFT122, IFT88, IGF2R, IGFBP2, IL11RA, IL23A, ILDR2, ILVBL, INADL, INO80D, INPP5B, INPP5D, INTS1, INTS3, IPO13, IQGAP2, ITGA9, ITPR3, ITSNI, JMD2A, KANK1, KANSL1, KANSL3, KBTBD4, KCTD21, KDM2A, KDR, KEAP1, KIAA0100, KIAA0182, KIAA0355, KIAA0753, KIF13A, KIF16B, KIF3B, KLF12, KLHL18, KLHL25, KLHL26, KMT2B, KPTN, LAMB2, LARPI, LASS1, LAT51, LGALS9, LHPP, LOC100137838, LOC100138392, LOC100295097, LOC100295263, LOC100296493, LOC100298868, LOC100299799, LOC100335642, LOC100336406, LOC100336508, LOC100336568, LOC100336586, LOC100336604, LOC100336756, LOC100336769, LOC100336841, LOC100336856, LOC100336912, LOC100337052, LOC100337072, LOC100337080, LOC100337088,</p>
4 h		

4 h	LOC100336452, LOC100336518, LOC100336625, LOC100336666, TNFSF18, LOC100337076, TWF1, LOC100337126, UBALD1, UFM1, LOC100337445, LOC407171, LOC508459, LOC509071, LOC509094, XCL2, LOC509506, LOC509911, XIRP1, YOD1, YWHAZ, LOC515823, LOC521081, LOC522171, LOC523389, LOC524181, LOC524703, LOC613460, LOC613882, LOC613970, LOC614643, LOC615482, LOC616520, LOC618696, LOC619061, LOC781102, LOC781142, LOC781416, LOC781462, LOC781612, LOC781807, LOC782021, LOC782266, LOC782348, LOC782402, ZFAND5, LOC782639, LOC782740, LOC782950, LOC783459, LOC784207, LOC784704, LOC785366, LOC785449, LOC785455, LOC785745, LOC786131, ZNF385B, LOC787187, LOC788284, LOC788496, LOC789095, LOC789126, LOC789920, ZSWIM6, #N/A, LRP12, LRRC58, LRRC8B, LRRN3, LSM1, LY96, MAN1A1, MANF, MAP1LC3C, MAP2K3, MAP4K5, MAPK6, MAPKSP1, MARCKSL1, MEMO1, METRNL, MEX3C, MGC127989, MGC143035, MICAL2, MIER1, MIR19A, MIR21, MIR2434, MIR2469, MMP1, MMP1, MOSPD2, MRPL39, MRPL42, MRPS16, MRPS18C, MSC, MT2A, MTCL1, MTMR12, MUSK, MYH1, MYL3, Myrn, MZT1, NAB1, NCALD, NDUFAF2, NEXN, NFKB1, NFKB1A, NIPAL1, NMU, NOS1AP, NRCAM, NRG1, NUCB2, NUDCD1, NUDT10, NUPL2, OAF, ODF2L, OSBPL11, OSTM1, OXT, PAG1, PAK1IP1, PAPD7, PCDH11X, PCNP, PDCD10, PDE4B, PDGFC, PDLIM4, PDPI, PELI1, PENK, PEX13, PICALM, PIGP, PIK3CA, PITPNC1, PKIB, PKNOX1, PLA2G7, PLEK, PLIN2, RND1, PLN, PLOD2, PNP, POLB, POLE4, POLR2K, PPAPDC3, PPARG-TSEN2, PPMIN, PPP1CB, PPP1R2, PPP1R3C, PPP4R4, PRKCD, PRORS1, PSMD14, PSTPIP2, PTGER2, RAB19, RAB40B, RABGGTB, RAI14, RASGEF1A, RASSF8, RBM7, RCHY1, RCN2, RDH11, RERG, RGCC, RHEB, RIPK4, RNF19B, RNFT1, RPF2, RPIA, RPL34, RPS12, RPS21, RPS23, RRAD, RRAS2, RSL24D1, RUBCNL, RUNX1, S100A12, S100A8, S100A9, S1PR3, SAMD4A, SDS, SEC61G, SELK, SEMA3C, SERPINA11, SERTAD4, SF3B14, SGPP1, SGTB, SH3GL3, SHTN1, SLC12A2, SLC20A2, SLC25A25, SLC25A33, SLC26A2, SLC33A1, SLC34A2, SLC38A1, SLC39A8, SLC46A2, SLITRK2, SLMO2, SMG9, SNAP25, SNRPD1, SNRPG, SNX13, SNX31, SNX4, SOCS1, SPCS3, SPHK1, SPPI, SRD5A1, SRXN1, SSTRI, STAMBP, STEAP1, STK17A, SUCO, TANK, TBCA, TERC, TET3, TFB2M, TGFBR1, TGIF1, THAP5, THBD, THBS1, THX1, TIAM1, TIMM17A, TIMM8A, TLR2, TMC1, TMEM126A, TMEM136, TMEM14A, TMEM165, TMEM188, TMEM189-UBE2V1, TMEM26, TMEM41B, TMEM45A, TMEM64, TMF1, TMOD1, TMX1, TNFAIP3, TNFAIP8L3, TNFRSF12A, TNFRSF6B, TNFSF4, TPM4, TRAM1, TREM1, TRH, TRPC4, TRPM6, TRPM7, TSPAN12, TUBB2A, TXN, TXNRD1, UAPI, UBE2B, UBE2N, UBE2W, UBE3A, UCHL3, UPRT, UXT, VAT1L, VBP1, VNN2, WASF1, WDR44, WDR89, XBPP1, YWHAQ, ZBTB43, ZNF469, ZNRD1, ACBD7, BCL2A1, CHSY3, GPR87, LOC100294744, LOC100297034, LOC100297127, LOC100337296, LOC509074, LOC514319, LOC520180, LOC616887, LOC782358, LOC785867, LOC787306, LOC788009, LOC789734, LRRC31, MBL2, NPPB, PAG6, PAG9, PAQR9, PDE1C, SERPINI1, TMIGD1, TRIM9, VSX1, WFDC11, WNT10B	LOC100337236, LOC505156, LOC505719, LOC508153, LOC511497, LOC526631, LOC526847, LOC529423, LOC534002, LOC539110, LOC539229, LOC540312, LOC616014, LOC616063, LOC616198, LOC619000, LOC783493, LOC786942, LOC788379, LPCAT1, LPHN1, LRFN3, LRIF1, LRP1, LRRC41, LRRK1, LRSAM1, LTBR, LYSMD4, MACF1, MAEA, MAMLD1, MAN2A2, MAP2K2, MAP3K4, MAP3K6, MAP4K2, AGTR1, MAPK7, MAPRE2, AHDC1, AKIP1, AMIGO1, MARK2, MARVELD1, MAVS, MAZ, MBD6, MBNL2, MCM9, MDC1, MDN1, MECP2, MED12, MED16, MED22, MED25, MEF2C, MEPC, AMOT, MFNG, AOC3, MGC134093, MGC159500, MGME1, MIB2, MICAL1, MID1IP1, ARHGAP20, MINK1, MIR1287, MIR2303, MIR2416, MIR2454, ARHGEF11, ARMCX6, MKKS, MKS1, MLH3, MLL, MLL2, MLLT10, MMP15, MMP2, MMS19, MOBKL2A, MON1B, MORC2, MOSPD3, MOV10, MPDZ, MPP5, ATAT1, MRPS24, MSH6, ATP1B2, BCL9L, MTF1, MTHFD1, BCOR, MTMR14, MTMR15, MTMR4, MTOR, BLES03, MTRR, BORCS5, MTSS1L, MUL1, MUM1, MXD4, MYCBP2, MYH11, MYL9, MYO18A, MYOF, MYST2, MYST4, NAAA, NADSYN1, NAGK, C16H1orf115, NAV2, NBEAL2, NCKAP5L, NCOA2, NCOA6, C25H7ORF26, NDST2, C28H1orf54, NEU3, NFATC1, NFIA, NFIC, NFIX, NFYC, NHSL2, NIPSNAP1, NIPSNAP3A, NISCH, CAMK2G, NOL4L, CBX7, NOSIP, CCDC125, NOVA2, NPEPL1, CCDC14, NPNT, CD34, NR0B2, CFAP126, CNM3, CRTCI, NR2F2, NR5A1, CTC1, NSD1, NUAKE1, CYR1, NUP214, NUP62, NUP85, OGFOD2, DAPK2, OIT3, DMD, ORA1, OSBP, OSBPL7, OXSM, DNASE1, PACS1, PALD1, PAN2, PAPSS1, PARG, PARP1, PARP4, PATL1, PATZ1, PBX1, DNM3, PCDHGA5, PCGF2, PCIF1, PCNT, PCNXL3, PCYOX1L, PCYT1B, PDE4DIP, PDE7B, DPFF3, PDPR, PDZD2, PEAK1, PELP1, FAM13C, PEX1, PEX10, FAM193B, PFKM, PGAP2, PGAP3, PGM5, FAM198B, PHC3, PHF14, PHF15, PHF20, PHF21A, FAM222B, PIK3C2B, PIK3CG, PIK3R1, PIM2, PIM3, PIP4K2B, PITPNM2, PJA2, PKD2L1, PKNOX2, FLT3LG, PLCG1, PLEKHM3, PLIN3, PLOD3, PLPP6, FOXL2, PLXNA2, PLXNB2, PLXND1, FSD1L, PMF1, PNKD, GAB1, PNPLA2, PNPLA6, POFUT1, POGZ, POLD1, POLD2, POLDIP3, POLL, POLR1A, POLR1E, POLR3A, POLR3B, POM121C, POMT1, POU6F1, PPARA, PPIL2, PPP1CA, PPP1R13B, HLX, PPP1R9A, HOXD3, PPP2R5D, IFT52, PRDM10, PRDM6, PRELP, PRICKLE1, PRKAB1, PRKACA, PRKCE, PRKCSH, PRKD2, PRKDC, PRPF19, IRF2, PRR14, PRR3, ISYNA1, PSMF1, PTCH1, JUB, PTH1R, PTHLH, PTPN14, PTPN23, PTPRF, PTPRG, PTPRS, KANK2, PXN, PYGB, RAB11B, RAB11FIP5, RAB1B, KANK3, RAB37, RAB3A, RABGGTA, RAD52, KIAA1462, LDB1, LDLRAP1, LENG8, RBM47, RBM5, LIN37, RECQL5, LIPE, REV3L, RFFL, LMAN2L, RFX1, RGL1, RHBDF1, RHOTB1, RHOG, RNASEN, LOC509283, RNF123, RNF135, RNF145, RNF169, LOC511229, RNF26, RNF31, RNF40, RNF44, RPAP1, RPRD2, RPS6KA5, RPTOR, RREB1, LOC515697, RUNXIT1, LRIG3, RWDD3, MAMSTR, SAP130, SAP30BP, SAP30L, SARS2, SART3, SCAF1, MFSD9, SEC16A, SEC24C, SELO, SEMA6D, SEPN1, SEPT4, SEPT8, SERPINA14, SETD1B, MPPED2, SF3A1, SF3A2, MSRA, MTP18, SFXN2, MTSS1, SHPRH, SIAH2, SIN3B, SIPA1, SIRT2, SLC10A5, NAIF1, SLC19A1, NFIB, SLC24A3, SLC27A1, NHSLI, NLRX1, NOTCH3, SLC2A9, SLC35A4, SLC35E2, NPHP3, SLC37A4, NPR3, SLC41A1, SLC46A3, SLC47A1, NR2C2, SLC7A8, SLC8A1, SLC9A1, SLC9A3R2, SLCO2B1, NR2F1, SMARCA2, NR5A2, SMARCC2, SMARCD2, SMC1A, SMG1, SMG6, NUMA1, SMPD2, SMYD4, SNRNP200, PCDH12, SOGA1, SORBS3, SOS1, PER3, SPG11, SPIDR, SPRY3, PHACTR4, PHLDB2, SPTAN1, SPTBN1, PIEZO2, SRCAP, SRGAP2, SRRM1, SRRM2, PLEKHA2, PNMA1, PODXL, STAP2, PPARGC1B, STAT1, STAT2,
4 h		

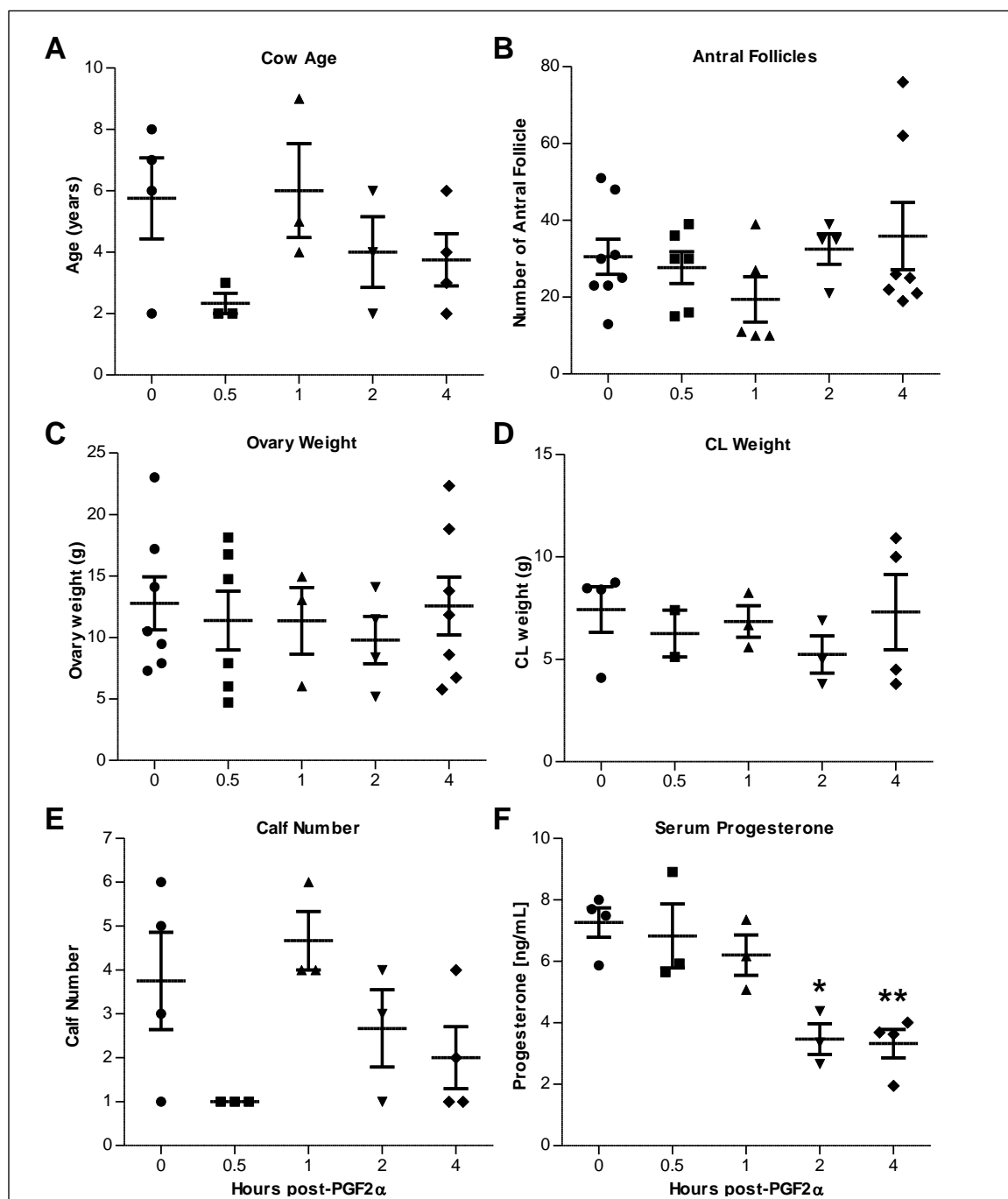
4 h		<p>STBD1,, PPP1R3B, STK36, PPP2R4, STOML1, PRR12, PTGDS, RAB7L1, SUN2, SYNE2, SYNPO2, SZT2, TAB1, TACC2, TAF4, TAF6L, TAF8, RARG, RASGRP3, TAOX2, TAPBP, TBC1D16, TBC1D2B, TBC1D4, TBC1D8, RMND5B, TBC1D9B, TBCD, TBXA2R, TCF7L2, LOC100337120, TCP11L1, TDRD7, RNF214, TENC1, RUBCN, TGFB2, TH1L, RXRB, TIE1, TIRAP, TJP1, TLDC1, TLN1, SETDB1, TMCC1, TMCO4, TMCO6, TMEM106A, TMEM127, TMEM138, TMEM204, TMEM214, TMEM265, SFRS14, TMEM41A, SFRS8, TMEM51, TMEM52, TMEM62, TMEM63A, SLC29A3, TMEM88, TMEM8A, TMEM94, SMIM10, LOC783362, TNKS, TNRC6A, TNRC6B, SPRY4, TNS1, ST5, ST6GAL1, TP53, TPCN1, TPCN2, TRAFD1, TRAPPC1, TRAPPC9, TRIB2, TRIL, TRIM11, TRIM21, TRIM25, TRIM41, TRIM44, TRIM45, STARD9, TANC1, TRIP10, TRM1L, TRPV2, TRRAP, TSC2, TSC22D3, TSNARE1, TSPAN11, TSPAN4, TSPAN5, TSPAN9, TTC21B, TTC28, TTC39A, TTC5, TTH1, TTL12, TTL4, TUBG1, TBC1D13, TULP4, TXNIP, UAP1L1, TCN2, UBAP2L, UBE4B, UBIAD1, UBR4, UFSP1, UNC119, UNC93B1, UNG, UNK, UPF1, TET1, USP19, USP20, USP21, USP22, USP24, USP48, THAP11, VAC14, TMEM42, VAV3, VIPAS39, TNFRSF19, VIPR2, VMAC, VPS11, VPS13D, VPS37C, VPS39, VPS52, VRK3, WDR11, WDR20, WDR34, WDR6, WDR76, WDR81, WDR91, WFDC5, WIPF3, WIZ, WNK1, WWC3, WWP2, TNRC6C, XDH, TNS3, XPC, XPNPEP3, XRCC1, TOR3A, TRIM62, TRIM65, ZBED5, ZBTB16, ZBTB20, ZBTB24, TRIM68, ZBTB45, USHBP1, ZBTB6, ZBTB7B, VAMP2, ZC3H4, ZC3H7B, ZC3HC1, ZCCHC11, VIPR1, ZER1, WDR59, ZFH3, ZFP3, ZFP62, ZFYVE26, ZHX3, ZBTB4, ZBTB40, ZMYND8, ZC2HC1C, ZNF142, ZC4H2, ZNF346, ZEB2, ZNF384, ZNF385A, ZNF395, ZNF414, ZNF423, ZMYM3, ZNF445, ZNF449, ZNF470, ZNF503, ZNF512B, ZNF518B, ZNF22, ZNF592, ZNF605, ZNF618, ZNF362, ZNF652, ZNF687, ZNF689, ZNF704, ZNF710, ZNF768, ZNF828, ZRANB3, ZNF585A, ZNF629, ZNF827, CCR10, CD6, CDK18, CEP135, ZNFX1, IQSEC2, LOC508648, LOC100138414, LOC100336686, LOC616365, PLEKHH1, PMS2, SLFN1, TRERF1, WDR62, YDJC, ZKSCAN2, ARHGAP25, CARD6</p>
4 h		



Appendix B-3 – Biological process annotation of differentially expressed genes from each time point

(A) Percent of mapped genes with “transcription factor activity, RNA polymerase II core promoter proximal region sequence-specific binding” or “protein binding” annotations based on DAVID molecular function analysis (GOTERM_MF_ALL) of all differentially expressed genes from each time point. (B) Percent of mapped genes with “transcription factor (PC00218)”, “hydrolase (PC00121)”, or “transferase (PC00220)” annotations based on Panther Protein Class analysis of differentially expressed genes from each time point.

Appendix B-5 – Physiological characteristics of the study animals



Appendix B-4 – Physiological characteristics of the study animals

Mid-cycle cows (n = 3/time point) were treated with 25 mg PGF2 α for 0.5, 1, 2, and 4 hours or saline (n = 4). Symbols indicate individuals or each ovary, with mean \pm SEM overlaid. (A) Age (in years) of cows at ovariectomy. (B) Number of antral follicles present on each ovary from study animals. (C) Total weight of each ovary from study animals. (D) Weight of corpus luteum (CL) from each study animal. (E) Previous number of calves from each study animal. (F) Serum progesterone concentrations of cows 0.5 - 4 hour post-PGF2 α treatment (n = 3/time point). * $P \leq 0.05$, ** $P \leq 0.01$ compared to saline-treated animals using one-way ANOVA followed by Bonferroni's multiple comparison test.

Appendix B-6 – Differentially expressed transcripts included within each SOM

	Up-Regulated Transcripts (33)	Down-Regulated Transcripts (144)
Immediate-Early Response	<i>ABT1, ADAMTS1, ADAMTS4, ANGPT2, APOLD1, CCND1, CDC42EP2, CIRH1A, CYR61, DLL1, DNAJB1, DNAJB4, EGR1, ERF, FOS, FZD4, IER2, JMJD6, JUN, KLF16, LOC100138911, LOC786156, NFKBIZ, NR4A2, PCF11, PDE7B, PER1, PLK2, PPP1R10, PPP1R16B, RAB7B, RABGEF1, RGS2, RND1, SNAI1, SNAI2, ZC3H12A</i>	<i>ABCA7, ABCC5, ABLIM1, ADAP2, AHDC1, AKIP1, AOC3, ARHGEF10L, ARMC2, ARMCX6, ARRB1, ATP1B2, BCAR3, BLES03, C13H20ORF27, C4H7orf23, C8H9orf23, CACNB2, CALB2, CBX7, CCDC125, CCDC14, CDC42EP1, CIRBP, CLEC3B, DGCR6L, DISP1, EML5, FAM193B, FAM82A1, FGD6, FIS1, FLVCR2, GLTPD1, GRIA1, GTF3C4, HES2, HLX, HOXD4, HSPA12B, IFT52, KCNN3, LBH, LDB1, LENG8, LIMS2, LIN37, LMAN2L, LOC100125412, LOC100139577, LOC100335299, LOC100335495, LOC100336920, LOC100337457, LOC508354, LOC510193, LOC513640, LOC514257, LOC514704, LOC514750, LOC515356, LOC522449, LOC540918, LOC616821, LOC618094, LOC618454, LOC786352, LOC787074, LOC789977, LOH12CR1, MAPK7, MAPRE3, MAST3, MFSD8, MFSD9, MGC139026, MGC151567, MGC165685, MIR2450A, MRM1, MSRA, MTMR11, MUSTN1, NHSL1, NPHP3, NPR3, NR1D1, OGT, PATZ1, PDRG1, PHF14, PHLDB2, PIGS, PNMA1, PRR3, PRRG3, RAB30, RAB3A, RASA3, REM1, RERE, RFTN2, RFX3, RMND1, RMND5B, RNF113A, SAP30L, SDPR, SF4, SLC25A42, SLC39A14, SNCAIP, ST5, STK19, SUFU, TADA3, TANC2, TBC1D30, TEK, THUMPD2, TMEM145, TMEM42, TNFSF10, TP53I11, TRIM41, TRIM65, TSC1, TUBGCP5, URGCP, VAMP2, VAMP5, WDR59, YPEL3, ZC4H2, ZFP2, ZFP62, ZMYND15, ZNF26, ZNF260, ZNF319, ZNF366, ZNF43, ZNF462, ZNF581</i>

	Up-Regulated Genes (136)	Down-Regulated Genes (240)
Early Response	<p>AATF, ACSL3, AMD1, ANKMY2, ANKRA2, ARC, ARL4C, ARL5B, ATF3, B3GALNT2, BAMBI, BCL6, BRIX1, BTA1F1, BTG2, C27H8orf4, CCDC85B, CCNYL1, CCRN4L, CCT2, CDK8, CEBPD, CH25H, CRISPLD2, CSRNP1, DCLK1, DCUN1D3, DHX15, DNAJB11, DNAJC21, DUSP1, DUSP2, EDNRB, EGR3, EGR4, EIF3B, EIF3J, EIF4A1, FAM49B, FBXO33, FGF18, FHOD3, FKBP5, FOSB, FOSL1, GADD45A, GADD45G, GJA1, GNE, GOLM1, GPRC5B, HAT1, HSPH1, IFRD1, IGFBP3, INSIG1, JUNB, JUND, KIAA0020, KLF5, KLF6, LOC100174924, LOC100295476, LOC100295973, LOC100296226, LOC100297981, LOC100299027, LOC100336279, LOC100337254, LOC524703, LOC529462, LOC539374, LOC541159, LOC613882, LOC784070, LOC785063, LOC785529, LOC787610, LTV1, LYSD3, MAP3K2, MAP7D2, MCL1, MGC137708, MGC142811, MGC148992, MXI1, MYC, MYL6B, NAB1, NEXN, NFIL3, NOP58, NPPC, NR4A1, NR4A3, ONECUT2, PDE4B, PEX12, PFDN6, PFKFB3, PHLDA1, PHLDA2, PLAT, PLSCR4, PPP1CC, PPP1R15A, RABEP1, RASD1, RDH12, RFK, RND3, RNF122, SEMA7A, SFPQ, SLC20A1, SLC2A3, SLC4A7, SLC04A1, SMARCA1, SMARCA5, SMOC1, SNX18, SPTY2D1, STC1, TEAD4, TIGAR, TLE3, TMEM2, TMEM65, TP53BP2, TRAF1, TRIB1, ZBTB10, ZBTB5, ZFP36</p>	<p>AASDH, ABCA1, ABCC3, ABHD14B, ACP2, ADCK2, AFF2, AKAP11, AKAP8L, AKR1A1, ALDH3A2, ALG8, AMIGO1, ANAPC5, ANGEL1, APEX2, ARHGAP19, ARHGAP20, ARHGAP25, ASB16, ATF7IP, ATXN7L1, C10H15orf41, C14H8ORF70, C23H6ORF47, C28H10ORF35, C2H2orf24, C9H6ORF203, CARD6, CC2D1A, CC2D2A, CCDC8, CCND3, CDON, CEP68, CHD8, CHST7, CIAO1, CLN6, CNOT8, COG1, COG8, CPT2, CSTF1, DACT1, DAG1, DBP, DCAF4, DDX31, DENND1A, DEPDC5, DNAJC16, DNAJC30, DPAGT1, DSCR3, DUSP10, EHMT2, EIF2C4, EIF4EBP2, ERAP1, ERCC3, ERCC5, FAM120B, FAM122A, FAM33A, FAM73B, FARP1, FBXL12, FBXO10, FIGN, FITM2, FKBP15, FLAD1, FN3KRP, FOXL2, GATSL3, GEMIN4, GON4L, GPAM, H1F0, HAUS4, HDAC6, HDGF2, HEATR5B, HEXIM1, HIG2, HLCS, INPP5B, IRF2, JMJD2A, KBTBD4, KCTD21, KEAP1, KIAA1539, KIF3B, LATS1, LNPEP, LOC100138392, LOC100140430, LOC100295097, LOC100295263, LOC100336406, LOC100336473, LOC100336856, LOC506615, LOC508153, LOC508720, LOC509858, LOC512910, LOC516630, LOC539472, LOC540169, LOC616198, LOC618190, LOC787062, LRIG3, MAP3K7IP1, MAPK8IP3, MARVELD1, MCM9, MEN1, MEPCE, MGC134150, MGC139126, MGC155141, MGC159500, MICAL1, MID1IP1, MKKS, MKS1, MRPS24, MSH6, MTHFD1, MTRR, MUM1, MYCBP2, MYST2, NCKAP5L, NDST2, NEK4, NEU3, NFYC, NGRN, NIPSNAP3A, NPEPL1, NR0B2, NR1H4, NR2F2, NR5A1, NSD1, NUP62, PAPSS1, PARG, PCDHGA5, PCIF1, PDE4DIP, PGAP2, PHF15, PHF20, PIK3C2B, PIP4K2B, PJA2, PNPLA6, POFUT1, POLDIP3, POLR1E, POLR3B, PRICKLE1, PRUNE, PSKH1, PTCH1, PTHLH, PYGB, RECQL5, RGL1, RHOBTB1, RNF135, RNF145, RNF169, RNF26, RNF31, RNF44, RNPEPL1, RPRD2, RWDD3, SEMA6D, SETD1B, SF3A1, SLC16A14, SMARCD2, SMPD2, SOS1, STBD1, STOML1, SYNPO2, TAF8, TBC1D13, TBC1D4, THAP11, TMEM164, TMEM214, TMEM62, TNFAIP8, TRIM21, TRIM62, TRIM68, TRIP6, TRM1L, TSPAN11, TTC21B, TTC5, TTLL12, TUBG1, TXNIP, UBIAD1, UNG, USP19, USP20, USP21, VPS11, VPS52, WDFY2, WDR11, WDR20, WDR76, XPNPEP3, XRCC1, ZBED5, ZBTB24, ZBTB45, ZBTB6, ZBTB7B, ZFP3, ZNF142, ZNF22, ZNF346, ZNF449, ZNF624, ZNF652, ZNF689</p>

	Up-Regulated Genes (286)	Down-Regulated Genes (288)
Delayed-Early Response	<p> <i>ABCE1, ABL2, AGFG1, AH11, AMIGO2, AP1S3, AREG, ARG2, ARID5B, ASAM, ATP11B, ATP13A3, ATP2A2, BACH1, BCAS2, BCL2L11, BCL3, BHLHB2, BTBD10, BTG1, BTG3, BZW1, BZW2, C12H13orf30, C15H11orf46, C1H21ORF91, C9H6ORF115, CBFB, CCDC41, CCDC80, CCL3, CCNC, CD83, CDC42SE2, CDK17, CDKN1A, CHAC1, CHIC2, CHKA, CHSY1, CLDND1, CNN1, COQ10B, CSRP2, CSRP3, CWC22, CXCL5, DAPP1, DDX39, DDX3X, DDX5, DNAJA1, DNAJB6, DNAJB9, DPH3, DUSP5, EDN2, EIF1B, EIF2C2, ELL2, ENTPD7, F2RL1, F2RL2, F3, FAM8A1, FBXL14, FERMT2, FGF2, FGF7, GASI, GCH1, GDF11, GPPD1, GEM, GLRX2, GPR137B, GPR155, GPR68, GPRC5A, GTF2E2, H2AFZ, HAUS3, HGF, HIGD1D, HK2, HMGA1, HOMER1, HPCA, HSPA5, ICOSLG, IER3, IFNARI, IL1A, IL1R1, IL33, CXCL8, INA, INHBA, IRAK2, ISG20L2, ITGA2, ITGAV, IVNS1ABP, JAK2, JARID2, JMD1C, JPH1, JPH2, KBTBD8, KRT18, KRT8, LDHA, LHFPL2, LIN7C, LMCD1, LOC100139161, LOC100270684, LOC100296849, LOC100297185, LOC100297291, LOC100298623, LOC100336688, LOC100336779, LOC100337139, LOC100337302, LOC286871, LOC510442, LOC510487, LOC513388, LOC515823, LOC521504, LOC533324, LOC538547, LOC540234, LOC540868, LOC617407, LOC617986, LOC768081, LOC782348, LOC782470, LOC782740, LOC784446, LOC784704, LOC785868, LOC786258, LOC788082, LONRF3, LRP12, LRRC8B, LRRN3, LSM1, LYPD2, MANF, MAP1LC3C, MAP2K3, MAP3K8, MARCKSL1, METAP2, MEX3C, MGC165939, MIR21, MIR220C-1, MMP12, MT2A, MUSK, MXD1, Mynn, NAP1L5, NDRG1, NET1, NFKB1, NIPAL1, NKAIN1, NP, NUPL2, OAF, OBFC2A, OSBPL1, P2RY6, PAK1IP1, PCP4L1, PDE8A, PDP1, PELI1, PICALM, PIK3CA, PIM1, PITPNC1, PKNOX1, PLAUR, PLIN2, PLK3, PLOD2, POLB, PPM1D, PPP1CB, PPP4R2, PPP4R4, PSME4, PTX3, RAB20, RAI14, RASA2, RASSF8, RBBP8, RCAN1, RERG, RGS16, RHEB, R1OK3, RNF125, RNF19B, RNF24, RPF2, RPS12, RRP15, RSBN1, RSL24D1, RUNX1, S1PR3, SAMD8, SBNO2, SDC4, SEL1, SERPINA11, SERPINB2, SERPINE1, SERTAD2, SETD8, SGMS2, SLC13A3, SLC20A2, SLC25A33, SLC26A2, SLC2A1, SLC37A3, SLITRK2, SMG9, SNAP25, SOCS1, SOCS3, SOX4, SPCS3, SPPI1, SPSB1, SRF, SRXN1, SSFA2, STEAP1, STK17B, STK38L, STX11, SUCLA2, TAF4B, TBC1D8B, TBC1D9, TFPI2, THBD, THBS1, TIAM1, TIMM17A, TIMM8A, TMEM30B, TMF1, TNFRSF12A, TRAM1, TUFT1, TWFI, TXN, UBE2B, UBE2N, UBE3A, UTP15, VAT1L, XCL2, XIRP1, YOD1, YWHAZ, ZBTB43, ZFAND2A, ZFAND5, ZNF385B, ZNF644, ZNRD1, ZSWIM4, ZSWIM6</i> </p>	<p> <i>ACBD4, ACD, ACP5, ACTN4, ADCY4, ADCY9, ADORA2A, ADPRHL2, ADRB1, AGAP2, AGFG2, AGTR1, AHNAK, ALAD, AMOT, ARHGAP17, ARHGAP23, ARID1A, ARRD1, ATF7, ATP2C2, B3GNT3, BCL9L, BCOR, BRPF1, C22H3ORF37, C25H7ORF26, C28H1orf198, C5H12ORF4, C8H9orf91, CABC1, CAMK2G, CASP9, CBFA2T2, CBRI, CBX6, CD34, CDC42EP4, CEACAM8, CHAD, CHMP1A, CHMP4C, CMTM4, CNNM3, COL4A3BP, COPS7A, CRT2, CTNS, CYR1, DCP1B, DEF6, DHRS12, DIP2A, DMD, DNAJC17, DNASE1, DTNBP1, DYSF, EIF4ENIF1, ENG, ERAL1, EVC2, EZH1, FAM115A, FBXO42, FBXW4, FLT3LG, FOXN3, FOXO4, FOXRED1, FOXS1, FUT1, FYCO1, GAB1, GATA4, GGA3, GNA14, GPIHBP1, GPR111, GPS2, GTF2I, H6PD, HAUS5, HCRTR1, HIP1, HPS1, HS1BP3, HSDL1, ID3, ILDR2, ILVBL, INPP5K, IPO13, JUB, KANK1, KANK2, KANK3, KDR, KIAA1462, KIF13A, KIF16B, KLHL26, LASS1, LDLRAP1, LGALS9, LIPE, LOC100294795, LOC100296837, LOC100302527, LOC100335169, LOC100335642, LOC100336568, LOC100336724, LOC100336733, LOC100336756, LOC100337051, LOC100337052, LOC100337088, LOC505156, LOC505719, LOC507983, LOC511229, LOC512933, LOC518003, LOC522631, LOC523424, LOC531539, LOC540132, LOC540480, LOC614014, LOC615144, LOC616063, LOC617808, LOC783807, LOC785034, LOC785776, LOC786652, LOC789017, LPHN1, MAMSTR, MAP4K2, MBNL2, MEF2C, MFNG, MICALL1, MINK1, MIR2416, MLLT10, MMP15, MMS19, MOBKL2B, MPDZ, MTF1, MTMR4, MTSS1, MYH11, NAAA, NBEAL2, NFATC1, NFIB, NHSL2, NIPSNAP1, NME6, NOVA2, NR1H3, NR2C2, NR2F1, NR5A2, NUMA1, OSBPL7, PACS1, PCDH12, PEX10, PFKM, PGM5, PHACTR4, PHF21A, PIK3CG, PITPNM2, PKDCC, PLCG1, PLEKHA2, PNKD, PNPLA2, PODXL, POLD2, PPARA, PPP1R3B, PPP1R9A, PRDM10, PRPF19, PRR12, PRR14, PTH1R, PTPN23, RAB11FIP5, RAB7L1, RABGGTA, RAD52, RARG, RASGRP1, RASGRP3, RBM5, RHOG, RNF213, RNF214, RPAP1, RXRB, SAP30BP, SEMA4C, SETDB1, SF3A2, SHANK3, SIPA1, SIRT2, SLC24A3, SLC29A3, SLCO2B1, SMARCA2, SORBS3, SPRY3, SPRY4, SPTBN1, ST6GAL1, STAB1, STAP2, STARD9, STAT1, STAT2, STK36, STYX11, TAF6L, TAOK2, TARBP1, TBC1D16, TBC1D2B, TBC1D9B, TBXA2R, TCEA2, TCN2, TCP11L1, TDRD7, TENC1, TGFB2, TIRAP, TMC06, TMEM106A, TMEM204, TMEM51, TMEM88, TNRC6C, TNS1, TOR3A, TPCN2, TRIB2, TRIM11, TRIM26, TRIP10, TSC22D3, TSPAN4, UBA7, UFSP1, UNC119, UNC93B1, UNK, USHBP1, VMAC, WDR91, WIPF3, WWP2, XDH, ZBTB4, ZBTB40, ZC3HC1, ZER1, ZMYM3, ZMYND8, ZNF362, ZNF384, ZNF395, ZNF423, ZNF445, ZNF592, ZNF687, ZNF704, ZNF768, ZNF827, ZNFX1</i> </p>

	Up-Regulated Genes (321)	Down-Regulated Genes (320)
Late-Response	<p> <i>ABHD12B, ABTB2, AEBP2, AHSB, AKAP4, AKIRIN1, ALCAM, ANKRD1, ANO6, ARF4, ARHGAP28, ARHGAP6, ATAD1, ATP2B1, ATP5I, ATP6V1C1, B4GALT5, BCAP29, BCHE, BIRC3, BMP2, BTBD1, C12H13orf27, C16H1ORF21, C17H12orf52, C23H6orf141, C29H11orf73, C6H4orf34, CA8, CAPZA2, CCDC58, CCK, CCL2, CCL4, CCL8, CCNG2, CD14, CD40, CD44, CDH1, CFLAR, CGRRF1, CLDN1, CLEC1A, CLEC1B, COMMD6, COX6C, CPNE8, CREB5, CRIPT, CRYAB, CSF1, CTLA4, CTNNA1, CXCL2, CYB5R4, CYSLTR2, DENND5A, DNAJC12, DSTN, DTWD1, DUSP11, DUSP14, EIF1AX, EIF4E, EVI2A, EXOSC1, FAM18B, FAM92A1, FBXO32, FGFR1OP2, FGR, FKBP14, GAL, GMCL1, GMFB, GMNN, GMPR, GNPAT1, GULO, HAUS6, HBXIP, HINT1, HINT3, HPCAL4, HS3ST5, HSPA13, IBSP, IFT20, IGFBP1, IL18, IL1B, IL1RN, IL21R, IL4R, IL7R, INHBB, INSIG2, IPMK, IRG1, ISCA1, ITGB8, KIAA1715, KLHL32, LLPH, LMO7, LOC100137875, LOC100138864, LOC100140212, LOC100140827, LOC100294784, LOC100294785, LOC100294863, LOC100294880, LOC100295254, LOC100295381, LOC100295586, LOC100295656, LOC100295757, LOC100295775, LOC100296216, LOC100296447, LOC100296475, LOC100296588, LOC100296684, LOC100296722, LOC100296944, LOC100297075, LOC100297131, LOC100297413, LOC100297496, LOC100297676, LOC100297932, LOC100298628, LOC100300164, LOC100301462, LOC100335253, LOC100335275, LOC100335936, LOC100336429, LOC100336518, LOC100336625, LOC100337076, LOC100337126, LOC100337445, LOC407171, LOC509094, LOC516629, LOC520588, LOC521363, LOC532603, LOC538197, LOC613460, LOC613970, LOC614438, LOC614643, LOC615784, LOC616520, LOC619061, LOC781142, LOC781416, LOC781612, LOC781807, LOC782021, LOC782162, LOC782266, LOC782402, LOC782950, LOC783459, LOC783838, LOC784097, LOC784207, LOC784931, LOC785449, LOC785455, LOC785745, LOC786131, LOC787187, LOC788496, LOC789095, LRRC57, LRRC58, MAGI3, MANIA1, MAP4K5, MAPK6, MAPKAPK3, MAPKSP1, MEMO1, METRNL, MGC127538, MGC127989, MGC133504, MGC143035, MGC148938, MGC148942, MICAL2, MIER1, MIR147, MIR2469, MMP1, MOSPD2, MRPL39, MRPL42, MRPS16, MRPS18C, NCALD, NDUFB1, NUCB2, NUDCD1, ODF2L, OLR1, OSTM1, PAG1, PAPD7, PCNP, PDCD10, PDGFC, PDLIM4, PEX13, PKIB, PLA2G7, PLN, POLE4, POLR2K, PPAPDC3, PPP1R2, PPP1R3C, PRDM1, PRKCD, PRR5L, PSMD14, PSTPIP2, PTGER2, RABGGTB, RBM18, RBM7, RCHY1, RCN2, RDH11, RNFT1, RPIA, RPL27, RPL34, RPS21, RRS2, S100A12, S100A9, SAMD4A, SEC61G, SELK, SELP, SEMA3C, SF3B14, SGPP1, SGTB, SH3GL3, SLC12A2, SLC19A2, SLC25A25, SLC33A1, SLC38A1, SLC39A8, SLC41A2, SLMO2, SNRPDI, SNRPG, SNX13, SNX31, SNX4, SOAT1, SPHK1, SRD5A1, STAMBP, STK17A, SUB1, TAF13, TANK, TBCA, TERC, TET3, TFB2M, TGFBR1, TGIF1, THAP5, THEX1, TMEM126A, TMEM136, TMEM14A, TMEM165, TMEM188, TMEM189-UBE2V1, TMEM26, TMEM40, TMEM41B, TMEM45A, TMEM64, TMOD1, TMX1, TNFAIP8L3, TNFSF4, TPM4, TRPC4, TRPM6, TRPM7, TSPAN12, TXNRD1, TYW3, UAP1, UBE2D1, UBE2W, UCHL3, UFM1, UPRT, UXT, VBPI, WDR44, WDR89, XBPP1, YWHAQ, ZCCHC10</i> </p>	<p> <i>AACS, AAK1, AARS, ABCF3, ABCG2, ABHD14A, ACACA, ACIN1, ADAMTS17, ADD1, AGK, AGRN, ALDH3B1, ANKLE2, APLNR, AR, ARFGEF2, ARHGAP18, ARHGEF7, ARID1B, ARSB, ASXL2, ATF5, ATN1, ATXN2, ATXN7, AUTS2, B3GNT9, BAT2, BAT2L1, BAZ1B, BAZ2A, BCL9, BNC2, CAPN1, CASC3, CBL, CBR4, CEP110, CHD2, CKAP5, CLASP1, CLMN, CNDP2, CNST, COL4A2, COQ4, CPE, CREBBP, CUL7, CUX1, CXORF36, CYB5R3, DAAM2, DAB2, DAGLA, DCLRE1B, DCTN1, DHX30, DHX37, DIP2B, DOCK6, DOCK9, DUSP15, DVLP3, EEF2K, EFTUD2, EHD2, EIF2B4, ELMO1, EMCN, EMP2, EPB41, FADS6, FAM59A, FASN, FBLIM1, FBLN5, FBN1, FBXL6, FBXL8, FES, FGD1, FIBIN, FLOT2, FLYWCH2, FOXJ2, FTSJD2, FUT4, FUT8, GALNS, GALNT10, GANAB, GBA2, GCC1, GCN1L1, GIT2, GLG1, GPR4, GTF3C1, GYS1, HCFC1, HECW2, HGS, HSD17B14, HSPG2, IFT122, IFT88, IGF2R, IGFBP2, IL11RA, INADL, INPP5D, INTS1, INTS3, IQGAP2, ITGA9, ITSN1, KDM2A, KLF12, KPTN, LAMA4, LARP1, LHPP, LNP1, LOC100137838, LOC100138783, LOC100295338, LOC100296937, LOC100298629, LOC100300734, LOC100336508, LOC100336586, LOC100336604, LOC100336651, LOC100336769, LOC100337072, LOC100337134, LOC100337236, LOC100337329, LOC507299, LOC509490, LOC510855, LOC511523, LOC511901, LOC512110, LOC512168, LOC512286, LOC517133, LOC517559, LOC518768, LOC523454, LOC524694, LOC524974, LOC527362, LOC527591, LOC529211, LOC533444, LOC537748, LOC538506, LOC539067, LOC616014, LOC767865, LOC783344, LOC785548, LOC785659, LOC790124, LRRC41, LRRK1, LRSAM1, MAP3K4, MAP3K6, MAPRE2, MCM4, MDN1, MECP2, MED12, MED22, MGC138976, MIB2, MLH3, MLL2, MMP2, MOBK12A, MON1B, MORC2, MOV10, MPP5, MTMR14, MTMR15, MTOR, MUL1, MXD4, MYO18A, MYOF, MYST4, NAGK, NFIA, NFIC, NFIX, NUA1, NUP214, NUP85, OIT3, OLFML1, OSBP, PAN2, PARP1, PARP4, PATL1, PBX1, PCNXL3, PCYOX1L, PCYT1B, PDZD2, PELP1, PEX1, PIK3R1, PKNOX2, PLIN3, PLOD3, PLXNB2, PLXND1, PMF1, POGZ, POLD1, POLL, POLR1A, POLR3A, POMT1, PPIL2, PPP1R13B, PPP2R5D, PRDM6, PRELP, PRKAB1, PRKACA, PRKCSH, PRKD2, PTPN14, PTPRF, PTPRS, RBM47, REV3L, RHBDF1, RNASEN, RNF123, RNF40, RPS6KA5, SAPI30, SARS2, SART3, SCAF1, SEC16A, SEC24C, SELO, SEPNI, SETMAR, SF3B4, SFXN2, SLC12A6, SLC19A1, SLC46A3, SLC47A1, SLC7A8, SLC8A1, SMC1A, SMG1, SMYD4, SNRNP200, SPG11, SREBF1, SRGAP2, SRRM1, SUN2, TBCD, TH1L, TJPI, TLN1, TMCC1, TMEM41A, TMEM52, TMEM63A, TMEM8A, TNKS, TNRC6A, TNS3, TRAPPC9, TRIM44, TRRAP, TSC2, TSPAN18, TTC39A, TLL4, UAP1L1, UBAP2L, UBE4B, UPF1, USP22, USP24, USP48, VAC14, VAV3, VPS39, WDR34, WDR81, WFDCC5, WIZ, WNK1, XPC, YLPM1, ZBTB16, ZC3H4, ZCCHC11, ZNF385A, ZNF503, ZNF518B, ZNF787, ZRANB3, ZZEF1</i> </p>

	Up-Regulated Genes (26)	Down-Regulated Genes (222)
BiPhasic Response	<i>CRABP2, DES, FAM148A, FCHSD2, IL18BP, LOC100140276, LOC100336666, LOC100337178, LOC789021, LY96, MIR2475, NFKBIA, OXT, PDE4D, PENK, PTBP2, RUNDC3B, RUSC2, SEPW1, SRGN, TM4SF1, TMEM14C, TNFAIP3, UNC50, USP2, XIST</i>	<i>ACAD10, ACAP3, ADAMTSL5, AEBP1, AFF1, AFF3, AGPAT1, AKAP13, ANXA11, APIB1, ARAP1, ARHGEF11, ARSG, ASAP1, ATF6B, B9D2, C9H6ORF70, CABIN1, CAMKK2, CASKIN2, CCDC106, CCS, CELSR2, CIZ1, CLIC5, CNOT3, CNOT4, COG7, CPEB2, CPSF1, CRTC1, CRY2, DAB2IP, DENND4B, DHX57, DIS3L2, DOPEY2, DPF3, DTX2, EGFLAM, EMD, EP400, ERN1, EXOC3L, FAM13A1, FANCG, FBR5, FBXW12, FHOD1, FNTB, FRY, FZR1, G6PD, GALT, GBF1, GPD5, GIPC1, GLE1, GRN, HADH, HEATR7A, HERC2, HEXDC, HOXC6, HSPA2, HUWE1, IKBKG, INO80D, ISYNA1, ITPR3, KIAA0406, KLHL18, KLHL25, LAMB2, LOC100297361, LOC100298868, LOC100336841, LOC100336912, LOC100337120, LOC100337133, LOC100337159, LOC100337193, LOC506074, LOC506315, LOC508226, LOC508997, LOC510844, LOC511420, LOC513500, LOC515954, LOC520505, LOC522998, LOC526847, LOC528987, LOC533805, LOC533894, LOC534002, LOC534434, LOC535053, LOC535946, LOC536128, LOC538693, LOC539015, LOC540077, LOC615274, LOC619120, LOC783362, LOC784903, LOC788113, LOC789485, LOC789747, LPCAT1, LRFN3, LTBR, MACF1, MAEA, MAMLD1, MAN2A2, MAP1S, MAP2K2, MARK2, MAVS, MDC1, MED25, MGC128008, MGC151975, MIR1287, MIR2450B, MIR2454, MLL, MOSPD3, MTP18, MTSS1L, MYL9, NADSYN1, NAV2, NCOA2, NCOA6, NGLY1, NLRX1, NOSIP, NOTCH1, NPNT, OGFOD2, ORAI1, PCGF2, PDPR, PEX6, PGAP3, PHC3, PIM2, PKD2L1, PLCB3, PLEKHM3, PLXNA2, PML, POU6F1, PPP1CA, PPP1R12C, PPP2R4, PRKCE, PRKDC, PSMF1, PTGDS, PTPRG, PXN, RAB11B, RAB1B, RFFL, RPTOR, RUNX1T1, SFRS14, SFRS8, SHROOM4, SLC27A1, SLC35A4, SLC37A4, SLC41A1, SLC9A1, SLC9A3R2, SMARCC2, SMG6, SNX29, SPTAN1, SRRM2, SYNE2, TACC2, TAF4, TAPBP, TBC1D8, TCF7L2, TIE1, TMEM127, TMEM138, TNRC6B, TP53, TPCN1, TRAFD1, TRAPPC1, TRIM25, TRIM45, TRPV2, TSNARE1, TSPAN5, TSPYL4, TTC28, TTL3, UBR4, VPS13D, VPS37C, VRK3, WDR6, ZBTB20, ZC3H7B, ZEB2, ZFYVE26, ZHX3, ZNF414, ZNF496, ZNF605, ZNF618, ZNF828</i>